

# Scientific Opportunities with the Long-Baseline Neutrino Experiment

October 17, 2013



## The LBNE Collaboration

C. Adams,<sup>66</sup> T. Akiri,<sup>17</sup> M. Andrews,<sup>18</sup> I. Anghel,<sup>28</sup> E. Arrieta-Diaz,<sup>36</sup> M. Artuso,<sup>56</sup> J. Asaadi,<sup>56</sup> X. Bai,<sup>53</sup> M. Baird,<sup>26</sup> B. Balantekin,<sup>65</sup> B. Baller,<sup>18</sup> B. Baptista,<sup>26</sup> D. Barker,<sup>58</sup> W. Barletta,<sup>39</sup> G. Barr,<sup>43</sup> A. Bashyal,<sup>60</sup> M. Bass,<sup>12</sup> V. Bellini,<sup>10</sup> B.E. Berger,<sup>12</sup> M. Bergevin,<sup>5</sup> E. Berman,<sup>18</sup> H. Berns,<sup>5</sup> A. Bernstein,<sup>31</sup> R. Bernstein,<sup>18</sup> V. Bhatnagar,<sup>25</sup> B. Bhuyan,<sup>24</sup> M. Bishai,<sup>4</sup> A. Blake,<sup>9</sup> E. Blaufuss,<sup>35</sup> B. Bleakley,<sup>54</sup> E. Blucher,<sup>11</sup> S. Blusk,<sup>56</sup> V. Bocean,<sup>18</sup> T. Bolton,<sup>29</sup> R. Breedon,<sup>5</sup> A. Brandt,<sup>60</sup> C. Bromberg,<sup>36</sup> R. Brown,<sup>4</sup> N. Buchanan,<sup>12</sup> B. Bugg,<sup>57</sup> L. Camilleri,<sup>14</sup> R. Carr,<sup>14</sup> G. Carminati,<sup>6</sup> F. Cavanna,<sup>66</sup> A. Chen,<sup>18</sup> H. Chen,<sup>4</sup> K. Chen,<sup>4</sup> D. Cherdack,<sup>12</sup> C. Chi,<sup>14</sup> S. Childress,<sup>18</sup> B. Choudhary,<sup>23</sup> C. Christofferson,<sup>53</sup> E. Church,<sup>66</sup> D. Cline,<sup>7</sup> T. Coan,<sup>55</sup> J. Coelho,<sup>61</sup> S. Coleman,<sup>13</sup> J. Conrad,<sup>39</sup> M. Convery,<sup>51</sup> R. Corey,<sup>53</sup> L. Corwin,<sup>53</sup> G.S. Davies,<sup>28</sup> S. Dazeley,<sup>31</sup> A. de Gouvea,<sup>41</sup> J.K. de Jong,<sup>43</sup> C. Escobar,<sup>18</sup> K. De,<sup>60</sup> D. Demuth,<sup>37</sup> M. Diwan,<sup>4</sup> Z. Djurcic,<sup>2</sup> J. Dolph,<sup>4</sup> G. Drake,<sup>2</sup> H. Duyang,<sup>52</sup> S. Dye,<sup>19</sup> D. Edmunds,<sup>36</sup> S. Elliott,<sup>33</sup> S. Eno,<sup>35</sup> S. Enomoto,<sup>63</sup> A. Farbin,<sup>60</sup> L. Falk,<sup>67</sup> J. Felde,<sup>5</sup> F. Feyzi,<sup>65</sup> L. Fields,<sup>41</sup> B. Fleming,<sup>66</sup> J. Fowler,<sup>17</sup> W. Fox,<sup>26</sup> A. Friedland,<sup>33</sup> B. Fujikawa,<sup>30</sup> H. Gallagher,<sup>61</sup> R. Gandhi,<sup>21</sup> G. Garvey,<sup>33</sup> V.M. Gehman,<sup>30</sup> G. Geronimo,<sup>4</sup> R. Gill,<sup>4</sup> M.C. Goodman,<sup>2</sup> J. Goon,<sup>58</sup> M. Graham,<sup>51</sup> R. Gran,<sup>38</sup> C. Grant,<sup>5</sup> H. Greenlee,<sup>18</sup> L. Greenler,<sup>65</sup> V. Guarino,<sup>2</sup> E. Guardincerri,<sup>33</sup> R. Guenette,<sup>66</sup> S. Habib,<sup>1</sup> A. Habig,<sup>38</sup> R.W. Hackenburg,<sup>4</sup> A. Hahn,<sup>18</sup> T. Haines,<sup>33</sup> T. Handler,<sup>57</sup> S. Hans,<sup>4</sup> J. Hartnell,<sup>67</sup> J. Harton,<sup>12</sup> R. Hatcher,<sup>18</sup> A. Hatzikoutelis,<sup>57</sup> S. Hays,<sup>18</sup> E. Hazen,<sup>3</sup> M. Headley,<sup>49</sup> A. Heavey,<sup>18</sup> K. Heeger,<sup>65</sup> J. Heise,<sup>49</sup> R. Hellauer,<sup>35</sup> A. Himmel,<sup>17</sup> M. Hogan,<sup>12</sup> A. Holin,<sup>32</sup> G. Horton-Smith,<sup>29</sup> J. Howell,<sup>18</sup> P. Hurh,<sup>18</sup> J. Huston,<sup>36</sup> J. Hylen,<sup>18</sup> R. Imlay,<sup>34</sup> J. Insler,<sup>34</sup> Z. Isvan,<sup>4</sup> C. Jackson,<sup>60</sup> D. Jaffe,<sup>4</sup> C. James,<sup>18</sup> M. Johnson,<sup>18</sup> R. Johnson,<sup>13</sup> S. Johnson,<sup>13</sup> W. Johnston,<sup>12</sup> J. Johnstone,<sup>18</sup> B. Jones,<sup>39</sup> H. Jostlein,<sup>18</sup> T. Junk,<sup>18</sup> R. Kadel,<sup>30</sup> G. Karagiorgi,<sup>14</sup> J. Kaspar,<sup>63</sup> T. Katori,<sup>39</sup> B. Kayser,<sup>18</sup> E. Kearns,<sup>3</sup> P. Keener,<sup>44</sup> S.H. Kettell,<sup>4</sup> M. Kirby,<sup>18</sup> J. Klein,<sup>44</sup> G. Koizumi,<sup>18</sup> S. Kopp,<sup>59</sup> W. Kropp,<sup>6</sup> V.A. Kudryavtsev,<sup>50</sup> A. Kumar,<sup>25</sup> J. Kumar,<sup>19</sup> T. Kutter,<sup>34</sup> K. Lande,<sup>44</sup> C. Lane,<sup>16</sup> K. Lang,<sup>59</sup> F. Lanni,<sup>4</sup> R. Lanza,<sup>39</sup> T. Latorre,<sup>44</sup> F. La Zia,<sup>10</sup> J. Learned,<sup>19</sup> D. Lee,<sup>33</sup> K. Lee,<sup>7</sup> S. Li,<sup>4</sup> Y. Li,<sup>4</sup> Z. Li,<sup>17</sup> J. Libo,<sup>52</sup> S. Linden,<sup>3</sup> J. Ling,<sup>4</sup> J. Link,<sup>62</sup> L. Littenberg,<sup>4</sup> H. Liu,<sup>20</sup> Q. Liu,<sup>33</sup> T. Liu,<sup>55</sup> J. Losecco,<sup>42</sup> W. Louis,<sup>33</sup> B. Lundberg,<sup>18</sup> T. Lundin,<sup>18</sup> C. Maesano,<sup>5</sup> S. Magill,<sup>2</sup> G. Mahler,<sup>4</sup> S. Malys,<sup>40</sup> F. Mammoliti,<sup>10</sup> S. Mandal,<sup>23</sup> A. Mann,<sup>44</sup> A. Mann,<sup>61</sup> P. Mantsch,<sup>18</sup> A. Marchionni,<sup>18</sup> W. Marciano,<sup>4</sup> C. Mariani,<sup>62</sup> J. Maricic,<sup>19</sup> A. Marino,<sup>13</sup> M. Marshak,<sup>37</sup> J. Marshall,<sup>9</sup> S. Matsuno,<sup>19</sup> C. Mauger,<sup>33</sup> N. Mayer,<sup>61</sup> E. McCluskey,<sup>18</sup> K. McDonald,<sup>46</sup> K. McFarland,<sup>48</sup> D. McKee,<sup>29</sup> R. McKeown,<sup>64</sup> R. McTaggart,<sup>54</sup> R. Mehdiyev,<sup>59</sup> D. Mei,<sup>58</sup> Y. Meng,<sup>7</sup> B. Mercurio,<sup>52</sup> M.D. Messier,<sup>26</sup> W. Metcalf,<sup>34</sup> R. Meyhandan,<sup>19</sup> R. Milincic,<sup>19</sup> W. Miller,<sup>37</sup> G. Mills,<sup>33</sup> S. Mishra,<sup>52</sup> S. Moed Sher,<sup>18</sup> N. Mokhov,<sup>18</sup> D. Montanari,<sup>18</sup> C.D. Moore,<sup>18</sup> J. Morfin,<sup>18</sup> W. Morse,<sup>4</sup> S. Mufson,<sup>26</sup> D. Muller,<sup>51</sup> J. Musser,<sup>26</sup> D. Naples,<sup>45</sup> J. Napolitano,<sup>47</sup> M. Newcomer,<sup>44</sup> E. Niner,<sup>26</sup> B. Norris,<sup>18</sup> T. Olson,<sup>61</sup> B. Page,<sup>36</sup> S. Pakvasa,<sup>19</sup> J. Paley,<sup>2</sup> O. Palamara,<sup>66</sup> V. Paolone,<sup>45</sup> V. Papadimitriou,<sup>18</sup> S. Park,<sup>60</sup> Z. Parsa,<sup>4</sup> B. Paulos,<sup>65</sup> K. Partyka,<sup>66</sup> Z. Pavlovic,<sup>33</sup> A. Perch,<sup>32</sup> J.D. Perkin,<sup>50</sup> S. Peeters,<sup>67</sup> R. Petti,<sup>52</sup> R. Plunkett,<sup>18</sup> C. Polly,<sup>18</sup> S. Pordes,<sup>18</sup> R. Potenza,<sup>10</sup> A. Prakash,<sup>39</sup> O. Prokofiev,<sup>18</sup> G. Perdue,<sup>48</sup> X. Qian,<sup>8</sup> J.L. Raaf,<sup>18</sup> V. Radeka,<sup>4</sup> R. Rajendran,<sup>18</sup> I. Rakhno,<sup>18</sup> R. Rameika,<sup>18</sup> J. Ramsey,<sup>33</sup> B. Rebel,<sup>18</sup> S. Rescia,<sup>4</sup> D. Reitzner,<sup>18</sup> M. Richardson,<sup>50</sup> K. Riesselman,<sup>18</sup> M. Robinson,<sup>50</sup> M. Ronquest,<sup>33</sup> M. Rosen,<sup>19</sup> C. Rosenfeld,<sup>52</sup> R. Rucinski,<sup>18</sup> S. Sahijpal,<sup>25</sup> H. Sahoo,<sup>2</sup> N. Samios,<sup>4</sup> M.C. Sanchez,<sup>28</sup> H. Schellman,<sup>41</sup> R. Schmitt,<sup>18</sup> D. Schmitz,<sup>11</sup> J. Schneps,<sup>61</sup> K. Scholberg,<sup>17</sup> S. Seibert,<sup>44</sup> M. Shaevitz,<sup>14</sup> P. Shanahan,<sup>18</sup> R. Sharma,<sup>4</sup> T. Shaw,<sup>18</sup> N. Simos,<sup>4</sup> V. Singh,<sup>22</sup> G. Sinnis,<sup>33</sup> W. Sippach,<sup>14</sup> T. Skwarnicki,<sup>56</sup> M. Smy,<sup>6</sup> H. Sobel,<sup>6</sup> M. Soderberg,<sup>56</sup> J. Sondericker,<sup>4</sup> W. Sondheim,<sup>33</sup> N.J.C. Spooner,<sup>50</sup> M. Stancari,<sup>18</sup> I. Stancu,<sup>1</sup> A. Stefanik,<sup>18</sup> J. Stewart,<sup>4</sup> S. Stone,<sup>56</sup> J. Strait,<sup>18</sup> M. Strait,<sup>11</sup> S. Striganov,<sup>18</sup> G. Sullivan,<sup>35</sup> L. Suter,<sup>2</sup> R. Svoboda,<sup>5</sup> B. Szczerbinska,<sup>15</sup> M. Szydagis,<sup>5</sup> A. Szelc,<sup>66</sup> R. Talaga,<sup>2</sup> M. Tamsett,<sup>67</sup> S. Tariq,<sup>18</sup> R. Tayloe,<sup>26</sup> C. Taylor,<sup>33</sup> D. Taylor,<sup>30</sup> D. Taylor,<sup>49</sup> A. Teymourian,<sup>7</sup> H. Themann,<sup>4</sup> M. Thiesse,<sup>16</sup> J. Thomas,<sup>32</sup> L.F. Thompson,<sup>50</sup> M. Thomson,<sup>9</sup> C. Thorn,<sup>4</sup> X. Tian,<sup>52</sup> D. Tiedt,<sup>53</sup> W. Toki,<sup>12</sup> N. Tolich,<sup>63</sup> M. Tripathi,<sup>5</sup> I. Tropin,<sup>18</sup> M. Tzanov,<sup>34</sup> J. Urheim,<sup>26</sup> S. Usman,<sup>40</sup> M. Vagins,<sup>27</sup> R. Van Berg,<sup>44</sup> R. Van de Water,<sup>33</sup> G. Varner,<sup>19</sup> K. Vaziri,<sup>18</sup> G. Velev,<sup>18</sup> B. Viren,<sup>4</sup> T. Wachala,<sup>12</sup> D. Wahl,<sup>65</sup> A. Waldron,<sup>67</sup> C.W. Walter,<sup>17</sup> H. Wang,<sup>7</sup> W. Wang,<sup>64</sup> D. Warner,<sup>12</sup> R. Wasserman,<sup>12</sup> B. Watson,<sup>60</sup> A. Weber,<sup>43</sup> W. Wei,<sup>58</sup> R. Wendell,<sup>27</sup> M. Wetstein,<sup>11</sup> A. White,<sup>60</sup> H. White,<sup>33</sup> L. Whitehead,<sup>20</sup> D. Whittington,<sup>26</sup> J. Willhite,<sup>49</sup> W. Willis,<sup>14</sup> R.J. Wilson,<sup>12</sup> L. Winslow,<sup>7</sup> E. Worcester,<sup>4</sup> T. Wyman,<sup>18</sup> T. Xin,<sup>28</sup> K. Yarritu,<sup>33</sup> J. Ye,<sup>55</sup> J. Yu,<sup>60</sup> M. Yeh,<sup>4</sup> B. Yu,<sup>4</sup> G. Zeller,<sup>18</sup> C. Zhang,<sup>4</sup> C. Zhang,<sup>58</sup> E.D. Zimmerman,<sup>13</sup> and R. Zwaska<sup>18</sup>

<sup>1</sup> Univ. of Alabama, Tuscaloosa, AL 35487-0324, USA

<sup>2</sup> Argonne National Laboratory, Argonne, IL 60437, USA

<sup>3</sup> Boston Univ., Boston, MA 02215, USA

- <sup>4</sup>Brookhaven National Laboratory, Upton, NY 11973-5000, USA
- <sup>5</sup>Univ. of California at Davis, Davis, CA 95616, USA
- <sup>6</sup>Univ. of California at Irvine, Irvine, CA 92697-4575, USA
- <sup>7</sup>Univ. of California at Los Angeles, Los Angeles, CA 90095-1547, USA
- <sup>8</sup>California Inst. of Tech., Pasadena, CA 91109, USA
- <sup>9</sup>Univ. of Cambridge, Cambridge CB3 0HE, United Kingdom
- <sup>10</sup>Univ. of Catania and INFN, I-95129 Catania, Italy
- <sup>11</sup>Univ. of Chicago, Chicago, IL 60637-1434, USA
- <sup>12</sup>Colorado State Univ., Fort Collins, CO 80521, USA
- <sup>13</sup>Univ. of Colorado, Boulder, CO 80309 USA
- <sup>14</sup>Columbia Univ., New York, NY 10027 USA
- <sup>15</sup>Dakota State University, Brookings, SD 57007, USA
- <sup>16</sup>Drexel Univ., Philadelphia, PA 19104, USA
- <sup>17</sup>Duke Univ., Durham, NC 27708, USA
- <sup>18</sup>Fermilab, Batavia, IL 60510-500, USA
- <sup>19</sup>Univ. of Hawaii, Honolulu, HI 96822-2216, USA
- <sup>20</sup>Univ. of Houston, Houston, Texas, 77204, USA
- <sup>21</sup>Harish-Chandra Research Institute, Allahabad-211 019, India
- <sup>22</sup>Banaras Hindu Univ., Varanasi UP 221005, India
- <sup>23</sup>Univ. of Delhi, Delhi 110007, India
- <sup>24</sup>Indian Institute of Technology Guwahati, Guwahati, 781 039, India.
- <sup>25</sup>Panjab Univ., Chandigarh 160014, U.T., India
- <sup>26</sup>Indiana Univ., Bloomington, Indiana 47405, USA
- <sup>27</sup>Kavli Institute for the Physics and Mathematics of the Universe, University of Tokyo, Chiba 277-8568, Japan
- <sup>28</sup>Iowa State Univ., Ames, IA 50011, USA
- <sup>29</sup>Kansas State Univ., Manhattan, KS 66506, USA
- <sup>30</sup>Lawrence Berkeley National Lab., Berkeley, CA 94720-8153, USA
- <sup>31</sup>Lawrence Livermore National Lab., Livermore, CA 94551, USA
- <sup>32</sup>University College London, London, W1C1E 6BT, England, UK
- <sup>33</sup>Los Alamos National Lab., Los Alamos, NM 87545, USA
- <sup>34</sup>Louisiana State Univ., Baton Rouge, LA 70803-4001, USA
- <sup>35</sup>Univ. of Maryland, College Park, MD 20742-4111, USA
- <sup>36</sup>Michigan State Univ., East Lansing, MI 48824, USA
- <sup>37</sup>Univ. of Minnesota, Minneapolis, MN 55455, USA
- <sup>38</sup>Univ. of Minnesota, Duluth, Duluth, MN 55812, USA
- <sup>39</sup>MIT Massachusetts Inst. of Technology, Cambridge, MA 02139-4307, USA
- <sup>40</sup>National Geospatial-Intelligence Agency, Reston, VA 20191, USA
- <sup>41</sup>Northwestern University, Evanston, IL 60208, USA
- <sup>42</sup>Univ. of Notre Dame, Notre Dame, IN 46556-5670, USA
- <sup>43</sup>Univ. of Oxford, Oxford OX1 3RH England, UK
- <sup>44</sup>Univ. of Pennsylvania, Philadelphia, PA 19104-6396, USA
- <sup>45</sup>University of Pittsburgh, Pittsburgh, PA 15260, USA
- <sup>46</sup>Princeton University, Princeton, NJ 08544-0708, USA
- <sup>47</sup>Rensselaer Polytechnic Inst., Troy, NY 12180-3590, USA
- <sup>48</sup>Univ. of Rochester, Rochester, NY 14627-0171, USA
- <sup>49</sup>Sanford Underground Research Facility, Lead, SD 57754, USA
- <sup>50</sup>Univ. of Sheffield, Sheffield, S3 7RH, England, UK
- <sup>51</sup>SLAC National Accelerator Laboratory, Menlo Park, CA 94025, USA
- <sup>52</sup>Univ. of South Carolina, Columbia, SC 29208, USA
- <sup>53</sup>South Dakota School of Mines and Technology, Lead, SD 57754, USA
- <sup>54</sup>South Dakota State Univ., Brookings, SD 57007, USA
- <sup>55</sup>Southern Methodist Univ., Dallas, TX 75275, USA
- <sup>56</sup>Syracuse Univ., Syracuse, NY 13244-1130, USA
- <sup>57</sup>Univ. of Tennessee, Knoxville TN 37996, USA
- <sup>58</sup>Univ. of South Dakota, Vermillion, SD 57069, USA
- <sup>59</sup>Univ. of Texas, Austin, Texas 78712, USA
- <sup>60</sup>Univ. of Texas at Arlington, Arlington, Texas 76019, USA
- <sup>61</sup>Tufts Univ., Medford, Massachusetts 02155, USA
- <sup>62</sup>Virginia Tech., Blacksburg, VA 24061-0435, USA
- <sup>63</sup>Univ. of Washington, Seattle, WA 98195-1560, USA
- <sup>64</sup>College of William and Mary, Williamsburg, VA 23187-8795, USA
- <sup>65</sup>Univ. of Wisconsin, Madison, WI 53706, USA
- <sup>66</sup>Yale Univ., New Haven, CT 06520, USA
- <sup>67</sup>Univ. of Sussex, Brighton, BN1 9RH, UK



## Abstract

In this document, we describe the wealth of science opportunities and capabilities of LBNE, the Long-Baseline Neutrino Experiment. LBNE has been developed to provide a unique and compelling program for the exploration of key questions at the forefront of particle physics. Chief among the discovery opportunities are observation of CP symmetry violation in neutrino mixing, resolution of the neutrino mass hierarchy, determination of maximal or near-maximal mixing in neutrinos, searches for nucleon decay signatures, and detailed studies of neutrino bursts from galactic supernovae. To fulfill these and other goals as a world-class facility, LBNE is conceived around four central components: (1) a new, intense wide-band neutrino source at Fermilab, (2) a fine-grained ‘near’ neutrino detector just downstream of the source, (3) the Sanford Underground Research Facility (SURF) in Lead, South Dakota at an optimal distance ( $\sim 1300$  km) from the neutrino source, and (4) a massive liquid argon time-projection chamber (LArTPC) deployed there as a ‘far’ detector. The facilities envisioned are expected to enable many other science opportunities due to the high event rates and excellent detector resolution from beam neutrinos in the near detector and atmospheric neutrinos in the far detector. This is a mature, well developed, world class experiment whose relevance, importance, and probability of unearthing critical and exciting physics has increased with time.

This document is being submitted as a white paper to the 2013 DPF Community Summer Study program.

# Contents

<b>Contents</b>	<b>iv</b>
<b>List of Figures</b>	<b>vii</b>
<b>List of Tables</b>	<b>xi</b>
<b>1 Introduction and Executive Summary</b>	<b>1</b>
1.1 Development of a World-Class Experiment . . . . .	4
1.2 The LBNE Physics Program . . . . .	8
1.2.1 Long-Baseline Neutrino Oscillation Physics . . . . .	8
1.2.2 Baryon Physics Motivated by Grand Unified Theories . . . . .	10
1.2.3 Supernova-Neutrino Physics and Astrophysics . . . . .	11
1.2.4 Precision Oscillation Measurements and Short-Baseline Neutrino Physics . . . . .	12
1.3 Summary . . . . .	13
<b>2 Overview of the LBNE Science Program</b>	<b>14</b>
2.1 Primary and Secondary Science Objectives . . . . .	14
2.2 Long-Baseline Neutrino Oscillation Physics . . . . .	16
2.2.1 Three-Flavor Mixing, CP Violation and the Mass Hierarchy . . . . .	16
2.2.1.1 Characterization of Three-Flavor Mixing . . . . .	17
2.2.1.2 CP Violation in the Quark and Lepton Sectors . . . . .	20
2.2.1.3 Observation of CP-Violating Effects in Long-Baseline Experiments . . . . .	21
2.2.1.4 Probing the Mass Hierarchy via the Matter Effect . . . . .	24
2.2.1.5 Disentangling Leptonic CPV and the Matter Effect . . . . .	27
2.2.1.6 Optimization of Baseline . . . . .	30
2.2.2 Disappearance of $\nu_\mu$ and Determination of $\theta_{23}$ . . . . .	31
2.2.3 Oscillation Physics with Atmospheric Neutrinos . . . . .	33
2.3 Baryon Physics Motivated by Grand Unified Theories . . . . .	35
2.3.1 Motivation from GUTs . . . . .	36
2.3.2 Proton Decay Modes . . . . .	38
2.4 Supernova-Neutrino Physics and Astrophysics . . . . .	39
<b>3 Overview of the LBNE Project and Design</b>	<b>44</b>
3.1 LBNE and the U.S. Neutrino-Physics Program . . . . .	44
3.2 The LBNE Far Site: Sanford Underground Research Facility . . . . .	46

3.3	The LBNE Near Site: Fermi National Accelerator Laboratory . . . . .	52
3.4	The LBNE Beamline . . . . .	57
3.5	The LBNE Near Detector . . . . .	63
3.6	The LBNE Far Detector . . . . .	66
3.6.1	Smaller Surface Detector for LBNE Phase 1 . . . . .	66
3.6.2	Larger Deep-Underground Detector . . . . .	72
<b>4</b>	<b>Long-Baseline Neutrino Oscillation Physics</b>	<b>77</b>
4.1	Experimental Requirements Based on Oscillation Phenomenology . . . . .	77
4.2	May want a new heading here, not sure what . . . . .	80
4.3	LBNE Detector Simulation and Reconstruction . . . . .	84
4.3.1	Far Detector Simulation . . . . .	84
4.3.2	Far Detector Reconstruction . . . . .	89
4.3.3	Fast Monte Carlo . . . . .	94
4.3.4	Simulation of Cosmic Ray Backgrounds for a 10-kt Surface Detector .	101
4.3.5	Detector Simulation using the GLOBES Package . . . . .	103
4.4	Measurements of Mass Hierarchy and the CP-Violating Phase . . . . .	108
4.5	Measurement of $\theta_{23}$ and Determination of the Octant . . . . .	118
4.6	Precision Measurements of the Oscillation Parameters in the Three-Flavor Model	123
4.7	Oscillation Studies Using Atmospheric Neutrinos . . . . .	126
4.8	Searches for Physics Beyond $\nu$ SM in Long-Baseline Oscillations . . . . .	138
4.8.1	Search for Non-Standard Interactions . . . . .	139
4.8.2	Long-Range Interactions . . . . .	141
4.8.3	Search for Active-Sterile Neutrino Mixing . . . . .	141
4.8.4	Sensitivity to Large Extra Dimensions . . . . .	142
<b>5</b>	<b>Near Detector</b>	<b>143</b>
5.1	Precision Measurements with Long-Baseline Oscillations . . . . .	145
5.1.1	Relative Neutrino and Antineutrino Flux . . . . .	149
5.1.2	Flavor Content of the Beam: $\nu_\mu, \bar{\nu}_\mu, \nu_e, \bar{\nu}_e$ . . . . .	149
5.1.3	Constraining the Unoscillated $\nu$ Spectral Shape with the Quasi-Elastic Interaction . . . . .	150
5.1.4	Low-Energy Absolute Flux: Neutrino-Electron Neutral Current Scattering	151
5.1.5	High-Energy Absolute Flux: Neutrino-Electron Charged Current Scattering . . . . .	151
5.1.6	Low-Energy Absolute Flux: QE in Water and Heavy-Water Targets . .	152
5.1.7	Neutral Pions, Photons, and $\pi^\pm$ in Neutral and Charged Current Events	152
5.2	Electroweak Precision Measurement: Weak Mixing Angle . . . . .	153
5.2.1	Deep Inelastic Scattering . . . . .	154
5.2.2	Elastic Scattering . . . . .	157
5.3	Observation of the Nucleon's Strangeness Content . . . . .	158
5.4	Tests of Isospin Physics and Sum-Rules . . . . .	161
5.5	Nucleon Structure, Parton Distribution Functions, and QCD Studies . . . . .	163
5.6	Studies of Neutrino-Nuclear Interactions and Nuclear Effects . . . . .	165

5.7	Search for Heavy Neutrinos . . . . .	167
5.8	Search for High $\Delta m^2$ Neutrino Oscillations . . . . .	169
5.9	Search for Non-Standard Interactions: High $\Delta m^2$ Neutrino Oscillations . . . . .	169
5.10	Light (sub-GeV) Dark Matter Searches . . . . .	172
<b>6</b>	<b>Baryon Physics Motivated by Grand Unified Theories</b>	<b>175</b>
6.1	Sensitivity to Nucleon Decay . . . . .	175
6.1.1	LBNE and the Current Experimental Context . . . . .	175
6.1.2	Signatures for Baryon Number Violation in LBNE . . . . .	176
6.1.2.1	Signatures for $p \rightarrow K^+ \bar{\nu}$ . . . . .	177
6.1.3	Background Levels and Rejection . . . . .	178
6.1.4	Expected Sensitivity . . . . .	180
<b>7</b>	<b>Core-Collapse Supernova Neutrinos</b>	<b>181</b>
7.1	Physics and Astrophysics From Core-Collapse Neutrinos . . . . .	181
7.2	Expected Signal and Detection in Liquid Argon . . . . .	183
7.3	Low-Energy Backgrounds . . . . .	185
7.3.1	Intrinsic Backgrounds . . . . .	186
7.3.1.1	Cleanliness Database . . . . .	188
7.3.2	Cosmogenic Backgrounds . . . . .	189
<b>8</b>	<b>Other Physics Opportunities with the LBNE Far Detector</b>	<b>190</b>
8.1	Solar Neutrinos . . . . .	190
8.2	Geoneutrinos . . . . .	191
8.3	Indirect Searches for WIMP Dark Matter . . . . .	192
8.4	GUT Monopoles . . . . .	193
8.5	Neutron Anti-neutron Oscillations ( $\Delta B = 2$ ) . . . . .	193
<b>9</b>	<b>Conclusion</b>	<b>194</b>
<b>A</b>	<b>Summary of the LBNE Reconfiguration Steering Committee Report</b>	<b>197</b>

# List of Figures

1-1	The expected $1\sigma$ resolution for $\delta_{cp}$ as a function of exposure for 700 kW proton beam power. . . . .	10
1-2	Sensitivity to the decay $p \rightarrow K^+\bar{\nu}$ with LAr detectors. . . . .	11
2-1	Neutrino oscillations vs energy, baseline and as a function of $\delta_{CP}$ , normal MH .	25
2-2	Neutrino oscillations vs energy, baseline and as a function of $\delta_{CP}$ , inverted MH	26
2-3	The CP asymmetry as a function of baseline . . . . .	29
2-4	$\nu/\bar{\nu}$ oscillation asymmetries vs $\delta_{CP}$ at the first two oscillation nodes . . . . .	30
2-5	Fraction of $3\sigma$ $\delta_{cp}$ values for CP violation and MH vs baseline . . . . .	32
2-6	Atmospheric neutrino flux and spectrum . . . . .	33
2-7	Probabilities of atmospheric $\nu_\mu \rightarrow \nu_e$ oscillations by zenith angle . . . . .	34
2-8	Proton decay lifetime limits compared to lifetime ranges predicted by GUTs . .	39
2-9	Number of supernova neutrino interactions in an LAr detector vs distance . . .	43
3-1	Homestake Mine development . . . . .	47
3-2	Predicted cosmic ray flux at SURF . . . . .	49
3-3	Photos from SURF . . . . .	50
3-4	Experiment timeline at SURF . . . . .	51
3-5	Fermilab's accelerator chain . . . . .	53
3-6	NuMI beamline performance . . . . .	54
3-7	The Fermilab proton plan for Intensity Frontier experiments . . . . .	54
3-8	Project X accelerator schematics . . . . .	55
3-9	Overall LBNE project layout at Fermilab . . . . .	58
3-10	Primary beamline elevation view . . . . .	58
3-11	Neutrino beamline components . . . . .	59
3-12	System of tertiary muon detectors . . . . .	64
3-13	Magnetized LArTPC and straw-tube tracker . . . . .	65
3-14	View of the far detector showing the building, overburden and access regions .	67
3-15	TPC modular construction concept . . . . .	69
3-16	Layout of the 34-kt LAr detector hall at the 4850-foot level of SURF . . . . .	74
3-17	Schematic of the 34-kt LArTPC design. . . . .	75
3-18	Possible layout for far detector modules at the 4,850-ft level . . . . .	76
4-1	Unoscillated spectrum of $\nu_\mu$ events and $\nu_\mu \rightarrow \nu_e$ oscillation probabilities . . . .	81
4-2	Event displays of beam interactions in an LArTPC . . . . .	85

4-3	2D clusterings of hits created by particles in two CC neutrino interactions in LAr	92
4-4	Distributions of the residuals between the reconstructed and MC primary vertices in MicroBooNE geometry using LBNE beam spectrum . . . . .	93
4-5	Distribution of $\nu_\tau$ transverse momentum. . . . .	97
4-6	Selection of $\nu_e$ appearance candidates in an LArTPC . . . . .	98
4-7	Selection of $\nu_\mu$ appearance candidates in an LArTPC . . . . .	99
4-8	Selection efficiency for $\nu_e$ appearance in an LArTPC . . . . .	99
4-9	Selection efficiency for $\nu_\mu$ appearance in an LArTPC . . . . .	100
4-10	Cosmic ray background event distribution in the 10-kt surface detector . . . . .	104
4-11	Disappearance spectra in an LArTPC . . . . .	106
4-12	Event spectra of neutrino interactions in an LArTPC . . . . .	107
4-13	Sensitivity to MH and CP violation in a 10 kiloton LArTPC . . . . .	110
4-14	Probability of determining the correct mass hierarchy for a given $\Delta\chi^2$ . . . . .	111
4-15	Mass hierarchy and CP-violation in LBNE with increased exposure in mass, beam power and time . . . . .	115
4-16	CP-violation in LBNE with increased exposure in mass, beam power and time - Project X phasing . . . . .	116
4-17	CP-violation in LBNE with increased exposure in mass and beam power compared to other proposed experiments . . . . .	117
4-18	Measurement of the mixing parameters from Fogli et. al. . . . .	119
4-19	Measurement of $\theta_{23}$ and $\Delta m_{31}^2$ with LBNE 10 . . . . .	120
4-20	Sensitivity of LBNE to the determination of the $\theta_{23}$ octant . . . . .	121
4-21	Sensitivity of LBNE to the determination of the $\theta_{23}$ octant with later phases and Project X upgrades. . . . .	122
4-22	Measurement of $\delta_{CP}$ and $\theta_{13}$ in LBNE with different exposures. . . . .	124
4-23	Expected $1\sigma$ resolution on different three-flavor oscillation parameters in a 700-kW beam . . . . .	125
4-24	Resolution on $\delta_{CP}$ in LBNE and other experiments . . . . .	128
4-25	Reconstructed L/E distribution of 'high-resolution' $\mu$ -like atmospheric neutrino events with a 350 kt-yr exposure . . . . .	132
4-26	Reconstructed zenith angle distributions in several ranges of energy for the FC electron-like, FC $\mu$ -like, and PC $\mu$ -like samples . . . . .	133
4-27	Reconstructed zenith angle distributions for 6-10 GeV events in the FC electron-like, FC $\mu$ -like, and PC $\mu$ -like samples . . . . .	134
4-28	Sensitivity of 350 kt-yr of atmospheric neutrino data to the mass hierarchy as a function of $\delta_{CP}$ . . . . .	136
4-29	Sensitivity to mass hierarchy using atmospheric neutrinos . . . . .	137
4-30	Sensitivity to octant and CPV using atmospheric neutrinos. . . . .	137
4-31	Sensitivity to mass hierarchy using atmospheric neutrinos and beam neutrinos . . . . .	138
4-32	Sensitivity to octant and CPV using atmospheric and beam neutrinos. . . . .	139
4-33	Sensitivity to non-standard interactions . . . . .	140
4-34	Long-range Interactions in LBNE . . . . .	141
5-1	MH and CP violation sensitivities as a function of exposure in kt-years . . . . .	146

5-2	MH and CP violation sensitivities from shape, rate, and shape+rate . . . . .	147
5-3	Feynman diagrams for the three main Neutral Current processes . . . . .	154
5-4	Expected sensitivity to $\sin^2 \theta_W$ from the LBNE ND for a 700-kW beam . . . . .	158
5-5	Sensitivity of NC/CC to the strange contribution to spin of nucleon . . . . .	161
5-6	Feynman diagrams pertaining to sterile neutrinos . . . . .	169
5-7	Production mechanisms for dark matter at neutrino beam experiments. . . . .	173
5-8	Expected number of neutral-current-like events from DM scattering . . . . .	174
6-1	Isolated Kaon observed during the ICARUS test run at Pavia . . . . .	178
6-2	Proton decay lifetime limit for $p \rightarrow K^+ \bar{\nu}$ as a function of time . . . . .	180
7-1	Expected core-collapse neutrino signal. . . . .	182
7-3	Supernova neutrino event rates in 17 kton of argon for a core collapse at 10 kpc, for the GKVM model [?] (events per 0.5 MeV), showing three relevant interaction channels. Left: interaction rates as function of true neutrino energy. Right: “smeared” rates as a function of detected energy, assuming resolution from reference [?]. . . . .	184
7-4	Comparison of total event rates for normal and inverted hierarchy, for a specific flux example, for a water Cherenkov detector (left) and for a 17 kt LAr (right) configuration, in events per 0.5 MeV. There are distinctive features in LAr for different neutrino mass hierarchies for this supernova model. . . . .	185
7-5	Observed $\nu_e$ spectra in 34 kton of LAr for a 10 kpc core collapse, representing about one second of integration time each at one second intervals during the supernova cooling phase. The solid line represents the best fit to a parameterized pinched-thermal spectrum. Clear “non-thermal” features in the spectrum that change with time are visible, on the left at around 20 MeV and on the right at around 35 MeV. Error bars are statistical. These features are present <i>only</i> for normal mass hierarchy. . . . .	186
7-6	Average $\nu_e$ energy from fit to SNOwGLoBES-smeared pinched-thermal spectrum as a function of time, for a flux model based on [?] and including collective oscillations, for two different hierarchy assumptions (34 kton at 10 kpc). The bands represent $1\sigma$ error bars from the fit. The solid red line is the truth $\langle E_\nu \rangle$ for the unoscillated spectrum. This plot shows that there is meaningful information to be obtained by tracking $\nu_e$ spectra as a function of time. . . . .	187
7-7	Left: raw event display of a typical 20-MeV event in the LBNE 10-kton geometry; the top panel shows the collection plane, and the lower two panels show the induction planes (with multiple images due to wire wrapping). Right: zoom of collection plane image. . . . .	187
8-1	Measurements of the solar MSW transition [?]. . . . .	191
8-2	$^{40}\text{Cl}$ production rates in a 10 kton detector produced by (n,p) reaction as a function of depth. . . . .	192
9-1	Evolution of LBNE CPV sensitivity in one scenario . . . . .	195





# List of Tables

2-1	Best fit values of the neutrino mixing parameters in the PMNS matrix . . . . .	19
3-1	Principal parameters of LBNE10 as defined at CD-1 . . . . .	46
3-2	The current and future experimental research programs planned for the Fermilab accelerator complex. . . . .	56
3-3	Impact of the beam improvements on the neutrino $\nu_\mu \rightarrow \nu_e$ . . . . .	62
4-1	Raw $\nu$ oscillation event rates at the LBNE far site with $E_\nu < 10$ GeV . . . . .	83
4-2	Cosmic ray induced backgrounds in the surface 10 kton detector . . . . .	103
4-3	Range of detector efficiencies and background rejection based on handscan studies	105
4-4	Expected number of $\nu$ oscillation signal and beam background events at LAr-FD	108
4-5	Summary of achieved systematic error performance in several select prior $\nu_\mu \rightarrow$ $\nu_e$ oscillation experiments . . . . .	112
4-6	Summary of surface 10-kt far detector sensitivities . . . . .	114
4-7	Summary of the oscillation measurements with different configurations given $\theta_{13} = 8.8^\circ, \theta_{23} = 40^\circ, \Delta m_{31}^2 = +2.27 \times 10^{-3} \text{eV}^2$ . . . . .	127
4-8	Expected event rates in 100 kt-yr for the Bartol flux and GENIE Argon cross sections (no oscillations). . . . .	130
4-9	Detector performance assumptions for the atmospheric neutrino and the com- bined atmospheric+beam neutrino analyses. . . . .	131
4-10	Systematic errors included in the atmospheric and beam+atmospheric neutrino analysis . . . . .	135
5-1	Estimated $\nu_\mu$ production rates per ton of detector for $1 \times 10^{20}$ POT at 459 m and a 120 GeV beam . . . . .	144
5-2	Exposures required to reach 3 and $5\sigma$ sensitivity to CP violation for $\geq 50\%$ of $\delta_{cp}$ values . . . . .	148
5-3	Precisions achievable from in situ $\nu_\mu$ and $\nu_e$ flux measurements . . . . .	153
5-4	Uncertainties on the $\mathcal{R}^\nu$ measurement, NuTeV vs LBNE . . . . .	155
5-5	Coefficients entering Equation 5.9 for NC elastic scattering . . . . .	159
5-6	Expected proton range for the low-density ( $\rho \sim 0.1 \text{ g/cm}^3$ ) tracker . . . . .	162
6-1	Efficiencies and background rates for nucleon decay modes of interest for a large underground LArTPC . . . . .	177

7-1	Event rates for different models in 17 kt of LAr for a core-collapse at 10 kpc. Event rates will simply scale by active detector mass. . . . .	184
-----	---	-----

# 1 Introduction and Executive Summary

**The Long-Baseline Neutrino Experiment will provide a unique, compelling and world-leading program for the exploration of key questions at the forefront of particle physics and particle astrophysics. Chief among them are matter/anti-matter asymmetries in the universe and the resolution of the neutrino mass ordering. Resolving the detailed mixing patterns and ordering of neutrino mass states and comparisons to the equivalent phenomenon in the quark sector could reveal fundamental underlying symmetries in physics that are as yet unknown. LBNE will offer unique opportunities to observe proton decay as predicted by Grand Unified Theories and elucidate the dynamics of galactic core-collapse supernovae using studies of neutrino bursts.**

In this document, we describe the wealth of science opportunities and capabilities of LBNE, the Long-Baseline Neutrino Experiment. LBNE has been developed to provide a unique and compelling program for the exploration of key questions at the forefront of particle physics. Chief among the discovery opportunities are observation of CP symmetry violation in neutrino mixing, resolution of the neutrino mass hierarchy as well as interactions with matter, searches for nucleon decay signatures, and detailed studies of neutrino bursts from galactic supernovae. To fulfill these and other goals as a world-class facility, LBNE has been conceived around four central components: (1) a new, intense wide-band neutrino source at Fermilab, (2) a fine-grained ‘near’ neutrino detector just downstream of the source, (3) the Sanford Underground Research Facility (SURF) in Lead, South Dakota at an optimal distance ( $\sim 1300$  km) from the neutrino source, and (4) a massive liquid argon time-projection chamber (LArTPC) deployed there as a ‘far’ detector. LBNE is an extensively-developed world-class experimental program whose relevance, importance, and probability of unearthing critical and exciting physics has only increased with time.

Neutrinos are the most abundant known particles with mass in the universe. Furthermore, neutrino mass is the only established evidence of physics beyond the Standard Model. Thus, understanding the nature of neutrinos is an essential goal for particle physics. The observation of charge-parity (CP) violation in the lepton sector, while groundbreaking on its own, would

provide an experimental underpinning for the basic idea of leptogenesis as an explanation for the baryon asymmetry of the universe. Resolution of the neutrino mass hierarchy along with precise determination of neutrino mixing would have significant theoretical, cosmological and experimental implications. The long baseline of LBNE enables a decisive determination of the mass hierarchy independent of the value of the CP-odd phase  $\delta_{CP}$ . LBNE will also determine with high precision many oscillation parameters (mixing angles and squared-mass differences). Such information will provide insight into the difference between the quark and lepton mixing patterns whose understanding is necessary for deciphering the flavor structure of physics in the Standard Model. Taken together, the above suite of measurements will thoroughly test the three neutrino-flavor paradigm that guides our current understanding, and will provide greatly extended sensitivity to signatures for non-standard neutrino interactions in matter. In the arena of non-accelerator physics, the observation of nucleon decay would be a watershed event for the understanding of physics at high energy scales. Neutrinos from supernovae are expected to provide key insights into the physics of gravitational collapse, and may likewise reveal fundamental properties of the neutrino.

The Liquid Argon Time Projection Chamber (LArTPC) technology is unmatched among massive detectors for precise spatial and energy resolution and for reconstruction of complex neutrino interactions with high efficiency over a broad energy range. It thus provides a compact, scalable approach to achieve sensitivity to the oscillation physics goals of LBNE. Although large underground water Cherenkov and/or scintillator-based detectors with specific strengths within non-accelerator physics may be operating in parallel, the LBNE far detector has unique capabilities here as well. For example, it is especially well-suited for challenging proton decay modes such as the SUSY-favored  $p \rightarrow K^+ \bar{\nu}$  mode, with high detection efficiency and background rejection sufficient to enable a discovery with single well-reconstructed events. Similarly the LArTPC technology opens up an avenue to precision studies of oscillation physics with atmospheric neutrinos. For supernova neutrino detection, liquid argon detectors are primarily sensitive to  $\nu_e$  interactions, which is complementary to water and organic scintillator-based detectors in which  $\bar{\nu}_e$  interactions are dominant. The highly-capable near detector envisioned will not only measure the absolute flux and energy scales of the neutrino species required for the oscillation parameter measurements, but will enable a broad range of precision neutrino interaction measurements. The unique combination of exceptional detector resolution, large target mass and deep underground location also opens the possibility of discovery of entirely unanticipated phenomena – history shows that Nature often rewards leading-edge instruments with unexpected signatures of new physics.

LBNE is a well-considered experiment whose execution has substantial impact on the overall direction of High Energy Physics (HEP) in the US. The US Department of Energy has endorsed the science goals of LBNE, which it envisions as a phased program, and for which it has given first stage (CD-1) approval with a budget of \$867M towards the initial phase. The science scope of this and subsequent phases will depend on the level of investment by additional national and international partners. This document aims to provide an overview of the LBNE physics program and how it may evolve for the US HEP community as it pursues long-term planning studies [?]. We summarize the physics reach of this program

under scenarios that are consistent with short, medium and long-term considerations.

The general conclusions are twofold: (1) a fully realized LBNE will provide an exciting broad-based physics program with exceptional capabilities for all of the primary physics goals, and many secondary ones; and (2) a first phase with a 10-kt\* LArTPC far detector will substantially advance the field of neutrino oscillation physics while, uniquely, laying the foundations for an experiment with the broad and exciting physics program described above in a later phase. In the following sections, we provide the context for development of LBNE as a phased program that maintains flexibility for future enhancements in each of its stages through the contributions of additional partners and summarize the physics reach of LBNE in the corresponding configurations.

---

\*Unless otherwise noted, this document will use fiducial mass for the far detector size.

## 1.1 Development of a World-Class Experiment

To pursue the transformative physics goals of LBNE in an era of highly constrained funding for basic research in the US, the conceptual design has evolved so as to provide a scalable, phased and global approach to achieving the scientific objectives while maintaining a US leadership role. International partnerships are being actively pursued to both globalize and accelerate the project. The key design elements of LBNE are as follows:

- **LBNE is envisioned as a long-baseline neutrino experiment utilizing a multi-megawatt neutrino beamline from the Fermilab Main Injector directed at a massive detector located 1300km away deep in Homestake Mine at the Sanford Underground Research Facility in Lead, South Dakota.**
- **A 50-kt (34-kt fiducial mass) Liquid Argon Time Projection Chamber installed deep underground at SURF is the full-scope vision for the LBNE far detector. The detector design is scalable and flexible allowing for a phased approach.**
- **The experimental hall at the 4,850-foot level is ideal for minimizing cosmic-ray muon backgrounds thus enabling the LBNE far detector to address key scientific questions such as searches for proton decay, and detailed studies of Supernova burst neutrinos.**
- **A fine-grained near neutrino detector located just downstream of the LBNE neutrino beamline at Fermilab will enhance the precision of the long-baseline oscillation studies and perform independent short-baseline measurements. The near detector is designed as a separate facility allowing maximal flexibility in phasing and deployment.**

The concept of a high intensity neutrino beam directed toward a distant massive underground detector to simultaneously investigate the nature of the neutrino, proton decay and neutrinos from astrophysical sources has been under serious investigation since the late 1990's. Since that time both the science goals and concepts for implementation have been the subject of intense study and review by distinguished panels including the National Academies Neutrino Facilities Assessment Committee in 2003 [?], the National Science and Technology Council Committee on Science strategic plan for federal research at the interaction of physics and astronomy in 2004 [?], the National Academies EPP2010 panel in 2006 [?], the HEPAP/NSAC Neutrino Scientific Assessment Group in 2007 [?], the HEPAP Particle Physics Project Prioritization Panel (P5) in 2008 [?], the National Academies ad hoc Committee to Assess the

Science Proposed for DUSEL in 2011 [?], and most recently the HEPAP Facilities Subpanel in 2013 [?]. High-level studies performed in Europe and Asia have come to similar conclusions [?].

**Long-Term Vision** LBNE as described in this document was developed by a collaboration that was established in 2009 and which currently comprises 377 collaborators from 62 institutions in five countries. Fermi National Accelerator Laboratory recognized LBNE as a central part of its long-term future planning and in January 2010 the US Department of Energy (DOE) formally recognized the LBNE science goals with approval of the mission need statement (CD-0) [?], this action established LBNE as a DOE project. It should be noted that it has taken more than a decade to reach this stage.

The central role of LBNE within the US particle physics program is also recognized in other documents prepared for the current community planning exercise [?], including the Project X Physics Book [?], and the reports from Intensity Frontier working groups on neutrino physics [?] and baryon number violation [?].

To pursue the transformative physics goals of LBNE in an era of highly constrained funding for basic research in the US, the conceptual design has evolved so as to provide a flexible and cost-effective approach to the science that maintains a world leadership role over the long term. The full scope LBNE detectors are defined as a 50-kt (34-kt fiducial) LArTPC in a new experimental hall to be excavated at the 4850L of the Homestake Mine at SURF (much larger detectors could be accommodated), and a fine-grained near neutrino detector located on the Fermilab site. Simultaneous construction of a new neutrino beam line at Fermilab would permit initial operations with 60 – 120 GeV protons extracted from the Main Injector at 700 kW of beam power. In anticipation of Project X [?], the beam line is designed to be upgradable to accommodate 2.3 MW. The 1300 km baseline is optimized for the neutrino oscillation program, as described in this and other documents. The shielding of cosmic rays provided by the deep underground far detector site enables the non-accelerator portion of the physics program, including nucleon decay searches, sensitive studies of neutrino bursts from galactic supernovae, and precision analyses of atmospheric neutrino samples.

With the choice of far detector technology and underground location, the overall physics reach of LBNE is predominantly limited by detector mass. From the outset, a guiding principle of the far detector design has been scalability. The conceptual design for the LBNE far detector consists of two identical 25-kt (17-kt fiducial) TPC modules housed within separate vessels (cryostats) exploiting technology developed by the liquefied natural gas (LNG) storage and transport industry. The TPC modules themselves consist of arrays of modular anode and cathode plane assemblies (APA's and CPA's) that are suspended from rails affixed to the top of the cryostats. The APA/CPA dimensions are chosen for ease of transportation and installation. Larger detector masses can be achieved by increasing the vessel size and installing additional APA/CPA units, thereby exploiting economies of scale and benefiting from increased volume to surface area ratio. Detector mass may also be increased after completion of the first phase through additional distinct detectors of the same or different

technology.

**Reconfiguration and CD-1 Approval** Since DOE CD-0 approval, the conceptual design for the fully realized LBNE configuration described above has been reviewed several times, most recently at a Fermilab Director’s CD-1 Readiness Review in March 2012 [?]. Contemporaneous with this review, however, cost considerations led the DOE to request a plan for implementing LBNE as a phased project, with a budget cap on the DOE contribution to the initial configuration cost (now stated as \$867M). An independent panel was established to review reconfiguration options that included consideration of using the existing neutrino beamline along with new massive detectors at the existing Soudan and Ash River sites (see Appendix A). The recommendation of this panel [?] led to a Phase-I configuration that we refer to as ‘LBNE10’. This configuration maintains the most important aspects of the full scope LBNE: the 1300 km baseline to the Sanford Underground Research Facility (SURF) located at the Homestake Mine and the large LArTPC far detector, and a multi-megawatt capable wide-band neutrino/antineutrino beam. However, to fit within the first phase DOE investment budget cap, the far detector fiducial mass was reduced to 10 kt (total mass 18.8 kt) and relocated to a surface site at SURF, and construction of the near neutrino detector was deferred. The conceptual design for this configuration [?] was reviewed in Fall 2012, leading to DOE CD-1 approval [?] in December 2012.

It is important to note that the DOE CD-1 approval document explicitly allows the LBNE Phase-I scope to be adjusted in advance of CD-2 should additional sources of funding be identified. *Using the CD-1 DOE funding as the foundation, the goal for the first phase of LBNE is an underground far detector of at least 10 kt and a highly capable near detector.* This goal has been endorsed by the collaboration, the project, the Fermilab directorate, and the DOE Office of High Energy Physics. Since a large portion of the LBNE10 project cost is in civil infrastructure ( $\sim$  \$500M) incremental funding from partners could have considerable impact on enhancing physics scope in the first phase.

**Global Partnerships** Global conditions are favorable for significant international partnerships with LBNE. As an example, the 2013 update [?] of the European Strategy for Particle Physics discusses long-baseline neutrino physics among the highest-priority large-scale activities for Europe requiring “significant resources, sizeable collaborations and sustained commitment”, with the primary recommendation of exploring “the possibility of major participation in leading long-baseline neutrino projects in the US and Japan.” At present the LBNE Collaboration includes institutions from Brazil, India, Italy, and the United Kingdom. Discussions with a number of potential international partners are under way, some of these already at an advanced stage. A summary of recent progress in these discussions can be found in the presentation of LBNE status to the Fermilab Program Advisory Committee in June 2013 [?].

To reflect the physics reach of various phasing scenarios, we present many of the parameter sensitivities for the accelerator-based neutrino topics as functions of exposure, defined as the product of detector fiducial mass, beam power and run time. However, we also explicitly highlight the capabilities of both the surface 10-kt Phase-I configuration and the 34-kt un-



derground detector, both operating at 700 kW for 10 years. Since the community planning exercise looks beyond the present decade, we also present the long-term physics impact of a fully realized LBNE operating with the beam power anticipated with the full implementation of Project X.

## 1.2 The LBNE Physics Program

**The technologies and configuration of the planned LBNE facilities offer a range of world-leading scientific opportunities:**

- **The broad-band, high power neutrino beam available from Fermilab coupled to the Fermilab-SURF baseline of 1300km presents the optimal sensitivity to neutrino charge-parity violation effects. A measurement of CP violation in the neutrino sector is the most promising avenue for understanding the matter/anti-matter asymmetry of the Universe.**
- **The long baseline of LBNE ensures a large matter induced asymmetry in the oscillations of neutrinos and anti-neutrinos thus providing a clear unambiguous signal of the mass ordering of the neutrino states.**
- **The very large underground Liquid Argon Time-Projection-Chamber technology chosen for the LBNE far detector provides superior sensitivities to proton decay modes with kaons in the final states. These modes are favored by many Grand Unified and Supersymmetric theoretical models.**
- **The neutrinos from a nearby core-collapse supernovae are emitted in a burst of a few tens of seconds duration, with about half in the first second. LAr has a unique sensitivity to the electron-neutrino component of the flux. A detection of a large neutrino signal in LBNE would help elucidate critical information on this key astrophysical phenomenon.**

In this section we summarize the reach of LBNE toward its primary physics goals based on our current understanding of (1) the experimental landscape, (2) scenarios for staging LBNE as described previously, and (3) the technical capabilities of LBNE at each stage. A detailed description of the physics goals of LBNE is provided in the main text of this document and in the LBNE Project controlled documents database [?]. A comprehensive study of the physics potential of the fully realized LBNE (including both LArTPC and water Cherenkov Detector (WCD) options for the far detector) is documented in a October 2011 collaboration report [?]. Key features of the LBNE10 physics program are documented in the introductory volume (Vol. 1) of the October 2012 LBNE Conceptual Design Report (CDR) [?].

### 1.2.1 Long-Baseline Neutrino Oscillation Physics

**Neutrino Mass Hierarchy** A key strength of LBNE is sensitivity to the matter effect due

to the 1300 km baseline, which leads to a large discrete asymmetry in the  $\nu_\mu \rightarrow \nu_e$  versus  $\bar{\nu}_\mu \rightarrow \bar{\nu}_e$  oscillation probabilities, the sign of which depends on the mass hierarchy. At 1300 km this asymmetry is larger than the CP-violating effect associated with  $\delta_{CP}$ , meaning that both the mass hierarchy and  $\delta_{CP}$  can be determined unambiguously within the same experiment, which is not the case for an experiment at much shorter baselines. For the mass hierarchy, recent studies indicate that LBNE on its own can distinguish between normal and inverted hierarchy at  $3\sigma$  significance<sup>†</sup> or better for all values of  $\delta_{CP}$  with less than 10 years of operation of an underground 10-kt far detector at 700 kW beam power coupled with concurrent analysis of the corresponding atmospheric neutrino samples. Exploitation of atmospheric neutrino interactions in a surface detector may also be possible. However, even without this, a 10-kt LArTPC on the surface can reach this level of coverage by incorporating constraints from NOvA and T2K data. For half of the range of possible  $\delta_{CP}$  values (which half depends on the actual hierarchy), the significance is at the level of  $5\sigma$  or better. For context, we note that even at four times its nominal exposure (of six years of operation at 700 kW), an extended NOvA program [?] would have coverage at the  $3\sigma$  level or better for only 40% of the  $\delta_{CP}$  range.

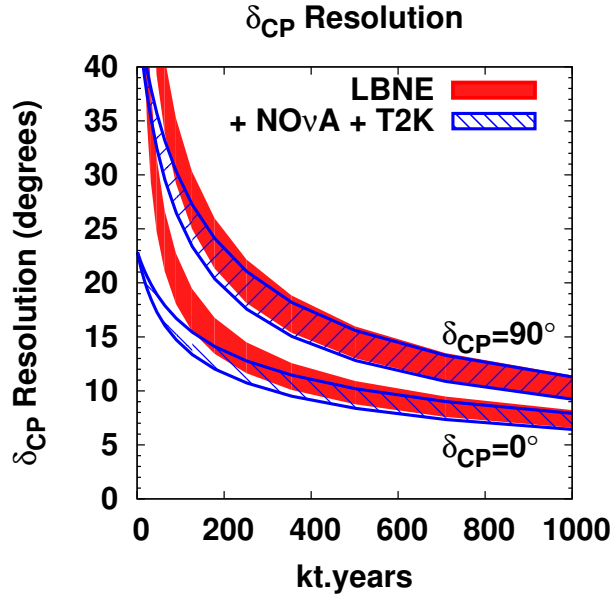
**CP Violation and the Measurement of  $\delta_{CP}$**  The LBNE program has two somewhat distinct goals with regard to CP symmetry violation in the  $\nu_\mu \rightarrow \nu_e$  oscillation channel. First, LBNE aims to make a precise determination of the value of  $\delta_{CP}$  within the context of the standard three-flavor mixing scenario described by the PMNS matrix. Second, and perhaps more significantly, LBNE aims to observe a signal for leptonic CP violation, independent of the underlying nature of neutrino oscillation phenomenology. Within the standard three-flavor mixing scenario such a signal will be observable, provided  $\delta_{CP}$  is not too close to one of the values (0 and  $\pi$ ) for which there is no CP violation. Together, the pursuit of these two goals provides a thorough test of the standard three-flavor picture.

Figure 1-1 shows the expected  $1\text{-}\sigma$  resolution for  $\delta_{cp}$  as a function of exposure for 700 kW proton beam power. We see that 10-kt far detector will be able to measure  $\delta_{CP}$  to  $\pm 20^\circ - 30^\circ$  (depending on its value), independent of other experiments, in a ten-year run on the surface at 700 kW. A fully realized LBNE operating with Project X in a later phase, will achieve a precision of less than  $\pm 10^\circ$ , comparable to the current precision on the CP phase in the CKM matrix of the quark sector.

As a second goal, a 10-kt LArTPC will, by itself, be able to cover between 40% and 50% of  $\delta_{CP}$  values at  $3\sigma$  significance or better in a ten-year run on the surface at 700 kW. To reach  $5\sigma$  for an appreciable fraction of the range of  $\delta_{CP}$ , a fully realized LBNE, including a near neutrino detector, will be needed to control systematic errors while accumulating large enough samples in the far detector to reach this level of sensitivity. Note that no experiment

<sup>†</sup>Unless otherwise specified, we employ the notation “ $3\sigma$ ” and “ $5\sigma$ ” as a shorthand to refer to significances corresponding to mean differences in  $\chi^2$  (or  $-2\ln\mathcal{L}$ ) of 9 and 25, respectively, relative to null or alternate hypotheses, as consistent with past common usage. For the case of the mass hierarchy determination, it has recently been pointed out that the assumption of Gaussian probability density implicit in this notation does not hold. Please see the discussion in Chapter 4.

will provide coverage at 100%, since CP violation effects vanish as  $\delta_{CP} \rightarrow 0$  or  $\pi$ .



**Figure 1-1:** The expected  $1\sigma$  resolution for  $\delta_{cp}$  as a function of exposure for 700 kW proton beam power. The red curve is the precision that could be obtained from LBNE alone, and the blue curve represents the combined precision from LBNE and the T2K and NO $\nu$ A experiments.

**Determination of  $\sin^2 2\theta_{23}$  and Octant Resolution.** In long-baseline experiments with  $\nu_\mu$  beams, the  $\nu_\mu$  disappearance and  $\nu_e$  appearance signals depend on the mixing angle  $\theta_{23}$  dominantly in proportion to  $\sin^2 2\theta_{23}$  and  $\sin^2 \theta_{23}$ , respectively, in the standard three-flavor mixing scenario. Current  $\nu_\mu$  disappearance data are consistent with maximal mixing,  $\theta_{23} = 45^\circ$ . To obtain the best sensitivity to both the magnitude of a deviation of  $\theta_{23}$  from  $45^\circ$  as well as its sign ( $\theta_{23}$  octant), a combined analysis of the two channels is needed [?]. As demonstrated in Chapter 4, LBNE10 will be able to resolve the  $\theta_{23}$  octant at the  $3\sigma$  level or better for true  $\theta_{23}$  values less than  $40^\circ$  or greater than  $50^\circ$ , provided  $\delta_{CP}$  is not too close to zero or  $\pi$ . A fully realized LBNE will attain a measurement of  $\theta_{23}$  of order  $1^\circ$  or less, even for values within a few degrees of  $45^\circ$ .

### 1.2.2 Baryon Physics Motivated by Grand Unified Theories

The LBNE far detector will be competitive for specific nucleon decay modes by virtue of its high detection efficiency and low background rates relative to water Cherenkov detectors. As an example, LBNE has good capability for the  $p \rightarrow K^+ \bar{\nu}$  channel, where predictions from Supersymmetric Models have lifetimes that extend beyond, but close to, the current (preliminary) Super-Kamiokande limit of  $\tau/B > 5.9 \times 10^{33}$  yr (90% CL) from a 260 kt-yr exposure [?]. The signature for an isolated semi-monochromatic charged kaon in an LArTPC

is distinctive, with multiple levels of redundancy. A 34-kt LBNE far detector deep underground will reach a limit of  $3 \times 10^{34}$  yr after 10 years of operation (see Fig. 1–2), and would see 9 events with a background of 0.3 should  $\tau/B$  be just around the corner at  $1 \times 10^{34}$  yr. Even a 10-kt detector (placed underground) would have an intriguing signal of a few events after a 10-year exposure in this scenario.

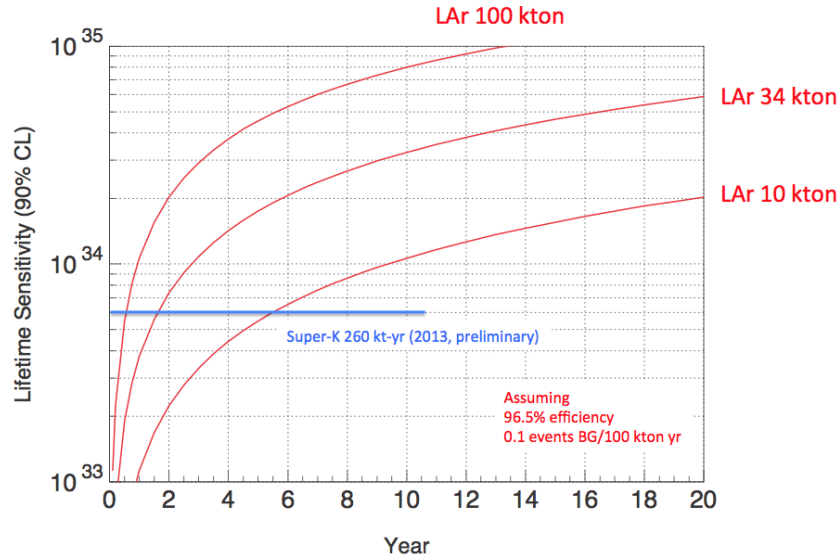


**Figure 1–2:** Sensitivity to the decay  $p \rightarrow K^+ \bar{\nu}$  as a function of time for underground LAr detectors with different masses.

### 1.2.3 Supernova-Neutrino Physics and Astrophysics

The neutrinos from a nearby core-collapse supernova are emitted in a burst of a few tens of seconds duration, with about half in the first second. Energies are in the few tens of MeV range, and the luminosity is divided roughly equally between flavors. Currently, world-wide sensitivity is primarily to electron anti-neutrinos, with detection through the inverse beta decay process on free protons, which dominates the interaction rate in water and liquid-scintillator detectors. LAr has a unique sensitivity to the *electron neutrino* component of the flux, via the absorption interaction on  $^{40}\text{Ar}$ ,  $\nu_e + ^{40}\text{Ar} \rightarrow e^- + ^{40}\text{K}^*$ . In principle, this interaction can be tagged via the coincidence of the emitted electron and accompanying photon cascade from the  $^{40}\text{K}^*$  de-excitation. About 900 events would be expected in a 10-kt fiducial LAr detector for a supernova at 10 kpc. In the neutrino channel the oscillation features are in general more pronounced, since the initial spectra of  $\nu_e$  and  $\nu_\mu$  ( $\nu_\tau$ ) are always significantly different. A detection of a large neutrino signal in LBNE would help elucidate critical information on key astrophysical phenomena such as 1) the neutronization burst, 2) formation of a black hole 3) shock wave effects 4) shock instability oscillations and 5) turbulence effects.

### 1.2.4 Precision Oscillation Measurements and Short-Baseline Neutrino Physics

The near neutrino detector (ND) will provide precision measurements of neutrino interactions which, in the medium to long term, are essential to control the systematic uncertainties in the long-baseline oscillation physics program. The ND, which will include an argon target, will measure the absolute flux and energy-dependent shape of all four neutrino species,  $\nu_\mu$ ,  $\bar{\nu}_\mu$ ,  $\nu_e$  and  $\bar{\nu}_e$  to accurately predict for each species the Far/Near flux ratio as a function of energy. It will also measure the 4-vectors of secondary hadrons, such as  $\pi^0$ ,  $\pi^+$ ,  $\pi^-$ , etc., produced in the neutral and charged current interactions that constitute the dominant backgrounds to the oscillation signals.

The near detector will also be the source of data for a rich program of neutrino interaction physics with 100,000 charged-current and 34,000 neutral current interactions per ton, per year, per  $10^{20}$  pot. This corresponds to  $10^7$  neutrino interactions per year for the range of beam configurations and near detector designs under consideration. Measurement of fluxes, cross sections, and particle production over a large energy range of 0.5–50 GeV (which can also help constrain backgrounds to the atmospheric neutrino and nucleon decay) are the key elements of this program. With very high statistics and precision event reconstruction capability, the near detector data can additionally be exploited for sensitive studies of electroweak physics and nucleon structure.

## 1.3 Summary

**The LBNE physics program has been identified as a priority of the global HEP community in the coming decades. The facilities available in the US are the best suited to carry out this program internationally. The LBNE design is technically advanced and is at the forefront of technical innovations in the field of HEP. Implementation of LBNE in a timely fashion will significantly advance the global HEP program and provide a means for continued intellectual leadership for the U.S. within the global HEP community.**

In this chapter, we have touched only briefly on a portion of the full suite of physics opportunities enabled by LBNE. The following chapters cover these in considerable detail, as well as topics that were omitted here in the interest of brevity and focus. In the final chapter (Chapter 9), we show progress toward LBNE physics milestones considering a particular scenario for the operation of successive stages of detector and Project X implementations. We also elaborate there on the broad role of LBNE in the context of such scenarios. For now, we conclude the present chapter by summarizing its key points.

The primary science goals of LBNE are drivers for the advancement of particle physics – the questions being addressed are of wide-ranging consequence: the origin of flavor and the generation structure of the fermions, the physical mechanism that provides the CP violation needed to generate the baryon asymmetry of the universe, and the high energy physics that would lead to instability of matter or proton decay. Achieving these goals requires a dedicated, ambitious and long term program. No other proposed long-baseline neutrino oscillation program with the scientific scope and reach of LBNE is as advanced in terms of engineering development and project planning. A phased program with a far detector of even modest size in the initial stage (LBNE10) will enable exciting physics in the intermediate term including a definitive mass hierarchy determination and a measurement of the CP phase without ambiguities, while providing the fastest route toward the full LBNE science goals. If the CP phase is not 0 or  $\pi$  there is good prospect for strong indications ( $> 3\sigma$ ) of leptonic CP violation. Global interest is favorable for contributions from international partners to accelerate this program, including enhancements to the LBNE Phase-I scope.

Implementing the vision that has brought LBNE to this point will provide a means for continued intellectual leadership for the U.S. within the global HEP community. Finally, we also note that the excitement generated by the technical challenges of mounting LBNE as well as the potential physics payoffs are widely felt—including among the young scientists for whom LBNE will provide numerous growth opportunities over the next two decades.

## 2 Overview of the LBNE Science Program

### 2.1 Primary and Secondary Science Objectives

The LBNE Science Collaboration, working with LBNE Project Management, has developed a prioritized set of science objectives, which was approved by the LBNE Collaboration Executive Committee and Co-Spokespersons, Project Director, Fermilab Director, and LBNE Federal Project Director. The science objectives for the full implementation of LBNE, presented in Version 1.0 of “Physics Research Goals of the LBNE Project” [?], have not changed as a result of the phased implementation currently planned for the program; rather, achieving them will also be done in a phased manner. The following discussion of the LBNE science objectives is based on that in the LBNE CDR [?], with some added clarification. Note that the objectives that cannot be addressed in the nominal (LBNE10) initial phase are shown in *italic font* below.

**Primary objectives** of LBNE, in priority order, are the following experiments:

1. precision measurements of the parameters that govern  $\nu_\mu \rightarrow \nu_e$  oscillations; this includes precision measurement of the third mixing angle  $\theta_{13}$ , measurement of the CP violating phase  $\delta_{CP}$ , and determination of the mass ordering (the sign of  $\Delta m_{32}^2$ )
2. precision measurements of  $\theta_{23}$  and  $|\Delta m_{32}^2|$  in the  $\nu_\mu$ -disappearance channel
3. *search for proton decay, yielding significant improvement in the current limits on the partial lifetime of the proton ( $\tau/BR$ ) in one or more important candidate decay modes, e.g.  $p \rightarrow e^+\pi^0$  or  $p \rightarrow K^+\nu$*
4. *detection and measurement of the neutrino flux from a core-collapse supernova within our galaxy, should one occur during the lifetime of LBNE*

The phase 1 configuration (LBNE10) is set to maximize the effectiveness of the facility to achieve the the first two objectives, above. The mass hierarchy determination and the



precision determination of  $\theta_{23}$  will most likely be complete in this configuration. The precision determination of CP violation will require later phases of LBNE, although an initial measurement of the CP phase parameter will be performed in phase 1.

*The second two require a deep underground location for the Far Detector, and can only be addressed in the initial phase should additional resources be identified for this purpose.*

**Secondary objectives**, which may also be enabled by the facility designed to achieve the primary objectives include:

1. other accelerator-based neutrino-oscillation measurements. These could include further sensitivity to Beyond Standard Model (BSM) physics such as non-standard interactions
2. *measurements of neutrino-oscillation phenomena using atmospheric neutrinos*
3. *measurement of other astrophysical phenomena using medium-energy neutrinos*

*Secondary objectives 2 and 3 most likely require a deep underground location for the Far Detector.*

*Secondary objectives 2 and 3 most likely require a deep underground location for the Far Detector, and would be best addressed in a subsequent phase of LBNE absent resources to enable this in the initial phase.*

**Additional secondary objectives**, the achievement of which may require upgrades to the facility that is designed to achieve the primary physics objectives (regardless of phase)**FIXME:** added, include:

1. *detection and measurement of the diffuse supernova-neutrino flux*
2. *measurements of neutrino-oscillation phenomena and of solar physics using solar neutrinos*
3. *measurements of astrophysical and geophysical neutrinos of low energy*

*All of the additional secondary objectives require very low backgrounds at low energies, thus a deep-underground Far Detector location. Furthermore, some of them may require deployment of additional detector mass or alternate detector technologies.*

Additionally, a rich set of science objectives enabled by a sophisticated near neutrino detector have been identified. These will be discussed in Chapter 5.

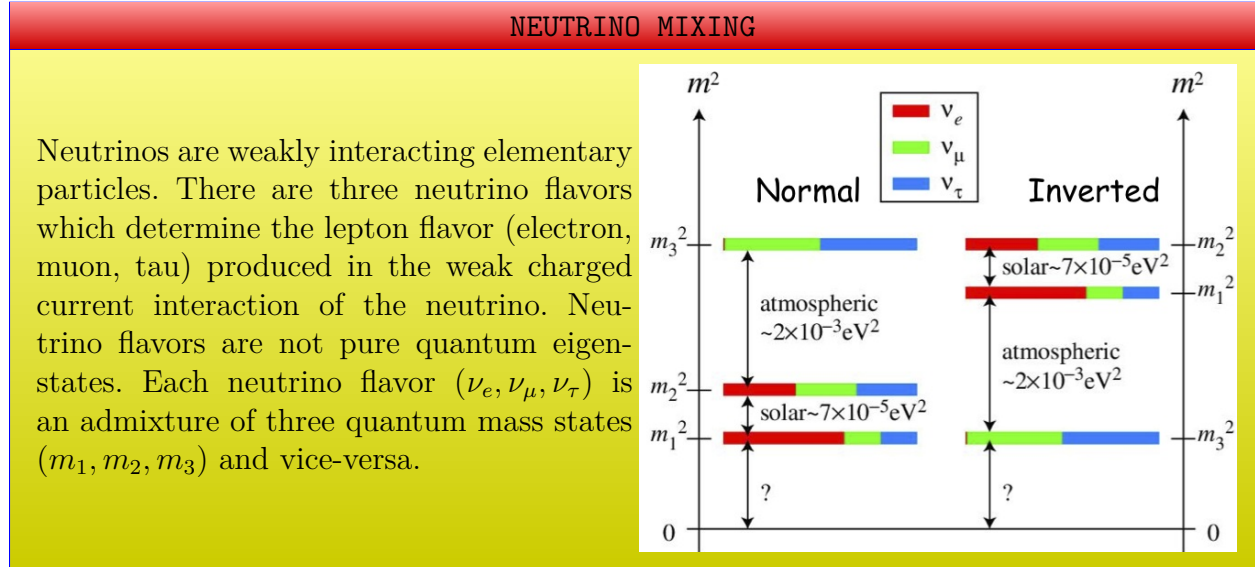
## 2.2 Long-Baseline Neutrino Oscillation Physics

The Standard Model of particle physics presents a remarkably accurate description of the elementary particles and their interactions. However, its limitations beg deeper questions about nature. The unexplained patterns of quarks and leptons, flavors and generations imply that a more fundamental underlying theory must exist. Results from the last decade, indicating that the three known types of neutrinos have non-zero mass, mix with one another and oscillate between generations, imply physics beyond the Standard Model [?] and the possibility of mass scales beyond those in the current model.

### 2.2.1 Three-Flavor Mixing, CP Violation and the Mass Hierarchy

**FIXME:** *Can we make each of the following subsections of the form: “Measurement/observation/blah of phenomenon X” ??*

**FIXME:** *Maybe add a 1-2 sentence intro that does what the long title was supposed to do. Here’s a strawman based on text from long-baseline phys chap: LBNE plans to pursue its primary science objectives using a  $\nu_\mu$  beam and making precision measurements of the parameters that govern the sub-dominant  $\nu_\mu \rightarrow \nu_e$  oscillations.*



### 2.2.1.1 Characterization of Three-Flavor Mixing

Neutrino oscillation arises from mixing between the weak-interaction (flavor) and mass eigenstates of neutrinos. This three-flavor-mixing scenario can be described by a rotation between the weak-interaction eigenstate basis ( $\nu_e, \nu_\mu, \nu_\tau$ ) and the basis of states of definite mass ( $\nu_1, \nu_2, \nu_3$ ). In direct correspondence with mixing in the quark sector, the transformations between basis states is expressed in the form of a complex unitary matrix that in full generality depends on just three mixing angles and a CP-odd phase. For neutrino mixing, this matrix is known as the PMNS matrix, and the mixing angles and phase are designated as ( $\theta_{12}, \theta_{23}, \theta_{13}$ ), and  $\delta_{CP}$ . The frequency of neutrino oscillation, among the weak-interaction eigenstates, also depends on the difference in the squares of the neutrino masses,  $\Delta m_{ij}^2 = m_i^2 - m_j^2$ ; three neutrinos implies two independent mass-squared differences ( $\Delta m_{21}^2$  and  $\Delta m_{32}^2$ ).

The PMNS matrix can be parameterized as the product of three two-flavor mixing matrices as follows:

$$U_{PMNS} = \underbrace{\begin{pmatrix} 1 & 0 & 0 \\ 0 & c_{23} & s_{23} \\ 0 & -s_{23} & c_{23} \end{pmatrix}}_{\text{I}} \underbrace{\begin{pmatrix} c_{13} & 0 & e^{i\delta_{CP}} s_{13} \\ 0 & 1 & 0 \\ -e^{i\delta_{CP}} s_{13} & 0 & c_{13} \end{pmatrix}}_{\text{II}} \underbrace{\begin{pmatrix} c_{12} & s_{12} & 0 \\ -s_{12} & c_{12} & 0 \\ 0 & 0 & 1 \end{pmatrix}}_{\text{III}} \quad (2.1)$$

where  $c_{\alpha\beta} = \cos \theta_{\alpha\beta}$  and  $s_{\alpha\beta} = \sin \theta_{\alpha\beta}$ .

The entire complement of neutrino experiments to date has measured five of the mixing parameters: the three angles  $\theta_{12}$ ,  $\theta_{23}$ , and recently  $\theta_{13}$ , and the two mass differences,  $\Delta m_{21}^2$  and  $\Delta m_{32}^2$ . The sign of  $\Delta m_{21}^2$  is known, but not that of  $\Delta m_{32}^2$ , which (since it is larger in magnitude) is the crux of the mass-hierarchy ambiguity. (The case of  $\Delta m_{32}^2 > 0$  is known as

the ‘normal hierarchy’, while  $\Delta m_{32}^2 < 0$  is referred to as the ‘inverted hierarchy’ case.) The values of  $\theta_{12}$  and  $\theta_{23}$  are large, while  $\theta_{13}$  has been determined to be macroscopic but smaller than the other two [?]. The value of  $\delta_{\text{CP}}$  is unknown.

The moduli **FIXME:** *Is this the modulus of the PMNS mixing matrix itself, or another level of abstraction: one modulus per entry of the PMNS matrix?* **FIXME:** *Can we say ‘determinants’?* of the entries of the PMNS mixing matrix **FIXME:** *how related to the above, or is that implicit in the matrix math?*, which contains information on the strength of flavor-changing weak decays in the lepton sector, can be expressed in approximate form as

$$|U_{\text{PMNS}}| \sim \begin{pmatrix} 0.8 & 0.5 & 0.2 \\ 0.4 & 0.6 & 0.7 \\ 0.4 & 0.6 & 0.7 \end{pmatrix}. \quad (2.2)$$

The three-flavor-mixing scenario for neutrinos is well established, albeit not nearly to the same precision as that in the corresponding quark sector, and with several key parameters, e.g.,  $\delta_{\text{CP}}$ , still undetermined. (In addition, several recent anomalous experimental results count among their possible interpretations phenomena that do not fit this model.) The relationships between the values of the parameters in the neutrino and quark sectors suggests that mixing in the two sectors is qualitatively different. Illustrating this difference, the moduli of the entries of the CKM mixing matrix (analogous to the PMNS matrix for neutrinos, and thus indicative of the strength of flavor-changing weak decays in the quark sector) can be expressed in approximate form as **FIXME:** *Same question about modulus*

$$|V_{\text{CKM}}| \sim \begin{pmatrix} 1 & 0.2 & 0.004 \\ 0.2 & 1 & 0.04 \\ 0.008 & 0.04 & 1 \end{pmatrix}. \quad (2.3)$$

Any organizing principle such as a unification model **FIXME:** *like a GUT? Relate this to the matrices we’ve just seen. This comes out of thin air.* leads to testable predictions such as sum rules between CKM and PMNS parameters [?,?,?]. Quoting the discussion in [?], “while the CKM matrix is almost proportional to the identity matrix plus hierarchically ordered off-diagonal elements, the PMNS matrix is far from diagonal and, with the possible exception of the  $U_{e3}$  element, all elements are  $\mathcal{O}(1)$ .” **FIXME:** *What are the implications? Need that before saying ‘this is crucial’.* These data **FIXME:** *the matrix values? the nu mixing parameters discussed above? which data?* are already proving crucial in the quest for a relationship between quarks and leptons and their seemingly arbitrary generation structure. **FIXME:** *I moved the first sentence in the paragraph to here from somewhere else; not sure if the next sentence follows properly. The paragraph doesn’t say much to me. Anne*

Table 2-1 displays the above comparison in terms of the fundamental parameters and the precision to which they are known\*, highlighting the limited precision of the neutrino-mixing

\*A global fit [?] to existing results from **FIXME:** *all? experiments sensitive to neutrino-oscillation effects* is the source for the PMNS matrix values.

parameter measurements.

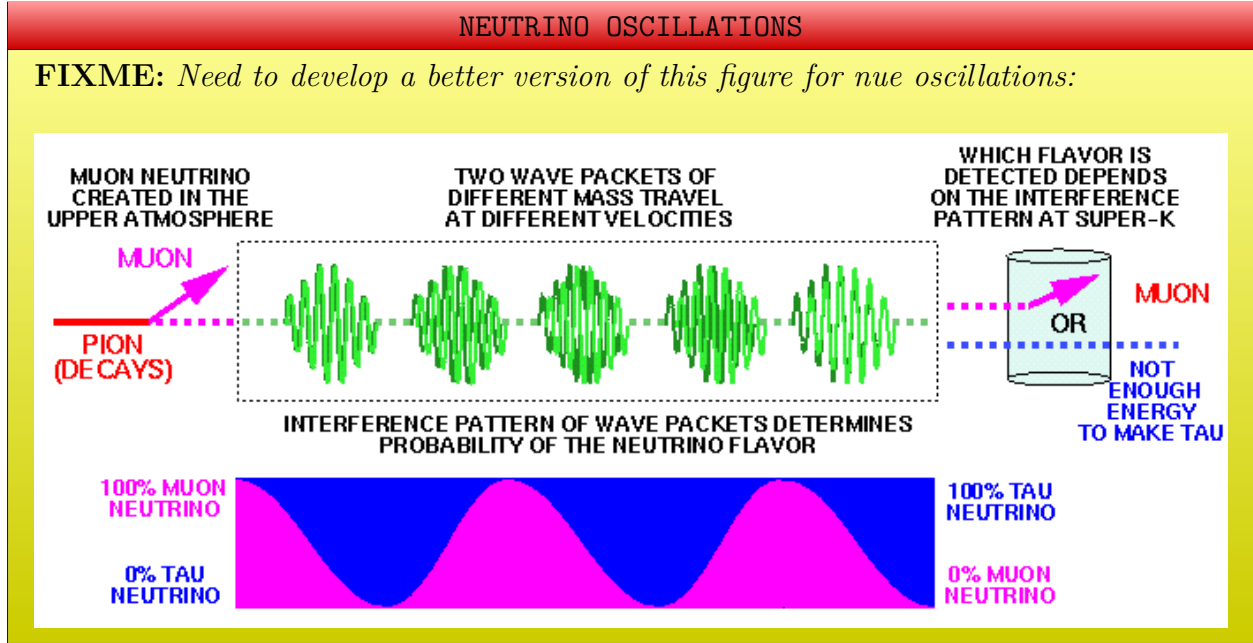
**Table 2-1:** Best fit values of the neutrino mixing parameters in the PMNS matrix (assumes normal hierarchy) and comparison to the **FIXME:** *analogous* equivalent values in the CKM matrix from [?,?].  $\Delta M^2$  is defined as  $m_3^2 - (m_1^2 + m_2^2)/2$ . **FIXME:** *Why for delta M do you not use the mid value +/- .08?*

Parameter	Value (neutrino PMNS matrix)	Value (quark CKM matrix)
$\theta_{12}$	$34 \pm 1^\circ$	$13.04 \pm 0.05^\circ$
$\theta_{23}$	$38 \pm 1^\circ$	$2.38 \pm 0.06^\circ$
$\theta_{13}$	$8.9 \pm 0.5^\circ$	$0.201 \pm 0.011^\circ$
$\Delta m_{21}^2$	$+(7.54 \pm 0.22) \times 10^{-5} \text{ eV}^2$	
$ \Delta M^2 $	$(2.43_{-0.06}^{+0.10}) \times 10^{-3} \text{ eV}^2$	$m_3 \gg m_2$
$\delta_{CP}$	$-170 \pm 54^\circ$	$67 \pm 5^\circ$

The neutrino mixing parameter values and their ‘ $1\sigma$ ’ uncertainties **FIXME:** *Is this the thing Mary said needs changing? If not, should it go in the caption?* shown in Table 2-1 are valuable from the standpoint of providing broad guidance to the particle physics community. However, as an encapsulation of the current knowledge they are somewhat more tenuous; both the values and the uncertainties must be interpreted carefully. The interpretation of the global fit results for  $\Delta m_{21}^2$ ,  $\Delta M^2$ ,  $\theta_{12}$  and  $\theta_{13}$ , on the one hand, is relatively straightforward; the values are dominated by results of direct experimental probing of these parameters (or of effects that are roughly linearly related), and the  $\chi^2$  surfaces for these parameters are correspondingly parabolic. On the other hand, the current input into the determination of the values and uncertainties for  $\theta_{23}$  and  $\delta_{CP}$  is less direct, and given the nature of what is directly measurable (i.e.,  $\sin^2(2\theta_{23})$  in long-baseline/atmospheric  $\nu_\mu$  disappearance measurements),  $\chi^2$  surfaces are strongly non-parabolic beyond  $\pm 1\sigma$ .<sup>†</sup> Furthermore, the combining of data from experiments from which systematic uncertainties are likely not Gaussian-distributed also complicates such global fits.

Clearly much work remains just to complete the standard three-flavor mixing picture, particularly with regard to  $\theta_{23}$  (is it maximal or not, and if not, is it less than or greater than  $45^\circ$ ?), mass hierarchy (normal versus inverted) and  $\delta_{CP}$  (even taking the global fit at face value, it is completely unconstrained at the  $2\sigma$  level). Additionally, there is great value in obtaining a set of measurements for multiple parameters *from a single experiment*, so that correlations and systematic uncertainties can be handled properly. Such an experiment would also be well positioned to extensively test the standard picture of three-flavor mixing. LBNE is designed to be this experiment.

<sup>†</sup>The authors of [?] take care to provide the  $\pm 2\sigma$  and  $\pm 3\sigma$  ranges as well; for  $\theta_{23}$  and  $\delta_{CP}$ , these are considerably less constraining than what might be inferred on the basis of the  $1\sigma$  ranges indicated in the table.



### 2.2.1.2 CP Violation in the Quark and Lepton Sectors

**FIXME:** *new* In the particular parameterization of the PMNS matrix shown in Equation 2.1, the central factor, labeled ‘II’, describes the mixing between the  $\nu_1$  and  $\nu_3$  mass states, and depends on the CP-violating phase  $\delta_{CP}$ . **FIXME:** *And it somehow represents or is indicative of CP violation? Maybe clarify this.* Leptonic CP violation in the three-flavor model thus occurs due to the interference of contributions to an oscillation mode from the terms in this factor – some of which contain  $\delta_{CP}$  (i.e., involve the above  $\nu_1$ - $\nu_3$  mixing directly) and some of which do not. The magnitude of the CP-violating effect depends most directly on the size of a particular function known as the Jarlskog Invariant [?]; it is a function of all three mixing angles and the (as yet unmeasured) CP phase **FIXME:** *How does  $J$  relate to factor II?  $J$  seems like it came out of thin air. :*

$$J_{CP}^{PMNS} \equiv \frac{1}{8} \sin 2\theta_{12} \sin 2\theta_{13} \sin 2\theta_{23} \cos \theta_{13} \sin \delta_{CP} \quad (2.4)$$

Given the current best fit values of the mixing angles [?], and assuming normal hierarchy,

$$J_{CP}^{PMNS} = 0.035 \sin \delta_{CP} \quad (2.5)$$

The relatively large values of the mixing angles in the lepton sector imply that leptonic CP violation effects may be quite large – depending on the value of the unknown phase  $\delta_{CP}$ .

This is in sharp contrast to the very small mixing in the quark sector, which leads to a very small value of the corresponding quark sector Jarlskog invariant [?]. (despite the large value of  $\delta_{CP}^{CKM}$  **FIXME:** *I thought it was small??? Oh, just the angles are small?*) of

$$J_{CP}^{CKM} \approx 3 \pm 1 \times 10^{-5}. \quad (2.6)$$

To date, all observed CP-violating effects have occurred in experiments involving systems of quarks, in particular strange and  $B$ -mesons [?]. Furthermore, in spite of several decades of experimental searches, all of these effects are explained by the CKM paradigm, and all are functions of a unique CP-odd phase parameter. **FIXME:** *What is significance of this statement? If they're functions of the 'large' phase parameter (not the 'small' angles, how does that lead to  $J$  is still too small to explain BAU?* CP-violation in the quark sector has not been able to explain the observed Baryon Asymmetry of the Universe (BAU), however, due to the small value of  $J_{CP}^{CKM}$ . The field now looks towards measurement of CP violation in the lepton sector to provide the explanation.

Leptogenesis, leading to baryogenesis, has therefore emerged as perhaps the most promising candidate for the origin of the observed BAU. Furthermore, the GUT-based *seesaw* mechanism<sup>‡</sup> may provide the simplest and most natural explanation of the observed superlight neutrino mass scales. Leptogenesis and baryogenesis may share a compelling origin within schemes of grand unification. **FIXME:** *meaning they may have a common origin, which within certain GUT schemes, could make a compelling explanation for BAU? Plz clarify* The goal of establishing an experimental basis for assessing this possibility should rank very high on the list of programmatic priorities within particle physics. **FIXME:** *Add: And by way of being able to measure delta CP, LBNE could provide this assessment?*

### 2.2.1.3 Observation of CP-Violating Effects in Long-Baseline Experiments

**FIXME:** *new* If CPT invariance is assumed, **FIXME:** *CPT has not been defined* then the probabilities of neutrino oscillation and antineutrino oscillation are equivalent, i.e.,  $P(\nu_l \rightarrow \nu_l) = P(\bar{\nu}_l \rightarrow \bar{\nu}_l)$ , **FIXME:** *Should this be  $P(\nu_l \rightarrow \nu_{l'})$  and  $P(\bar{\nu}_l \rightarrow \bar{\nu}_{l'})$ ?* where  $l = e, \mu, \tau$ . CPT has been tested by measurements from the MINOS experiment of  $\nu_\mu \rightarrow \nu_\mu$  and  $\bar{\nu}_\mu \rightarrow \bar{\nu}_\mu$  oscillations [?] **FIXME:** *With what results?* Therefore **FIXME:** *I don't see the 'therefore'* CP-violating effects in neutrino oscillations can only be accessed in appearance experiments. Because of the intrinsic challenges of producing and detecting  $\nu_\tau$ 's, the oscillation modes  $\nu_{\mu,e} \rightarrow \nu_{e,\mu}$  provide the most promising experimental signatures of leptonic CP violation.

<sup>‡</sup>**FIXME:** *need short def;* e.g., a model that depends on the neutrino being a Majorana particle and involves ... help! from wikipedia: the seesaw mechanism is a generic model used to understand the relative sizes of observed neutrino masses, of the order of eV, compared to those of quarks and charged leptons, which are millions of times heavier.

**FIXME:** *Add: The LBNE beamline is designed to produce a beam selectively composed of (to what percentage?) either muon neutrinos or muon antineutrinos.*

**FIXME:** *new* For  $\nu_{\mu,e} \rightarrow \nu_{e,\mu}$  oscillations that occur as the neutrinos propagate through matter, as in terrestrial long-baseline experiments, the coherent forward scattering of  $\nu_e$ 's on electrons in matter modifies the energy and path-length dependence of the vacuum oscillation probability in a way that depends on the magnitude *and* sign of  $\Delta m_{32}^2$ . This is the Mikheyev-Smirnov-Wolfenstein (MSW) effect [?,?] that has already been observed in solar neutrino oscillation experiments [?,?,?]. The oscillation probability of  $\nu_{\mu,e} \rightarrow \nu_{e,\mu}$  through matter in a constant density approximation, keeping terms up to second order in  $|\alpha| \equiv |\Delta m_{21}^2|/|\Delta m_{31}^2|$  and  $\sin^2 \theta_{13}$ , is [?,?]

$$P(\nu_{\mu} \rightarrow \nu_e) \cong P(\nu_e \rightarrow \nu_{\mu}) \cong P_0 + \underbrace{P_{\sin \delta}}_{\text{CP violating}} + P_{\cos \delta} + P_3 \quad (2.7)$$

where

$$P_0 = \sin^2 \theta_{23} \frac{\sin^2 2\theta_{13}}{(A-1)^2} \sin^2[(A-1)\Delta], \quad (2.8)$$

$$P_3 = \alpha^2 \cos^2 \theta_{23} \frac{\sin^2 2\theta_{12}}{A^2} \sin^2(A\Delta), \quad (2.9)$$

$$P_{\sin \delta} = \alpha \frac{8J_{cp}}{A(1-A)} \sin \Delta \sin(A\Delta) \sin[(1-A)\Delta], \quad (2.10)$$

$$P_{\cos \delta} = \alpha \frac{8J_{cp} \cot \delta}{A(1-A)} \cos \Delta \sin(A\Delta) \sin[(1-A)\Delta], \quad (2.11)$$

where

$$\alpha = \Delta m_{21}^2 / \Delta m_{31}^2, \quad \Delta = \Delta m_{31}^2 L / 4E, \quad A = \sqrt{3} G_F N_e 2E / \Delta m_{31}^2.$$

**FIXME:** *new* In the above, the effect of the CP-odd phase  $\delta_{CP}$  appears in the expressions for  $P_{\sin \delta}$  (via  $J_{cp}$ ), which switches sign in going from  $\nu_{\mu} \rightarrow \nu_e$  to the  $\bar{\nu}_{\mu} \rightarrow \bar{\nu}_e$  channel, and  $P_{\cos \delta}$ , which does not. Additionally, the matter effect described above introduces a CP asymmetry as well, the origin of which is simply the presence of electrons and absence of positrons in the matter comprising the Earth. The Earth is therefore naturally CP-violating, and this is represented by the factors proportional to  $\Delta m_{31}^2$  (namely  $A$ ,  $\Delta$  and  $\alpha$ ) changing sign in going from the normal to the inverted neutrino mass hierarchy. This provides a means for determining the currently-unknown mass hierarchy.

**FIXME:** *new* Recall that in Equation 2.1, the CP phase appears in the PMNS matrix through the mixing of the 1-3 states. The physical characteristics of the appearance experiment are therefore determined by the baseline and neutrino energy at which the mixing between the 1-3 state is maximal, as follows:

$$\frac{L(\text{km})}{E_{\nu}(\text{GeV})} = (2n-1) \frac{\pi}{2} \frac{1}{1.27 \times \Delta m_{31}^2 (\text{eV}^2)} \quad (2.12)$$



$$\approx (2n - 1) \times 510 \text{ km/GeV} \quad (2.13)$$

where  $n = 1, 2, 3 \dots$  denotes the oscillation nodes at which the appearance probability is maximal. For long-baseline experiments such as LBNE where the neutrino beam propagates through the Earth, the leptonic CP-violation effects must be disentangled from the matter effects, which will be described further in Section 2.2.1.4.

**THE MATTER EFFECT**

L. Wolfenstein, 1978

Elastic forward scattering

→

Pot  
 $V_e$

- $V \sim 10^{-13}$  eV inside the Earth for  $E =$
- Difference of potentials is important
- Refraction index:
 

$n - 1 = V / p$
- $n - 1 \begin{cases} \sim 10^{-20} & \text{inside the} \\ < 10^{-18} & \text{inside the} \\ \sim 10^{-6} & \text{inside the} \end{cases}$
- Neutrino optics

FIXME: From a presentation by Smirnov - need to redo for GeV  $\nu$

#### 2.2.1.4 Probing the Mass Hierarchy via the Matter Effect

The dependence of the matter effect on the mass hierarchy is illustrated in the oscillograms plotted on the left hand side of Figures 2-1 and 2-2, and can be characterized as follows:

**FIXME:** *minor edits to figure captions; added short caption for inclusion in list of figures*

**FIXME:** *Why do right-hand figures have  $E$  sub  $\nu$  on the vertical axis?  $P$  would depend on  $E$  sub  $\nu$ , not the other way around...? Seems reversed.*

- For normal hierarchy,  $P(\nu_\mu \rightarrow \nu_e)$  is enhanced and  $P(\bar{\nu}_\mu \rightarrow \bar{\nu}_e)$  is suppressed. The effect increases with baseline at a fixed  $L/E$ .
- For inverted hierarchy,  $P(\nu_\mu \rightarrow \nu_e)$  is suppressed and  $P(\bar{\nu}_\mu \rightarrow \bar{\nu}_e)$  is enhanced. The effect increases with baseline at a fixed  $L/E$ .
- The matter effect has the largest impact on the probability amplitude at the first oscillation maximum.
- The matter effect introduces a phase shift in the oscillation pattern, shifting it to a

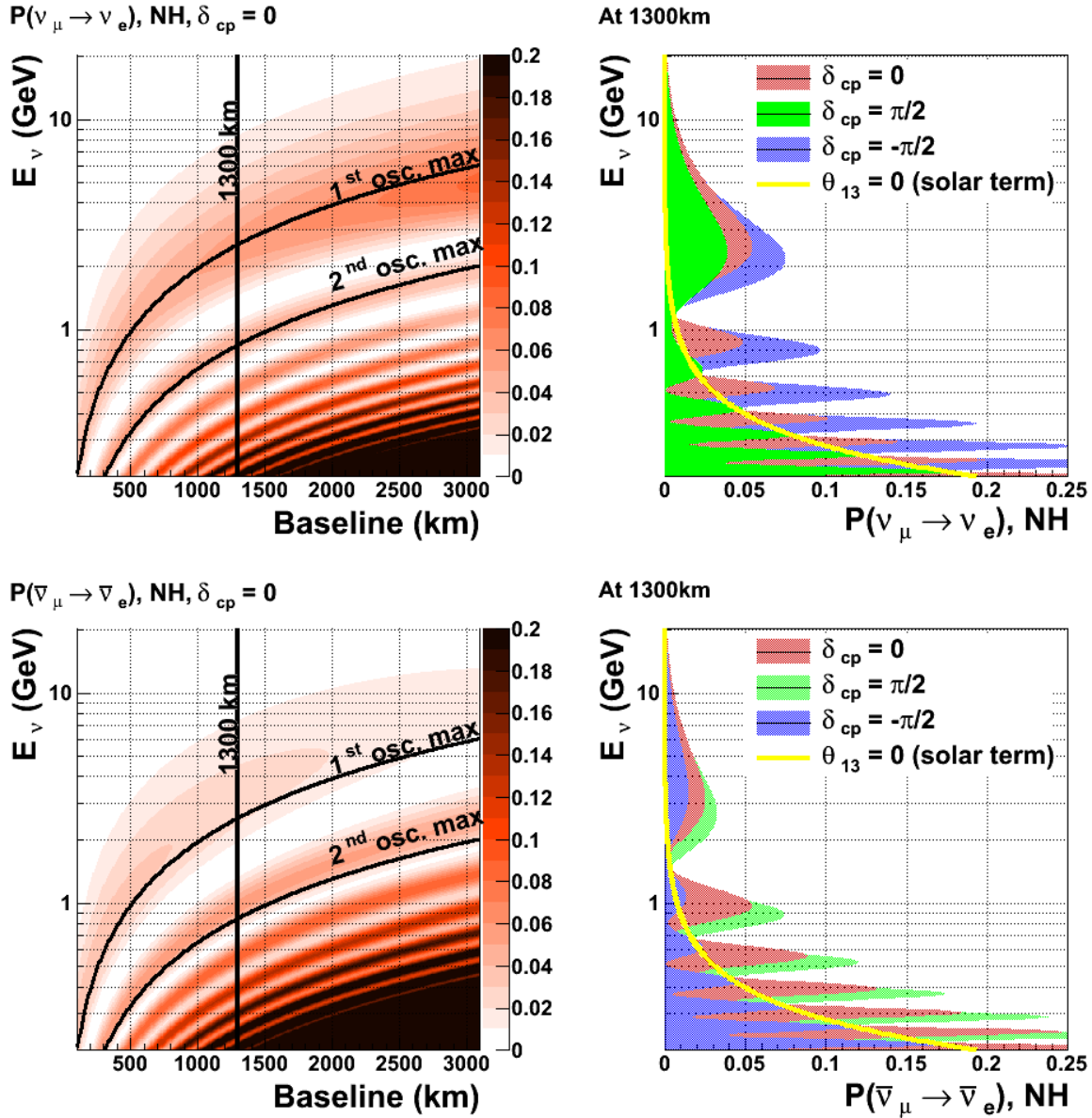


**Figure 2-1:** Neutrino oscillations vs energy, baseline and as a function of different values of  $\delta_{CP}$ . The oscillograms on the left show the  $\nu_\mu \rightarrow \nu_e$  oscillation probabilities as a function of baseline and energy for *neutrinos* (top left) and *antineutrinos* (bottom left) with  $\delta_{CP} = 0$  and a *normal hierarchy*. The figures on the right show the projection of the oscillation probability on the neutrino energy axis at a baseline of 1300 km for  $\delta_{CP} = 0$  (red),  $\delta_{CP} = +\pi/2$  (green), and  $\delta_{CP} = -\pi/2$  (blue) for neutrinos (top right) and antineutrinos (bottom right). The yellow curve is the  $\nu_e$  appearance solely from the “solar term” due to 1-2 mixing as given by Equation 2.9.

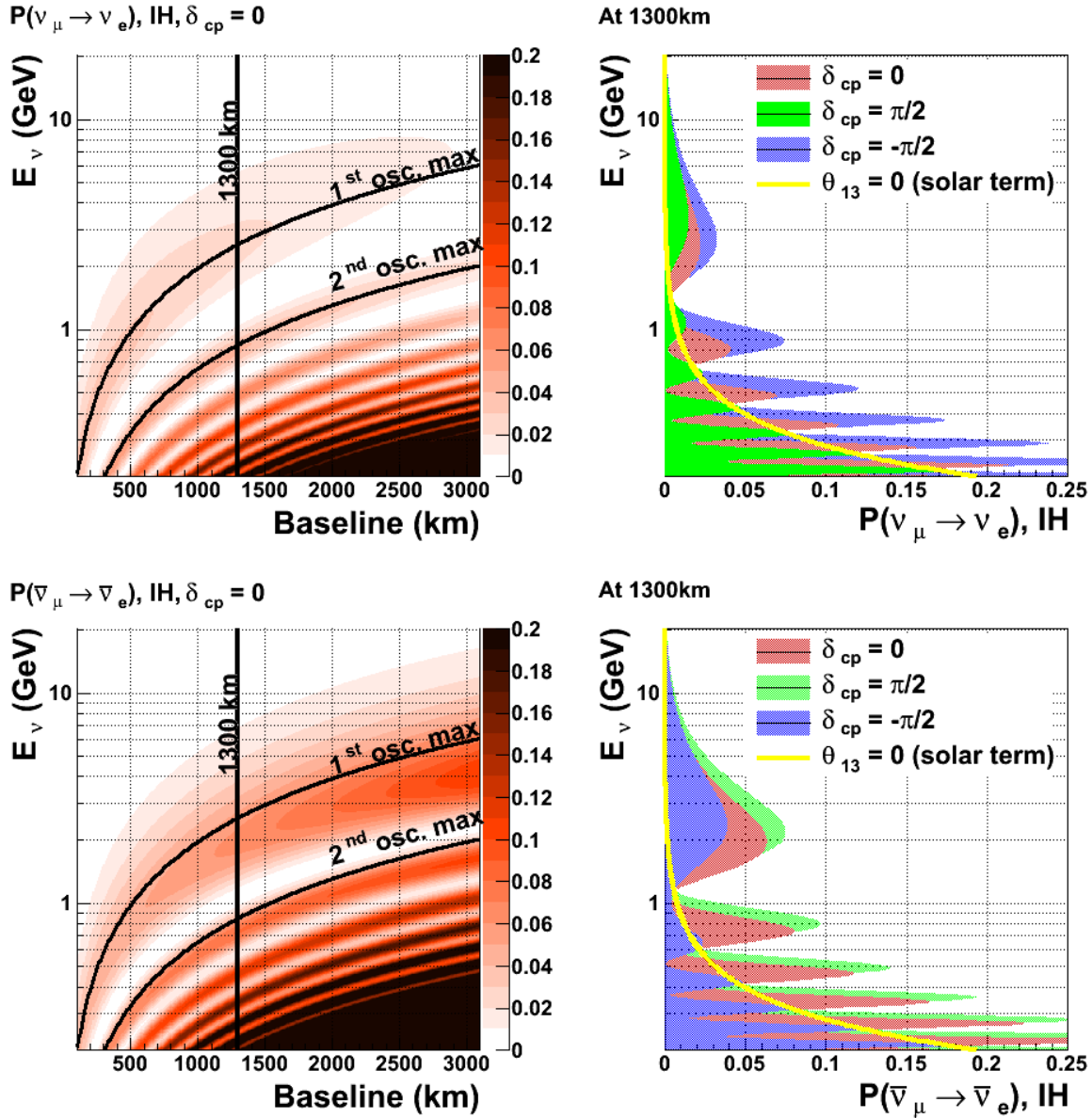


**Figure 2-2:** Neutrino oscillations vs energy, baseline and as a function of different values of  $\delta_{CP}$ . The oscillograms on the left show the  $\nu_\mu \rightarrow \nu_e$  oscillation probabilities as a function of baseline and energy for *neutrinos* (top left) and *antineutrinos* (bottom left) with  $\delta_{CP} = 0$  and an *inverted hierarchy*. The figures on the right show the projection of the oscillation probability on the neutrino energy axis at a baseline of 1300 km for  $\delta_{CP} = 0$  (red),  $\delta_{CP} = +\pi/2$  (green), and  $\delta_{CP} = -\pi/2$  (blue) for neutrinos (top right) and antineutrinos (bottom right). The yellow curve is the  $\nu_e$  appearance solely from the “solar term” due to 1-2 mixing as given by Eqn. 2.9.

lower energy for a given baseline when the hierarchy changes from normal to inverted. The shift is  $\approx -100$  MeV.

**FIXME:** *new* The oscillation probabilities given in Equations 2.7 to 2.11 for  $\nu_\mu \rightarrow \nu_e$  as a function of baseline in km and energy in GeV are shown in the Figure 2-1 and 2-2 oscillograms for  $\delta_{CP} = 0$  for normal and inverted hierarchies, respectively. The oscillograms include the matter effect assuming a constant **FIXME:** *uniform?* density of the Earth's mantle of  $2.8 \text{ g/cm}^3$ . The solid black curves on the oscillograms indicate the location of the first and second oscillation maxima as given by Equation 2.13, assuming oscillations in a vacuum; matter effects will distort the scale at which the mixing between the 1 and 3 states is maximal. **FIXME:** *'scale at which blah is maximal'? Seems like it could distort the scale, thereby changing the maximal value or something... Plz clarify.* The large impact of the matter effect on the appearance probabilities of  $\nu_e$  and  $\bar{\nu}_e$  at longer baselines implies that appearance measurements over long distances through the Earth provide a powerful probe into the neutrino mass hierarchy.

### 2.2.1.5 Disentangling Leptonic CPV and the Matter Effect

**FIXME:** *new* The dependences on  $E_\nu$  of the oscillation probability for a baseline of  $L = 1, 300$  km are plotted on the right in Figures 2-1 and 2-2. The colored curves demonstrate the variation in the  $\nu_e$  appearance probability as a function of the value of  $\delta_{CP}$ . **FIXME:** *Seems like as a function of E sub nu, for 4 different values of delta CP.* The variation in the  $\nu_\mu \rightarrow \nu_e$  oscillation probabilities with the value of  $\delta_{CP}$  indicates that it is experimentally possible to measure the value of  $\delta_{CP}$  at a fixed baseline using only the observed shape of the  $\nu_\mu \rightarrow \nu_e$  or  $\bar{\nu}_\mu \rightarrow \bar{\nu}_e$  appearance signal measured over an energy range that encompasses at least one full oscillation interval. A measurement of the value of  $\delta_{CP} \neq 0$  or  $\pi$ , assuming that neutrino mixing follows the three-flavor model, would imply CP violation. The CP asymmetry,  $\mathcal{A}_{CP}$ , is defined as

$$\mathcal{A}_{CP} = \frac{P(\nu_\mu \rightarrow \nu_e) - P(\bar{\nu}_\mu \rightarrow \bar{\nu}_e)}{P(\nu_\mu \rightarrow \nu_e) + P(\bar{\nu}_\mu \rightarrow \bar{\nu}_e)} \quad (2.14)$$

In the three-flavor model the asymmetry can be approximated to leading order in  $\Delta m_{21}^2$  as [?]:

$$\mathcal{A}_{CP} \sim \frac{\cos \theta_{23} \sin 2\theta_{12} \sin \delta}{\sin \theta_{23} \sin \theta_{13}} \left( \frac{\Delta m_{21}^2 L}{4E_\nu} \right) + \text{matter effects} \quad (2.15)$$

Regardless of the value obtained for  $\delta_{CP}$ , it is clear that the explicit observation of an asymmetry between  $P(\nu_l \rightarrow \nu_{l'})$  and  $P(\bar{\nu}_l \rightarrow \bar{\nu}_{l'})$  is required in order to claim evidence for CP violation in the neutrino sector.

**FIXME:** *new* In Figure 2-3, the asymmetries induced by matter and maximal CP violation (at  $\delta_{CP} = \pm\pi/2$ ) are shown separately as 2-D oscillograms in baseline and neutrino energy. The matter effect induces an asymmetry in  $P(\nu_l \rightarrow \nu_{l'})$  and  $P(\bar{\nu}_l \rightarrow \bar{\nu}_{l'})$  that adds to the CP asymmetry. At longer baselines ( $> 1000$  km), the matter asymmetry in the energy region of the first oscillation node is driven primarily by the change in the  $\nu_e$  appearance amplitude. At shorter baselines ( $\mathcal{O}(100$  km)) the asymmetry is driven by the phase shift. In general:

$$\mathcal{A}_{cp} \propto L/E, \quad (2.16)$$

$$\mathcal{A}_{matter} \propto L \times E. \quad (2.17)$$

**FIXME:** *new* The phenomenology of  $\nu_\mu \rightarrow \nu_e$  oscillations described above implies that the experimental sensitivity to CP violation and the mass hierarchy from measurements of the total asymmetry between  $P(\nu_l \rightarrow \nu_{l'})$  and  $P(\bar{\nu}_l \rightarrow \bar{\nu}_{l'})$  requires the disambiguation of the asymmetries induced by the matter effect and those induced by CP violation. **FIXME:** *Plural asymmetries for each cause? Not ‘the (single) asymmm from matter and the asymmm from CPV’?* This is particularly true for experiments designed to access the 1-3 mixing scale using neutrino beams of  $\mathcal{O}(1$  GeV). Such beams require baselines of  $\mathcal{O}(100$  km), at which the matter asymmetries are significant. The currently known values of the oscillation parameters permit calculation of the magnitude of the matter asymmetry **FIXME:** *plural in prev sentence* within an uncertainty of  $< 10\%$ ; only the sign of the asymmetry – which depends on the sign of  $\Delta m_{31}^2$  – is unknown. **FIXME:** *End with a sentence about how LBNE will disambiguate these asymmetries.*

**FIXME:** *new* An example shown in Figure 2-4 illustrates the ambiguities that can arise from the interference of the matter and CP asymmetries. The plots show the total asymmetry as a function of  $\delta_{CP}$  at four baseline values (clockwise from top left): 290 km, 810 km, 2300 km and 1300 km. The curves in black and red are the asymmetries at the first and second oscillation nodes, respectively. The solid lines represent normal hierarchy and the dashed lines inverted. The plots demonstrate that measurements of the asymmetry (as calculated in Equation 2.14) **FIXME:** *whoa, measurements or calculations?* at the first oscillation node yield ambiguous results for short baselines if the hierarchy is unknown. **FIXME:** *Not obvious to me, but if it is to intended audience, ok* This occurs in regions of the  $(L, E, \delta_{CP})$  phase space where the matter and CP asymmetries cancel partially or totally. For example, the green lines in Figure 2-4 indicate the asymmetry at the first node for maximal CP violation ( $\delta_{CP} = \pi/2$ ) with an inverted hierarchy. At a baseline of 290 km the measured asymmetry ( $\delta_{CP} = \pi/2$ , inverted hierarchy) is degenerate ( $\delta_{CP} \sim 0$ , normal hierarchy) at the first node. Measurements of the asymmetry at different  $L/E$  or at different baselines can break the degeneracies (Equation 2.17). At very long baselines where the matter asymmetry exceeds the maximal CP asymmetry, there are no degeneracies and the mass hierarchy and CP asymmetries can be resolved within the same experiment. For the current best fit values of

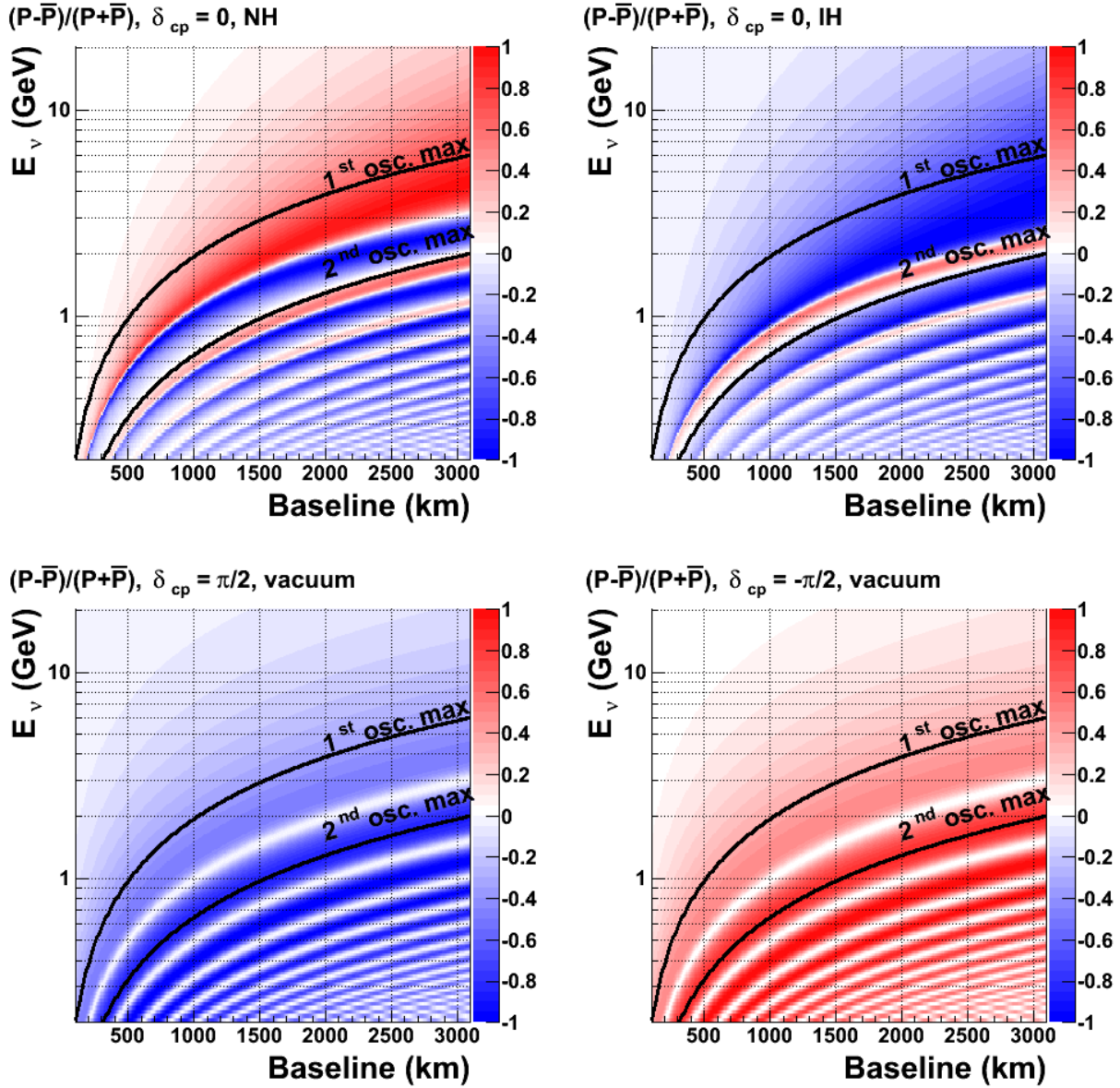


**Figure 2-3:** The CP asymmetry as a function of baseline. The top two figures are for the asymmetry induced by the matter effect only for normal (top left) and inverted (top right) hierarchies. The bottom figures are for the asymmetry induced through the CP violating phase  $\delta_{CP}$  in vacuum, for  $\delta_{CP} = +\pi/2$  (bottom left) and  $\delta_{CP} = -\pi/2$  (bottom right)



the oscillation parameters the degeneracies in measurements at the first oscillation maximum are optimally resolved at a baseline of  $\sim 1200$  km. **FIXME:** *I don't see all this in the plots; just FYI*

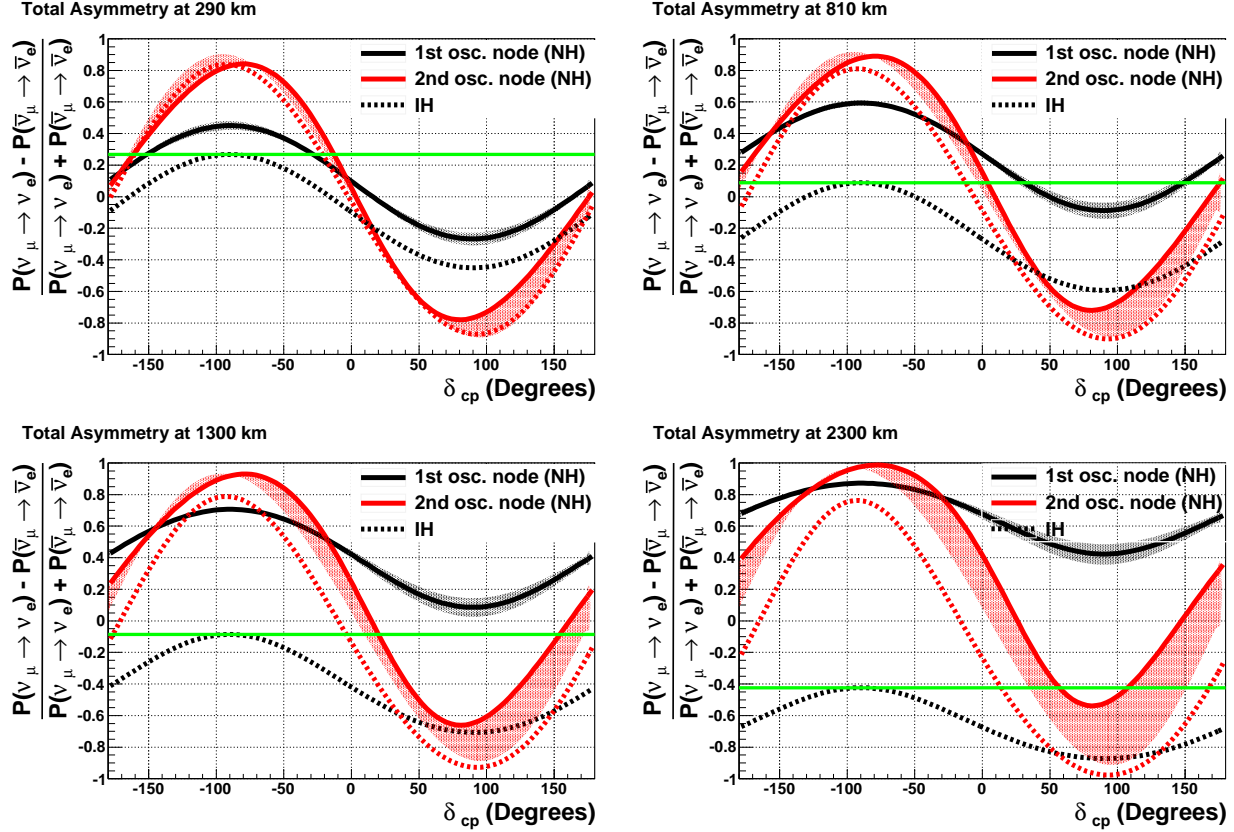


**Figure 2-4:**  $\nu/\bar{\nu}$  oscillation asymmetries vs  $\delta_{CP}$  at the first two oscillation nodes. Clockwise from top left: 290 km, 810 km, 2300 km and 1300 km.

### 2.2.1.6 Optimization of Baseline

**FIXME:** *All the other subsubsections here are physics studies; this is the oddball. Suggestion: summarize it in intro to 2.2 'Long-Baseline...' and move longer discussion to chapter about long baseline phys.*

**FIXME:** *new* To understand the performance of a long-baseline experiment as a function of baseline using more realistic experimental conditions **FIXME:** *'more' realistic compared to what?*, a study of the sensitivities to CP violation and the mass hierarchy as a function of baseline was carried out using different realistic **FIXME:** *word needed again?* beamline designs for each baseline **FIXME:** *one design per baseline, or several designs for each baseline?* and a 35-kt LArTPC. A large LArTPC was chosen for the far detector since it has a high  $\nu_e$  identification efficiency that is flat over a large range of energies (see Chapter 4). **FIXME:**



*No mention that this matches conceptual design of full scope from march 2012; seems funny* The beamline design was based on the NuMI beamline utilizing the 120 GeV, 700 kW beam from the Fermilab Main Injector and was fully simulated using GEANT3. **FIXME:** *Need geant3 ref?* Varying the distance between the target and the first horn allowed selection of a beam spectrum that covers the first oscillation node and part of the second. The design incorporated an evacuated decay pipe of 4 m diameter and a length that varied from 280 to 580 m. For baselines less than 1000 km, an off-axis beam was simulated, **FIXME:** *why? and this is in contrast to 'on-axis' for longer baselines?* with the off-axis angle chosen to provide the most coverage of the first oscillation nodes. **FIXME:** *plural because one node per baseline?* The results of this study are summarized in Figure 2-5. The sensitivity to CP violation (bottom plot) assumes that the mass hierarchy is unknown.

**FIXME:** *new* The baseline study indicates that with realistic experimental conditions, baselines between 1000-1300 km are near optimal for determination of CP violation. With baselines  $> 1500$  km the mass hierarchy could be determined with a minimum of  $5\sigma$  for all values of  $\delta_{cp}$  with a large LArTPC far detector, however, in one of the neutrino polarities, **FIXME:** *Can you say which polarity?* the the event rate suppression due to the beam's traversal through matter becomes very large, making it difficult to determine the CP violation asymmetry.

### 2.2.2 Disappearance of $\nu_\mu$ and Determination of $\theta_{23}$

**FIXME:** *new - 2 paragraphs* The study of  $\nu_\mu$  disappearance probes  $\theta_{23}$  and  $|\Delta m_{32}^2|$  with very high precision. Combining the disappearance of  $\nu_\mu$  with the  $\nu_e$  appearance signal can help determine the  $\theta_{23}$  octant. **FIXME:** *How does determining the 'octant' relate to the parameters we've been discussing?* Non-standard physics can manifest itself in differences observed in higher-precision measurements of  $\nu_\mu$  and  $\bar{\nu}_\mu$  disappearance over long baselines. In addition, experiments at long enough baselines and sufficient neutrino flux  $> 3$  GeV, coupled with high-resolution tracking detectors, as for the LBNE design, can also probe  $\nu_\mu \rightarrow \nu_\tau$  appearance with higher precision than is currently possible using  $\nu_\tau$  charged-current interactions. With long enough exposures, the combination of  $\nu_\mu \rightarrow \nu_\mu$ ,  $\nu_\mu \rightarrow \nu_e$ , and  $\nu_\mu \rightarrow \nu_\tau$  can overconstrain the three-flavor model of neutrino oscillations both in neutrino and antineutrino modes. **FIXME:** *"Overconstrain" sounds like a bad thing...?*

**FIXME:** *The above paragraph doesn't hang together very well, maybe better as a bullet list?*

The precision with which the current set of neutrino-oscillation parameters are known ensures that the compelling physics program outlined for LBNE is feasible with the proposed combination of baseline, detector mass and beam. **FIXME:** *relate this to nu sub mu disapp or move it*

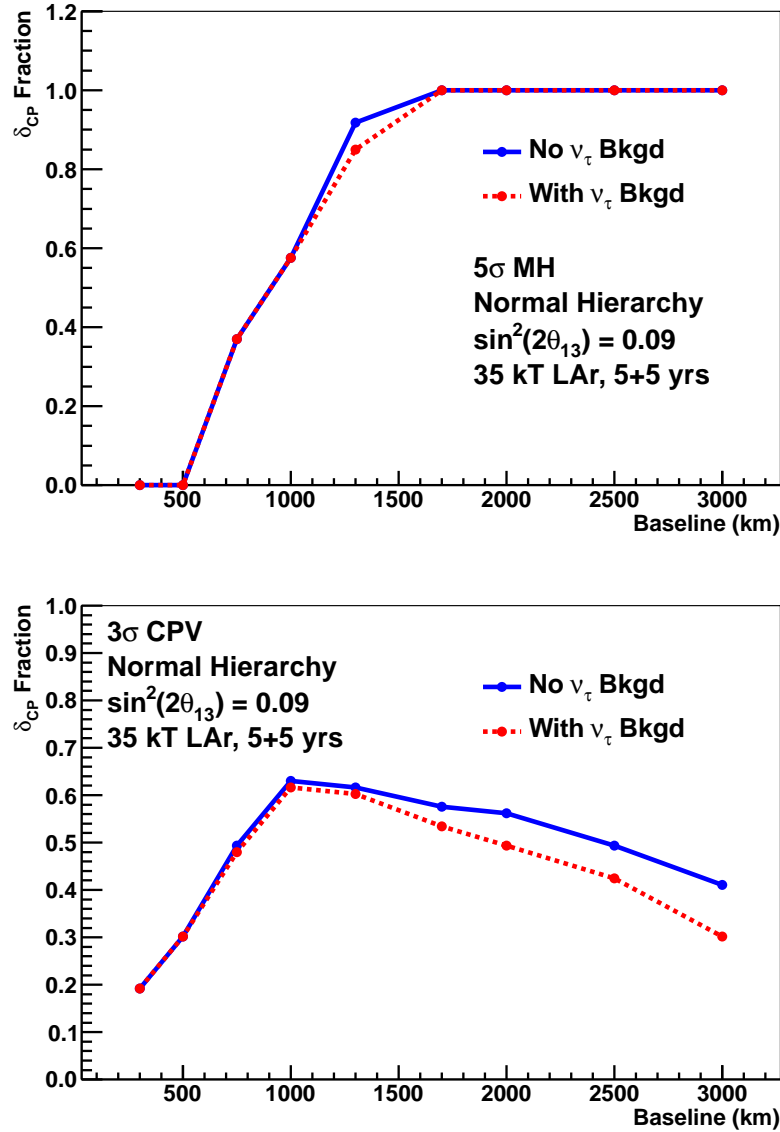


**Figure 2-5:** The fraction of  $\delta_{cp}$  values for which the mass hierarchy can be determined at the  $5\sigma$  level or greater as a function of baseline (top) and the fraction of  $\delta_{cp}$  values which CP violation can be determined at the  $3\sigma$  level or greater as a function of baseline (bottom). A NuMI-based beam design with a 120 GeV, 708 kW beam was optimized for each baseline. Projections assume  $\sin^2 2\theta_{13} = 0.09$  and a 35-kt LArTPC as the Far Detector [?]. An exposure of 5yrs+5yrs neutrino+antineutrino running is assumed at each baseline.

### 2.2.3 Oscillation Physics with Atmospheric Neutrinos

**FIXME:** *new* Atmospheric neutrinos are unique among sources used to study oscillations: the flux contains neutrinos and antineutrinos of all flavors, matter effects play a significant role, both  $\Delta m^2$  values contribute **FIXME:** *to what?*, and the oscillation phenomenology occurs over several decades in both energy (see Figure 2-6) and path length. The probabilities of atmospheric  $\nu_\mu \rightarrow \nu_e$  and  $\bar{\nu}_\mu \rightarrow \bar{\nu}_e$  oscillations for normal and inverted hierarchies as a function of zenith angle are shown in Figure 2-7.

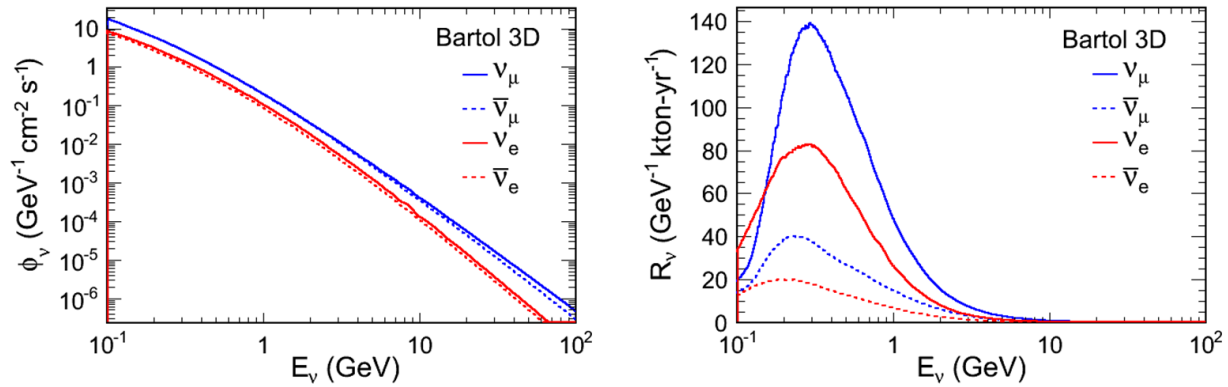


**Figure 2-6:** The atmospheric neutrino flux in neutrinos per second per steradian as a function of neutrino energy for different flavors (left). The atmospheric neutrino spectrum per GeV per kt per year for the different species (right).

**FIXME:** *new* These characteristics make atmospheric neutrinos ideal for the study of oscillations (in principle sensitive to all of the remaining unmeasured quantities in the PMNS matrix) **FIXME:** *‘sensitive’ is funny - are they ‘sensitive’ to these quantities or do their characteristics make them good probes?* and provide a laboratory suitable to search for exotic phenomena for which the dependence of the flavor-transition and survival **FIXME:** *survival? not ‘appearance’ or some such?* probabilities on energy and path length can be defined.

**FIXME:** *new, 2 pgraphs* Even with dedicated long-baseline experiments exploring the large mass splitting **FIXME:** *new term, not defined* for nearly a decade, atmospheric data continues to contribute substantially to our understanding of the neutrino sector **FIXME:** *lepton or neutrino sector? Or neutrino physics?* in three areas, broadly speaking:

- The data demonstrate *complementarity* with beam results via two- and three-flavor fits and the measurement of a tau appearance signal consistent with expectations
- The data serve to increase measurement *precision* through global fits, given that the sensitivity of atmospheric neutrinos to the mass hierarchy **FIXME:** *again I question ‘sensitivity’* is largely independent of the CP phase and the octant of  $\theta_{23}$ .

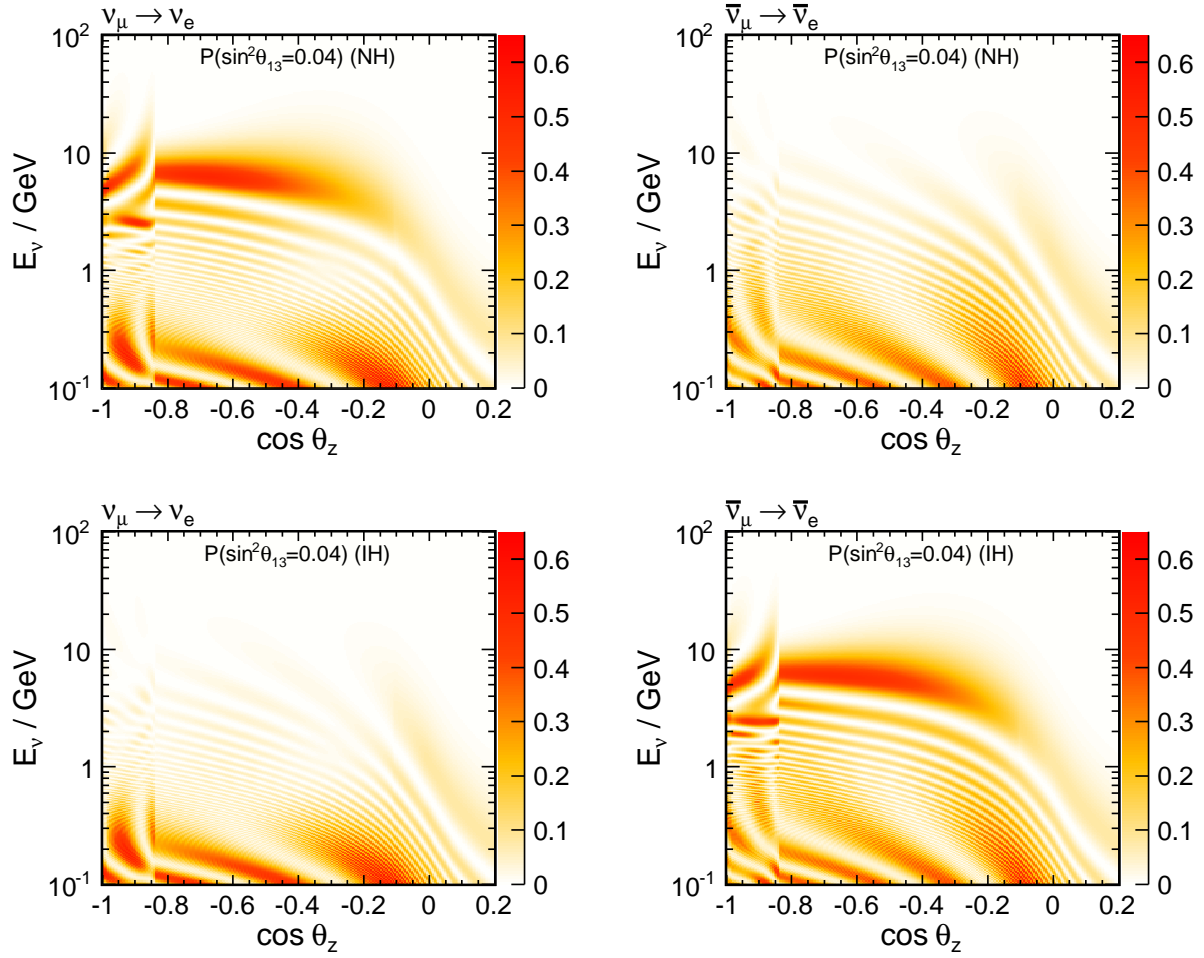


**Figure 2-7:** The probabilities of atmospheric  $\nu_\mu \rightarrow \nu_e$  (left) and  $\bar{\nu}_\mu \rightarrow \bar{\nu}_e$  (right) oscillations for normal (top) and inverted (bottom) hierarchies as a function of zenith angle.

- *New physics* searches with atmospheric neutrinos have placed limits on CPT violation, non-standard interactions, mass-varying neutrinos and Lorentz invariance violation.

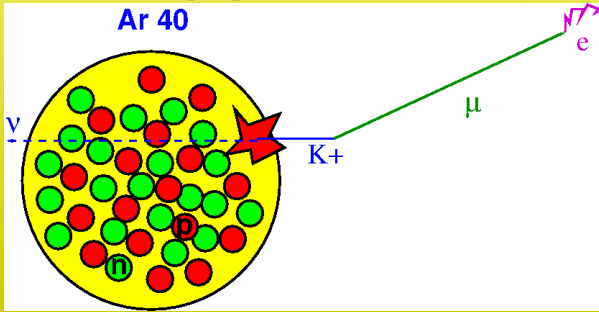
Atmospheric neutrinos can continue to play these roles in the LBNE era if the detector is located deep underground. In particular, complementarity will be vital in a future where, worldwide, the number of high-precision, long-baseline beam/detector facilities is small. The physics potential of a large underground liquid argon detector for measuring atmospheric neutrinos is discussed in Section 4.7.

## 2.3 Baryon Physics Motivated by Grand Unified Theories

**FIXME:** *Made title same as in exec summ; easier to follow*

**PROTON DECAY**

**FIXME:** *text taken verbatim from Wikipedia:* In the Standard Model, protons, are theoretically stable because baryon number (quark number) is conserved. Therefore, protons will not decay into other particles on their own, because they are the lightest (and therefore least energetic) baryon. Some beyond-the-Standard Model grand unified theories (GUTs) explicitly break the baryon number symmetry, allowing protons to decay via the Higgs particle, magnetic monopoles or new X bosons. Proton decay is one of the few observable effects of the various proposed GUTs. To date, all attempts to observe these events have failed.



**FIXME:** *new* Proton decay, bound neutron decay and similar processes such as di-nucleon decay and neutron-antineutron oscillation test **FIXME:** *processes don't test it, they may demonstrate it or provide a means of probing it...?* the apparent but unexplained conservation law of baryon number. These decays are already known to be rare based on decades of prior searches, all of which have produced negative results. If measurable event rates or even single-candidate events were to be found, it would be sensible to presume that they occurred via unknown virtual processes based on physics beyond the Standard Model. The impact of demonstrating the existence of a baryon-number-violating process would be profound.

### 2.3.1 Motivation from GUTs

**FIXME:** *new pgraph + list* The class of theories known as Grand Unified Theories (GUTs) make predictions about both baryon number violation and the proton lifetime that may be within reach of the full-scope LBNE experiment. The grand unified theoretical motivation for the study of proton decay has a long and distinguished history [?, ?, ?], and has been reviewed many times [?, ?, ?]. Early GUTs provided the original motivation for putting kiloton-scale detectors underground. **FIXME:** *need connection - underground to limit background?* The 22.5 kiloton Super-Kamiokande (SK) experiment extended the search for proton decay by more than an order of magnitude. Contemporary reviews [?, ?, ?] discuss the strict limits already set by SK and the context of proposed multi-100-kiloton scale experiments such as Hyper-Kamiokande and LBNE. **FIXME:** *LBNE is not this scale (unless you say WCE), since WCD days*

Although no evidence of proton decay has been detected, the strict limits from these experiments constrain the construction of contemporary GUTs and indeed, a tension between experiment and theory is now commonly discussed. **FIXME:** *Gist of last part of prev sentence is not clear; is it a competitive thing, the idea that thry and expt will never converge?* The current limits point naturally towards continuing the search with 100-kiloton-scale detectors. A range of scientific questions motivates these studies:

- Conservation of baryon number is unexplained, corresponding to no known long-range force. **FIXME:** *not sure what connection is: just that no known forces explain this conservation? Clarify*
- Baryon number non-conservation has cosmological consequences, such as a role in the inflation and the baryon asymmetry of the universe.
- Proton decay is predicted by a wide range of GUTs.
- Some GUTs can accommodate massive neutrinos with characteristics as discovered over the last decade. **FIXME:** *vague - need at least a ‘for instance’ and/or a reference!*
- GUTs incorporate other unexplained features of the Standard Model such as the relationship between quark and lepton electric charges.
- The unification scale is suggested experimentally and theoretically by the apparent convergence of the running coupling constants of the Standard Model. It is **FIXME:** *singular or plural* in excess of  $10^{15}$  GeV.
- The unification scale is not accessible by any accelerator experiment, and can only be probed by virtual processes such as proton decay.
- GUTs usually predict the relative branching fractions of different nucleon decay modes, requiring of course a sizeable sample of proton decay events to test.
- The dominant proton decay mode of a GUT is often sufficient to roughly identify the likely characteristics of the GUT, such as gauge mediation or the involvement of supersymmetry.

**FIXME:** *new* The observation of even a single unambiguous proton decay event would strongly corroborate the idea of unification and would give strong guidance as to which theories are correct. One or two events would also provide guidance as to the size of detector needed to explore the physics in more detail.

### 2.3.2 Proton Decay Modes

**FIXME:** *still part of the last 'new'* From the body of literature, two decay modes emerge that dominate the LBNE experimental design. The more well-known of the two, the decay mode of  $p \rightarrow e^+\pi^0$ , arises from gauge mediation. It is often predicted to have the higher branching fraction, and is also demonstrably the more straightforward experimental signature for a water Cherenkov detector. In this mode, the total mass of the proton is converted into the electromagnetic shower energy of the positron and the two photons from  $\pi^0$  decay, with a net momentum vector near zero.

**FIXME:** *new* The second key mode is  $p \rightarrow K^+\nu$ . This mode is dominant in most supersymmetric-GUTs, which also often favor several other modes involving kaons in the final state. This decay mode with a charged kaon is uniquely interesting; since the momentum of the kaon will result in high ionization density (which can be compared to the range of the kaon) a liquid argon TPC could detect it with extremely high efficiency. In addition, the unique final states of  $K^+$  decay would be fully reconstructed. **FIXME:** *reconstructable?*

**FIXME:** *new - 2 pg* Of the 27 allowed modes of proton or bound neutron into anti-lepton plus meson (conserving  $B-L$ ), none will influence the design of a next-generation experiment. The most stringent limits besides  $p \rightarrow e^+\pi^0$  include  $p \rightarrow \mu^+\pi^0$  and  $p \rightarrow e^+\eta$ , both of which must have partial lifetimes greater than  $4 \times 10^{33}$  years. Any experiment that will do well for  $e^+\pi^0$  will also do well for these decay modes. The decay  $p \rightarrow \nu\pi^+$  or  $n \rightarrow \nu\pi^0$  may have large theoretically predicted branching fractions, but they are experimentally difficult due to the sizeable backgrounds from atmospheric neutrino interactions. The decay  $p \rightarrow \mu^+K^0$  is detected relatively efficiently by either water Cherenkov or LArTPC detectors.

A number of other possible modes exist, such as those that conserve  $B+L$  **FIXME:** *as opposed to B-L like above?*, that violate only baryon number, or that decay into only leptons. These possibilities are less well-motivated theoretically, as they do not appear in a wide range of theories, and are therefore not considered here.

**FIXME:** *new* Figure 2-8 shows a comparison of experimental limits, dominated by recent results from Super-Kamiokande, to the ranges of lifetimes predicted by an assortment of GUTs. At this time, the theory literature does not attempt to precisely predict lifetimes, concentrating instead on suggesting the dominant decay modes and relative branching fractions. The uncertainty in the lifetime predictions come from details of the theory, such as masses and coupling constants of unknown heavy particles, as well as poorly known details of matrix elements for quarks within the nucleon.

**FIXME:** *new, 2 pgrphs* It is apparent from Figure 2-8 that a continued search for proton decay is by no means assured of obtaining a positive result. With that caveat, an experiment with sensitivity between  $10^{33}$  and  $10^{35}$  years is searching in the right territory over a wide range of GUTs and even if no proton decay is detected, the stringent lifetime limits will



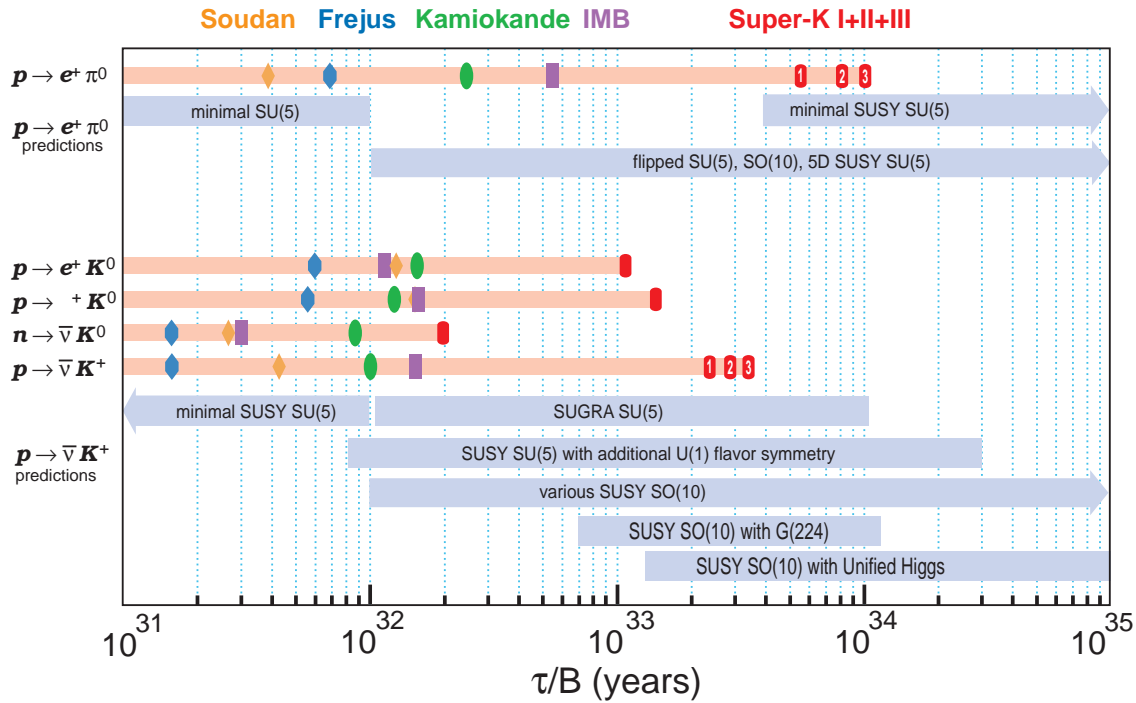


**Figure 2-8:** Proton decay lifetime limits compared to lifetime ranges predicted by Grand Unified Theories. The upper section is for  $p \rightarrow e^+ \pi^0$ , most commonly caused by gauge mediation. The lower section is for SUSY motivated models, which commonly predict decay modes with kaons in the final state. The marker symbols indicate published limits by experiments, as indicated by the sequence and colors on top of the figure.

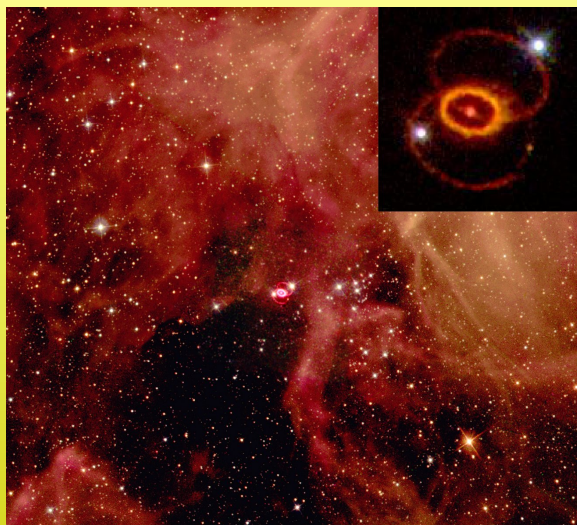
provide strong constraints on such theories. Minimal SU(5) was ruled out by the early work of IMB and Kamiokande; minimal SUSY SU(5) is considered to be ruled out by SK. In most cases, another order of magnitude in limit will not rule out specific theories, but will constrain their allowed parameters, perhaps leading to the conclusion that some are fine-tuned. **FIXME:** or ‘perhaps fine-tuning them’?

In summary, while the detector masses required to qualitatively extend the sensitivity to proton decay are inhibiting, an observation would have tremendous impact. As Chapter 6 will show, the performance and scalability of the LArTPC technology opens up nucleon decay channels that are not as readily accessible in water Cherenkov detectors, providing LBNE with a unique opportunity for discovery. **FIXME:** Is it really unique, or just rare or compelling?

## 2.4 Supernova-Neutrino Physics and Astrophysics

**FIXME:** changed title to match exec summ

### SUPERNOVA BURST NEUTRINOS



1987A supernova remnant near the center. Composite of two public domain NASA images taken from the Hubble Space Telescope.

**FIXME:** *taken verbatim from Wikipedia*

In 1966 Colgate and White calculated that neutrinos carry away most of the gravitational energy released by the collapse of massive stars, events now categorized as Type Ib and Ic and Type II supernovae. When such stars collapse, matter densities at the core becomes so high ( $10^{17} \text{ kg/m}^3$ ) that the degeneracy of electrons is not enough to prevent protons and electrons from combining to form a neutron and an electron neutrino. A second and more important neutrino source is the thermal energy (100 billion kelvins) of the newly formed neutron core, which is dissipated via the formation of neutrino-antineutrino pairs of all flavors.

**FIXME:** *new* Neutrinos from a core-collapse supernova are emitted in a burst of a few tens of seconds duration, with about half in the first second. Energies are in the few tens of MeV range, and luminosity is divided roughly equally between flavors. The high-statistics neutrino signal from a nearby supernova of this type would clearly provide a wealth of information, shedding light on a variety of physics and astrophysics topics (see [?,?] for reviews). The baseline model of core collapse was confirmed by the observation of 19 neutrino events in two water Cherenkov detectors for SN1987A in the Large Magellanic Cloud, 55 kpc away [?,?].

**FIXME:** *new* Core-collapse supernovae are rare events: the expected rate is 2-3 per century in the Milky Way. As for the Homestake **FIXME:** *which is this?* and Super-Kamiokande detectors, the large LBNE detector, once constructed, may operate for decades. On this time scale, the likelihood of a supernova event in our galaxy is significant. In a 20-year run of an experiment, the probability of observing a core-collapse is about 40%. The detection of the neutrino burst from such an event would dramatically expand the science reach of the experiment, allowing measurement of the neutrino mass hierarchy and the  $\theta_{13}$  mixing angle, observation of the development of the explosion in the core of the star, probing of the equation of state of matter at nuclear densities, and constraints on physics beyond the Standard Model. Each of these questions represents an important outstanding problem in modern physics, worthy of a separate, dedicated experiment. The opportunity of targeting them all at once is very attractive, especially since it may come only at incremental cost to the LBNE project. The expected harvest of physics is rich enough to warrant investing the effort required to enable collection of as much information as possible when a core collapse

occurs.

**FIXME:** *new - 3 pg* In contrast to the SN1987A, for which only 19 neutrinos were observed, the detectors currently on the drawing board would register thousands or tens of thousands of interactions from a core-collapse supernova. The type of interactions observed depends on the detector technology: a water-Cherenkov detector would be primarily sensitive to the electron antineutrinos, whereas a LArTPC detector has excellent sensitivity to electron neutrinos. In each case, the high event rate implies that it should be possible to measure not only the time-integrated spectra, but also their second-by-second evolution. This is the key reason behind the physics potential of the planned LBNE experiment.**FIXME:** *a key 'element of' the physics potential, maybe?*

The interest in establishing the explosion mechanism observationally comes from the key role supernovae of this type have played in the history of the universe. Ancient supernovae have in very large measure shaped our world. Without taking supernova feedback into account, for example, modern simulations of galaxy formation cannot reproduce the structure of our galactic disk. Star formation is – and always has been – triggered by shock waves from ancient supernovae. Even the iron in our blood was once synthesized inside a massive star and ejected in a supernova explosion.

For over half a century, researchers have been grappling to understand the physics of the core collapse. The challenge of reconstructing the explosion mechanism from the light curves and the structure of the remnants is akin to reconstructing the cause of a plane crash from a debris field. The supernova neutrinos serve as a kind of black box: they record the information about the physical processes in the center of the explosion during the first several seconds – as it is happening.

**FIXME:** *new - 3 pg* The explosion mechanism is thought to have three distinct stages: the collapse of the iron core, with the formation of the shock and its breakout through the neutrinosphere; the accretion phase, in which the shock temporarily stalls at the radius of about 200 km, while the material keeps raining in; and the cooling stage, in which the hot proto-neutron star loses its energy and trapped lepton number, while the re-energized shock expands to push out the rest of the star. Each of these three stages is predicted to have a distinct signature in the neutrino signal. Thus, it should be possible to directly observe, for example, how long the shock is stalled. More exotic features of the collapse may be observable in the neutrino flux, as well, such as possible transitions to quark matter or to a black hole. (An observation in conjunction with a gravitational wave detection would be especially interesting.)

Over the last **FIXME:** *two?* decades, neutrino flavor oscillations have been firmly established in solar neutrinos and a variety of terrestrial sources, and to correctly interpret the supernova neutrino signal, they must be accounted for. As it turns out, in fact, the physics of the oscillations in the supernova environment is **FIXME:** *promises to be?* much richer than in any of the cases measured to date, for a variety of reasons.

- Neutrinos travel through the changing profile of the explosion with stochastic density fluctuations behind the expanding shock and, due to their coherent scattering off of each other, their flavor states are coupled.
- The oscillation patterns come out very differently for the normal and inverted mass hierarchies.
- The expanding shock and turbulence leave a unique imprint in the neutrino signal.
- Additional information on oscillation parameters, free of supernova model-dependence, will be available if matter effects due to the Earth can be observed in detectors at different locations around the world [?,?].
- The observation of this potentially copious source of neutrinos will also allow limits on coupling to axions, large extra dimensions, and other exotic physics (*e.g.* [?,?]).
- The oscillations of neutrinos and antineutrinos from a core-collapse supernova manifest very differently. In the neutrino channel the oscillation features are in general more pronounced, since the initial spectra of  $\nu_e$  and  $\nu_\mu$  ( $\nu_\tau$ ) are always significantly different. It would be extremely valuable to detect both channels with high statistics.

**FIXME:** *still new*

The problem is truly multidisciplinary. The neutrino physics and astrophysics go hand-in-hand, therefore both need to be modeled, and both fields will receive payback simultaneously. The sign of the neutrino hierarchy, the speed at which the shock expands, and the density profile of the star, for example – all of which are interesting to both fields – will be learned “all in one package”. The better the astrophysics is understood, the better the quality of information about neutrino physics, and vice-versa. It is therefore important to gather as much high-quality information as possible, and to disentangle the flavor components of the flux.

Currently, experiments world-wide are sensitive primarily to electron antineutrinos, via inverse-beta decay on free protons, which dominates the interaction rate in water and liquid-scintillator detectors. Liquid argon exhibits a unique sensitivity to the *electron neutrino* component of the flux, via the absorption interaction on  $^{40}\text{Ar}$ ,  $\nu_e + ^{40}\text{Ar} \rightarrow e^- + ^{40}\text{K}^*$ . In principle, this interaction can be tagged via the coincidence of the electron and the  $^{40}\text{K}^*$  de-excitation gamma cascade. About 900 events would be expected in a 10-kt fiducial LAr detector for a supernova at 10 kpc. The number of signal events scales with mass and the inverse square of distance, as shown in Figure 2-9.

For a collapse in the Andromeda galaxy, detectors of 100 kilotons of mass would be required to observe a handful of events. However even a small 10-kt detector would gather a unique  $\nu_e$  signal from supernovae within the Milky Way.

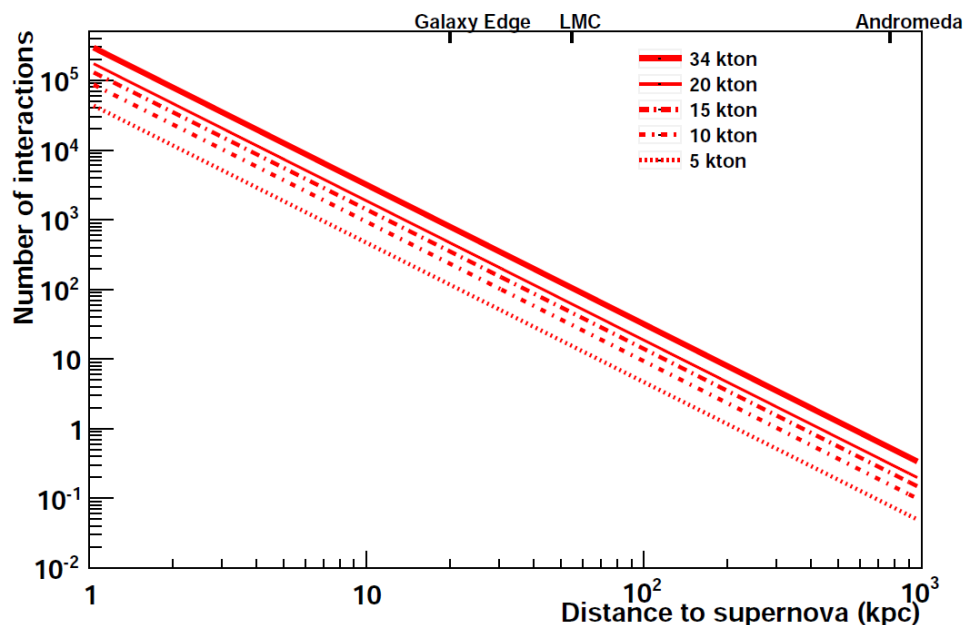


**Figure 2-9:** Number of supernova neutrino interactions in an LAr detector as a function of distance to the supernova, for different detector masses. Core collapses are expected to occur a few times per century, at a most-likely distance of about 10–15 kpc.

**FIXME:** *new 2 pg* As a final note, because the neutrinos emerge promptly after core collapse, in contrast to the electromagnetic radiation which must beat its way out of the stellar envelope, an observed neutrino signal can provide a prompt supernova alert [?,?]. This would allow astronomers to find the supernova in early light turn-on stages, which could yield information about the progenitor (in turn, important for understanding oscillations). The LBNE detector should be designed to allow prompt alert capability.

Due to the magnitude of the expected neutrino flux and the complexity of the neutrino signal, understanding core collapse through this mechanism requires supercomputers as well as state-of-the-art analytical models. Further, observations and measurements by multiple, geographically separated detectors during a core collapse – of which several are expected to be online over the next few decades [?,?] – will enhance the potential science yield from a rare event such as this [?].

## 3 Overview of the LBNE Project and Design

### 3.1 LBNE and the U.S. Neutrino-Physics Program

**FIXME:** *new - 4 pgrph* In its 2008 report, the Particle Physics Project Prioritization Panel (P5) recommended a world-class neutrino-physics program as a core component of the U.S. particle-physics program [?]. Included in the report is the long-term vision of a large far detector at the site of the former Homestake Mine in Lead, SD, and a high-intensity, broad-band neutrino source at Fermi National Accelerator Laboratory (Fermilab). At the time, the far detector site was the proposed Deep Underground Science and Engineering Laboratory (DUSEL); it is now the Sanford Underground Research Facility (SURF).

On January 8, 2010 the Department of Energy approved the Mission Need [?] for a new long-baseline neutrino experiment that would enable this world-class program and firmly establish the U.S. as the leader in neutrino science. The LBNE experiment is designed to meet this Mission Need. **FIXME:** *the ‘project was formed to’ or ‘experiment is designed to’ meet the need*

With the facilities provided by the LBNE Project and the unique features of the experiment – in particular the long baseline of 1,300 km, the broad-band beam and the high resolution of the far detector – the LBNE Science Collaboration proposes to mount a broad attack on the physics of neutrino oscillations with sensitivity to all poorly known **FIXME:** *searching for better phrase* parameters in a single experiment. **FIXME:** *Can’t we just say ‘as described in chapter blah’ and leave the rest of this pgraph off? This info should be in the exec summ, too - why say it 3 times?* The focus of the program will be the explicit demonstration of leptonic CP violation, if it exists, by precisely measuring the asymmetric oscillations of muon-type neutrinos and antineutrinos into electron-type neutrinos and antineutrinos. The experiment will enable precise measurements of the neutrino-oscillation parameters, in particular, the CP-violating phase in the three-flavor framework, and the search for new physics that would show up as deviations from this model.

It is currently planned to implement LBNE as a phased program, with increased scientific capabilities at each phase. The initial phase project (LBNE10), which received CD-1 approval

in December 2012, consists of a new neutrino beamline at Fermilab, tertiary-beam muon detectors to monitor the beam, and a 10-kt liquid argon TPC far detector located at SURF, placed at the surface under several meters of shielding. Table 3-1 summarizes the principal parameters of LBNE10, as defined at CD-1:

**FIXME:** *old* In its 2008 report, the Particle Physics Project Prioritization Panel (P5) recommended a world-class neutrino-physics program as a core component of the U.S. particle-physics program [?]. Included in the report is the long-term vision of a large detector at the formerly proposed Deep Underground Science and Engineering Laboratory (DUSEL, now SURF, the Sanford Underground Research Facility) at the site of the Homestake Mine in Lead, SD, and a high-intensity neutrino source at Fermi National Accelerator Laboratory (Fermilab). The baseline between Fermilab and SURF is 1300 km.

On January 8, 2010, the Department of Energy approved the Mission Need [?] for a new long-baseline neutrino experiment that would enable this world-class program and firmly establish the U.S. as the leader in neutrino science. The LBNE Project is designed to meet this Mission Need.

With the facilities provided by the LBNE Project and the unique features of the experiment – in particular the long baseline, the broad-band beam and the high resolution of the detector – the LBNE Science Collaboration proposes to mount a broad attack on the physics of neutrino oscillations with sensitivity to all poorly known parameters in a single experiment. The focus of the program will be the explicit demonstration of leptonic CP violation, if it exists, by precisely measuring the asymmetric oscillations of muon-type neutrinos and antineutrinos into electron-type neutrinos and antineutrinos. The experiment will enable precise measurements of the neutrino-oscillation parameters, in particular, the CP-violating phase in the three-flavor framework, and the search for new physics that would show up as deviations from this model.

It is currently planned to implement LBNE as a phased program, with increased scientific capabilities at each phase. The initial phase project (LBNE10), which received CD-1 approval in December 2012, consists of a new neutrino beamline at Fermilab, tertiary muon detectors to monitor the beam, and a 10-kt liquid argon TPC far detector located at SURF, placed at the surface under several meters of shielding. Table 3-1 summarizes the principal parameters of LBNE10, as defined at CD-1:

**FIXME:** *new- 2 pgph* Subsequent phases of LBNE are envisioned to include the construction of a near neutrino detector on the Fermilab site and construction of a larger far detector 4,850 feet underground at SURF.

A configuration of the LBNE facility in which the far detector is located deep underground would also provide opportunities for research in other areas of physics, such as nucleon decay and neutrino astrophysics, including studies of neutrino bursts from supernovae in our galaxy. In a 20-year run, the probability of observing such a supernova is about 40%.

**Table 3-1:** Principal parameters of LBNE10 as defined at CD-1

Project Element Parameter	Value
Near- to Far-Site Baseline	1,300 km
Primary Proton Beam Power	708 kW, upgradable to 2.3 MW
Protons on Target per Year	$6.5 \times 10^{20}$
Primary Beam Energy	60 – 120 GeV (tunable)
Neutrino Beam Type	Horn-focused with decay volume
Neutrino Beam Energy Range	0.5 – 5 GeV
Neutrino Beam Decay Pipe Diameter $\times$ Length	4 m $\times$ 200 m
Far Detector Type	LArTPC
Far Detector Active (Fiducial) Mass	13.5 (10) kt

**FIXME:** *old* Subsequent phases of LBNE will include the construction of a near neutrino detector on the Fermilab site and construction of a larger detector underground at SURF.

A configuration of the LBNE facility in which the Far Detector is located deep underground would also provide opportunities for research in other areas of physics, such as nucleon decay and neutrino astrophysics, including studies of neutrino bursts from locally occurring supernovae.

## 3.2 The LBNE Far Site: Sanford Underground Research Facility

**FIXME:** *new* The Sanford Underground Research Facility [?] is a laboratory located on the site of the former Homestake mine in Lead, SD that is dedicated to underground science. Underground neutrino experiments in the mine date back to 1967 when nuclear chemist Ray Davis installed a solar neutrino experiment 4,850 feet below the surface. Ray Davis earned a share of the Nobel Prize for physics in 2002 for his experiment, which ran until 1993. This former mine offers the deepest caverns in the western hemisphere with extensive drifts both vertically and laterally. A vertical cross-section of the underground areas developed for mining is shown in Figure 3-1.

**FIXME:** *old* The Sanford Underground Research Facility [?] is a laboratory dedicated to underground science located at the former Homestake gold mine in Lead, South Dakota. Underground neutrino experiments at Homestake Mine date back to 1967 when nuclear chemist Ray Davis installed a solar neutrino experiment 4,850 feet underground. Ray Davis earned a share of the Nobel Prize for Physics in 2002 for the Homestake mine solar neutrino experiment which ran until 1993. Homestake mine is the deepest mine in the western hemisphere with extensive drifts both in depth and laterally. A cross-section of the Homestake mine development is shown in Figure 3-1.



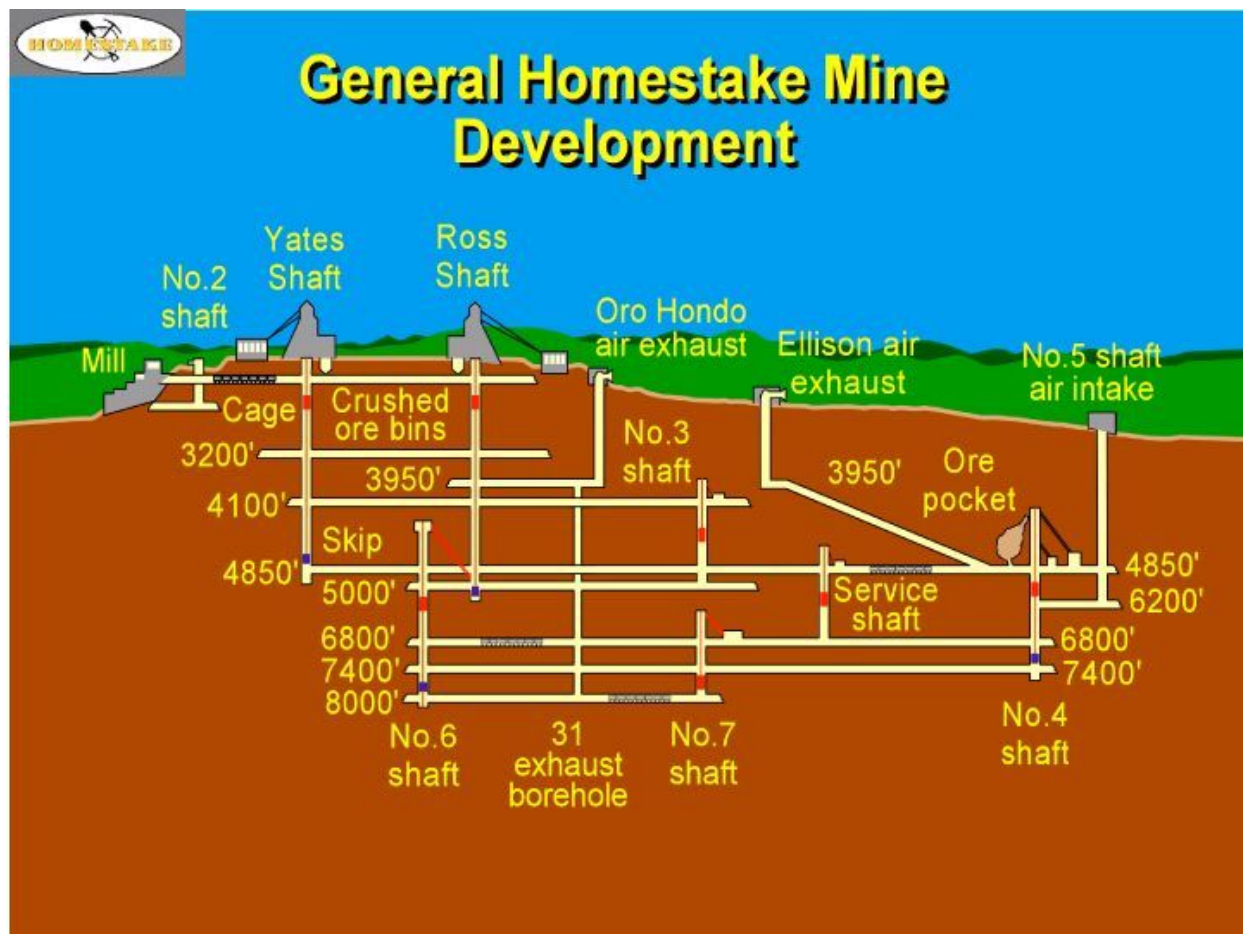


**Figure 3–1:** Vertical cross-section of the the former Homestake mine indicating the areas developed for mining. SURF is currently developing levels down to the 4850-foot level for science applications.

**FIXME:** *new* The Homestake mine closed in 2003, and in 2006 the company donated the property to the state of South Dakota for use as an underground laboratory. The South Dakota state legislature created the South Dakota Science and Technology Authority to operate the laboratory. The state legislature has since committed more than \$40 million in state funds to the project, and the state has also obtained a \$10 million Community Development Block Grant to help rehabilitate the site. In addition, a \$70 million donation from philanthropist T. Denny Sanford has been used to reopen the site for science and to establish a Sanford Center for Science Education.

The depth of the areas currently being developed for science at SURF make it an extremely competitive location in terms of cosmic ray background suppression for a large underground detector, like that envisioned for LBNE. Figure 3-2 shows the predicted cosmic ray flux at this site [?] as compared to other underground laboratories worldwide.

**FIXME:** *old* Homestake mine closed in 2003, but the company donated the property to the state of South Dakota in 2006 for use as an underground laboratory. The South Dakota state legislature created the South Dakota Science and Technology Authority to operate the lab. The state Legislature has committed more than \$40 million in state funds to the project, and South Dakota also obtained a \$10 million Community Development Block Grant to help rehabilitate Homestake. In addition, a \$70 million donation from philanthropist T. Denny Sanford was used to reopen the gold mine for science and to establish a Sanford Center for Science Education. The depth of the areas currently being developed for science at SURF make it an extremely competitive location for a large underground detector like that envisioned for LBNE. The predicted cosmic ray flux at Homestake mine [?] as compared to other underground laboratories world wide is shown in Figure 3-2.

**FIXME:** *new* The first two major physics experiments at SURF are being installed 4,850 feet underground (“at the 4850L”) in an area called the Davis Campus, named for the late Ray Davis. The Large Underground Xenon (LUX) experiment has been installed in the cavern first excavated for Davis in the 1960s. LUX will be the most sensitive detector yet to search for dark matter. The Majorana Demonstrator experiment, also being installed in 2013 in a newly excavated space adjacent to the original Davis cavern, **FIXME:** *since 2013 is 3/4 over, can we say either ‘currently being installed’ or ‘has recently been installed’?* will search for neutrinoless double-beta decay. Figure 3-3 shows four photographs of facilities and activities at SURF related to the LUX and Majorana Demonstrator at the 4850L.

**FIXME:** *old* The first two major physics experiments at the Sanford Lab are being installed 4,850 feet underground in an area called the Davis Campus, named for the late Ray Davis. The Large Underground Xenon (LUX) experiment has been installed in the same cavern excavated for Ray Davis in the 1960s. LUX will be the most sensitive detector yet to search for dark matter. The Majorana Demonstrator experiment, also being installed in 2013, will search for neutrinoless double-beta decay. The Majorana Demonstrator experiment is in a newly excavated space in the Davis Campus, adjacent to the original Davis cavern. Sample images from the LUX and Majorana Demonstrator activities at the 4850 foot level are shown

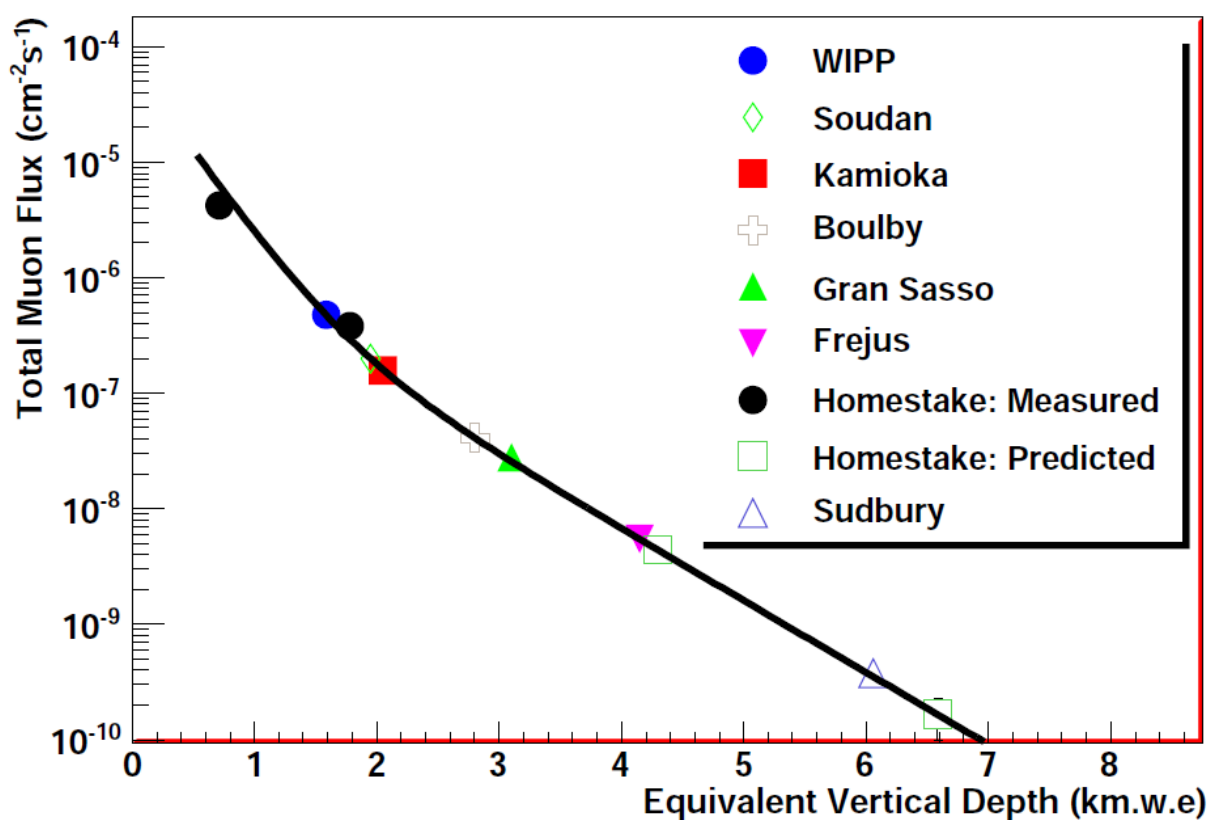


**Figure 3-2:** Open green squares indicate the predicted cosmic ray flux at the 4850L (left) and 8000L (right) at the SURF (Homestake) site. Values predicted for other underground laboratories are shown [?]. **FIXME:** Any comment about the measured vs predicted?

in Figure 3-3.



**Figure 3-3:** Sanford Underground Research Facility: Administration building and Yates shaft headframe (top left); corridor at 4850-ft (1480-m) depth leading to clean rooms and experimental halls (top right); billet of radiopure electroformed copper for the Majorana Demonstrator experiment being placed on a lathe in a clean room at 4850-ft depth (bottom left); LUX experiment at 4850-ft depth (bottom right).

**FIXME:** *new* The U.S. Department of Energy is also considering SURF as the site for proposed longer-term experiments in addition to LBNE, including, for example, a project entitled Dual Ion Accelerators for Nuclear Astrophysics (DIANA). Figure 3-4, prepared by SURF Director Mike Headley and Head of Operations Kevin Lesko, demonstrates the long-term potential for experiments at SURF. **FIXME:** *quality of figure not very good*

**FIXME:** *old* The U.S. Department of Energy is also considering the Sanford Underground Research Facility as the site for proposed longer term experiments in addition to LBNE, including, for example, a project entitled Dual Ion Accelerators for Nuclear Astrophysics (DIANA). Figure 3-4 prepared by Sanford Lab Director Mike Headley and Head of Operations Kevin Lesko demonstrates the long term potential for experiments at SURF.

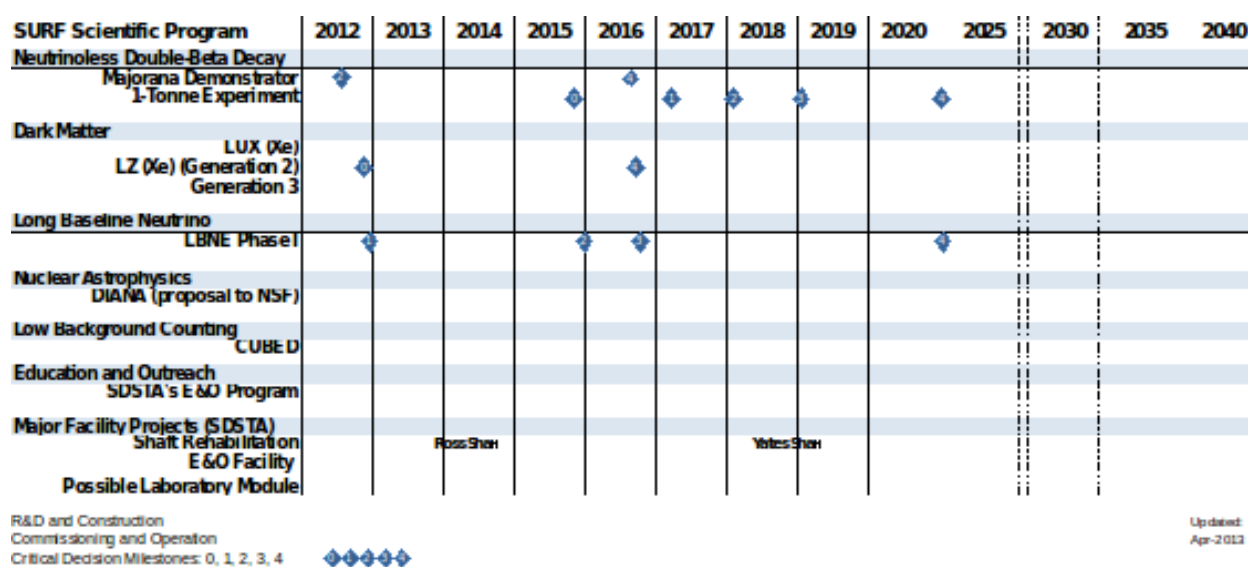


**Figure 3-4:** Timeline exploring the long-term potential of deep science experiments at SURF.

### 3.3 The LBNE Near Site: Fermi National Accelerator Laboratory

**FIXME:** *new* Fermi National Accelerator Laboratory (Fermilab), located 40 miles west of Chicago, Illinois, produces the world's most powerful neutrino beams. The neutrino beams come from two of the lab's proton accelerators (see Figure 3-5), the 8-GeV Booster which feeds the *Booster Neutrino Beamline* (BNB) and the 120-GeV Main Injector which feeds the *Neutrinos at the Main Injector* beamline (NuMI).

**FIXME:** *old* Fermi National Accelerator Laboratory (Fermilab), located 40 miles east of Chicago, Illinois produces the worlds most powerful neutrino beams. The neutrino beams come from two of the lab's proton accelerators (see Figure 3-5), the 8 GeV Booster which feeds the Booster Neutrino Beamline (BNB) and the 120 GeV Main Injector which feeds the Neutrinos at the Main Injector beamline (NuMI).

**FIXME:** *new - 3 pgph* NuMI is a high-energy neutrino beam that has been operating since 2004. It was designed for steady 400-kW operation and achieved that goal by the end of the MINOS experimental run in 2012. As shown in Figure 3-6, the NuMI beamline was integrating an average of  $9 \times 10^{18}$  protons per week ( $\approx 2.7 \times 10^{20}$  protons-on-target per year) in mid 2012.

The Fermilab accelerator complex has just completed an upgrade for the next phase of operations. The proton improvement plan is shown in Figure 3-7. The Main Injector will deliver 708 kW to the neutrino program starting in 2014 ( $\approx 6 \times 10^{20}$  protons-on-target per year). **FIXME:** *time scale still right?*

Fermilab has proposed a series of upgrades, collectively known as Project X [?], to the current complex, to take place during the decade beyond 2020. Project X proposes to replace the existing injector complex in stages, first replacing the 400-MeV conventional pulsed linac with a 1-GeV superconducting CW linac, and later replacing the 8-GeV Booster synchrotron with a superconducting pulsed linac, as shown in Figure 3-8. The planned stages of Project X and the future experimental research programs planned are summarized in Table 3-2.

**FIXME:** *old* NuMI is a high energy neutrino beam that has been operating since 2004. NuMI was designed for steady 400 kW operation and achieved that goal by the end of the MINOS experimental run in 2012. As shown in Figure 3-6, the NuMI beamline was integrating an average of  $9 \times 10^{18}$  protons per week ( $\approx 2.7 \times 10^{20}$  protons-on-target per year) in mid 2012.

The Fermilab accelerator complex is currently undergoing an upgrade for the next phase of operations. The proton improvement plan is shown in Figure 3-7. The Main Injector will deliver 708 kW to the neutrino program starting in 2014 ( $\approx 6 \times 10^{20}$  protons-on-target per year).



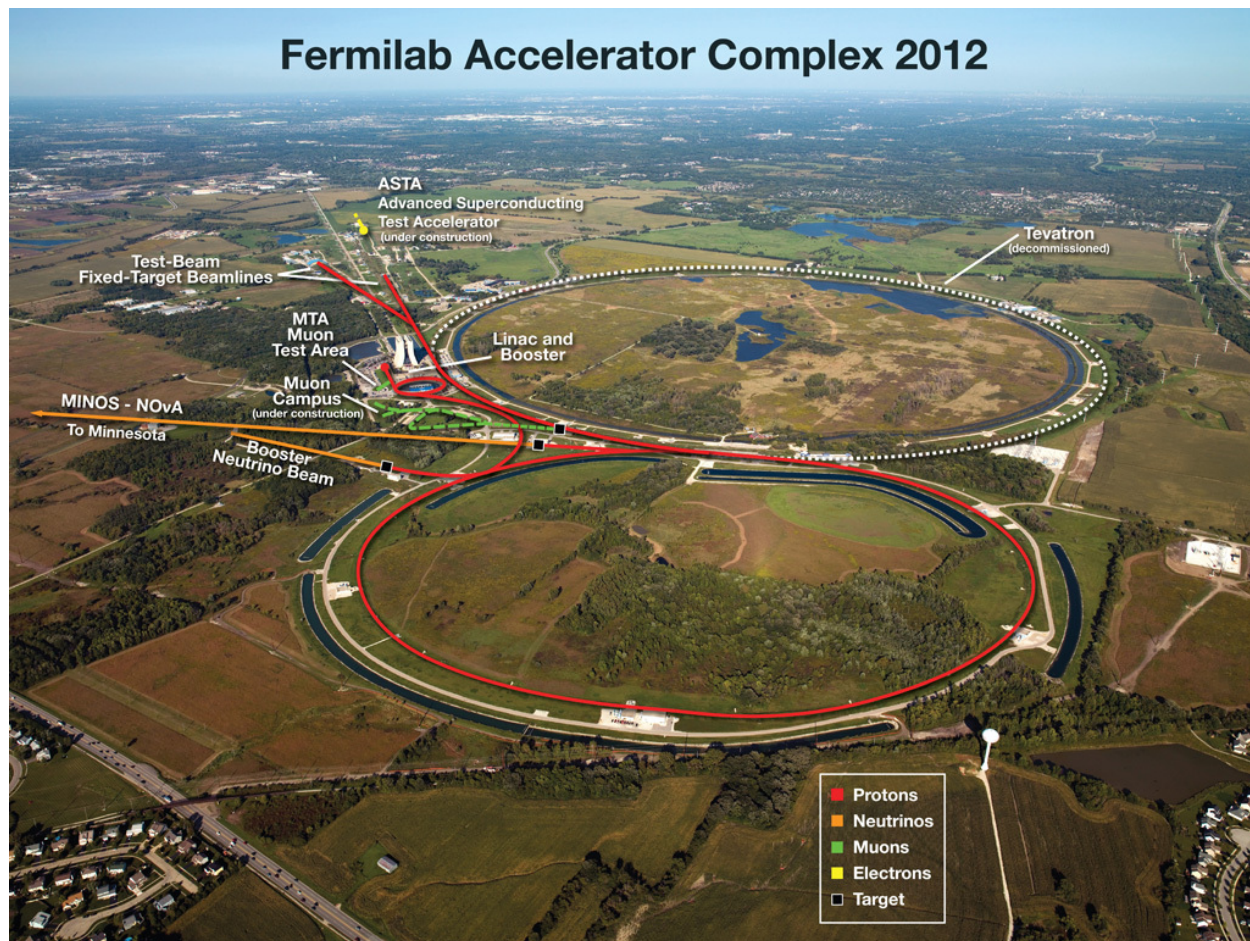


**Figure 3-5:** The accelerator chain at Fermi National Accelerator Laboratory. A 400-MeV linac feeds into the 15-Hz Booster which produces an 8-GeV beam. The Booster beam is used for the Booster Neutrino Beamline experiments. The Booster feeds into the 120-GeV Main Injector which operates at 708 kW as of September 2013. The Main Injector is the source for the NuMI beamline, which supplies a high-power, high-energy neutrino beam to the MINOS/MINOS+ and NOvA experiments.

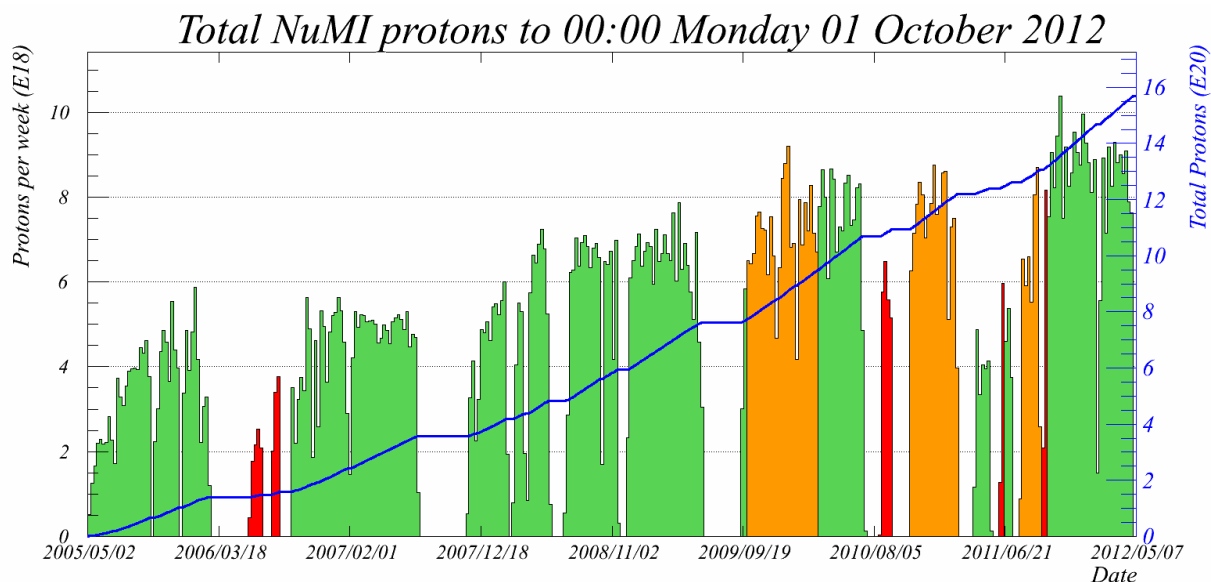


**Figure 3-6:** The NuMI beamline performance

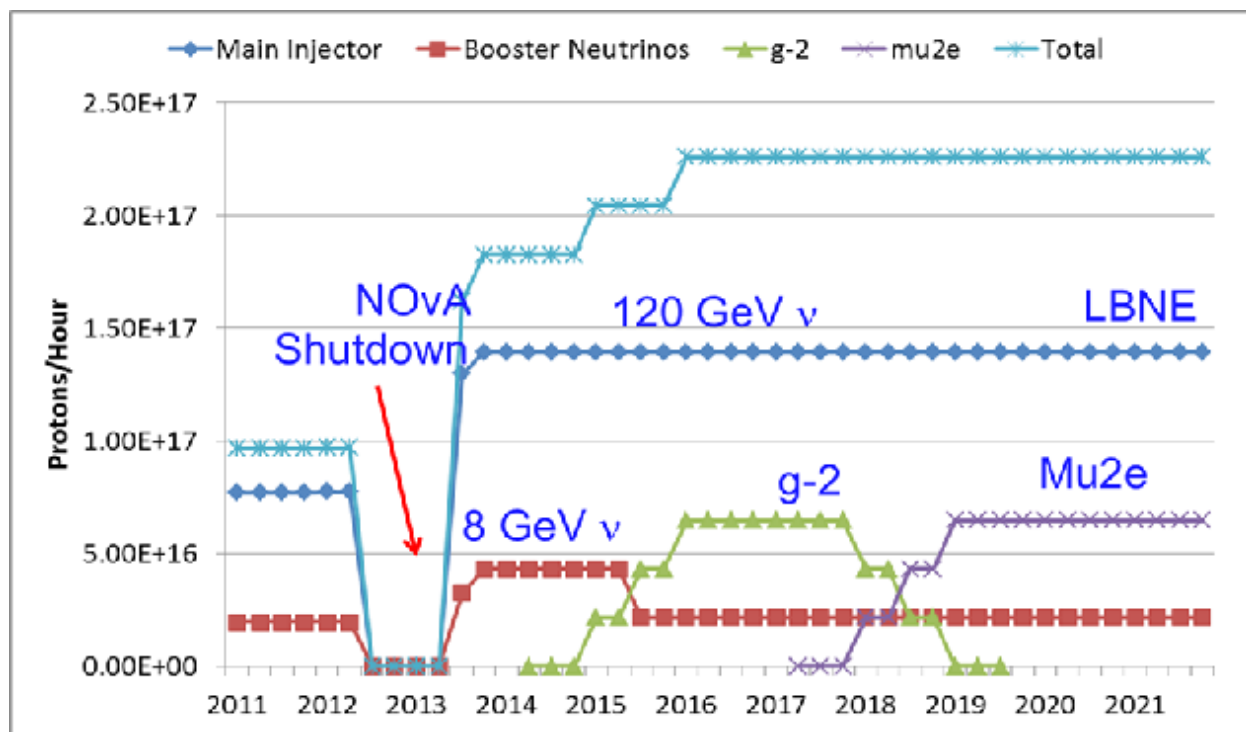


**Figure 3-7:** Fermilab proton source proton flux ramp up expectations for the Intensity Frontier experiments.



In the decade beyond 2020, Fermilab has proposed a series of upgrades to the current complex known as Project X [?]. The Project X upgrades propose to replace the existing injector complex in stages, first replacing the 400 MeV conventional pulsed linac with a 1 GeV superconducting CW linac, and later replacing the 8 GeV Booster synchrotron with a superconducting pulsed linac, as shown in Figure 3-8

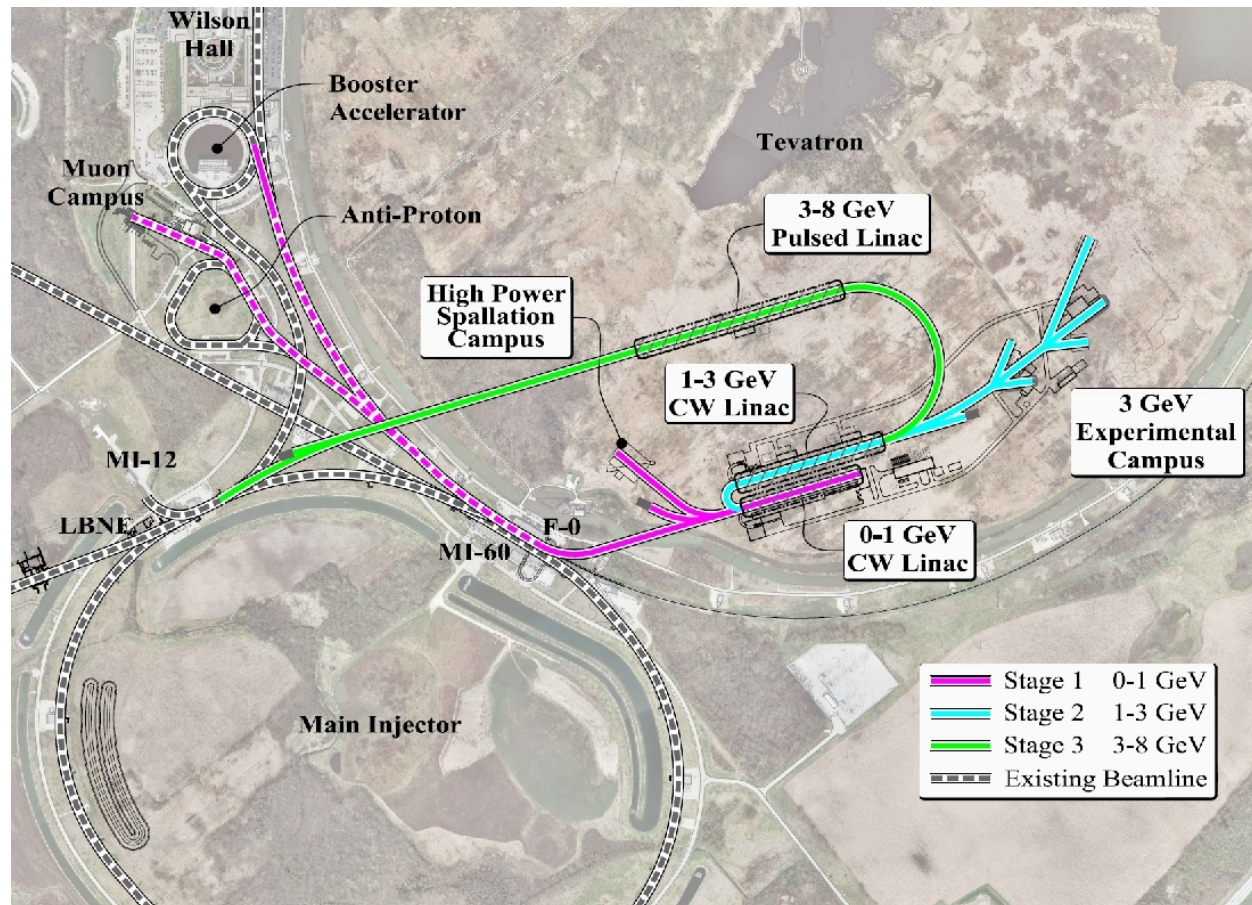


**Figure 3-8:** Proposed upgrades to the Fermilab accelerator complex under Project X

**FIXME: new** The LBNE beamline, described in Section 3.4, will utilize the Main Injector 120-GeV beam. The beamline is heavily modeled on the highly successful NuMI beamline and is planned to initially use the same targeting and focusing technology as NuMI does.

**FIXME: old** The LBNE beamline which is described in detail in Section 3.4 will utilize the Main Injector 120 GeV beam and is heavily modeled on the highly successful NuMI beamline. LBNE is planned to initially use the same targeting and focusing technology as NuMI.

**Table 3–2:** The current and future experimental research programs planned for the Fermilab accelerator complex.

Program Description	2013 NO $\nu$ A	PROJECT X			
		Stage 1 (2025 ?) 1 GeV CW linac	Stage 2 3 GeV CW linac	Stage 3 RDR	Stage 4 beyond RDR
60-120 GeV MI $\nu$ s	470-700 kW	515-1200 kW	1200 kW	2450kW	2450-4000 kW
8 GeV $\nu$ s	15 kW	0-42kW	0-84 kW*	0-172 kW*	3000kW
	+0-50kW**	+0-90 kW**			
8 GeV Muons	20 kW	0-20 kW*	0-20 kW*	0-172 kW*	1000 kW
1-3 GeV Muons	—	80 kW	1000 kW	1000 kW	1000 kW
Kaons	0-30 kW**	0-75 kW**	1100 kW	1870 kW	1870 kW
	(< 30% df)	(< 45% df)			
	(from MI)	(from MI)			
Nuclear edm ISOL	none	0-900 kW	0-900 kW	0-1000 kW	0-1000 kW
Ultra-cold neutrons	none	0-900 kW	0-900 kW	0-1000 kW	0-1000 kW
Nuclear technology	none	0-900 kW	0-900 kW	0-1000 kW	0-1000 kW
# Programs	4	8	8	8	8
Total max power	735 kW	2222 kW	4284 kW	6492 kW	11870kW

\* Operating point in range depends on Main Injector (MI) proton beam energy for neutrinos.

\*\* Operating point in range depends on MI inject or slow-spill duty factor (df) for kaon program.

## 3.4 The LBNE Beamline

**FIXME:** *new - 2 pgrph* The LBNE beamline facility, located at Fermilab (the LBNE *Near Site*), will aim a beam of neutrinos toward the LBNE far detector located 1,300 km away at SURF. The beamline facility, which is expected to be fully contained within Fermilab property, will consist of a primary (proton) beamline, a neutrino beamline, and conventional facilities to support the technical components of the primary and neutrino beamlines. **FIXME:** *seems premature to head reader off to another source* More detailed information can be found in the Conceptual Design Report [?].

The primary beam, composed of protons in the energy range of 60-120 GeV, will be extracted from the MI-10 straight section of Fermilab's Main Injector using single-turn extraction. The beam will then be transported to the target area within a beam enclosure embedded in an engineered earthen embankment (hill). The primary beam transport section is designed for very low losses. The embankment's dimensions are designed to be commensurate with the bending strength of the required dipole magnets so as to provide a net  $5.8^\circ$  downward vertical bent to the neutrino beam (see Figures 3-9 and 3-10).

**FIXME:** *old* LBNE will utilize a Beamline facility located at Fermilab to carry out a compelling research program in neutrino physics. The facility will aim a beam of neutrinos with a net  $5.8^\circ$  downward vertical bent toward a detector placed at the Sanford Underground Research Facility (SURF) in South Dakota, about 1,300 km away. The main elements of the facility, which is expected to be fully contained within Fermilab property, are a primary proton beamline, a neutrino beamline, and conventional facilities to support the technical components of the proton and neutrino beamlines. More detailed information can be found in the Conceptual Design Report [?].

The primary proton beam, in the energy range of 60-120 GeV, will be extracted from the MI-10 straight section of Fermilab's Main Injector using single-turn extraction. The beam is then transported to the target area with very low losses within a beam enclosure embedded in an earthen, engineered filled embankment (hill) whose dimensions are commensurate with the bending strength of the required dipole magnets (see Figures 3-9 and 3-10).

**FIXME:** *new* For 120-GeV operation and with the Main Injector upgrades implemented for the NOvA experiment [?], the fast, single-turn extraction will deliver  $4.9 \times 10^{13}$  to the LBNE target in  $10 \mu\text{s}$ . This represents all the protons in one machine cycle, which lasts 1.33 sec. The initial operating beam power of the facility is expected to be  $\sim 708$  kW. The design includes the capability to support the Project X [?] upgrade to 2.3 MW, which includes the replacement of the existing proton source that feeds the Main Injector. At 708-kW operation the accelerator and primary beamline complex are expected to deliver  $6.5 \times 10^{20}$  protons per year to the neutrino target. Approximately 85% of the protons interact with the solid target, producing pions and kaons that subsequently get focused by a set of magnetic horns into a decay pipe where they decay into muons and neutrinos (Figure 3-11). The neutrinos form a





**Figure 3-9:** Plan view of the overall Near Site Project layout showing the LBNE Beamline extraction point from the Main Injector, the primary beamline, target hall, decay pipe and absorber.

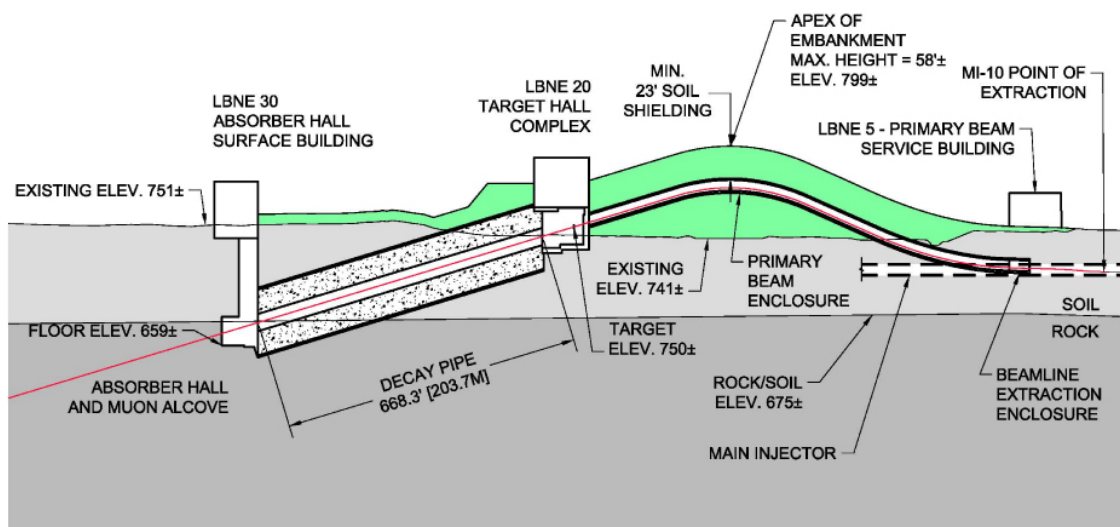


**Figure 3-10:** Longitudinal section of the LBNE Beamline facility. The beam enters from the right in the figure, the protons being extracted from the MI-10 extraction point at the Main Injector.

wide-band, sign-selected neutrino beam, designed to provide flux in the energy range 0.5 to 5 GeV. This energy range will cover the first and second neutrino oscillation maxima, which for a 1,300 km baseline are at approximately 2.5 and 0.8 GeV, respectively.

**FIXME:** *old* For 120 GeV operation and with the Main Injector upgrades implemented for the NOvA experiment [?], the fast, single turn extraction will deliver all the protons ( $4.9 \times 10^{13}$ ) in one machine cycle (1.33 sec) to the LBNE target in  $10 \mu\text{s}$ . The initial operation of the facility is expected to be at a beam power of 708 kW, with the capability to support an upgrade to 2.3 MW with Project X [?], which includes the replacement of the existing proton source that feeds the Main Injector. The accelerator complex and the primary beamline are planned to deliver  $6.5 \times 10^{20}$  primary protons to the neutrino target per year for 708 kW operation. Neutrinos are produced after protons from the Main Injector hit a solid target where approximately 85% of the protons interact producing pions and kaons which are subsequently focused by a set of magnetic horns into a decay pipe where they decay into muons and neutrinos (Figure 3-11). A wide-band sign-selected neutrino beam is needed to cover the first and second neutrino oscillation maxima, which for a 1,300 km baseline are at approximately 2.5 and 0.8 GeV respectively. The beam therefore must provide neutrino flux in the energy range 0.5 to 5 GeV covering both oscillation peaks.

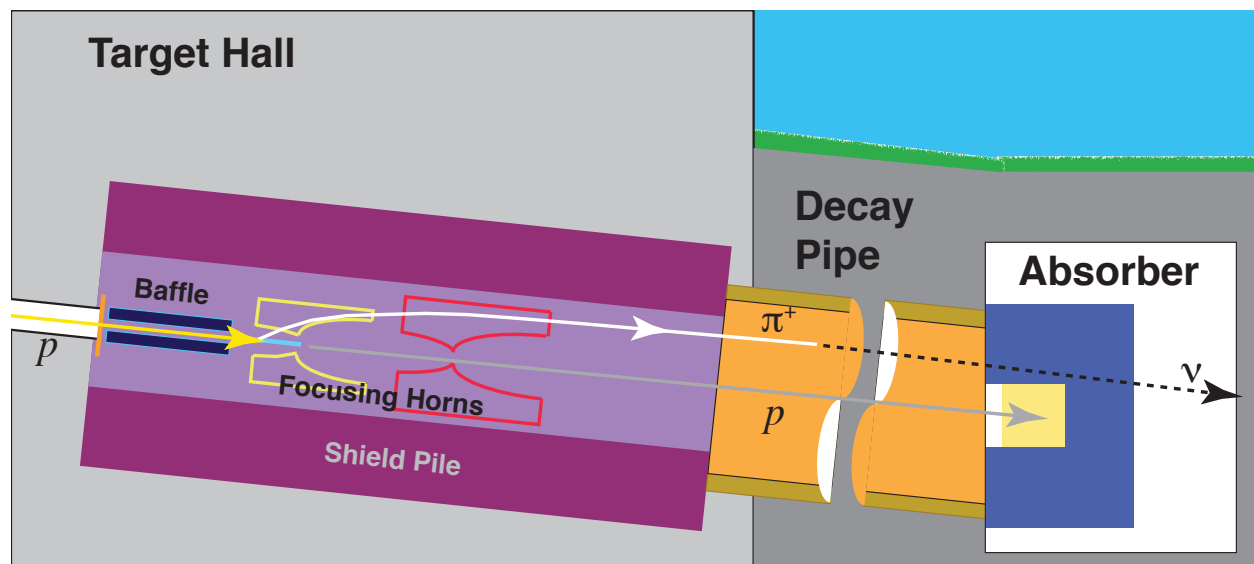


**Figure 3-11:** A cartoon of the LBNE neutrino beamline showing the major components of the neutrino beam. From left to right (the direction of the beam): the beam window, horn-protection baffle, target, the two toroidal focusing horns, decay pipe and absorber.

**FIXME:** *new* The reference target design for LBNE is an upgraded version of the NuMI-LE (Low Energy) target that was used for seven years to deliver beam to the MINOS experiment. The target consists of 47 segments, each 2-cm long, of POCO graphite ZXF-5Q. Focusing of charged particles is achieved by two magnetic horns in series, the first of which partially surrounds the target. They are both NuMI/NOvA-design horns with double-paraboloid inner conductor profiles that support currents up to 200 kA.

The decay volume in the LBNE reference design is an air-filled, air-cooled pipe of circular cross section with its diameter (4 m) and length (204 m) optimized such that decays of the pions and kaons result in neutrinos in the energy range useful for the experiment.

At the end of the decay region, the absorber, a water-cooled structure of aluminum and steel, is designed to remove any residual particles. This complex device, which must absorb a large fraction of the incident beam power of up to 2.3 MW, is also instrumented to measure the transverse distribution of the resultant hadronic showers to monitor the beam on a pulse-by-pulse basis.

An array of muon detectors in a small alcove immediately downstream of the absorber measures tertiary muons and thereby indirectly provides information on the direction, profile and flux of the neutrino beam.

**FIXME:** *old* The reference target design for LBNE is an upgraded version of the NuMI-LE (Low Energy) target that was used for 7 years to deliver beam to the MINOS experiment. The target consists of 47 segments, each 2 cm long, of POCO graphite ZXF-5Q. Focusing of charged particles is achieved by two magnetic horns in series, the first of which partially surrounds the target. They are both NuMI/NOvA design horns with double paraboloid inner conductor profiles and currents of up to 200 kA. The decay volume in the LBNE reference design is an air-filled, air-cooled pipe of circular cross section with its diameter (4m) and length (204m) optimized such that decays of the pions and kaons result in neutrinos in the energy range useful for the experiment. At the end of the decay region, the absorber, a water cooled structure of aluminum and steel, is needed to remove the residual particles remaining at the end of the decay pipe. This complex device, which must absorb a large fraction of the incident beam power of up to 2.3 MW, is also instrumented to measure the transverse distribution of the resultant hadronic showers to monitor the beam on a pulse-by-pulse basis. An array of muon detectors in a small muon alcove immediately downstream of the absorber provide information on the direction, profile and flux of the neutrino beam.

**FIXME:** *new* The Fermilab (Near Site) Conventional Facilities include the civil construction required to house the beamline components in their planned layout as shown in Figures 3-9 and 3-10. Following the beam from southeast to northwest, or roughly from right to left in Figure 3-9, the elements include the underground Extraction Enclosure, the Primary Beam Enclosure (inside the embankment) and its accompanying surface-based Service Building (LBNE 5), the Target Complex (LBNE 20) located in the embankment, the Decay Pipe, the underground Absorber Hall with the muon alcove, and its surface-based Service Building (LBNE 30). The embankment will need to be approximately 290 m long and 18 m above grade at its peak. The planned near neutrino detector facility is located as near as is feasible to the west site boundary of Fermilab, along the line-of-sight indicated in red in Figure 3-9.

**FIXME:** *Do we want all the elements capitalized in this pgraph?*

**FIXME:** *old* The Fermilab Conventional Facilities include the civil construction required to house the Beamline components and their layout as shown in Figs. 3-9 and 3-10. Following

the beam from southeast to northwest, or from right to left in the figure, is the underground Extraction Enclosure, the Primary Beam Enclosure inside the embankment and its accompanying surface-based Service Building (LBNE 5), the Target Complex (LBNE 20) located in the embankment, the Decay Pipe, the underground Absorber Hall with the muon alcove, and its surface-based Service Building (LBNE 30). The embankment will need to be approximately 290m long and 18 m high above grade at its peak. The planned near neutrino detector facility is located as near as is feasible to the west site boundary of Fermilab, along the line-of-sight indicated in red in Figure 3-9.

**FIXME:** *new - two sm changes only: ‘Beamline’ to ‘beamline’ and 2.3 MW ‘operation’; old deleted* The parameters of the beamline facility were determined taking into account several factors including the physics goals, the Monte Carlo modeling of the facility, spatial and radiological constraints and the experience gained by operating the NuMI facility at Fermilab. The relevant radiological concerns, prompt dose, residual dose, air activation and tritium production have been extensively modeled and the results implemented in the system design. The beamline facility design described above minimizes expensive underground construction and significantly enhances capability for ground-water radiological protection. In general, components of the LBNE beamline system which cannot be replaced or easily modified after substantial irradiation at 700-kW operation are being designed for 2.3-MW operation. Examples of such components are the shielding of the target chase and decay pipe and the absorber with its associated shielding.

In order to increase the neutrino event rates, the LBNE beamline project team is studying the following design improvements before baselining the experiment:

- Increase the length of the decay pipe up to 250 m (the maximum length allowed by the existing Fermilab site boundaries), and also possibly increase its diameter up to 6 m. Increases to the decay pipe size would require additional cost of the order several tens of millions of dollars. Increasing the length of the decay pipe from 200 to 250m increases the overall event rate in the oscillation region by 12%. Increases in the decay pipe diameter produces a 6% increase in the low energy neutrino event rate as shown in Table 3-3.
- Fill the decay pipe with helium instead of air. The total  $\nu_\mu$  event rate increases by about 11%, with a decrease in  $\bar{\nu}$  contamination in the neutrino beam. Introducing He in the decay pipe would require the design and construction of a decay pipe window; designs and different options for cooling this configuration are under study.
- Increase the horn current of the NuMI design horns by a modest amount (from 200 kA to 230 kA); this is expected to increase the neutrino event rates by about 10-12% at the first oscillation maximum [?]. A Finite Element Analysis simulation and a cooling test of the horns are underway to evaluate this option.
- Use an alternate material to the POCO graphite for the target to increase the target

longevity. This would involve additional R&D effort and design work. A Be target, for example, could be made shorter, potentially improving the horn focusing.

- Develop more advanced horn designs that could boost the low-energy flux in the region of the second oscillation maximum. It should be noted that the target and horn systems can be modified or replaced even after operations have begun if improved designs promise to enable higher instantaneous or integrated beam flux.

Table 3-3 summarizes the impact of the beam design improvements currently under consideration by the LBNE beamline project team. Together, the changes are anticipated to result in an increase of  $\sim 50\%$  in the  $\nu_e$  appearance signal rate at the far detector. These improvements will require an additional investment of approximately \$50M - 60M (U.S.).

**Table 3-3:** Impact of the beam improvements under study on the neutrino  $\nu_\mu \rightarrow \nu_e$  CC appearance rates at the far detector in the range of the first and second oscillation maxima, shown as the ratio of appearance rates: the “improved” rate divided by the rate from the beam design described in the CDR.

Changes	0.5-2 GeV	2-5 GeV
DP Air $\rightarrow$ He	1.07	1.11
DP length 200m $\rightarrow$ 250m	1.04	1.12
Horn current 200 kA $\rightarrow$ 230 kA	1.00	1.12
Proton beam 120 $\rightarrow$ 80 GeV, 700 kW	1.14	1.05
Target graphite $\rightarrow$ Be	1.10	1.00
DP diameter 4 m $\rightarrow$ 6 m	1.06	1.02
Total	1.48	1.50



## 3.5 The LBNE Near Detector

**FIXME:** *new* According to the plan for LBNE phase 1 approved at CD-1, the neutrino beam will be monitored with a sophisticated array of muon detectors placed just downstream of the absorber, as shown in Figure 3-12. The ionization chamber array will provide pulse-by-pulse monitoring of the beam profile and direction. The variable-threshold gas Cherenkov detectors will map the energy spectrum of the muons exiting the absorber on an on-going basis. The stopped muon detectors will sample the lowest-energy muons, which are known to correlate fully with the neutrino flux above 3 GeV. **FIXME:** *what does it mean to ‘correlate fully’? Doesn’t sound quantified enough to be physics-speak* These detectors therefore sample the equivalent of about half the neutrino flux near the first oscillation maximum, and a decreasing fraction of it at lower energy. **FIXME:** *The connection leading to ‘therefore’ (was ‘thus’) isn’t clear to me, but if it is to physicists, then ok* Preliminary studies show that this system, augmented by the existing level of understanding of the similar NuMI beam and experience in previous neutrino oscillation experiments, will be adequate for the initial period of LBNE operations. With its excellent particle identification capabilities, an LArTPC far detector relies less on the near detector systems for calibration and neutrino interaction response studies **FIXME:** *than would WHAT? a water Cherenkov detector??*

**FIXME:** *old* According to the current plan for LBNE Phase-I, the neutrino beam will be monitored with a sophisticated array of muon detectors placed just downstream of the absorber, as shown in Figure 3-12. The ionization chamber array will provide pulse-by-pulse monitoring of the beam profile and direction. The variable-threshold gas Cherenkov detectors will map the energy spectrum of the muons exiting the absorber on an on-going basis. The stopped muon detectors will sample the lowest energy muons. The muons measured by this system correlate fully with the neutrino flux above 3 GeV. Thus, they sample the equivalent of about half the neutrino flux near the first oscillation maximum, and sample a decreasing fraction at lower energy. Preliminary studies show that this system, augmented by the existing level of understanding of the similar NuMI beam and experience in previous neutrino oscillation experiments, will be adequate for the initial period of LBNE running. We note that with its excellent particle identification capabilities, the choice of an LArTPC far detector results in less reliance on the near detector systems for calibration and neutrino interaction response studies.

**FIXME:** *new - 3 pgr* Nevertheless, a full near neutrino detector coupled with the tertiary-beam muon measurements is needed to achieve the full scientific agenda of LBNE. Discussions are in progress with potential international partners who could help build a highly-capable near neutrino detector in the initial phase or soon after LBNE begins operating. **FIXME:** *‘help’ build or just plain ‘build’? India would build it.*

The near neutrino detector needs to measure the unoscillated flux spectrum for all neutrino species in the beam:  $\nu_\mu$ ,  $\nu_e$ ,  $\bar{\nu}_\mu$ , and  $\bar{\nu}_e$ . This requires a magnetized detector with high efficiency for identifying and measuring electrons and muons. If, in addition, the detector is

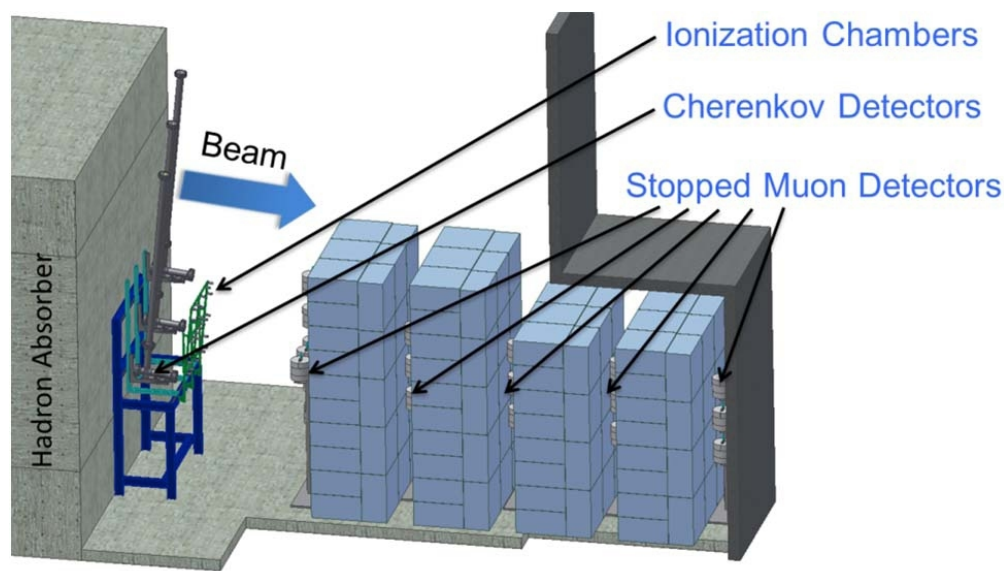


**Figure 3-12:** System of tertiary muon detectors, which will monitor the LBNE neutrino beam in the LBNE10 configuration

required to distinguish  $e^+$  from  $e^-$ , it would need to have a low-density and a commensurately long physical radiation length. **FIXME:** *How/when would it be decided that the detector needs this functionality?* To allow cancellation of systematic errors, the near detector would ideally use the same argon target nucleus and the same detection technique as the far detector, which suggests the use of a magnetized LArTPC.

The multiple requirements being somewhat at odds, **FIXME:** *This didn't jump out at me, should it have?* LBNE has considered two candidate near neutrino detector designs: a magnetized LArTPC and a magnetized straw-tube tracker with embedded high-pressure Ar gas targets (see Figure 3-13). Both designs are placed inside a 0.4 T dipole magnet, with muon detectors in the yoke steel and downstream steel absorbers. The lower-density straw-tube detector would be surrounded by an electromagnetic calorimeter inside the dipole coil.

**FIXME:** *old* Nevertheless, a full near neutrino detector coupled with the tertiary muon measurements is highly desirable in the long term, and is needed to achieve the full scientific agenda of LBNE. We are working with potential international partners who could help build a highly-capable near neutrino detector in the initial phase or soon after the operation of LBNE.

The neutrino near detector needs to measure the unoscillated flux spectrum for all species in the beam:  $\nu_\mu$ ,  $\nu_e$ ,  $\bar{\nu}_\mu$ , and  $\bar{\nu}_e$ . This requires a magnetized detector with has good efficiency for identifying and measuring electrons and muons. If, in addition, we require the detector to distinguish  $e^+$  from  $e^-$ , a low-density detector with a long physical radiation length would be required. The near detector should also make measurements using the same argon target nucleus as the far detector, and ideally should use the same detection technique as the far

detector to allow cancellation of systematic errors. The last requirement suggests the use of a magnetized LArTPC.

However the multiple requirements are somewhat at odds, and as a consequence LBNE has considered two candidate neutrino near detector designs: a magnetized LAr TPC and a magnetized straw-tube tracker with embedded high-pressure Ar gas targets (see Figure 3–13). Both are placed inside a 0.4 T dipole magnet, with muon detectors in the yoke steel and downstream steel absorbers. The lower-density straw-tube detector is also surrounded by an electromagnetic calorimeter inside the dipole coil.

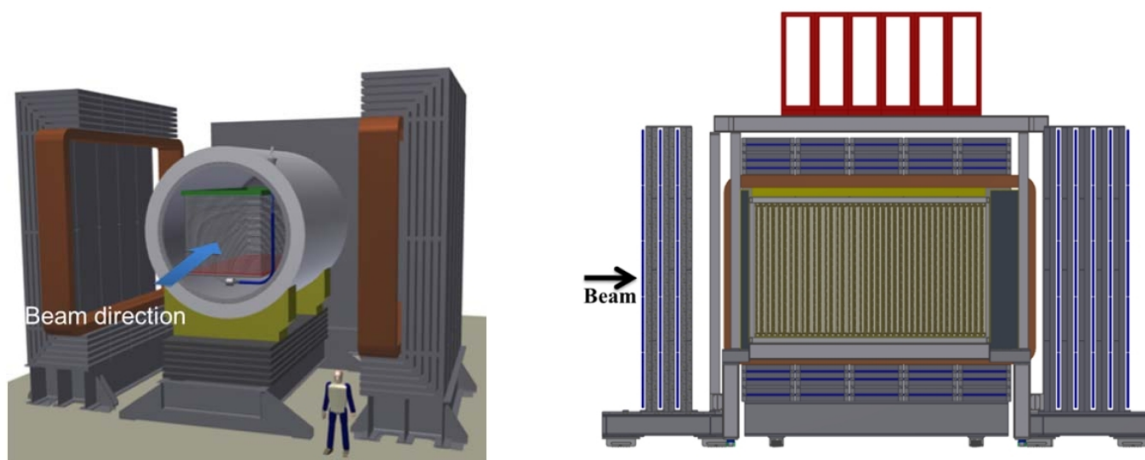


**Figure 3–13:** Two candidate near detectors: a magnetized LArTPC (left) and a magnetized straw-tube tracker with embedded high-pressure Ar gas targets (right)

**FIXME:** *new - 2 pgr* A full description of these two candidate detectors can be found in the March 2012 LBNE CDR (see Volume 3 of [?]). A more complete description of the straw-tube tracker design, including extensive discussion of its physics capabilities, can be found in [?].

The addition of a high-resolution near neutrino detector to LBNE, coupled with the precision absolute flux measurements from the tertiary muon detectors, will enable a diverse range of physics measurements as discussed in Chapter 4.

**FIXME:** *old* A full description of these two candidate detectors can be found in the March 2012 LBNE CDR (see Volume 3 of Ref. [?]). A more complete description of the straw-tube tracker design, including extensive discussion of its physics capabilities, can be found in Ref. [?].

The addition of a high resolution neutrino near detector to LBNE coupled with the precision absolute flux measurements from the tertiary muon detectors will enable a diverse range of physics measurements as discussed in Chapter 4.

## 3.6 The LBNE Far Detector

**FIXME:** *new - 2 pgr* Scalability has been a design consideration of critical importance for the LBNE project, and for the far detector in particular, since the project's inception in 2009. The surface 10-kt liquid argon time projection chamber (LArTPC) far detector configuration (LBNE10) has received CD-1 approval for the initial phase of LBNE. Other, more capable, configurations could be accomplished either in the initial phase with the identification of additional resources, or at a later stage (i.e., the fully realized LBNE configuration), assuming that scalability commensurate to the upgrade(s) is built in.

Other important considerations for the construction of a large LArTPC far detector include: (1) cryogenic safety and the elimination of hazards associated with large cryogenic liquid volumes, (2) attainment of stringent argon purity requirements ( $< 0.2$  ppb  $O_2$  concentration, for example) with respect to electronegative contaminants, (3) ease of transport and assembly of TPC mechanical systems, and (4) efficient deployment of high-sensitivity/low-noise electronics for readout of the ionization signal.

**FIXME:** *old* In this section we summarize the key features of the LBNE far detector. As mentioned earlier, the central design consideration throughout the LBNE development process has been the importance of scalability, and the flexibility that it enables. This has been of critical importance for the project as it has evolved since its inception in 2009. Thus, we start with a description of the surface 10-kt LArTPC far detector configuration that has been selected for the initial phase of LBNE and presented at CD-1. We also discuss the significant differences associated with other configurations that could be accomplished in the initial phase with the identification of additional resources, or at a later stage (i.e., the fully realized LBNE configuration). Because of the emphasis on scalability, these differences are modest and easily implemented.

Aside from scalability, general considerations for the construction of a large LArTPC include: (1) cryogenic safety and the elimination of hazards associated with large cryogenic liquid volumes, (2) attainment of stringent argon purity requirements ( $< 0.2$  ppb  $O_2$  concentration, for example) with respect to electronegative contaminants, (3) ease of transport and assembly of TPC mechanical systems, and (4) efficient deployment of high sensitivity/low-noise electronics for readout of the ionization signal.

### 3.6.1 Smaller Surface Detector for LBNE Phase 1

**FIXME:** *new* The far detector option presented at CD-1 for the LBNE phase 1 project (LBNE10) consists of two 9.4-kt liquid argon vessels, each designed to hold a 5-kt fiducial mass LArTPC as shown in Figure 3-14 [?]. The detector vessels will be constructed and operated at SURF in a detector hall on the surface, above the former Homestake mine. The

detector will require some overburden to shield against hadronic and electromagnetic showers from cosmic ray interactions. Construction of the detector hall thus requires excavation of a pit of depth 17.6 m, width 37.4 m, and length 30 m in which the vessels will sit, and the building containing this hall is designed to support the required three meters of overburden.

**FIXME:** *old* The far detector option presented at CD-1 for the LBNE Phase-I project (LBNE10) consists of two 9.4 kt liquid argon vessels, each designed to hold a 5-kt fiducial mass Liquid Argon Time Projection Chamber (LArTPC) as shown in Figure 3-14 (see Ref. [?]). The detectors will be constructed and operated in a detector hall on the surface of the SURF site, above the former Homestake mine. Construction of the detector hall requires excavation of a pit of depth 17.6m, width 37.4m, and length 30m such that the vessels will be below grade. The building in which this hall will be located is designed to support three meters of overburden to shield the detector against hadronic and electromagnetic showers from cosmic ray interactions.

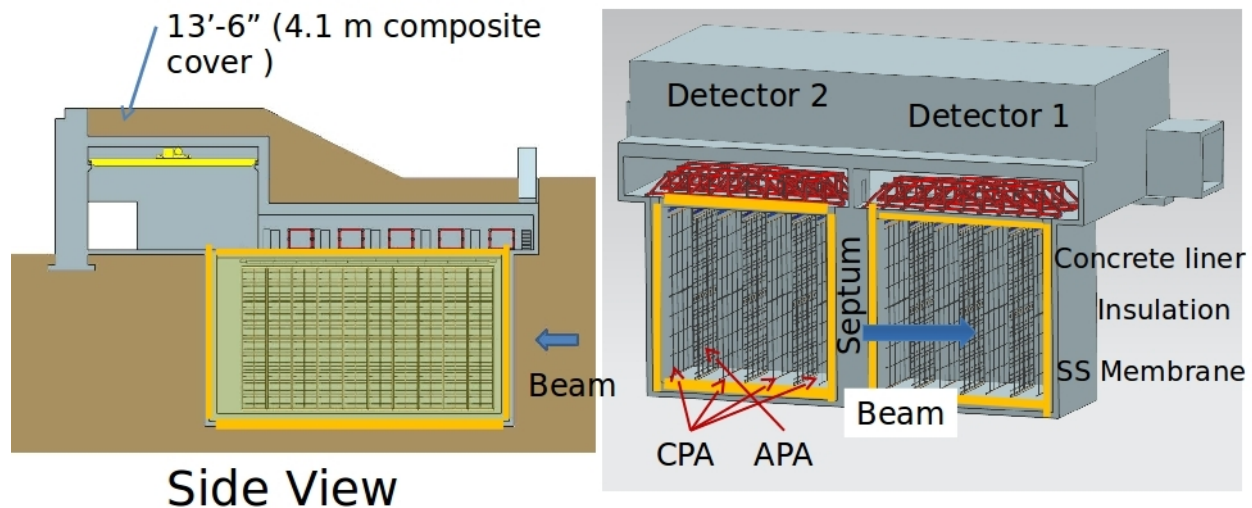


**Figure 3-14:** View of the far detector showing the building, overburden and access regions (left). 3D view of the detector showing the two modules and the orientation with the neutrino beam (right). **FIXME:** *Doesn't look professional enough to have the beam pointing in opposite directions in these two images.*

**FIXME:** *new* The choice of outfitting the far detector complex with two separately-instrumented detector vessels instead of a single, larger vessel has several benefits. First, this design enables each cryostat and TPC to be filled and commissioned while the other remains available for liquid storage, allowing for repairs to be made after the start of commissioning should that be necessary. Secondly, it allows deployment of TPCs of different designs. This may attract, for example, international partners with the resources to contribute a detector of an alternate design, enabling them to make a significant contribution to the project that unequivocally bears their stamp and/or addresses a particular research interest.

**FIXME:** *old* The choice of outfitting the far site detector complex with two separately-

instrumented detector vessels has several benefits. First, this design enables each cryostat and TPC to be filled and commissioned while the other cryostat is available for liquid storage. Thus this setup allows for repairs to be made after the start of commissioning should that be necessary. This two-vessel configuration also allows TPCs of different designs to be deployed. For example, international partners with the resources to construct a TPC of alternate design would be able to make a significant impact with such a contribution.

**FIXME:** *new - 2 pg* The detector vessels, as configured for LBNE10, will be constructed using technology standards from the liquid natural gas (LNG) industry. With similar requirements and geometries, adaptation of industrial LNG cryostat design provides a high-performance, extensively tested approach to the challenge of liquid argon containment for LBNE. The cryostats in large LNG tanker ships are constructed using a thin (1–2 mm), polished, stainless steel inner membrane surrounded by thick foam passive insulation. With stainless steel as the only wetted surface, this is an inherently clean design, ideal for liquid argon detectors where high purity is essential.

The cryogenics systems consist of three 55-kW liquid nitrogen liquefaction plants, a liquid argon receiving station, a liquid argon circulation system with liquid purifiers, and a liquid argon re-condensing system with gas purifiers. All the cryogenics systems are similar to large-scale systems found in industry applications.

**FIXME:** *old* The detector vessels will be constructed using technology standards used in the liquid natural gas (LNG) industry. With similar requirements and geometries, adaptation of industrial LNG cryostat design provides a high-performance, extensively tested approach to the challenge of the construction of large vessels for the containment of liquid argon for LBNE. The cryostats in large LNG tanker ships are constructed using thick foam insulation and a thin (1–2mm) stainless steel inner membrane, supported by the hull. This construction gives a completely passive cryostat with only stainless steel as the wetted surface, making it ideal for liquid argon detectors where high purity is essential.

The cryogenics systems consist of ... **FIXME:** *no change in new; deleted old*

**FIXME:** *new - 2 pgrph* The LBNE TPC design consists of four rows of cathode plane assemblies (CPAs) interspersed with three rows of anode plane assemblies (APAs), as shown in Figure 3-15 bottom right, with readout electronics mounted directly on the APA frames (Figure 3-15, left). These elements run the length of a cryostat module, save for space at one end allocated to the cryogenics systems. A field cage for shaping the electric field covers the top, bottom, and ends of the detector. In the surface detector, the CPA-APA spacing is 2.3 m, and the cathode planes will be operated at  $-114$  kV, establishing a drift field of 500 V/cm and a corresponding maximum drift time of 1.4 ms.

The APAs and CPAs are designed in a modular fashion as illustrated in Figure 3-15, top right. Each APA/CPA is constructed with a channel frame 2.5-m long and 7-m high; **FIXME:** *what does ‘channel frame’ mean?* these dimensions are chosen for ease of trans-

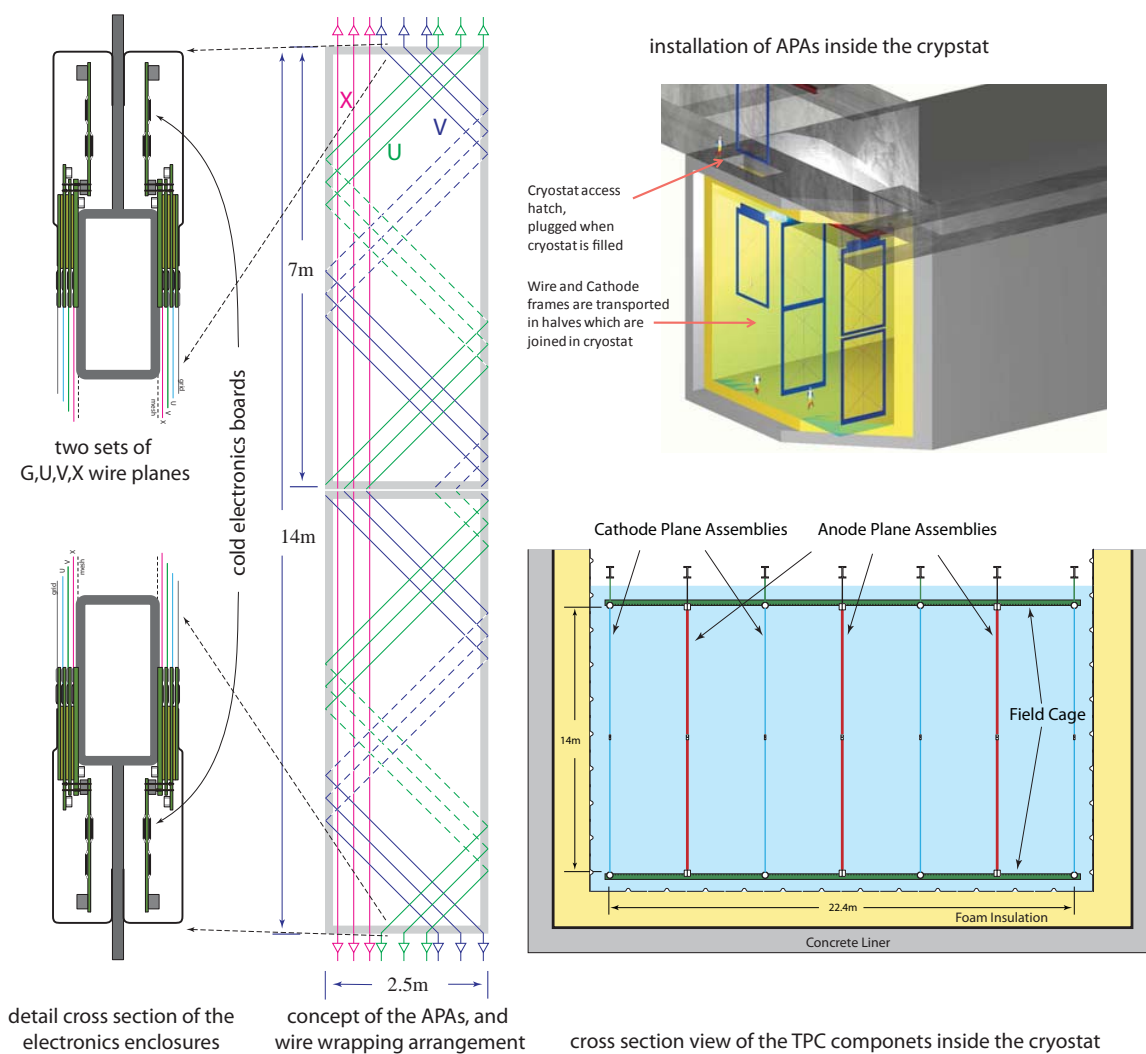


**Figure 3-15:** TPC modular construction concept

portation to the detector site and installation within the cryostat. During installation, two APAs are connected end-to-end to form a 14-m-tall, 2.5-m-long unit, which is transported to its final position in the detector and suspended there using a rail system at the top of the detector. Pairs of CPAs are installed in a similar fashion. This system of 2.5-m-long detector elements is easily scalable to any desired detector size. A total of 60 APAs and 80 CPAs per cryostat are needed for the LBNE10 detector design.

**FIXME:** *old* The LBNE TPC (see Figure 3-15) consists of 4 rows of cathode plane assemblies (CPA's) interspersed with three rows of anode plane assemblies (APA's) with readout electronics mounted directly on the APA frames. These elements run the length of a cryostat module, save for space at one end allocated for cryogenics systems. A field cage to shape the electric field covers the top, bottom, and ends of the detector. For the surface detector, the CPA-APA spacing is 2.3 meters, and the cathode planes will be operated at  $-114\text{ kV}$ , establishing a drift field of  $500\text{ V/cm}$  and a corresponding maximum drift time of 1.4 ms.

The APA's and CPA's are designed in a modular fashion as illustrated in Figure 3-15. Each APA/CPA is constructed with a channel frame 2.5m long and 7m high; these dimensions are chosen for ease of transportation to the detector site and installation within the cryostat. During installation two APAs are connected end-to-end to form a 14m tall 2.5m long unit, which is transported to its final position in the detector and suspended there using a rail system at the top of the detector. Pairs of CPA's are installed in a similar fashion. This system of 2.5m long detector elements enables easy scalability to any desired detector size. A total of 60 APAs and 80 CPAs per cryostat are needed for the present LBNE10 detector design.

**FIXME:** *new - 2 pg* Three sense wire planes (two *induction* planes and one *collection* plane) with wire pitches of 4.8 mm are mounted on each side of an APA frame, for sensitivity to ionization signals originating within the TPC cell on either side. The wires on these planes are oriented vertically (collection) and at  $\pm 45^\circ$  (induction). The induction plane wires are wrapped around the APA frame, and are therefore sensitive to charge arriving from either side of the APA, depending on where the charge arrives along the length of the wires. **FIXME:** *how does placement along the length of the wire relate to which side of the APA it's on?* **FIXME:** *Anything to say about the collection plane?* This configuration allows placement of readout electronics at the top and bottom of each two-APA unit. **FIXME:** *are the following details needed?* (Cables from the bottom APA are routed up through the channel frame, thereby eliminating any obstruction they would otherwise cause.) In this way, adjacent APA-pairs can be abutted so as to minimize the uninstrumented region in the gaps between them along the length of the detector.

Low-noise, low-power CMOS preamplifier and ADC ASICS have been developed for deployment on circuit boards mounted directly on the APA frames as indicated above. **FIXME:** *no prev mention of circuit bds* This scheme ensures good signal-to-noise performance, even allowing for some attenuation of long-drift ionization signals due to residual impurities in the argon. It also offers the possibility of digital signal processing, including multiplexing



and zero suppression at the front end, thereby limiting the cable plant within the cryostat and the number of penetrations required, while also easing requirements on the downstream readout/DAQ systems located outside the cryostat. The ASICs have been laid out following design rules developed explicitly for long-term operation at cryogenic temperatures.

**FIXME:** *old* Three sense wire planes with wire pitches around 5mm are mounted on each side of an APA frame, for sensitivity to ionization signals originating within the TPC cell on either side. These planes are oriented vertically (collection plane) and at  $\pm 45^\circ$  (induction planes). The wires on the induction planes are wrapped around the APA frame, thereby viewing charge arriving from different sides of the APA, depending on where the charge arrives along the length of the wires. This configuration allows placement of readout electronics at the top and bottom of the two-APA unit. (Cables from the bottom APA are routed up through the channel frame, thereby eliminating any obstruction they would otherwise cause.) In this way, adjacent APA-pairs can be abutted so as to minimize the uninstrumented region in the gaps between them along the length of the detector.

Low-noise, low-power CMOS preamplifier and ADC ASICs have been developed for deployment on circuit boards mounted directly on the APA frames as indicated above. This scheme ensures good signal-to-noise performance, even allowing for some attenuation of long-drift ionization signals due to residual impurities in the argon. It also offers the possibility of digital signal processing, including multiplexing and zero suppression, at the front end, thereby limiting the cable plant within the cryostat and the number of penetrations required, while also easing requirements on the downstream readout/DAQ systems located outside the cryostat. The ASICs have been laid out following design rules developed explicitly for long-term operation at cryogenic temperatures.

**FIXME:** *new* In order to operate on the surface it is necessary to accurately determine the event time relative to the neutrino beam crossing **FIXME:** *‘crossing’ refers to what point in time/space?* window. If the event time is known at the microsecond level then out-of-time cosmic ray backgrounds can be rejected to the level of  $10^{-5}$  (the beam spill duty factor), which is necessary to reduce the background rates to an acceptable level. The slow ionization-electron drift velocity gives the TPC its 3-D imaging capability, but an independent fast signal is required to localize events in time and in space along the drift direction. The excellent scintillation properties of liquid argon ( $\mathcal{O}(10^4)$  photons per MeV of energy deposition) are exploited to address this issue. A photon detection system is planned for detection of the 128-nm scintillation light that, in turn, allows determination of the event timing. Several photon detector designs are under study at present. The most advanced design uses cast acrylic bars coated with wavelength shifter, and SiPMs at the ends for read out. These bars will be assembled into paddles of dimensions 10 cm by 2 m, and mounted on the APA frames, fitting within the 5-cm gap between the sets of wire planes located on both sides of the frames. Initial studies indicate a light yield of 0.1 - 0.5 photoelectrons per MeV.

**FIXME:** *old* In order to operate on the surface it is necessary to accurately determine the

event time relative to the neutrino beam crossing window. If the event time is understood at the microsecond level then out-of-time cosmic ray backgrounds can be rejected to the level of  $10^{-5}$  (the beam spill duty factor), which is necessary to reduce the background rates to an acceptable level. The slow ionization electron drift velocity gives the TPC its 3-D imaging capability, but an independent fast signal is required to localize events in time and in space along the drift direction. For this we capitalize on the excellent scintillation properties of liquid argon ( $\mathcal{O}(10^4)$  photons per MeV of energy deposition). A photon detection system is planned to detect the 128nm scintillation light and thereby determine the event timing. Several detector designs are under study at present with the most advanced design being made of cast acrylic bars coated with wavelength shifter and read out at the ends with SiPM's. These bars would be assembled into paddles of dimensions 10cm by 2m, and would be able to be mounted on the APA frames, fitting within the 5cm gap between the sets of wire planes located on the two sides of the frames. Initial studies indicate a light yield of 0.1 – 0.5 photoelectrons per MeV is expected.

### 3.6.2 Larger Deep-Underground Detector

**FIXME:** *new* The physics for a surface experiment is likely to be limited to the neutrino beam program, as all other physics channels are compromised by cosmic ray backgrounds. If the detector can be moved deep underground, then sensitivity to supernova core collapse neutrinos, detection of nucleon decay and precision studies of atmospheric neutrinos all become viable. These additional physics programs would greatly broaden the scientific impact of LBNE.

**FIXME:** *old* The physics for a surface experiment is likely to be limited to the neutrino beam program, as all other physics channels are compromised by cosmic ray backgrounds. If the detector can be moved underground, then sensitivity to supernova core collapse neutrinos, detection of nucleon decay and precision studies of atmospheric neutrinos all become viable. These additional physics programs would greatly broaden the scientific impact of LBNE.

**FIXME:** *new* LBNE considers a deep underground placement of the detector to be of paramount importance. **FIXME:** *I removed 'goal' because its goals are the measurements it wants to make* The underground detector option was studied in detail during the conceptual design phase of LBNE and presented at the Fermilab Director's Independent Conceptual Design Review in March of 2012 [?]. Although significant effort was invested to minimize the (dominant) cost of the far site conventional facilities, the underground option was eventually deferred due to financial constraints, as described in Chapter 1.

The layout of a 34-kt fiducial mass detector at the 4850-foot level of SURF, with the detector modules placed end-to-end instead of side-by-side, is shown in Figure 3-16. The detailed design of this configuration is shown in Figure 3-17. The detector design is very similar to that for the surface detector. The modules are of the same design and similar photon

detectors are needed underground to provide triggers for non-beam related events. In order to reduce channel counts, and hence cost, however, the drift distance is increased to 3.5 m as allowed by the lower cosmic ray rate at depth.

The differential cost between the 10-kt detector at the surface versus the same detector underground is estimated to be \$140M (U.S. accounting), mainly due to the underground excavation and infrastructure costs. As an “incremental cost” of putting the LBNE far detector underground, it is clearly much less expensive than the cost of constructing an independent detector elsewhere dedicated to achieving non-beam objectives similar to LBNE’s (Section 2.1). The LBNE project is thus well positioned to place the detector underground at any stage should additional resources be identified by international partners. **FIXME:** *At any stage? I doubt it - after it’s installed at the surface, for example?*

**FIXME:** *old* The goal of LBNE is to place the detector deep underground. To that end, the underground detector option was studied in detail during the conceptual design phase of LBNE and presented at the Fermilab Director’s Independent Conceptual Design Review in March of 2012 [?]. The layout of a 34-kt fiducial mass detector at the 4850-foot level of SURF as shown in Figure 3-16. The detailed design of a 34-kt (fiducial) detector located at the 4850-foot level of SURF is shown in Figure 3-17. For this configuration the detector modules are end to end instead of side by side as on the surface. Significant effort has been invested to minimize the cost of the conventional facilities, but the underground option was eventually deferred due to financial constraints as described in Chapter 1. The underground detector design is very similar to that for the surface detector. It is constructed of modules of the same design as the surface detector. However, as a means of saving costs by reducing channel counts, the drift distance is increased to 3.5 m as allowed by the lower cosmic ray rate at depth. Similar photon detectors are needed underground to provide triggers for non-beam related events. The differential cost between a 10-kt surface detector and a 10-kt underground detector is estimated to be \$140M (U.S. accounting), mainly due to the underground excavation and infrastructure costs. Thus, constructing a dedicated detector elsewhere capable of performing the non-beam measurements listed above would cost much more than the incremental cost of taking the LBNE far detector underground. The project is thus well positioned to place the detector underground at any stage should the enabling funding be identified. The possibility of expanding the scope of the initial phase of LBNE is open, and would be enabled by resources brought in by international partners.

**FIXME:** *new* Given the modular design of the detector and the use of industrial technologies in the cryogenics system there is a great deal of flexibility in possible contributions from new international partners to expand the size of the detector, and/or liberate U.S. funds for the additional cost of moving the detector underground. The details of any scope change would depend on the interests, capabilities and resources of the new partners.

**FIXME:** *old* Given the modular design of the detector and the use of industrial technologies in the cryogenics system there is a great deal of flexibility in possible contributions from new international partners that could expand the size of the detector, and/or free up U.S. funds

for the additional cost of moving the detector underground. The details of any scope change would depend on the interests, capabilities and resources of the new partners.

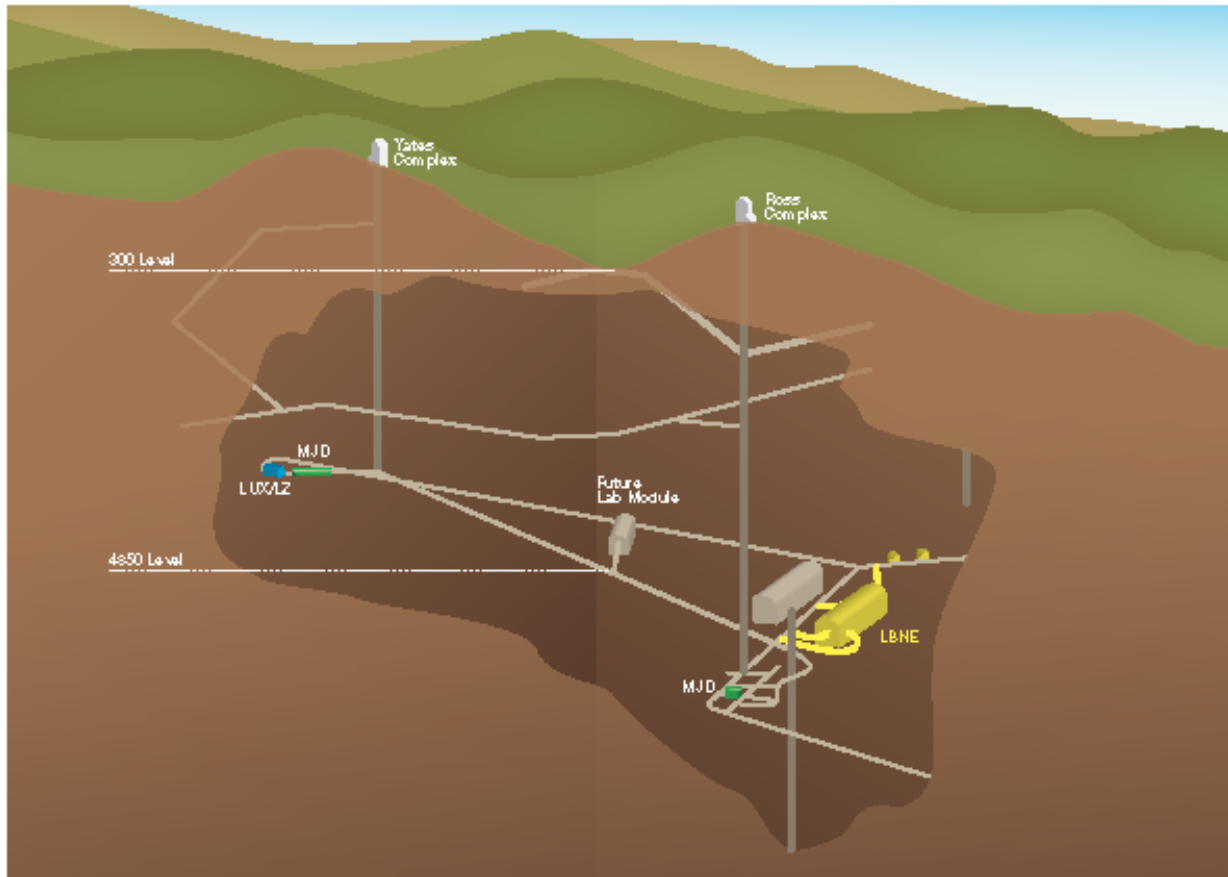


**Figure 3–16:** Layout of the 34-kt LAr detector hall at the 4850-foot level of SURF (yellow). A possible layout for an additional 34-kt LAr module is shown to the left of the LBNE module.

**FIXME:** *new* Information about the rock quality at the proposed underground location is available and simulations of the rock stress and resulting ground support have been performed. The LBNE far detector project team is embarking on an underground geotechnical exploration program that will map out in detail the location of the 34-kt module at the 4840 ft level of SURF. Demonstrating the expansion potential of the 4850 ft location, a schematic of the layout for an additional 70-kt module is shown in Figure 3–18. This location is estimated to accommodate a total of 100 kilotons of LArTPC detectors.

**FIXME:** *old* Information about the rock quality is available and simulations of the rock stress and resulting ground support have been performed. The LBNE far detector project team is embarking on an underground geo-technical exploration program that will map out in detail the location of the 34-kt module at the 4840 ft level of SURF. A schematic of the layout for an additional 70 kt module is shown in Figure 3–18. This schematic demonstrates

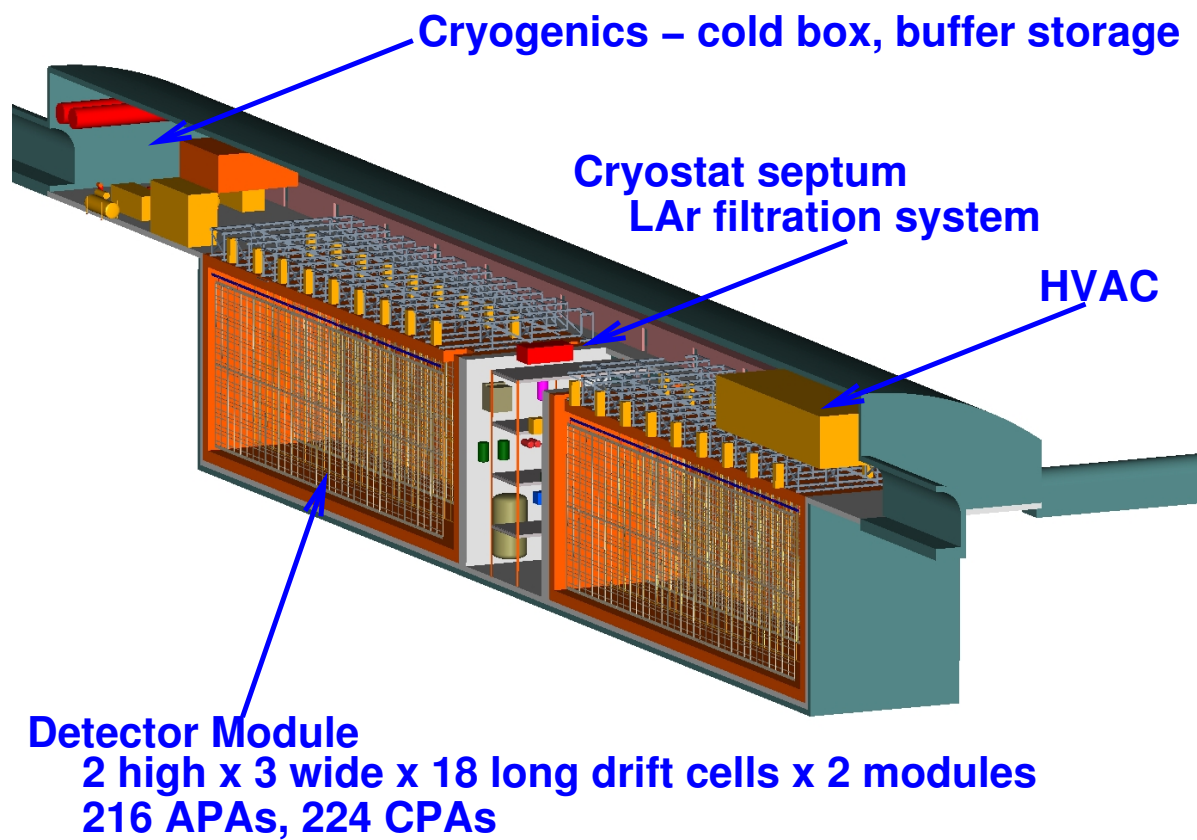


**Figure 3–17:** Schematic of the 34-kt LArTPC design.

the expansion potential of the 4850 ft location to accommodate a total of 100 kilotons of LArTPC detectors.

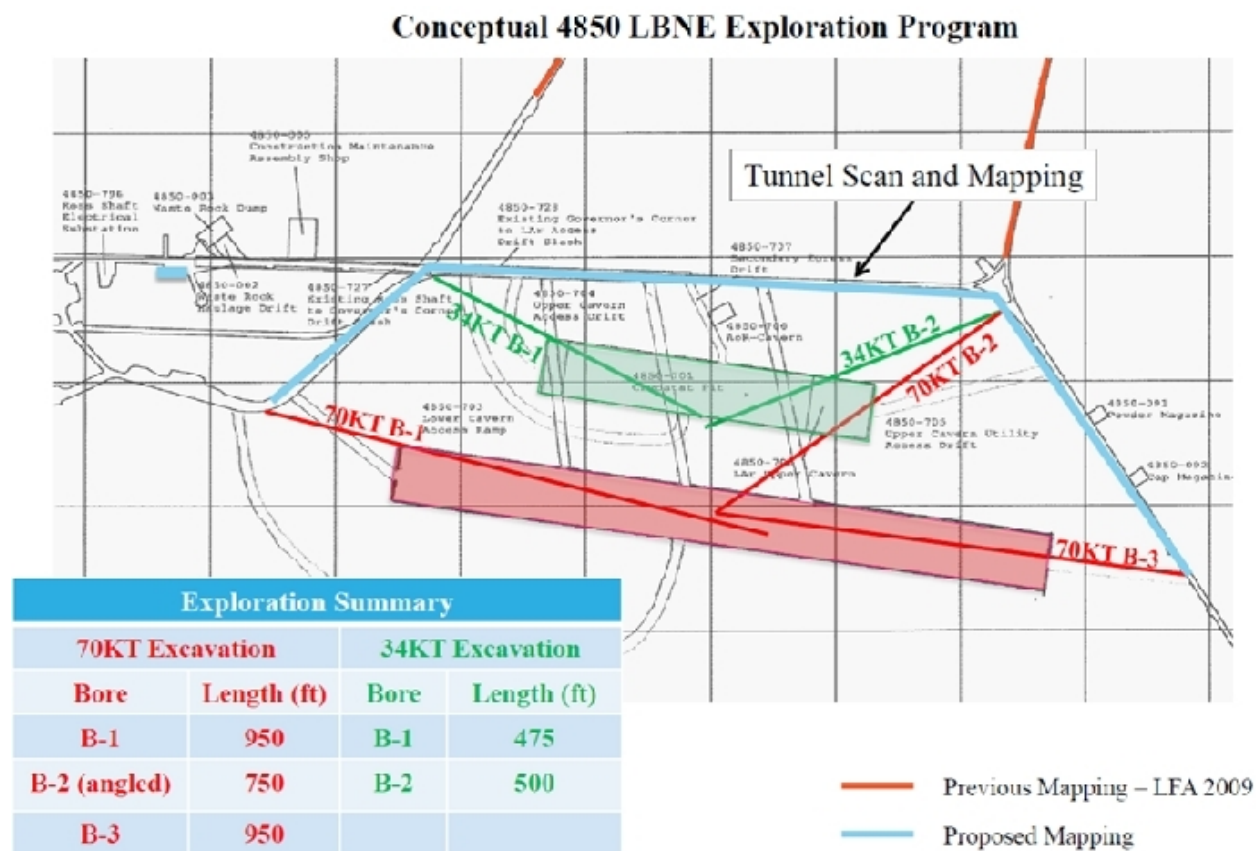


**Figure 3-18:** Possible layout for 70-kt + 34-kt LArTPC detector modules at the 4,850-ft level.

## 4 Long-Baseline Neutrino Oscillation Physics

**FIXME:** *I changed the few references to a 708 kW beam to 700 for consistency. Anne*

The LBNE Science Collaboration proposes to mount a broad investigation of the science of neutrino oscillations with sensitivity to all known mixing parameters in a single experiment, in particular,

1. precision measurements of the parameters that govern  $\nu_\mu \rightarrow \nu_e$  and  $\bar{\nu}_\mu \rightarrow \bar{\nu}_e$  oscillations; this includes precision measurement of the third mixing angle, measurement of the CP violating phase  $\delta_{CP}$ , and determination of the mass ordering (the sign of  $\Delta m_{32}^2$ );
2. precision measurements of  $\sin^2 2\theta_{23}$  and  $|\Delta m_{32}^2|$  in the  $\nu_\mu/\bar{\nu}_\mu$ -disappearance channel;
3. determination of the  $\theta_{23}$  octant using combined precision measurements of the  $\nu_e/\bar{\nu}_e$  appearance and  $\nu_\mu/\bar{\nu}_\mu$ -disappearance channels.
4. search for non-standard physics that can manifest itself in differences observed in higher-precision measurements of  $\nu_\mu$  and  $\bar{\nu}_\mu$  disappearance over long baselines.

### 4.1 Experimental Requirements Based on Oscillation Phenomenology

The general experimental parameters **FIXME:** *requirements* for designing a successful **FIXME:** *remove word, should be assumed* neutrino oscillation experiment to simultaneously address neutrino CP violation and the mass hierarchy can be extrapolated as follows **FIXME:** *moved* from the phenomenology summarized in Chapter 2:

1. *Phenomenology: An appearance experiment is necessary to extract the CP-violating effects.* Experimental requirements:

- The experiment probes oscillations of  $\nu_{\mu,e} \rightarrow \nu_{e,\mu}$
  - **FIXME:** *new* The experiment shall identify  $\nu_e$  and  $\nu_\mu$  with high efficiency and purity in order to tag (or otherwise know) the flavor of the neutrino at production and after flavor transformations.
  - **FIXME:** *old* The flavor of the neutrino at production and after flavor transformations must be tagged or known, therefore the experiment needs to identify  $\nu_e$  and  $\nu_\mu$  with high efficiency and purity.
  - **FIXME:** *new* The experiment shall perform flavor-tagging of muon neutrinos using the lepton flavor produced in a charged-current interaction such that  $\nu_\mu + N \rightarrow \mu N' X$  requires  $E_\nu > 100$  MeV. **FIXME:** *The original is ambiguous and I can't parse it properly*
  - **FIXME:** *old* The flavor tagging of muon neutrinos using the lepton flavor produced in a charged-current interaction such that  $\nu_\mu + N \rightarrow \mu N' X$  requires  $E_\nu > 100$  MeV.
2. **FIXME:** *new Phenomenology: In the three-flavor mixing model, the CP-violating Jarlskog invariant arises in the interference term  $P_{\sin\delta}$  as given by Equation 2.10; the oscillation scale where the interference term is maximal is that determined by the mixing between the 1-3 states.*
  3. **FIXME:** *old Phenomenology: In the 3 flavor mixing model, the CP violating Jarlskog invariant arises in the interference term  $P_{\sin\delta}$  as given by Equation 2.10, the oscillation scale where the interference term is maximal is that determined by the mixing between the 1-3 states.*

Experimental requirements:

- **FIXME:** *sm chgs only* The experimental baseline and corresponding neutrino energy are chosen according to Equation 2.13 such that  $L/E = 510$  km/GeV to maximize sensitivity to the CP-violating term in the neutrino flavor mixing.
  - **FIXME:** *sm chgs only* Flavor-tagging of muon neutrinos that can be produced either at the source or after flavor-mixing requires  $E_\nu > 100$  MeV; therefore, the experimental baselines over which to measure neutrino oscillations are  $L > 50$  km. \*
4. *Phenomenology: In the three-flavor model  $\nu_{\mu,e} \rightarrow \nu_{e,\mu}$  oscillations depend on all parameters in the neutrino mixing matrix as well as **FIXME:** on the mass differences, as shown in Equations 2.7 to 2.10.*

Experimental requirements:

---

\*Neutrino experiments using beams from pion decay-at-rest experiments such as DAE $\delta$ ALUS are exceptions since the  $\bar{\nu}_\mu$  production spectrum is well known and only the  $\bar{\nu}_e$  flavor after oscillations is tagged through inverse-beta decay. The neutrino energies are  $\sim 50$  MeV below the CC muon production threshold.



- **FIXME:** *This is not a requirement, it's just a statement. What's the requirement on LBNE? Is it 'precision measurement of all the mixing parameters within the three-flavor model'? What is the requirement on LBNE relative to other experiments in case it can't do it all by itself?* The precision with which  $\delta_{CP}$  can be determined - and the sensitivity to small CP violating effects or CP violation outside the 3-flavor model - requires precision determination of all the other mixing parameters - preferably in the same experiment.

5. *Phenomenology: Evidence for CP violation necessitates the explicit observation of an asymmetry between  $P(\nu_l \rightarrow \nu_{l'})$  and  $P(\bar{\nu}_l \rightarrow \bar{\nu}_{l'})$ .*

Experimental requirements:

- The experiment must **FIXME:** *shall* probe the oscillations of both neutrinos and antineutrinos in an unambiguous way.
- **FIXME:** *new* The experiment shall be capable of charge tagging in addition to flavor tagging. Charge tagging can be achieved at detection using the lepton charge and/or at production by selecting beams of pure neutrinos or antineutrinos.
- **FIXME:** *old* Charge tagging in addition to flavor tagging is required. Charge tagging can be achieved at detection using the lepton charge and/or at production by selecting beams of pure neutrinos or anti-neutrinos.
- **FIXME:** *new* The experiment shall be capable of resolving degeneracies between matter and potential CP asymmetries in order to determine the mass hierarchy. This can be achieved by using a baseline of  $> 1200$  km or with measurements probing oscillations over different  $L/E$ .
- **FIXME:** *old* The mass hierarchy is as yet undetermined. The experiment must be designed to resolve degeneracies between matter and potential CP asymmetries. This can be achieved by using a baseline of  $> 1200$  km or with measurements probing oscillations over different  $L/E$ .

6. *Phenomenology: CP asymmetries are maximal at the secondary oscillation nodes.*

Experimental requirements:

- **FIXME:** *what is the requirement?* Coverage of the  $L/E$  scale of the secondary oscillation nodes improves experimental sensitivity to small values of  $\delta_{CP}$  by enabling measurements of the asymmetry at the secondary nodes where the CP asymmetries are much larger and where there are no degeneracies with the matter asymmetries.
- **FIXME:** *new* The experimental baseline shall be  $> 150$  km, given that muon flavor tagging is required at either production or detection. The secondary oscillation nodes are located at scales set by Equation 2.13 where  $n > 1$ . The second oscillation maximum is located at scales given by  $L/E \sim 1500$  km/GeV.

- **FIXME:** *old* The secondary oscillation nodes are located at scales set by Equation 2.13 where  $n > 1$ . The second oscillation maximum is located at scales given by  $L/E \sim 1500 \text{ km/GeV}$ . If muon flavor tagging is required at production and/or detection, the experimental baseline is required to be  $> 150 \text{ km}$ .

**FIXME:** *new* Based on the experimental requirements prescribed by the neutrino oscillation phenomenology detailed above, pursuit of the primary science objectives for LBNE dictates the need for very large mass (10-100 kiloton-scale) neutrino detectors located at a distance of  $> 1000 \text{ km}$  from the neutrino source. A large mass coupled with a powerful wide-band beam and long exposures is required to accumulate enough neutrino interactions –  $\mathcal{O}(1000)$  events – to make precision measurements of the parameters that govern the sub-dominant  $\nu_\mu \rightarrow \nu_e$  oscillations. At 1,300 km, the baseline chosen for LBNE, both the first and second oscillation nodes are at neutrino energies  $> 0.5 \text{ GeV}$  as shown in Figure 4-1. This places both neutrino oscillation nodes in a region that is well matched to the energy spectrum of the high-power conventional neutrino beams that can be obtained using the 60-120 GeV Main Injector (MI) proton accelerator at Fermilab.

**FIXME:** *old* Based on the experimental requirements prescribed by the neutrino oscillation phenomenology detailed above, pursuit of the primary science objectives for LBNE dictates the need for very large mass (10-100 kiloton-scale) neutrino detectors located at a distance of  $> 1000 \text{ km}$  from the neutrino source. A large mass coupled with a powerful wide-band beam and long exposures is required to accumulate enough neutrino interactions –  $\mathcal{O}(1000)$  events – to make precision measurements of the parameters that govern the sub-dominant  $\nu_\mu \rightarrow \nu_e$  oscillations. At 1300 km, the baseline chosen for LBNE, both the first and second oscillation node are at neutrino energies  $> 0.5 \text{ GeV}$  as shown in Figure 4-1. This places both neutrino oscillation nodes in a region which is well matched to the energy spectrum of the high power conventional neutrino beams that can be obtained using the 60-120 GeV Main Injector (MI) proton accelerator at Fermilab.

## 4.2 May want a new heading here, not sure what

**FIXME:** *Physics to accomplish?...study shape of spectrum,  $\nu$  interaction rates*

**FIXME:** *new* The unoscillated  $\nu_\mu$  spectrum (flux  $\times$  cross-section) at 1,300 km obtained from the LBNE beamline using 80-GeV protons from the MI is shown as the black histogram in Figure 4-1. At this baseline, neither matter nor CP degeneracies occur at the first node where the LBNE neutrino beam spectrum peaks, phenomena that would limit the sensitivities of experiments with baselines  $< 1,000 \text{ km}$ . The wide coverage of the oscillation patterns enables the search for physics beyond the three-flavor model — physics that otherwise interferes with the standard oscillations and induces a distortion in the oscillation patterns. As a next-generation neutrino oscillation experiment, LBNE aims to study in detail the full spectral

shape of neutrino mixing where the mixing effects are largest. **FIXME:** *the full shape, or only where effects are largest? Plz clarify.* This is crucial for advancing the science beyond the current generation of experiments, which depend primarily on rate asymmetries. **FIXME:** *figure* The LBNE reconfiguration study [?] determined that the far detector location at SURF provides an optimal baseline for precision measurement of neutrino oscillations using a conventional neutrino beam from Fermilab. The 1,300-km baseline optimizes sensitivity to CP violation and is long enough to resolve the mass hierarchy with a high level of confidence, as shown in Figure 2-5.

**FIXME:** *old* The LBNE unoscillated  $\nu_\mu$  spectrum (flux  $\times$  cross section) at 1300 km obtained from the LBNE beamline using 80 GeV protons from the MI is shown as the black histogram in Figure 4-1. In addition, at this baseline, there are no matter and CP degeneracies at the first node where the Fermilab neutrino beam spectrum peaks. These degeneracies limit the sensitivities of experiments with baselines  $< 1000$  km. The wide coverage of the oscillation patterns also enables the search for physics beyond the 3 flavor model that interferes with the standard oscillations and induces a distortion in the oscillation patterns. As a next generation neutrino oscillation experiment, LBNE aims to study in the detail the full spectral shape of neutrino mixing where the mixing effects are largest. This is crucial for advancing the science beyond the current generation of experiments which depend primarily on rate asymmetries. The LBNE reconfiguration study [?] determined that the Far Detector location at SURF

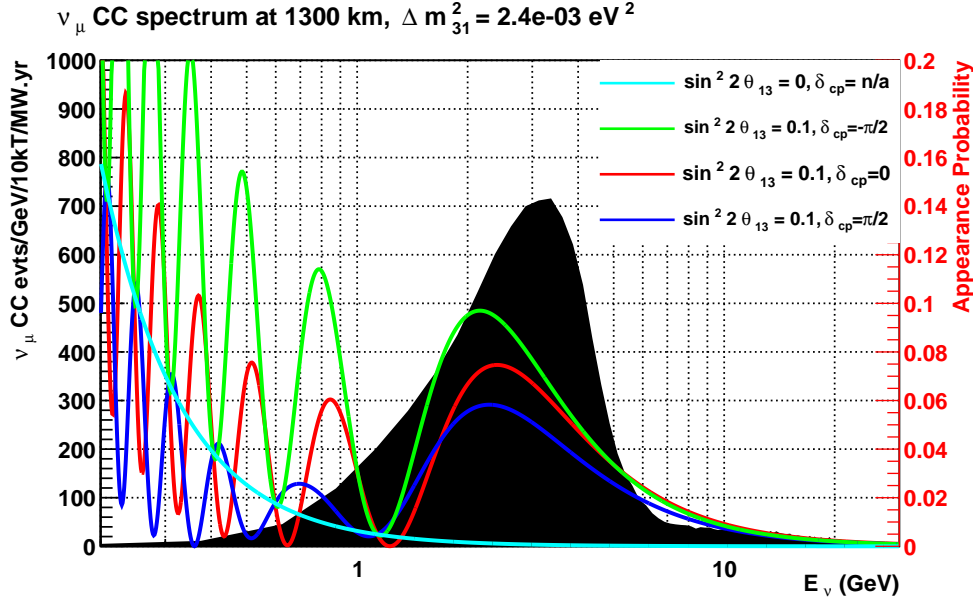


**Figure 4-1:** The **FIXME:** *simulated* unoscillated spectrum of  $\nu_\mu$  events from the LBNE beam (black histogram) overlaid with the  $\nu_\mu \rightarrow \nu_e$  oscillation probabilities (colored curves) for different values of  $\delta_{CP}$  and normal hierarchy.

provides an optimal baseline (1,300 km) for precision measurement of neutrino oscillations using a conventional neutrino beam from Fermilab. The 1300 km baseline produces the best

sensitivity to CP violation and is long enough to resolve the mass hierarchy with a high level of confidence, as shown in Figure 2–5.

**FIXME: new** Table 4–1 lists the beam neutrino interaction rates for all three known species of neutrinos as expected at the LBNE far detector. A tunable beam spectrum, obtained by varying the distance between the target and the first focusing horn (Horn 1), is assumed. The higher-energy tunes are chosen to enhance the  $\nu_\tau$  appearance signal and improve the oscillation fits to the three-flavor paradigm. For comparison, the rates at current neutrino oscillation experiments such as T2K, MINOS and NO $\nu$ A are shown for similar exposure in mass and time. For LBNO, the event rates are obtained using the optimized beam from the HP-PS2 50-GeV synchrotron [?] with an exposure of  $3 \times 10^{21}$  POT/year. This would correspond to a beam power of  $\sim 1.2$  MW if a duty cycle of  $\sim 2 \times 10^7$  s/year is assumed. Note that for Stage 1 and Stage 2 of the NuMAX neutrino factory proposal [?], Project X beams at 3 GeV with 1 and 3 MW, respectively, are needed. Table 4–1 shows only the raw interaction rates. No detector effects are included. It is clear that the LBNE beam design and baseline produce high rates of  $\nu_e$  appearance coupled with larger rate asymmetries when CP-violating effects are included. LBNE has higher appearance rates with a 700-kW Main Injector beam even when compared to Stage 1 of the NuMAX neutrino factory with a 1-MW beam from Project X upgrades <sup>†</sup>.

**FIXME: old** Table 4–1 lists the beam neutrino-interaction rates for all three known species of neutrinos as expected at the LBNE Far Detector site. A tunable beam spectrum, obtained by varying the distance between the target and the first focusing horn (Horn 1), is assumed. The higher energy tunes are chosen to enhance the  $\nu_\tau$  appearance signal, and improve the oscillation fits to the 3 flavor paradigm. For comparison, the rates at current neutrino oscillation experiments such as T2K, MINOS, NO $\nu$ A are shown for similar exposure in mass and time. For LBNO, the event rates are obtained using the optimized beam from the HP-PS2 50 GeV synchrotron [?] with an exposure of  $3 \times 10^{21}$  POT/year. This would correspond to a beam power of  $\sim 1.2$  MW if a duty cycle of  $\sim 2 \times 10^7$  s/year is assumed. Note that for Stage 1 and Stage 2 of the NuMAX neutrino factory proposal presented here [?], Project X beams at 3 GeV with 1 and 3 MW respectively are needed. Table 4–1 shows only the raw interaction rates. No detector effects are included. It is clear that the LBNE beam design and baseline produce high rates of  $\nu_e$  appearance coupled with larger rate asymmetries when CP violating effects are included. LBNE has higher appearance rates with a 700 kW Main Injector beam even when compared to Stage 1 of the NuMAX neutrino factory with a 1 MW beam from Project X upgrades <sup>‡</sup>.

---

<sup>†</sup>The corresponding MI power would be 1.2 MW for the neutrino program with this phase of Project X

<sup>‡</sup>The corresponding MI power would be 1.2 MW for the neutrino program with this phase of Project X

**Table 4-1:** Raw  $\nu$  oscillation event rates at the LBNE far site with  $E_\nu < 10$  GeV. Assumes  $1.8 \times 10^7$  seconds/year (Fermilab). Oscillation parameters used are:  $\theta_{12} = 0.587$ ,  $\theta_{13} = 0.156$ ,  $\theta_{23} = 0.670$ ,  $\delta m^2 = 7.54 \times 10^{-5} eV^2$ , and  $\Delta m^2 = 2.47 \times 10^{-3} eV^2$ . The NC event rate is for events with visible energy  $> 0.5$  GeV. The rate is given for an exposure of 50 kt.yrs. For comparison, the rates at other neutrino oscillation experiments (current and proposed) are shown for similar exposure in mass and time. Note that for the first 2 stages of the NuMAX proposal the beam power requires Project X upgrades and is higher than that assumed for LBNE. The duty factor for the JPARC beam is  $\sim 1/3$  of NuMI/LBNE. There are no detector effects included.

Beam	$\nu_\mu$ unosc. CC	$\nu_\mu$ osc. CC	$\nu_e$ beam CC	$\nu_\mu$ NC	$\nu_\mu \rightarrow \nu_\tau$ CC	$\nu_\mu \rightarrow \nu_e$ CC $\delta_{CP} = -\pi/2, 0, \pi/2$		
LBNE low energy beam 80 GeV, 700 kW $9 \times 10^{20}$ POT/year								
50 kt-years $\nu$	7421	2531	63	1953	91	353	280	204
50 kt-years $\bar{\nu}$	2478	812	20	876	28	30	50	62
LBNE medium energy beam 120 GeV, 700 kW $6 \times 10^{20}$ POT/year								
50 kt-years $\nu$	11441	7185	42	3388	400	254	233	171
T2K: 295 km 30 GeV, 750 kW $9 \times 10^{20}$ POT/year								
50 kt-years $\nu$	2100	898	41	360	$< 1$	73	58	39
MINOS: 735 km 120 GeV, 700 kW $6 \times 10^{20}$ POT/year LE Beam								
50 kt-years $\nu$	17574	11223	178	4806	115	345	326	232
50 kt-years $\bar{\nu}$	5607	3350	56	2017	32	58	85	88
NOvA: 810 km 120 GeV, 700 kW $6 \times 10^{20}$ POT/year								
50 kt-years $\nu$	4676	1460	74	1188	10	196	168	116
50 kt-years $\bar{\nu}$	1388	428	19	485	2	22	35	41
LBNO: 2300 km 50 GeV $\sim 1.2$ MW $3 \times 10^{21}$ POT/year								
50 kt-years $\nu$	8553	2472	48	2454	570	534	426	336
50 kt-years $\bar{\nu}$	3066	828	15	1140	255	24	45	54
Neutrino Factory	$\nu_\mu$ unosc. CC	$\nu_\mu$ osc. CC		$\nu_\mu$ NC	$\nu_\mu \rightarrow \nu_\tau$ CC	$\nu_e \rightarrow \nu_\mu$ CC $\delta_{CP} = -\pi/2, 0, \pi/2$		
NuMAX Stage 1: 1300km 3 GeV, 1MW, no cooling $0.94 \times 10^{20}$ $\mu$ decays/year								
50 kt-years $\mu^+$	1039	339		484	28	71	97	117
50 kt-years $\mu^-$	2743	904		945	89	24	19	12
NuMAX Stage 2: 1300km 3 GeV, 3MW $5.6 \times 10^{20}$ $\mu$ decays/year								
50 kt-years $\mu^+$	6197	2018		2787	300	420	580	700
50 kt-years $\mu^-$	16349	5390		5635	534	139	115	85

## 4.3 LBNE Detector Simulation and Reconstruction

A 10-kt-scale LArTPC far detector, the LAr-FD (or FD), fulfills the high-mass requirement for LBNE and provides excellent particle identification with high signal-selection efficiency ( $\geq 80\%$ ) over a wide range of energies as described in the LBNE Conceptual Design Report Volume 1 [?]. The status of the LBNE LArTPC simulation and reconstruction efforts, and expected performance is summarized in this section.

### 4.3.1 Far Detector Simulation

Interactions of events **FIXME:** *Can't we just say 'events'?* in the LAr-FD are simulated with GEANT4 [?] using the LArSoft [?] package. LArSoft is being developed to provide an integrated, experiment-agnostic set of software tools to perform simulation, data reconstruction and analysis for LArTPC neutrino experiments. The experiments provide experiment-specific pieces of the analysis code that interface to LArSoft, and contribute to the development effort required to produce the LArSoft software. LArSoft is based on *art*, an event-processing framework developed and supported by the Fermilab Scientific Computing Division as a way to share a single framework across many experiments. LArSoft is also managed by the Fermilab Scientific Computing Division.

*Art* is used by several intensity frontier experiments, including NOvA, Mu2e, MicroBooNE, and ArgoNeuT. The latter two experiments are based on liquid argon TPCs, and thus share many event-simulation challenges with LBNE. Besides offering a shared code base, LArSoft has the advantage that reconstruction algorithms advanced by ArgoNeuT and MicroBooNE can readily benefit LBNE. Examples of neutrino beam interactions in an LArTPC obtained from the LArSoft package using the MicroBooNE detector geometry are shown in Figure 4-2.

**FIXME:** *new* The LBNE FD design is summarized in Section 3.6. The LBNE FD geometries that are available in LArSoft currently are the LBNE10 10-kT surface detector and the 34-kt underground detector. The 35-ton prototype geometry is also included.

Following the MicroBooNE example, the LBNE FD geometries are specified in GDML files, which are created using Perl scripts. These scripts are easily customizable in order to modify detector design parameters, such as the wire spacing and angles, drift distances, and materials. The photon detectors are included as acrylic bars coated with wavelength-shifting TPB, and are read out with SiPMs.

GEANT4 is used to model particles traveling through the active and inactive detector volumes and the surrounding materials such as the cryostat and rock. The simulation of photons and electrons produced by the ionized argon however is parameterized as there are tens of

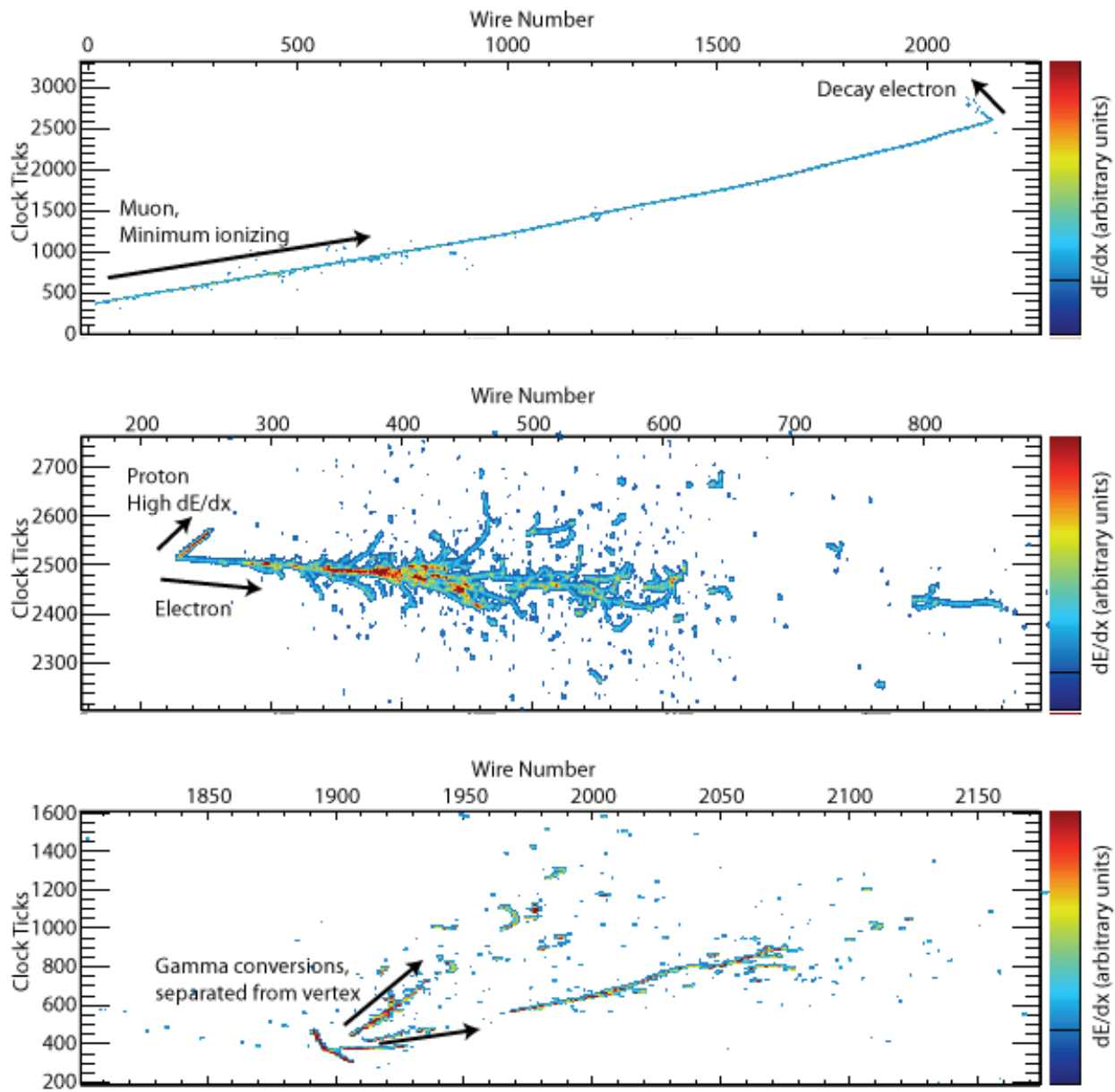


**Figure 4-2:** Examples of neutrino beam interactions in an LArTPC obtained from a GEANT4 simulation [?]. A CC  $\nu_\mu$  interaction with a stopped  $\mu$  followed by a decay Michel electron (top), a CCQE  $\nu_e$  interaction with a single electron and a proton (middle), an NC interaction which produced a  $\pi^0$  that then decayed into two  $\gamma$ 's with separate conversion vertices (bottom)

thousands of these quanta per MeV of energy deposited. **FIXME:** *why 'however'? What would they be if not parametrized? Clarify prev sentence.* The drifting electrons are parameterized by many small clouds of charge that diffuse as they travel towards the collection wires. These electrons are recorded as functions of drift time. **FIXME:** *do you 'record' as a function of something? or maybe 'process'?* The response of the channels to the drifting electrons is modeled parametrically with a separate response function for collection and induction wires. The signals on the induction plane wires are **FIXME:** *simulated as?* measurements of the induced currents as functions of time and are thus bipolar as charge drifts past the wires. The signals on the collection plane wires are unipolar. **FIXME:** *Is it obvious why?* The response functions include the expected response of the electronics. For the 10-kt FD, a 1.5 ms readout of the TPC signals 2 MHz gives a data volume of just under 2 GB per event. **FIXME:** *come back to* More will be required if the readout is extended before and after the drift time including the beam window, which will be required in order to collect charge deposited by cosmic rays which would otherwise be partially contained.

**FIXME:** *old* The LBNE far detector (FD) design is summarized in Section 3.6. The LBNE FD detector geometries that are available in LArSoft currently are the 10 kT surface detector and the 34-kt underground detector. The 35t prototype geometry is also included. Following the MicroBooNE example, the LBNE FD geometries are specified in GDML files, which are created using Perl scripts. These scripts are easily customizable in order to modify detector design parameters, such as the wire spacing and angles, drift distances, and materials. The photon detectors are included as acrylic bars coated with wavelength-shifting TPB, and are read out with SiPM's. GEANT4 is used to model particles traveling through the active and inactive detector volumes and the surrounding materials such as the cryostat and rock. The simulation of photons and electrons produced by the ionized argon however is parameterized as there are tens of thousands of these quanta per MeV of energy deposited. The drifting electrons are parameterized by many small clouds of charge that diffuse as they travel towards the collection wires. These electrons are recorded as functions of drift time. The response of the channels to the drifting electrons is modeled parametrically with a separate response function for collection and induction wires. The signals on the induction plane wires are measurements of the induced currents as functions of time and are thus bipolar as charge drifts past the wires. The signals on the collection plane wires are unipolar. The response functions include the expected response of the electronics. For the 10-kt FD, a 1.5 ms readout of the TPC signals 2 MHz gives a data volume of just under 2 GB per event. More will be required if the readout is extended before and after the drift time including the beam window, which will be required in order to collect charge deposited by cosmic rays which would otherwise be partially contained.

**FIXME:** *new* Noise is simulated with **FIXME:** *modeled on?* a realistic spectrum measured in the ArgoNeuT detector. The decays of  $^{39}\text{Ar}$  are included, but some work is required to make them more realistic. In order to reduce the data volume and speed up the calculation, long strings of consecutive ADC counts below a specifiable threshold are suppressed in the readout. Huffman coding of the remaining data is also included in the digitization. **FIXME:** *what does huffman coding do vis-a-vis noise?*



The photon system likewise requires a full simulation of the particle steps. **FIXME:** *particle steps?* Photons propagating from the TPC to the acrylic bars have been fully simulated using GEANT4, and their probabilities of striking each bar as functions of the emission location and the position along the bar at which the photon strikes have been computed. Smooth parameterizations of these functions are currently used in the simulation to compute the average numbers of photons expected to strike a bar as a function of position along the bar.

Given the current design of the optical detectors, approximately 2-3% of VUV photons produced uniformly in the fiducial detector volume strike the bars. This low number is largely due to the small fraction of the total area in contact with the argon that is represented by the bars, and the low reflectivity of the stainless steel cathode planes, field cage, and CuBe wires. A second function is used to parameterize the attenuation of light within the bar as a function of position along the bar. The expected number of photons surviving propagation, downconversion, attenuation in the bar and the detection efficiency of the SiPM is then used as the mean of a Poisson distribution for simulating individual photons **FIXME:** *I can't parse this unambiguously.* The measured waveforms for cold SiPMs are used in simulating the digitized response. Measurements in prototype dewars will be used to normalize the yield for signals on the SiPMs as a function of the incident location of the VUV photon on the bar. The NEST [?] model, which describes the conversion of ionization energy into both electrons and photons in an anticorrelated manner, and which has been shown to model a large range of data from noble liquid detectors, is currently being incorporated into the LBNE detector simulation.

**FIXME:** *old* Noise is simulated with a realistic spectrum measured in the ArgoNeuT detector. The decays of  $^{39}\text{Ar}$  are included, but some work is required to make them more realistic. In order to reduce the data volume and speed calculation, long strings of consecutive ADC counts below a specifiable threshold are suppressed in the readout. Huffman coding of the remaining data is also included in the digitization.

The photon system likewise requires a full simulation of the particle steps. Photons propagating from the TPC to the acrylic bars have been fully simulated using GEANT4, and their probabilities of striking each bar as functions of the emission location and the position along the bar at which the photon strikes have been computed. Smooth parameterizations of these functions are currently used in the simulation to compute the average numbers of photons expected to strike a bar as a function of position along the bar. Given the current design of the optical detectors, approximately 2-3% of VUV photons produced uniformly in the fiducial detector volume strike the bars. This low number is largely due to the small fraction of the total area in contact with the argon that is represented by the bars, and the low reflectivity of the stainless steel cathode planes, field cage, and CuBe wires. A second function is used to parameterize the attenuation of light within the bar as a function of position along the bar. The expected number of photons surviving propagation, downconversion, attenuation in the bar and the detection efficiency of the SiPM is then used as the mean of a Poisson distribution for simulating individual photons. The measured waveforms for cold SiPM's are used in simulating the digitized response. Measurements in prototype

dewars will be used to normalize the yield for signals on the SiPM's as a function of the incident location of the VUV photon on the bar. The NEST [?] model which describes the conversion of ionization energy into both electrons and photons in an anticorrelated manner is currently being incorporated into the LBNE detector simulation. The modeling of NEST has been shown to model a large range of data from noble liquid detectors.

**FIXME:** *new 3 pgrph* A variety of different event generators is available for use in simulating events. Neutrino hard scattering interactions and subsequent nuclear breakup are simulated using GENIE [?], though other generators are possible. Cosmic rays are simulated with CRY [?]. Single particles can be generated one at a time, and general text-file interfaces are available allowing arbitrary generators to be used without linking them in with LArSoft.

Currently, samples of single electrons, muons, charged and neutral pions, protons and tau leptons have been generated and simulated using the 10-kT surface geometry and the 35-ton geometry, though without photon detector simulation. These samples are being used to develop reconstruction algorithms.

Future directions include interfacing the simulation to a calibration database, updating the response functions with measured responses from MicroBooNE, which uses an electronics design very similar to LBNE's (including the effects of space charge buildup in the drift volume) and more detailed maps of the drift in the gaps between the APAs and for charge that is deposited between the wire planes.

**FIXME:** *old* A variety of different event generators is available for use in simulating events. Neutrino hard scattering interactions and subsequent nuclear breakup are simulated using GENIE [?], though other generators are possible. Cosmic rays are simulated with CRY [?]. Single particles can be generated one at a time, and general text-file interfaces are available allowing arbitrary generators to be used without linking them in with LArSoft.

Currently, samples of single electrons, muons, charged and neutral pions, protons, and tau leptons have been generated and simulated using the 10 kT surface geometry and the 35 ton geometry, though without photon detector simulation. These samples are being used to develop reconstruction algorithms.

Future directions include interfacing the simulation to a calibration database, updating the response functions with measured responses from MicroBooNE which uses electronics which are very similar to LBNE's design, including the effects of space charge buildup in the drift volume, and more detailed maps of the drift in the gaps between the APA's and for charge that is deposited between the wire planes.

### 4.3.2 Far Detector Reconstruction

**FIXME:** *new* The first stage of reconstruction of TPC data is unpacking and deconvoluting the electronics and field response of the wire planes. The deconvolution function includes a noise filter that currently is parameterized with ArgoNeuT’s noise, but will be tuned for the eventual noise observed in the LBNE detector.

The deconvolution makes sharp, unipolar pulses from the bipolar induction-plane signals and also sharpens the response to collection-plane signals. Hits are then identified in the deconvoluted signals by fitting Gaussian functions, allowing for sums of several overlapping hits in each cluster. The inefficiencies specific to LBNE at this stage — in CPU and memory — arise largely from the quantity of channels in the FD, and will be addressed by rearrangement of the processing.

In ArgoNeuT and MicroBooNE the next step, reconstruction, proceeds with Hough line-finding and clustering in 2D using an algorithm called “fuzzy clustering.” [?] This clustering is performed in each view separately. **FIXME:** *What’s a view?* Three-dimensional track-fitting is performed using a Kalman filter [?], and dedicated algorithms have been developed to optimize electromagnetic shower reconstruction and energy resolution. **FIXME:** *I can’t tell which things are related. Would the sentence be better as “This clustering is performed in each view separately and 3D track-fitting is performed using a Kalman filter [?]. Dedicated algorithms have been developed to optimize electromagnetic shower reconstruction and energy resolution.”*

**FIXME:** *old* The first stage of reconstruction of TPC data is unpacking and deconvoluting the electronics and field response of the wire planes. The deconvolution function includes a noise filter which must be tuned for the eventual noise observed in the detector but is parameterized with ArgoNeuT’s noise for the moment. The deconvolution makes sharp, unipolar pulses from the bipolar induction-plane signals and also sharpens the response to collection-plane signals. Hits are then identified in the deconvoluted signals by fitting Gaussian functions, allowing for sums of several overlapping hits in each cluster. The challenges specific to LBNE at this stage largely arise from the large numbers of channels in the FD, and requires rearrangement of the processing in order to be efficient in CPU and memory.

Reconstruction in ArgoNeuT and MicroBooNE then proceeds with Hough line-finding and clustering in 2D using an algorithm called “fuzzy clustering.” [?]. This clustering is performed in each view separately. Three-dimensional track-fitting is performed using a Kalman filter [?], and dedicated algorithms have been developed to optimize electromagnetic shower reconstruction and energy resolution.

**FIXME:** *new 2 pgph* LBNE poses unique challenges for reconstruction for a couple of reasons: the APA frames are located within the fiducial volume and the induction-plane wires wrap around the edges of the APA frames. Since the hit data on LArTPCs are inherently

two-dimensional – wire number and arrival time of the charge, if the deposition time is unknown, the location of the initial ionization point has a 2D ambiguity. For beam events, the  $t_0$  is known, and thus only a one-dimensional ambiguity remains. This 1D ambiguity is broken by angling the induction plane wires relative to the collection plane wires, in order to measure the  $y$  location of the hits for which  $t$  (thus  $x$ ) and  $z$  are known. For (non-beam) cosmic-ray signals which arrive uniformly in time, the photon system provides  $t_0$ .

LBNE’s wrapping of the induction plane wires introduces discrete ambiguities that are not present in other LArTPC designs, however. Whereas a hit on a collection-plane wire identifies uniquely the side of the APA from which it came, this is not known for a hit on an induction-plane wire. The angles between the  $U$  and  $V$  plane wires **FIXME:** *have these been defined?* are slightly different from  $45^\circ$  and from each other in order to assist **FIXME:** *or enable?* breaking the ambiguities. A combinatoric issue arises, however, if many hits arrive on different wires at nearly the same time, for instance when a track, or even a track segment, propagates in a plane parallel to the wire planes (i.e., at constant drift distance). Showers will also contain many hits on different wires that arrive at similar times. Hits that arrive at different times can be uniquely associated in the  $Z$ ,  $U$ , and  $V$  views **FIXME:** *associated together or each associated with its appropriate view or vertex or something?*, while hits that arrive at similar times must be associated **FIXME:** *same question* using a topological pattern-recognition technique. LBNE is developing a version of the fuzzy clustering tool for use as a pattern recognition step. This will allow association of  $Z$ ,  $U$ , and  $V$  hits, a step that is needed to assign the correct  $y$  position to a track segment or portion of a cluster. This process is called “disambiguation” of the induction hits. Misassignment can affect particle ID performance and reconstructed energy resolution. Fully-contained tracks may appear partially contained and vice versa **FIXME:** *because of misassignment?*. After this step, standard track, vertex, and cluster reconstruction algorithms are applied. **FIXME:** *this pgraph needs work*

**FIXME:** *old*LBNE poses unique challenges for reconstruction due to the fact that the APA frames are located within the fiducial volume, and because the induction-plane wires wrap around the edges of the APA frames. Since the hit data on LAr TPC’s is inherently two-dimensional – wire number vs. arrival time of the charge, the location of the initial ionization point has a two-dimensional ambiguity (if the deposition time is unknown). For beam events, the  $t_0$  is known, and thus only a one-dimensional ambiguity remains. This ambiguity is broken by angling the induction plane wires relative to the collection plane wires, in order to measure the  $y$  location of the hits for which  $t$  (thus  $x$ ) and  $z$  are known. The photon system provides  $t_0$  for cosmic-ray signals which arrive uniformly in time.

The wrapping of the induction plane wires however introduces discrete ambiguities that are not present in other LAr TPC designs. A hit on a collection-plane wire identifies uniquely which side of the APA from which it came, while this is not known for a hit on an induction-plane wire. The angles between the  $U$  and  $V$  plane wires are slightly different from  $45^\circ$  and from each other in order to assist breaking the ambiguities. A combinatoric issue arises, however, if many hits arrive on different wires at nearly the same time. This occurs if a track, or even a track segment, propagates in a plane parallel to the wire planes (constant

drift distance). Showers will also contain many hits on different wires that arrive at similar times. Hits that arrive at different times can be uniquely associated in the  $Z$ ,  $U$ , and  $V$  views, while hits that arrive at similar times must be associated using a topological pattern recognition technique. We are developing a version of the fuzzy clustering tool that is to be used as a pattern recognition step in order to associate  $Z$ ,  $U$ , and  $V$  hits together, which is a step needed in order to assign which of the discrete choices of wire segment an induction hit falls on. This process is called “disambiguation” of the induction hits, and is needed to assign the correct  $y$  position to a track segment or portion of a cluster. Once the induction hits have been disambiguated, standard track, vertex, and cluster reconstruction algorithms are applied. Misassignment of the  $y$  locations for pieces of tracks and clusters can affect particle ID performance and reconstructed energy resolution. Fully-contained tracks may appear partially contained and vice versa.

**FIXME: new** A promising suite of algorithms for event reconstruction is provided by the PANDORA toolkit [?], which provides a framework for reconstruction algorithms and visualization tools. Currently it is being used to develop pattern-recognition algorithms and to reconstruct primary vertices. PANDORA’s pattern-recognition algorithm merges hits based on proximity and pointing **FIXME: and on direction?** to form 2D clusters. Vertices are then identified from the clusters that best connect the event. **FIXME: Other clusters?** Clusters that correspond to particles emitted from the primary vertex **FIXME: that some clusters were used to identify** are identified in 2D. These particle candidates are then used to seed 3D reconstructed particles, and a 3D primary vertex is identified. Examples of PANDORA’s 2D clustering are shown in Figure 4-3 for two simulated charged-current neutrino scattering events. Figure 4-4 shows the primary vertex spatial resolution in 3D with well-contained simulated beam neutrino events, using the nominal LBNE spectrum and MicroBooNE geometry. **FIXME: this pgraph needs work**

**FIXME: old** A promising suite of algorithms for event reconstruction is provided by the PANDORA toolkit [?], which provides a framework for reconstruction algorithms and visualization tools. Currently it is being used to develop pattern recognition algorithms, and also to reconstruct the primary vertex. PANDORA’s pattern recognition merges hits based on proximity and pointing to form 2D clusters. Vertices are identified from the clusters that best connects the event, and clusters that correspond to particles emitted from the primary vertex are identified in 2D. These particle candidates are then used to seed 3D reconstructed particles, and a 3D primary vertex is identified. Examples of PANDORA’s 2D clustering are shown in Fig. 4-3 for two simulated charged-current neutrino scattering events. Fig. 4-4 shows the primary vertex spatial resolution in 3D using well-contained simulated beam neutrino events using the nominal LBNE spectrum and MicroBooNE geometry.

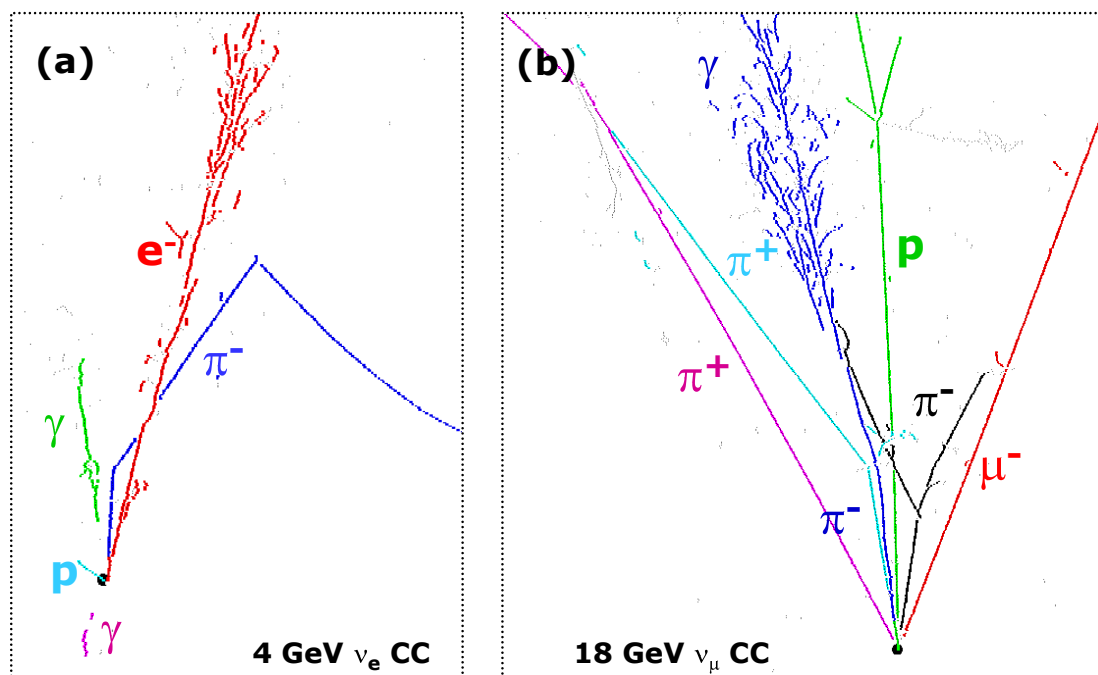


**Figure 4-3:** PANDORA's two-dimensional clusterings of hits created by the particles in two charged-current neutrino interactions in liquid argon. Panel (a) shows a 4 GeV  $\nu_e$  interaction, and panel (b) shows an 18 GeV  $\nu_\mu$  interaction. The colors indicate the clusters into which PANDORA has divided the hits, and the particle labels are from the MC truth.

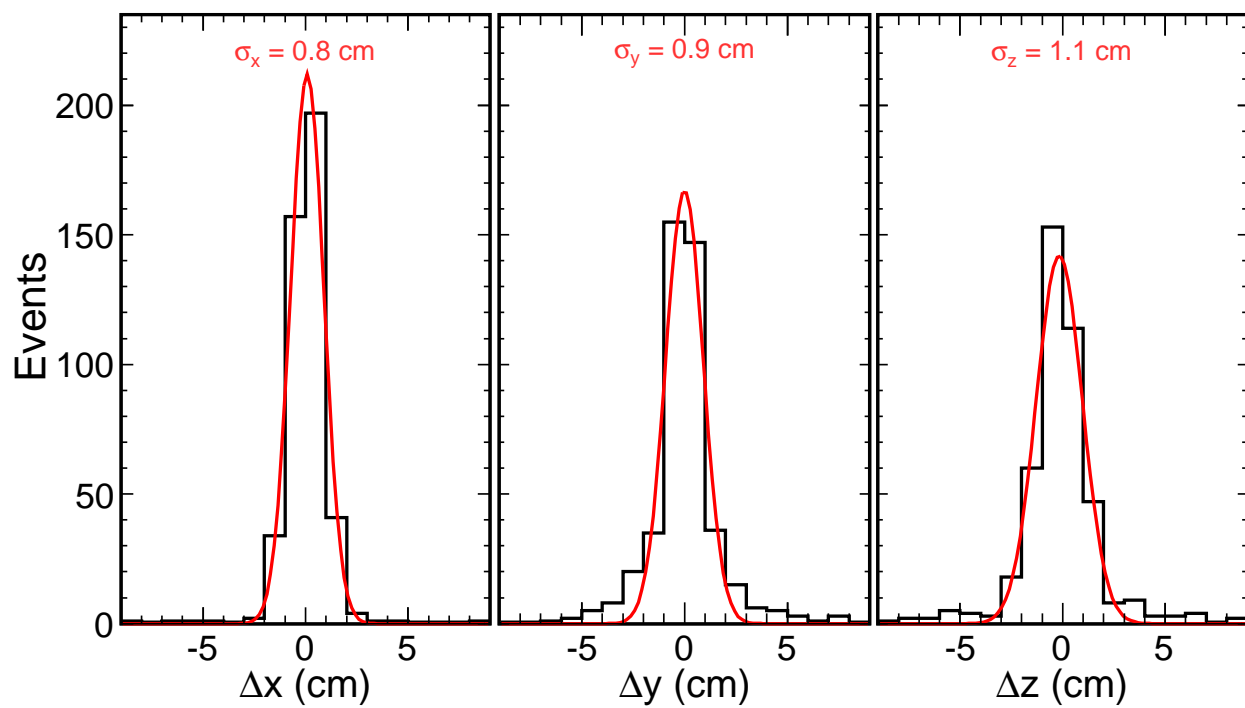


**Figure 4-4:** Distributions of the residuals between the reconstructed and the Monte Carlo true locations of primary vertices in neutrino interactions in the MicroBooNE geometry using the LBNE beam spectrum. The  $x$  axis is oriented along the drift field, the  $y$  axis is parallel to the collection-plane wires, and the  $z$  axis points along the beam direction.

### 4.3.3 Fast Monte Carlo

**FIXME:** *Do we want to start with ‘what is a fast MC’ and why is it important?*

**FIXME:** *new* A Fast Monte Carlo (Fast MC) is **FIXME:** ? and is important for modeling the entire analysis chain for an experiment. The output of the Fast MC simulations is a set of analysis-level ‘reconstructed’ quantities that mimic the output of a full MC simulation, and physics analysis sample classification **FIXME:** *this phrase not clear*. To produce a Fast MC, LBNE developed a parameterized detector response and has combined it with flux simulations and the GENIE event generator. The detector response is informed by GEANT4 simulations of particle trajectories in LAr, studies of detector response simulation in MicroBooNE, results reported by the ICARUS collaboration, and the geometry of a detector design. The Fast MC files can be used to construct the inputs required for GLoBES simulations on an event-by-event basis. This functionality allows for the propagation of realistic flux, cross section, and detector response systematic uncertainties. In total, the Fast MC allows for a full implementation of the LBNE analysis chain starting from the beam flux and propagating detector acceptance, smearing and uncertainties through to the oscillation parameter sensitivities.

**FIXME:** *old* A parameterized detector response was developed and has been combined with flux simulations and the GENIE event generator to produce a fast MC simulation (Fast MC).

**FIXME:** *Does the fast mc INCLUDE the geant and genie processes or is it considered to be separate, following those?* The detector response is informed by GEANT4 simulations of particle trajectories in LAr, studies of detector response simulation in MicroBooNE, results reported by the ICARUS collaboration, and the geometry of a detector design. The output of the Fast MC simulations are a set of analysis-level ‘reconstructed’ quantities that mimic the output of a full MC simulation, and physics analysis sample classification. These Fast MC files can be used to construct the inputs required for GLoBES simulations on an event-by-event basis. This functionality allows for the propagation of realistic flux, cross section, and detector response systematic uncertainties. In total the Fast MC allows for a full implementation of the LBNE analysis chain starting from the beam flux and propagating detector acceptance, smearing and uncertainties through to the oscillation parameter sensitivities.

**FIXME:** *new replaced old; not much change* The flux simulations are generated from a full GEANT4 simulation of the LBNE beamline described in Section 3.4. The GENIE neutrino event generator is used to simulate interactions of neutrinos on  $\text{Ar}_{40}$  nuclei. For each interaction a record of the interaction process, event kinematics, and a list of final-state particles and their associated four-vectors is produced **FIXME:** *by which process/app: geant, genie or the fast mc itself?*. The parameterized detector response applies spatial and energy/momentum smearing to each of the final-state particles based on the particle properties and encoded detector-response parameters. Detection thresholds are applied to determine if a final state particle will deposit energy in the detector, and if that energy deposition pattern will allow for particle identification. The detector response functions for neutrons and charged pions



include a variety of interactions depending on the ways in which they deposit energy in the detector. These interaction categories are referred to as ‘fates.’ Neutral pions are decayed into two photons. The vertex positions of the resulting EM showers are selected randomly from an exponential **FIXME:** *exponential what?* with a characteristic length based on the radiation length in LAr. Tau leptons are also decayed. The spatial extent of tracks and showers are simulated and energy deposition patterns with respect to detector boundaries are taken into account when assigning associated energy resolutions.

**FIXME:** *new* The Fast MC reconstructs the kinematics of the event ( $E_\nu, Q^2, x, y, etc$ ) based on the smeared four-vectors of particles that are above detection threshold. Next, it searches interaction final-state particle lists for lepton candidates that it then uses in an event classification algorithm. The resulting classifications are used to isolate analysis samples for  $\nu_e$  appearance and  $\nu_\mu$  disappearance, which are in turn used to build energy spectra on an event-by-event basis. The final oscillation fits **FIXME:** *this is the fast mc output?* are produced by the GLoBES [?] oscillation analysis package. The output of the Fast MC is used to generate matrices that relate the true energy **FIXME:** *of each particle?* to the reconstructed energy. These matrices provide input to GLoBES, which converts oscillated true-energy spectra to reconstructed-energy spectra. In addition, alternate cross section models, flux simulations and detector response assumptions are incorporated into the Fast MC as event weights that can be used to generate covariance matrices for propagation of systematic uncertainties. Specialized GLoBES functions can read in the covariance matrices generated by the Fast MC and apply realistic simulations of systematic uncertainties to sensitivity studies.

**FIXME:** *old* The kinematics of the event ( $E_\nu, Q^2, x, y, etc$ ) are reconstructed based on the smeared four-vectors of particles above detection threshold. Next, interaction final-states particle lists are searched for lepton candidates which are used in an event classification algorithm. The resulting classifications are used to isolate analysis samples for  $\nu_e$  appearance and  $\nu_\mu$  disappearance which are used to build energy spectra on an event-by-event basis. The GLoBES [?] oscillation analysis package is used for the final oscillation fits. The output of the Fast MC is used to generate matrices which relate the true energy to the reconstructed energy which are used as input to GLoBES to convert oscillated true energy spectra to reconstructed energy spectra. Furthermore alternate cross section models, flux simulations, and detector response assumptions are incorporated into the Fast MC as event weights and can be used to generate covariance matrices for propagation of systematic uncertainties. Specialized GLoBES functions can read in the covariance matrices generated by the Fast MC and apply realistic simulations of systematic uncertainties to sensitivity studies.

The event classification algorithm uses the following criteria to identify lepton candidates:

- An event with a candidate is assumed to be a CC  $\nu_\mu$  interaction. To be selected as a  $\mu$  candidate, a track must pass the following criteria:
  - The longest MIP-like track is evaluated for consistency **FIXME:** *to be consistent with?* with a  $\mu$  hypothesis.

- The track must be at least 2.0 m long. (The probability for a charged lepton to exhibit ranging behavior becomes minimal above this length.)
  - If the track is produced by a charged pion its fate must produce a topology consistent with a  $\mu$ . This includes:
    - \* tracks exiting the detector
    - \* pions that range out
    - \* pions that are absorbed (assumed to be 15% of non-ranging pions)
  - To account for the expected reduction in selection efficiency for low-energy muon candidates in high-multiplicity events, an additional selection probability of the form  $P(E_{track}) = (E_{track} - m)/(E_{track} - m * n)$ , where  $m$  is a tunable parameter set to 0.8 GeV and  $n$  is the  $\mu$  detection threshold, is applied as a function of MIP-like track energy to the  $\mu$  candidates. The falling edge of the applied pdf is well below the energy required to generate a 2.0 m track, thus the effect of this additional selection requirement is minimal. **FIXME:** *Needs clarification: what does  $P$  need to be in order for the candidate to pass?*
- An event with no muon candidate and an electron candidate is assumed to be a CC  $\nu_e$  interaction. An EM shower passing the following criteria is selected as a muon candidate: **FIXME:** *seems like we need another begin itemize here, but I don't know where to end it. I'm giving it a try.*
  - The highest energy EM shower is evaluated for consistency with an  $e\pm$  hypothesis.
  - The vertex of the shower must be within 2.0 cm of the event vertex.
  - The shower is paired with each other EM showers in the event above the identification threshold, and the invariant mass is calculated. **FIXME:** *this is not a criterion*
  - If the invariant mass is consistent ( $135 \pm 40$  MeV) with the  $\pi^0$  mass, the candidate is rejected and the next-highest-energy EM shower is considered.
  - To account for proposed  $e/\gamma$  separation algorithms and for the expected reduction in selection efficiency for low energy  $e\pm$  candidates in high multiplicity events, additional selection probabilities are applied as a function of EM shower energy to the  $e\pm$  candidates.
    - \* The  $e/\gamma$  separation algorithm is tuned to preserve 95% of the signal ( $e\pm$ ) across all energies, and selection probability of 0.9 is applied to each true  $e\pm$  candidate.
    - \* The  $e/\gamma$  separation algorithm gives the fraction of background ( $\gamma$ ) rejected as a function of candidate energy. This fraction is used as the selection probability for each true  $\gamma$  candidate
    - \* The current implementation rejects 50% of  $\gamma$  induced EM showers at 0.25 GeV, and 92% of  $\gamma$  induced EM showers above 1.5 GeV (linear interpolation is applied between these points).

- \* A selection probability of the form  $P(E_{\text{shower}}) = (E_{\text{shower}} - m)/(E_{\text{shower}} - m * n)$ , where  $m$  is a tunable parameter set to  $-5.0$  GeV and  $n$  is the  $e^\pm$  detection threshold, is applied as a function of EM shower energy to the  $e^\pm$  candidates. The parameter  $m$  is tuned to agree with hand scan studies.
- An event with no muon candidate and no electron candidate is assumed to be a NC interaction.
- Currently no attempt is made to identify tau lepton candidates, either to isolate a tau sample, or to reject  $\tau \rightarrow \mu + \nu + \nu$  or  $\tau \rightarrow e + \nu + \nu$  from their constituent samples.

Algorithms for  $\tau$  event selection are under development. Efforts focus on using event kinematics and topological variables. Candidates for kinematic discriminants include the transverse momentum imbalance (see Figure 4-5) with respect to the incoming neutrino direction, and

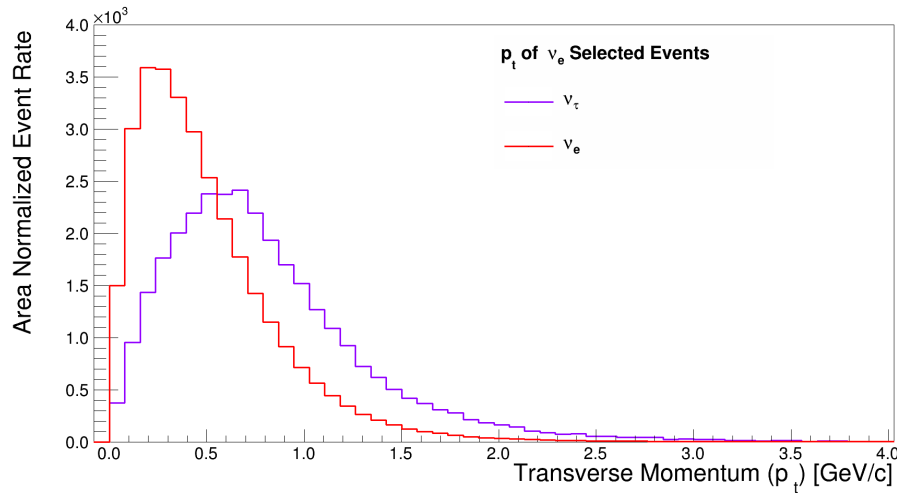


**Figure 4-5:** Transverse momentum profile - measured with respect to the neutrino beam direction - of  $\nu_e$  and  $\nu_\tau$  events that pass  $\nu_e$  selection cuts.

reconstruction of a  $\rho$  mass from hadronic decay products. Topological discriminants will focus on identification of a second hadronic shower vertex at the termination of a MIP-like track originating at the primary vertex. This topology is consistent with the high-energy charged pions produced in  $\tau$  decays.

**FIXME:** new Figures 4-6 and 4-7 show for  $\nu_e$  and  $\nu_\mu$ , respectively, the output appearance spectrum and the backgrounds from the Fast MC. The bottom insert in each plot shows the variation in the spectrum of each component of the spectrum **FIXME:** variation in the spectrum... of the spectrum? Plz clarify. Same comment for the figure captions. induced by changing the value of  $CCM_A^{QE}$ , the axial mass parameter appearing in the axial form factor describing QE interactions in GENIE. This particular example of the cross section

and nuclear effect systematic studies demonstrates the strong correlation in cross section systematics in the  $\nu_\mu \rightarrow \nu_e$  and  $\nu_\mu \rightarrow \nu_\mu$  analyses.

**FIGME:** *old* Figures 4-6 and 4-7 shows the output  $\nu_e$  and  $\nu_\mu$  appearance spectrum and the backgrounds from the Fast MC respectively. The bottom insert in each plot shows the variation in the spectrum of each component of the spectrum induced by changing the value of  $CCM_A^{QE}$ , the axial mass parameter appearing in the axial form factor describing QE interactions in GENIE. This particular example of the cross-section and nuclear effect systematic studies demonstrates the strong correlation in cross-section systematics in the  $\nu_\mu \rightarrow \nu_e$  and  $\nu_\mu \rightarrow \nu_\mu$  analyses.

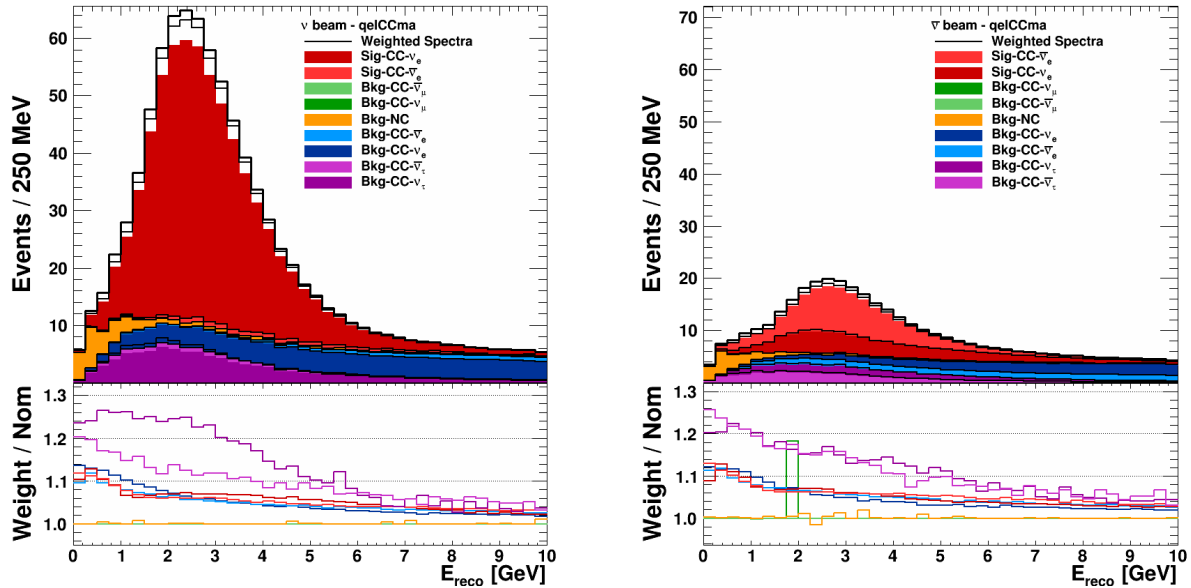


**Figure 4-6:** The  $\nu_e$  (left) and  $\bar{\nu}_e$  (right) appearance signal produced by the Fast MC simulation package. The bottom insert in each plot shows the variation in the spectrum of each component of the spectrum induced by changing the value of  $M_A^{QE}$  in the simulation.

The left-hand side plots of Figures 4-8 and 4-9 show the acceptance (efficiency) of the signal and the background samples for the Fast MC  $\nu_e$  appearance and  $\nu_\mu$  disappearance selections, respectively. The effects of the low-energy selection probabilities induce the observed low-energy fall off in the  $\nu_e$  appearance sample. On the other hand the 2.0-m track length requirement is mainly responsible for the low-energy behavior in the  $\nu_\mu$  disappearance sample. The corresponding plots on the right-hand side show the relative fraction (purity) of each signal and background sample for the Fast MC  $\nu_e$  appearance and  $\nu_\mu$  disappearance selections. The increased wrong-sign contamination is evident in the  $\bar{\nu}$  beam samples as compared to the  $\nu$  beam samples. No attempt has been made to reduce the tau backgrounds in this analysis.

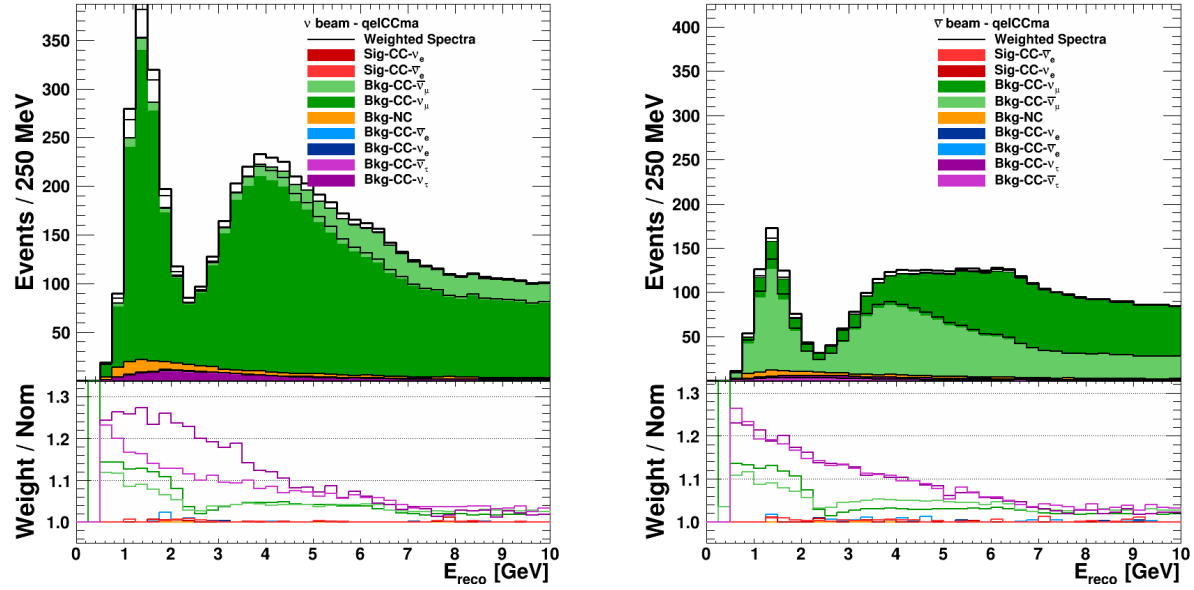


**Figure 4-7:** The  $\nu_\mu$  (left) and  $\bar{\nu}_\mu$  (right) appearance signal produced by the Fast MC simulation package. The bottom insert in each plot shows the variation in the spectrum of each component of the spectrum induced by changing the value of  $M_A^{QE}$ .

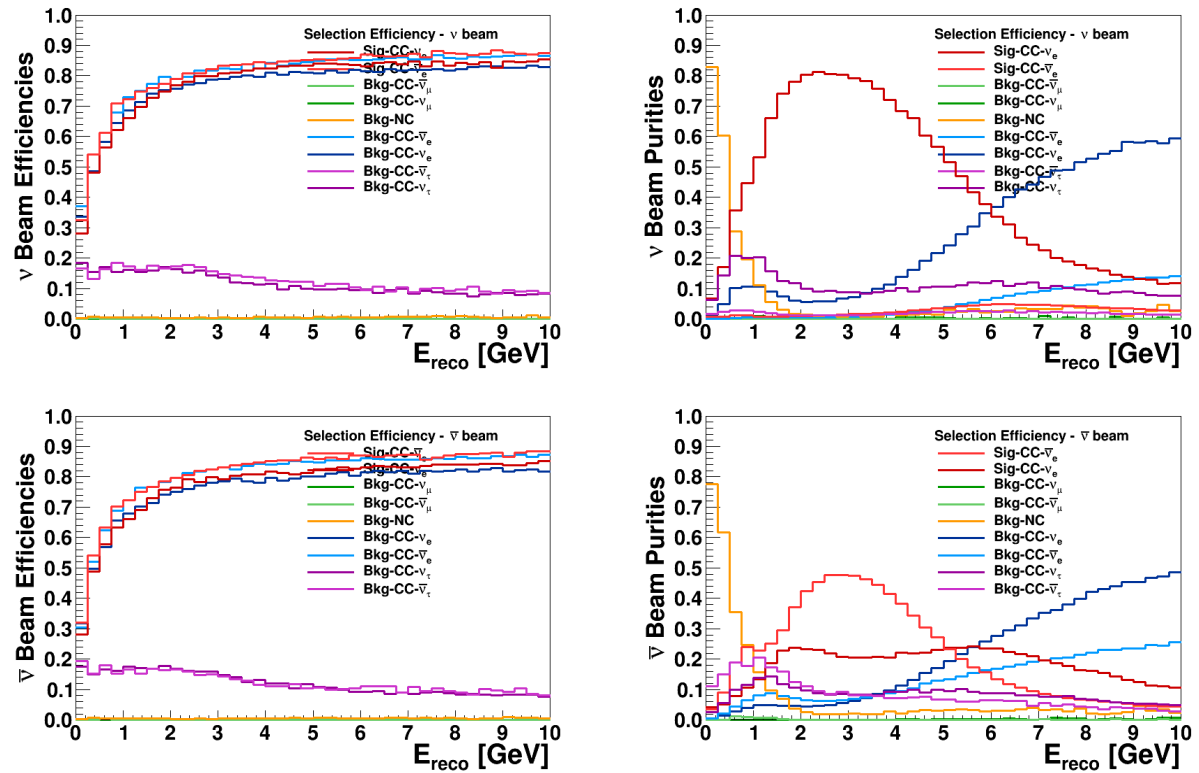


**Figure 4-8:** The expected efficiencies and purities of selecting  $\nu_e$  appearance events in an LArTPC obtained from the Fast MC.

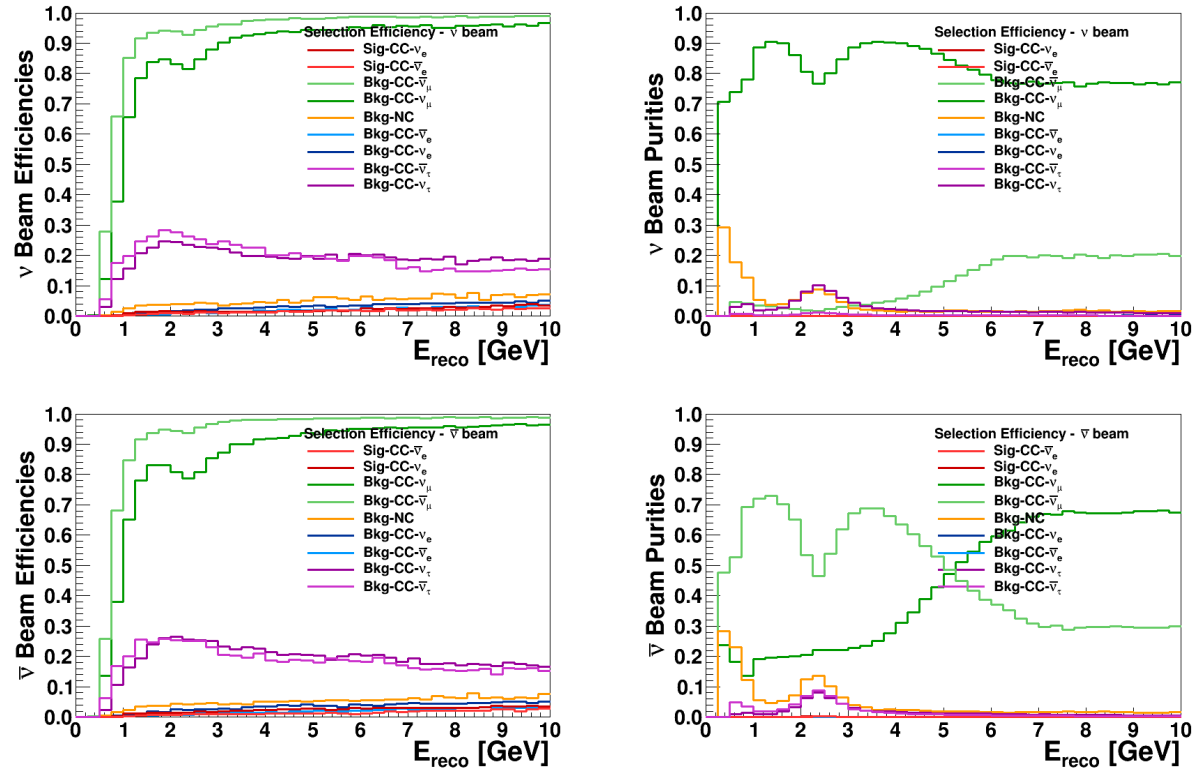


**Figure 4-9:** The expected efficiencies and purities of selecting  $\nu_\mu$  appearance events in an LArTPC obtained from the Fast MC.

#### 4.3.4 Simulation of Cosmic Ray Backgrounds for a 10-kt Surface Detector

**FIXME: new** A preliminary study of the non-beam **FIXME: aren't they by def 'non-beam'?** background events expected from cosmic rays in the 10-kt FD installed near the surface at SURF is detailed in [?]. The study simulated cosmic-ray interactions in the FD and focused on cosmic-ray induced signals from neutrons and muons that mimic electron-neutrino interactions, such as electromagnetic cascades from knock-on electrons, muon Bremstrahlung, and hadronic cascades with electromagnetic components from photons and  $\pi^0$ 's. Backgrounds from decays of neutral hadrons into electrons such as  $K_L^0 \rightarrow \pi e \nu$  were also studied. The energy of the cascades was required to be  $> 0.1$  GeV.

**FIXME: old** A preliminary study of the expected non-beam background events expected from cosmic rays in the 10-kton LAr-FD located near the surface at SURF is detailed in [?]. The study simulated cosmic-ray interactions in the LAr-FD and focused on cosmic-ray induced signals from neutrons and muons that mimic electron-neutrino interactions, such as electromagnetic cascades from knock-on electrons, muon Bremstrahlung, and hadronic cascades with electromagnetic components from photons and  $\pi^0$ 's. Backgrounds from decays of neutral hadrons into electrons such as  $K_L^0 \rightarrow \pi e \nu$  were also studied. The energy of the cascades was required to be  $> 0.1$  GeV.

These initial studies indicate that a combination of simple kinematic and beam timing cuts will help in significantly reducing the cosmic-ray background event rate in this FD configuration. In particular:

1. Only electromagnetic cascades with energies greater than 0.25 GeV are considered background (for the neutrino oscillation sensitivity calculations, only neutrino energies  $\geq 0.5$  GeV are considered).
2.  $e^\pm$  background candidates are tracked back to the parent muon; the distance between the muon track and the point-of-closest-approach (PoCA) to the muon track is required to be  $> 10$  cm.
3. The vertex of the  $e^\pm$  shower is required to be within the fiducial volume of the detector (defined as 30 cm from the edge of the active detector volume).
4. The  $e^\pm$  cascade is required to be within a cone around the beam direction (determined from the angular distribution of the beam signal  $e^\pm$  and the incoming neutrino beam).
5. It is assumed that em showers initiated by  $\gamma$ 's and  $\pi^0 \rightarrow \gamma\gamma$  can be effectively distinguished from primary electron interactions using particle ID techniques such as  $dE/dX$ .
6. Events are timed with a precision of  $\leq 1 \mu\text{s}$  using the photon detection system, which limits backgrounds to events occurring within the  $10\mu\text{s}$  of the beam spill.

**FIXME: new** The result of applying these selection criteria to the electromagnetic showers initiated by cosmic rays is summarized in Table 4-2 and Figure 4-10. The background rates given in Table 4-2 include the recalculation for the cosmic flux at 1,500 m above sea level, which was not included in the previous study [?] (and is not included in Figure 4-10). In the table, the initial background event rate is calculated for one calendar year assuming a 1.4-ms drift time per beam pulse, a beam pulse every 1.33 seconds and  $2 \times 10^7$ s of running/year. The expected event rate/yr after various selection criteria is applied from left to right in the table. The rates in all columns except the last are given for a time window of 1.4 ms, corresponding to the maximum electron drift time. The last column shows the rate reduction assuming an efficient photon detection system. The first three rows show events with a muon in the detector where a PoCA cut (column 3) can be applied. The row labeled ‘Missing  $\mu$ ’ shows events without a muon in the detector, thus for which PoCA cannot be applied (no muon track). The detector is assumed to be on the surface with 3 m of rock overburden.

The most dominant background is found to be 12 out of 16 total events per year **FIXME: 12 out of 16 events; I don't get it.** coming from  $\pi^0$ 's originating in cosmic showers. The study does not yet include specific  $\pi^0$  reconstruction, only individual  $e/\gamma$  separation. More sophisticated reconstruction techniques should further reduce the  $\pi^0$  background. The studies indicate that application of these selection criteria coupled with a more detailed background event reconstruction can potentially reduce the background from cosmic rays to a few events per year — mostly in the energy region  $< 1$  GeV.

**FIXME: old** The result of applying these selection criteria to the electromagnetic showers initiated by cosmic rays are summarized in Table 4-2 and Figure 4-10. The background rates given in Table 4-2 include the recalculation for the cosmic flux at 1500m above sea level which was not included in the previous study [?]. The most dominant background is found to be 12 out of 16 total events per year coming from  $\pi^0$  from cosmic showers. The study does not yet include specific  $\pi^0$  reconstruction only individual  $e/\gamma$  separation. We expect with more sophisticated reconstruction techniques that the  $\pi^0$  background can be further reduced. The studies indicate that application of these selection criteria coupled with a more detailed background event reconstruction can potentially reduce the background from cosmic rays to a few events per year – mostly in the energy region  $< 1$  GeV.

**FIXME: Anne adds:** In Figure 4-10, black filled circles show events before any cuts are applied. The other point icons represent successively applied cuts in the order listed below and in the figure's legend.

1. Blue squares: only events with PoCA to the muon track greater than 30 cm
2. Red triangles: angle with respect to the beam such that 99% of signal events are retained
3. Green triangles: application of energy-dependent  $e/\gamma$  discrimination



**Table 4-2:** Cosmic ray induced backgrounds (at 1500m above sea level) to the beam  $\nu_e$  appearance signal in the 10 kton detector.

Processes	$E_e > 0.25$ GeV	PoCA $> 10$ cm and $D > 30$ cm	Beam angle	$e/\gamma$ PID	Beam timing
$\pi^0 \rightarrow \gamma \rightarrow e^\pm$	$2.2 \times 10^6$	$9.7 \times 10^4$	$4.8 \times 10^4$	$1.7 \times 10^3$	12
$\mu \rightarrow \gamma \rightarrow e^\pm$	$7.1 \times 10^6$	12	0	0	$< 0.003$
Ext $\gamma \rightarrow e^\pm$	$1.9 \times 10^6$	660	340	13	0.1
$\pi^0, K^0 \rightarrow e^\pm$	$1.4 \times 10^6$	810	240	240	1.7
Missing $\mu$	$1.3 \times 10^6$	$1.8 \times 10^3$	580	20	0.1
Atm $n$	$2.9 \times 10^6$	$1.6 \times 10^4$	$6.5 \times 10^2$	240	1.7
Total	$1.1 \times 10^7$	$1.2 \times 10^5$	$5.6 \times 10^4$	$2.2 \times 10^3$	16

4. Magenta open circles: efficient photon detection is assumed to allow the reduction of the time window from a maximum drift time of 1.4 ms down to a beam spill of 10  $\mu$ s.

**FIXME:** *can we state this as a cut?*

### 4.3.5 Detector Simulation using the GLoBES Package

For the current set of sensitivity studies, the full implementation of the FastMC had not yet been developed, and the GLoBES package [?,?] was used to simulate the detector response using much simpler smearing and detector efficiency values based on results from ICARUS and earlier simulation efforts as documented in [?]. The values used in GLoBES are shown in Table 4-3.

**FIXME:** *new* Studies from ICARUS have estimated and measured single-particle energy resolutions in LAr. Below 50 MeV, the energy resolution of electrons is  $11\%/\sqrt{E[\text{MeV}]} + 2\%$ . The energy resolution of an electromagnetic shower with energy in the range (50–5000) MeV is  $33\%/\sqrt{E(\text{MeV})} + 1\%$  [?], and that of hadronic showers is  $\approx 30\%/\sqrt{E(\text{GeV})}$ . A significant fraction of the  $\nu_e$  CC signal in LBNE in the range of 1–6 GeV is non-quasi-elastic CC interactions with a large component of the visible energy in the hadronic system. From recent simulations of neutrino interactions in the region of 1–6 GeV it has been determined that  $< E_{\text{lepton}}/E_\nu > \approx 0.6$ . For this reason, the total electron-neutrino energy resolution for the neutrino oscillation sensitivity calculation is chosen to be  $15\%/\sqrt{E(\text{GeV})}$ . In a non-magnetized LArTPC the muon momentum can be obtained from range and multiple scattering **FIXME:** *sentence feels incomplete*. The muon-momentum resolution is found to be in the range 10 – 15% [?] [?] for muons in the 0.5–3 GeV range. Therefore the total muon-neutrino energy resolution in LBNE is assumed to be  $20\%/\sqrt{E(\text{GeV})}$ . **FIXME:** *I don't follow the math that leads to 20%, but maybe others do.*

**FIXME:** *old* Studies from ICARUS have estimated and measured single-particle energy

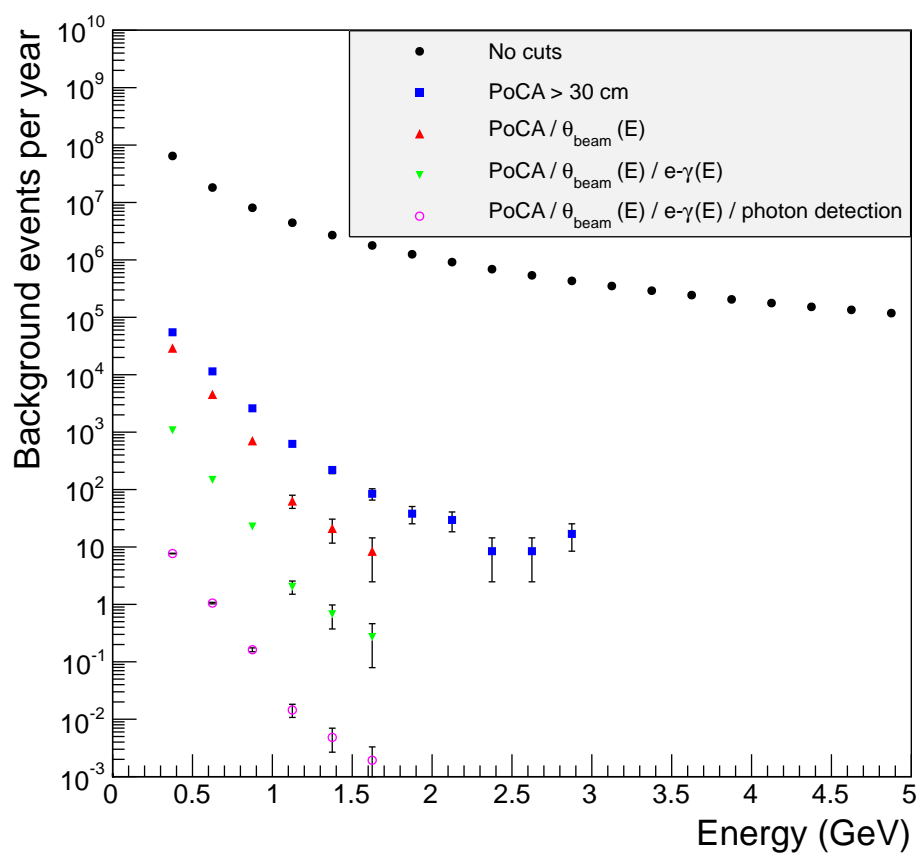


**Figure 4-10:** Energy spectra of muon-induced background events for successively applied background rejection cuts. **FIXME:** *portion of caption moved to text* Simulations have been done for a muon spectrum at sea level. Correction for an altitude of 1,500 m above sea level has not been applied to the data on this graph.

**Table 4–3:** Estimated range of the LAr-TPC detector performance parameters for the primary oscillation physics. Signal efficiencies, background levels, and resolutions are obtained from the studies described in this chapter (middle column) and the value chosen for the baseline LBNE neutrino-oscillation sensitivity calculations (right column).

Parameter	Range of Values	Value Used for LBNE Sensitivities
For $\nu_e$ CC appearance studies		
$\nu_e$ CC efficiency	70-95%	80%
$\nu_\mu$ NC mis-identification rate	0.4-2.0%	1%
$\nu_\mu$ CC mis-identification rate	0.5-2.0%	1%
Other background	0%	0%
Signal normalization error	1-5%	1-5%
Background normalization error	2-15%	5-15%
For $\nu_\mu$ CC disappearance studies		
$\nu_\mu$ CC efficiency	80-95%	85%
$\nu_\mu$ NC mis-identification rate	0.5–10%	0.5%
Other background	0%	0%
Signal normalization error	1-10%	5–10%
Background normalization error	2-20%	10-20%
For $\nu$ NC disappearance studies		
$\nu$ NC efficiency	70-95%	90%
$\nu_\mu$ CC mis-identification rate	2-10%	10%
$\nu_e$ CC mis-identification rate	1-10%	10%
Other background	0%	0%
Signal normalization error	1-5%	under study
Background normalization error	2-10%	under study
Neutrino energy resolutions		
$\nu_e$ CC energy resolution	$15\%/\sqrt{E(\text{GeV})}$	$15\%/\sqrt{E(\text{GeV})}$
$\nu_\mu$ CC energy resolution	$20\%/\sqrt{E(\text{GeV})}$	$20\%/\sqrt{E(\text{GeV})}$
$E_{\nu_e}$ scale uncertainty	under study	under study
$E_{\nu_\mu}$ scale uncertainty	1-5%	2%

resolutions in LAr. Below 50 MeV, the energy resolution of electrons is  $11\%/\sqrt{E[\text{MeV}]} + 2\%$ . The energy resolution of an electromagnetic shower with energy in the range (50–5000) MeV is  $33\%/\sqrt{E(\text{MeV})} + 1\%$  [?]. The energy resolution of hadronic showers in an LArTPC is  $\approx 30\%/\sqrt{E(\text{GeV})}$ . A significant fraction of the  $\nu_e$  CC signal in LBNE in the range of 1–6 GeV is non-quasi-elastic CC interactions with a large component of the visible energy in the hadronic system. From recent simulations of neutrino interactions in the region of 1–6 GeV it has been determined that  $\langle E_{\text{lepton}}/E_\nu \rangle \approx 0.6$ . For this reason, the total electron-neutrino energy resolution for the neutrino-oscillation sensitivity calculation is chosen to be  $15\%/\sqrt{E(\text{GeV})}$ . In a non-magnetized LArTPC the muon momentum can be obtained from range and multiple scattering. The muon-momentum resolution is found to be in the range 10–15% [?] [?] for muons in the 0.5–3 GeV range. Therefore the total muon-neutrino energy resolution in LBNE is assumed to be  $20\%/\sqrt{E(\text{GeV})}$ .

The predicted spectrum of oscillated  $\nu_\mu$  and  $\bar{\nu}_\mu$  CC events in LBNE produced from the GLoBES implementation is shown in Figure 4–11.

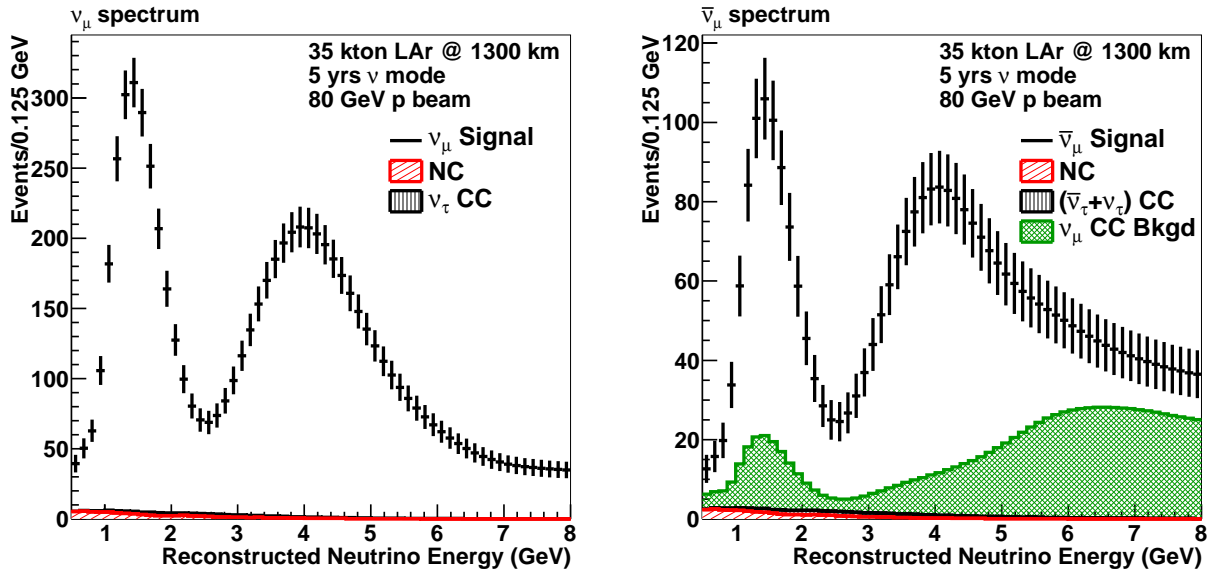


**Figure 4–11:** The expected spectrum of  $\nu_\mu$  or  $\bar{\nu}_\mu$  events in a 35-kt LArTPC for five years of neutrino (left) and anti-neutrino (right) running with a 700-kW beam.

The GLoBES implementation used in the sensitivity studies appears to be in good agreement with the more recent results from the Fast MC. Updated sensitivity and systematic studies are currently underway using the Fast MC for detector simulation and GLoBES for the oscillation fits and propagation of systematics.

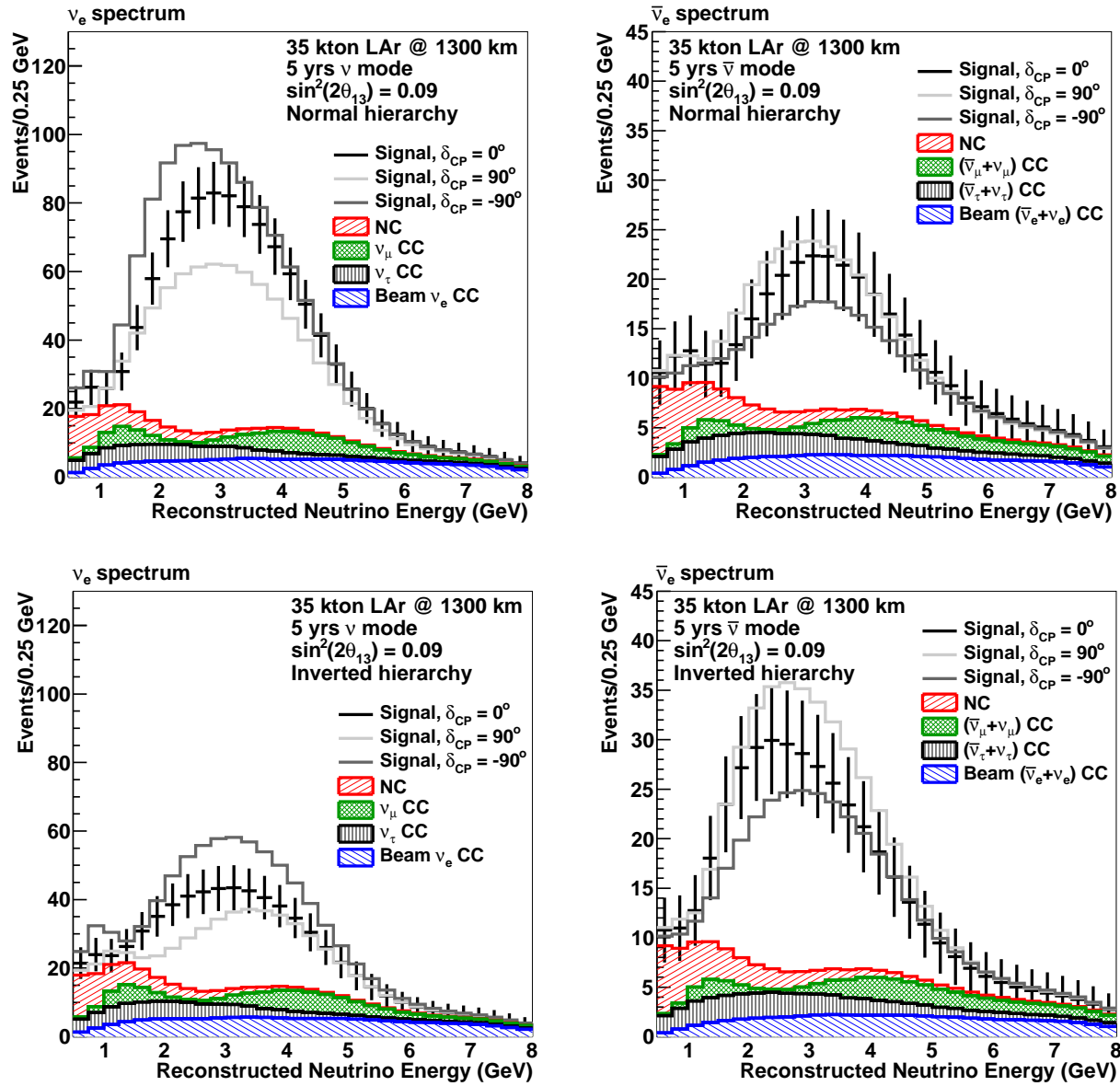


**Figure 4-12:** The expected spectrum of  $\nu_e$  or  $\bar{\nu}_e$  oscillation events in a 35-kt LArTPC for 5 years of neutrino (left) and anti-neutrino (right) running with a 700-kW, 80-GeV beam assuming  $\sin^2(2\theta_{13}) = 0.09$ . The plots on the top are for normal hierarchy and the plots on the bottom are for inverted hierarchy.

**Table 4-4:** Expected number of neutrino oscillation signal and background events in the energy range (0.5 – 8.0) GeV at the LAr-FD after detector smearing and event selection. The calculation assumes  $\sin^2(2\theta_{13}) = 0.1$  and  $\delta_{CP} = 0$ . The event rates are given per 10 kt LArTPC FD and 5 years of running with the improved 80 GeV LBNE beam at 700 kW ( $9 \times 10^{20}$  protons-on-target/year).

	Signal Events	Background Events				Total
	$\nu_e$	$\nu_\mu$ NC	$\nu_\mu$ CC	$\nu_e$ Beam	$\nu_\tau$ CC	
Neutrino Normal Hierarchy	222	19	24	42	14	99
Neutrino Inverted Hierarchy	98	19	23	44	15	100
Anti-neutrino Normal Hierarchy	54	11	11	23	9	54
Anti-neutrino Inverted Hierarchy	80	11	11	23	9	54

## 4.4 Measurements of Mass Hierarchy and the CP-Violating Phase

**FIXME:** *Pretty dry intro; does it make sense to start with something like:*

Something about the LBNE science objectives... Measuring the sign of  $\Delta m_{32}^2$  would resolve the mass-hierarchy ambiguity. As discussed in Section **FIXME:** 2.2.1.3, CP-violating effects in neutrino oscillations can only be accessed in appearance experiments, and the oscillation modes  $\nu_{\mu,e} \rightarrow \nu_{e,\mu}$  provide the most promising experimental signatures of leptonic CP violation. The phase 1 configuration (LBNE10) is set to maximize the effectiveness of the facility to determine the mass hierarchy. **FIXME:** *come back to; this needs thought*

**FIXME:** *new 2 pgph* The expected performance of LBNE10, the phase 1 configuration that implements a 10-kt far detector installed near the surface 1,300 km downstream from a 700-kW beam, is detailed in the LBNE Conceptual Design Report Volume 1 [?]. The sensitivity calculation **FIXME:** *in the CDR for determining the mass hierarchy and CP violation (one calculation for both?)* uses the GLoBES package. The detector response is summarized here in Table 4-3. The sensitivities are obtained by fitting the  $\nu_\mu \rightarrow \nu_e$  and  $\nu_\mu \rightarrow \nu_\mu$  oscillated spectra simultaneously (Figures 4-12 and 4-11). Neither the cosmogenic backgrounds discussed in Section 4.3.4 nor the  $\nu_\tau$  backgrounds are used in the sensitivity calculations since it is expected that further analysis will reduce these backgrounds to negligible levels.

Figure 4-13 summarizes the sensitivities for determining the mass hierarchy and CP violation ( $\delta_{CP} \neq 0$  or  $\pi$ ) as a function of the true value of  $\delta_{CP}$  after 10 years of running in the LBNE10 configuration.

**FIXME:** *old* The performance of first phase of LBNE which is a 10-kt far detector and

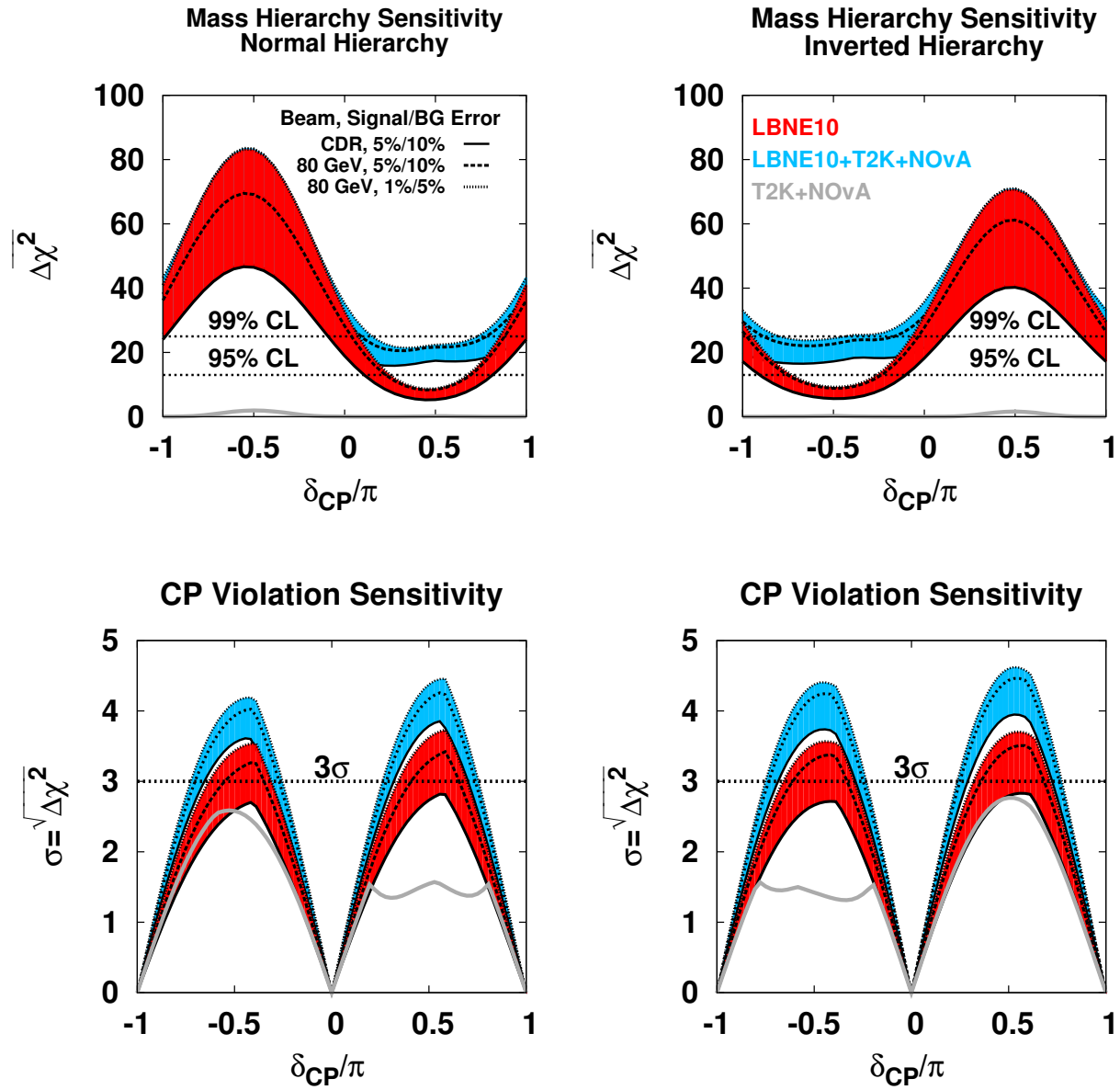
a 708 kW beam are detailed in the LBNE Conceptual Design Report Volume 1 [?]. The sensitivity calculation uses the GLoBES package with the detector response as summarized in Table 4-3. The sensitivities are obtained by fitting simultaneously both the  $\nu_\mu \rightarrow \nu_e$  and  $\nu_\mu \rightarrow \nu_\mu$  oscillated spectra (Figures 4-12 and 4-11). Cosmogenic backgrounds discussed in Section 4.3.4 and the  $\nu_\tau$  backgrounds are not used in the sensitivity calculations since it is expected that further analysis will reduce these backgrounds to negligible levels.

Figure 4-13 summarizes the sensitivities for determining the mass hierarchy and CP violation ( $\delta_{CP} \neq 0$  or  $\pi$ ) as a function of the true value of  $\delta_{CP}$  after 10 years of running with a 10-kt detector.

**FIXME: new** The mass hierarchy determination has only two possible outcomes: normal or inverted. Reference [?] carefully examines the statistical nature of properly interpreting the mass hierarchy physics sensitivity. In particular, an experiment with physics sensitivities determined by  $\Delta\chi^2 = 9, 16$ , and  $25$  (corresponding to  $3\sigma, 4\sigma$  and  $5\sigma$  for an ideal two-hypothesis testing problem) would have 93.32%, 97.72%, and 99.38% probabilities of determining the correct mass hierarchy, respectively. The corresponding *average* probabilities for determining the correct mass hierarchy are 90.14%, 96.57%, and 99.06%, respectively. These numbers are in general smaller than those based on the simple Gaussian expectation for  $3\sigma, 4\sigma$  and  $5\sigma = \sqrt{\chi^2}$  (corresponding to 99.73%, 99.994%, and 99.99994% probabilities). Figure 4-14 shows the probabilities with which the mass hierarchy can be correctly determined given a value of  $\Delta\chi^2$  using the statistical treatment discussed in reference [?] and comparing to the simple Gaussian expectation.

**FIXME: old** To properly interpret the mass hierarchy physics sensitivity, special attention should be paid, as the mass hierarchy determination has only two possible outcomes (normal vs. inverted hierarchy). Ref. [?] carefully examines the statistical nature of this problem. In particular, an experiment with physics sensitivities determined by  $\Delta\chi^2 = 9, 16$ , and  $25$  (corresponding to  $3, 4$ , and  $5-\sigma$  for an ideal two hypotheses testing problem) would have 93.32%, 97.72%, and 99.38% probability of determining the correct mass hierarchy, respectively. The corresponding average probabilities of determining the correct mass hierarchy are 90.14%, 96.57%, and 99.06%, respectively. These numbers are in general smaller than those based on the simple Gaussian expectation for  $3, 4$ , and  $5-\sigma = \sqrt{\chi^2}$  (corresponding to 99.73%, 99.994%, and 99.99994% probabilities). Figure 4-14 shows the probabilities with which the mass hierarchy can be correctly determined given a value of  $\Delta\chi^2$  using the statistical treatment discussed in ref. [?] and comparing to the simple Gaussian expectation. On the other hand, since there are only two outcomes in the mass hierarchy determination problem, the standards for “evidence” and “discovery” may arguably be lower than those in other commonly encountered problems (e.g., determination of a non-zero  $\theta_{13}$ ).

**FIXME: new** The sensitivity band **FIXME: in Figure 4-13?** represents the variation in sensitivity as a function of the beam designs and normalization uncertainties on the signal and background. The solid red curve **FIXME: it looks black** at the lower end of the red band represents the beamline design described the LBNE CDR Volume 2 [?]. The dashed



**Figure 4-13:** The significance with which the mass hierarchy (top) and CP-violation -  $\delta_{CP} \neq 0$  or  $\pi$  (bottom) can be determined as a function of the value of  $\delta_{CP}$  with a 10-kt fiducial volume LAr-FD. The plots on the right **FIXME: left?** are for normal hierarchy and the plots on the bottom **FIXME: right?** are for inverted hierarchy. The beam exposure is taken to be 5+5 yrs ( $\nu + \bar{\nu}$ ) in a 700-kW beam. The red band shows the sensitivity that is achieved by the LBNE10 configuration alone. The cyan band shows the sensitivity obtained by combining LBNE10 with T2K ( $5 \times 10^{21}$  protons-on-target  $\nu$  only) and NOvA (3+3  $\nu + \bar{\nu}$  yrs). The bands indicate the sensitivity range corresponding to different assumptions on background and signal normalization uncertainties, and on beam design improvements. The gray curves are the expected sensitivities for the combination of NOvA and T2K. For the CP violation sensitivities, the mass hierarchy is assumed to be unknown. **FIXME: too long; should move some to text**



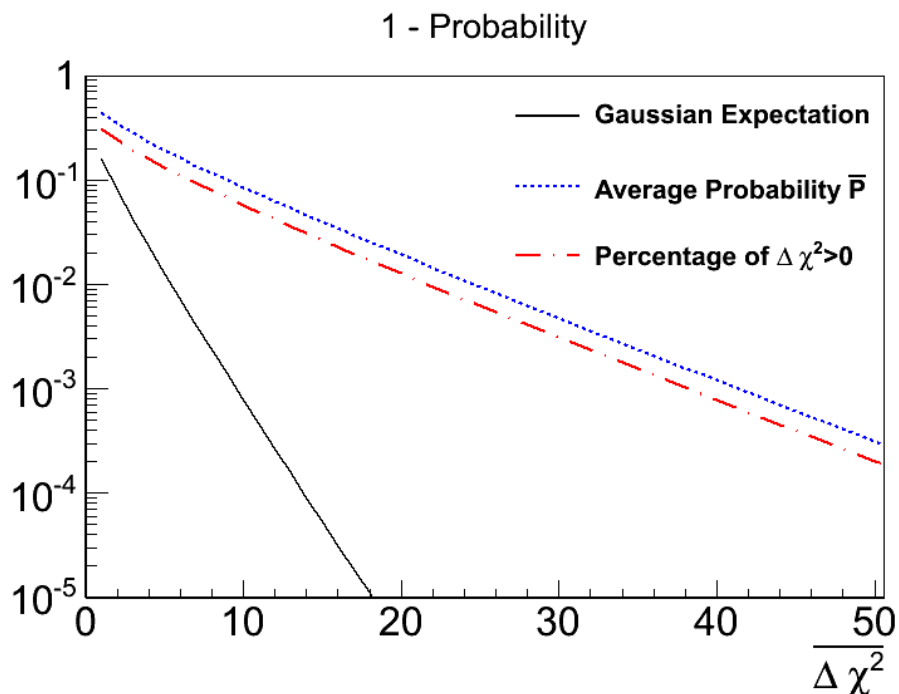


**Figure 4–14:** Mass hierarchy sensitivity metrics (subtracted from 1 for clarity) plotted versus  $\overline{\Delta\chi^2}$ , the average value of the expected  $\Delta\chi^2$  that ranges from 1 to 50. Three different metrics are presented: the Gaussian interpretation derived from the one-sided p-value with one degree of freedom (black line),  $\bar{P}$ , the average probability to give the correct mass hierarchy (dashed blue line), and the percentage of  $\Delta\chi^2 > 0$ , i.e., the probability of determining the correct mass hierarchy (dashed red line). The Gaussian interpretation appears overly optimistic in describing the ability of the experiment to differentiate the two hypotheses. Note that in the sensitivity plots shown in this Chapter,  $\Delta\chi^2$  is used to represent  $\overline{\Delta\chi^2}$ . **FIXME:** This last fact may be buried here; revisit **FIXME:** caption too long

line above the solid curve represents the sensitivity with the beam design improvements currently under study as described in Section 3.4. In the case where there is no near neutrino detector, we expect the uncertainties on signal and background to be 5% and 10%, respectively, extrapolating from (1) the performance and detailed knowledge of the NuMI beam on which the LBNE beamline is modeled, (2) in situ measurements of the muon flux at the near site as described in [?], (3) the expectation of improved target hadron production measurements with the NA61 and MIPP experiments, and (4) the experience of previous  $\nu_e$  appearance experiments as summarized in Table 4-5.

**FIXME:** *old* The sensitivity band represents the variation in sensitivity as a function of the beam designs and normalization uncertainties on the signal and background. The solid red curve at the lower end of the red band is the beam design described the LBNE CDR Volume2 [?]. The dashed line above the solid curve represents the sensitivity with the beam design improvements currently under study as described in Section 3.4. In the case where there is no near neutrino detector, we expect the uncertainties on signal and background to be 5% and 10% respectively extrapolating from 1) the performance and detailed knowledge of the NuMI beam on which the LBNE beam is modeled, 2) in-situ measurements of the muon flux at the near site as described in [?], 3) the expectation of improved target hadron production measurements with the NA61 and MIPP experiments, and 4) the experience of previous  $\nu_e$  appearance experiments as summarized in Table 4-5.

Experiment	NC/CC ( $\pi^0$ ) Events	Beam- $\nu_e$ Events	Syst.Error	Comment
BNL E734 [?]	235	418	20%	No ND
BNL E776(89)(NBB) [?]	10	9	20%	No ND
BNL E776 (WBB)	95	40	14%	No ND
MiniBooNE (>450MeV) [?]	140	250	9%	No ND
NOMAD	<300	5500	< 5%	No ND
MINOS [?]	111	12	3.8%	ND-FD

**Table 4-5:** Summary of achieved systematic error performance in several select prior  $\nu_\mu \rightarrow \nu_e$  oscillation experiments. These numbers were extracted from publications to the best of our ability and may not correspond exactly to the description in the text. NBB indicates a narrow band beam and WBB indicates a wide-band beam. No ND indicates there was no near detector, and ND-FD indicates a two detector experiment with extrapolation of the expected background and signal from the near to the far detector.

**FIXME:** *no old/new; this is current* In Chapter 3.5, a detailed discussion of the precision with which the unoscillated spectrum at the far detector can be predicted using a high-resolution tracking near detector is presented. The flux measurement precision expected from the near neutrino detector using different techniques is summarized in Table 5-3. The combination of different techniques in a highly capable near detector is expected to enable a prediction of the far detector  $\nu_e$  appearance signal with a precision of 1-2%. The background

uncertainty in a near-far extrapolation is expected to be at least as good as the  $\sim 5\%$  [?] achieved by the  $\nu_e$  appearance search in the MINOS experiment. The known mixing parameters are allowed to float in the fit, but are constrained to remain within the uncertainties from the current global fits [?]. The reactor mixing angle,  $\sin^2 2\theta_{13}$ , is constrained to be  $\sin^2 2\theta_{13} = 0.094 \pm 0.003$ , which is the expected ultimate precision from the current generation of reactor experiments.

**FIXME: new** As is obvious from this study, for a 10 kt detector, the statistical uncertainties dominate the systematic uncertainties. Combining **FIXME: uncertainties? data?** from LBNE10 with the expected knowledge from the NO $\nu$ A and T2K experiments <sup>§</sup> would allow a 10-kt detector to achieve a  $\geq 4\sigma$  sensitivity for 23% of the allowed values of  $\delta_{CP}$  and a  $\geq 3\sigma$  sensitivity for 50% of these values. It is clear that the LBNE10 sensitivity would be the single most dominant contribution in the combined sensitivities and would therefore represent a significant advance in the search for leptonic CP violation over the current generation of experiments, particularly in the region where the CP and matter effects are degenerate. The combination with T2K and NO $\nu$ A would allow the mass hierarchy to be determined with a precision of  $\geq 5\sigma$  over 60% of the allowed values of  $\delta_{CP}$  and  $\geq 3.8\sigma$  for all possible values of  $\delta_{CP}$ . **FIXME: Is ‘allowed’ different than ‘possible’ here?** The combination with NO $\nu$ A and T2K only helps the sensitivity in the region of  $\delta_{CP} > 0$  (normal hierarchy) or  $\delta_{CP} < 0$  (inverted hierarchy) where there are residual degeneracies between matter and CP-violating effects due to the low event statistics with the small detector. Alternatively, as will be discussed in Section 4.7, the combination with atmospheric neutrino oscillation studies can also be used to improve the mass hierarchy sensitivity in this region using only a 10 kton detector, but placed deep underground.

**FIXME: old** As is obvious from this study, for a 10 kt detector, the statistical uncertainties dominate and the impact of the systematic uncertainties on the sensitivity is small. The combination with the expected knowledge from the NO $\nu$ A and T2K ¶ experiments would allow a 10 kt detector to achieve a  $\geq 4\sigma$  sensitivity for at 23% of the allowed values of values of  $\delta_{CP}$  and a  $\geq 3\sigma$  sensitivity for 50% of the allowed values of  $\delta_{CP}$ . We note that the LBNE10 sensitivity is the single most dominant contribution in the combined sensitivities and would represent a significant advance in the search for leptonic CP violation over the existing experiments, particularly in the region where the CP and matter effects are degenerate in the current generation of experiments. The combination with T2K and NO $\nu$ A would allow the mass hierarchy to be determined with a precision of  $\geq 5\sigma$  over 60% of the allowed values of  $\delta_{CP}$  and  $\geq 3.8\sigma$  for all possible values of  $\delta_{CP}$ . We note that the combination with NO $\nu$ A and T2K only helps the sensitivity in the region of (normal hierarchy,  $\delta_{CP} > 0$ ) or (inverted hierarchy,  $\delta_{CP} < 0$ ) where there are residual degeneracies between matter and CP violating effects due to the low event statistics with the small detector. Alternatively, as will

<sup>§</sup>The exposure assumed for T2K in these studies was  $5 \times 10^{21}$  protons-on-target in neutrino mode only. It should be noted that the T2K collaboration’s official expected exposure is  $7.8 \times 10^{21}$  protons-on-target.

¶The exposure assumed for T2K in these studies was  $5 \times 10^{21}$  protons-on-target in neutrino mode only. It should be noted that the T2K collaboration’s official expected exposure is  $7.8 \times 10^{21}$  protons-on-target.

be discussed in Section 4.7, the combination with atmospheric neutrino oscillation studies can also be used to improve the mass hierarchy sensitivity in this region using only a 10 kton detector placed underground.

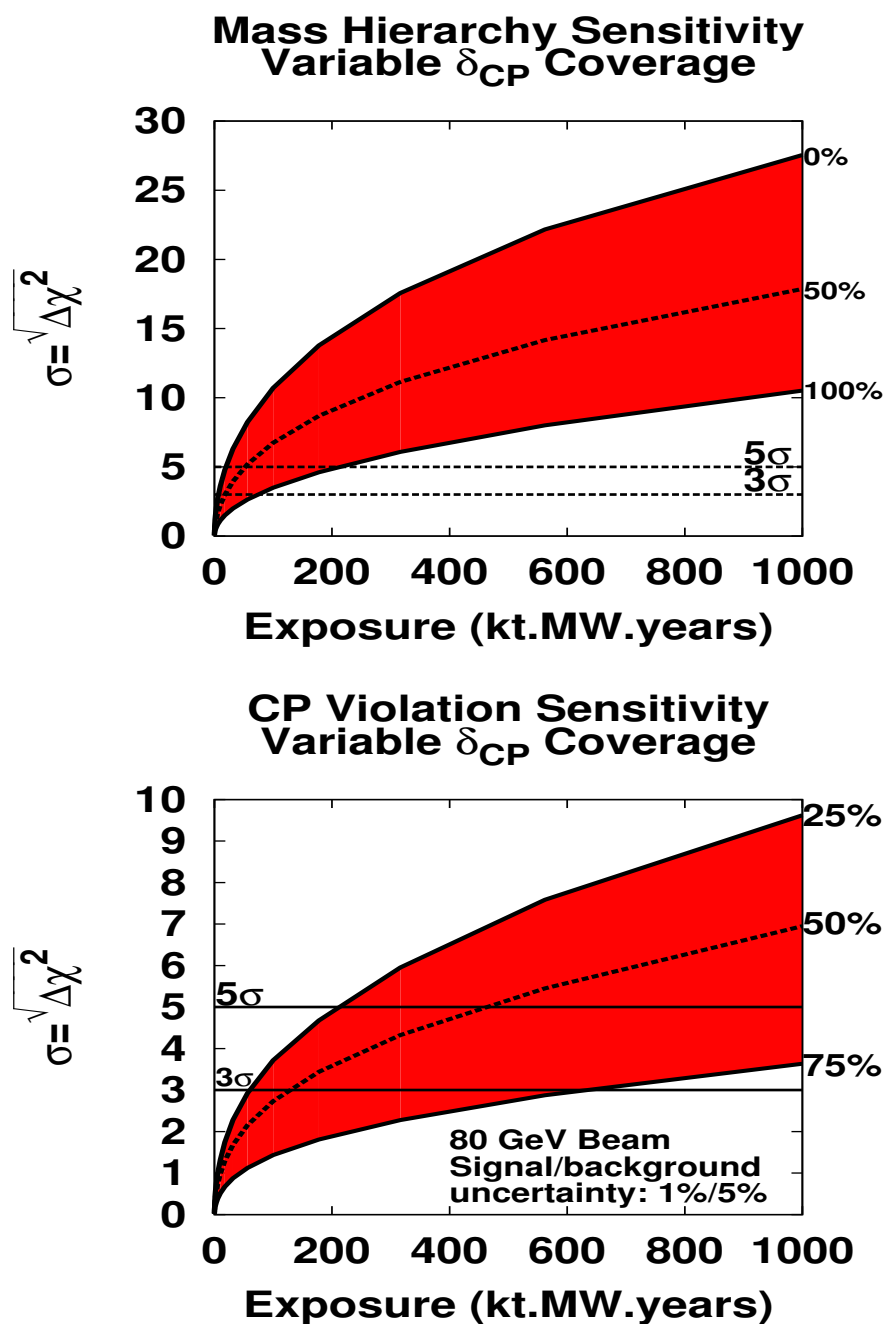
Table 4-6 summarizes the mass hierarchy and CP sensitivities that can be reached by the LBNE10 configuration assuming a running time of 5+5 ( $\nu + \bar{\nu}$ ) years with a 700-kW beam under a variety of scenarios.

**Table 4-6:** The mass hierarchy and CP sensitivities that can be reached by the LBNE10 configuration with a 700-kW beam and a run time of 5+5 ( $\nu + \bar{\nu}$ ) years under a variety of beam and systematic scenarios. As discussed in the text, the significance of the mass hierarchy determination should not be interpreted using Gaussian probabilities.

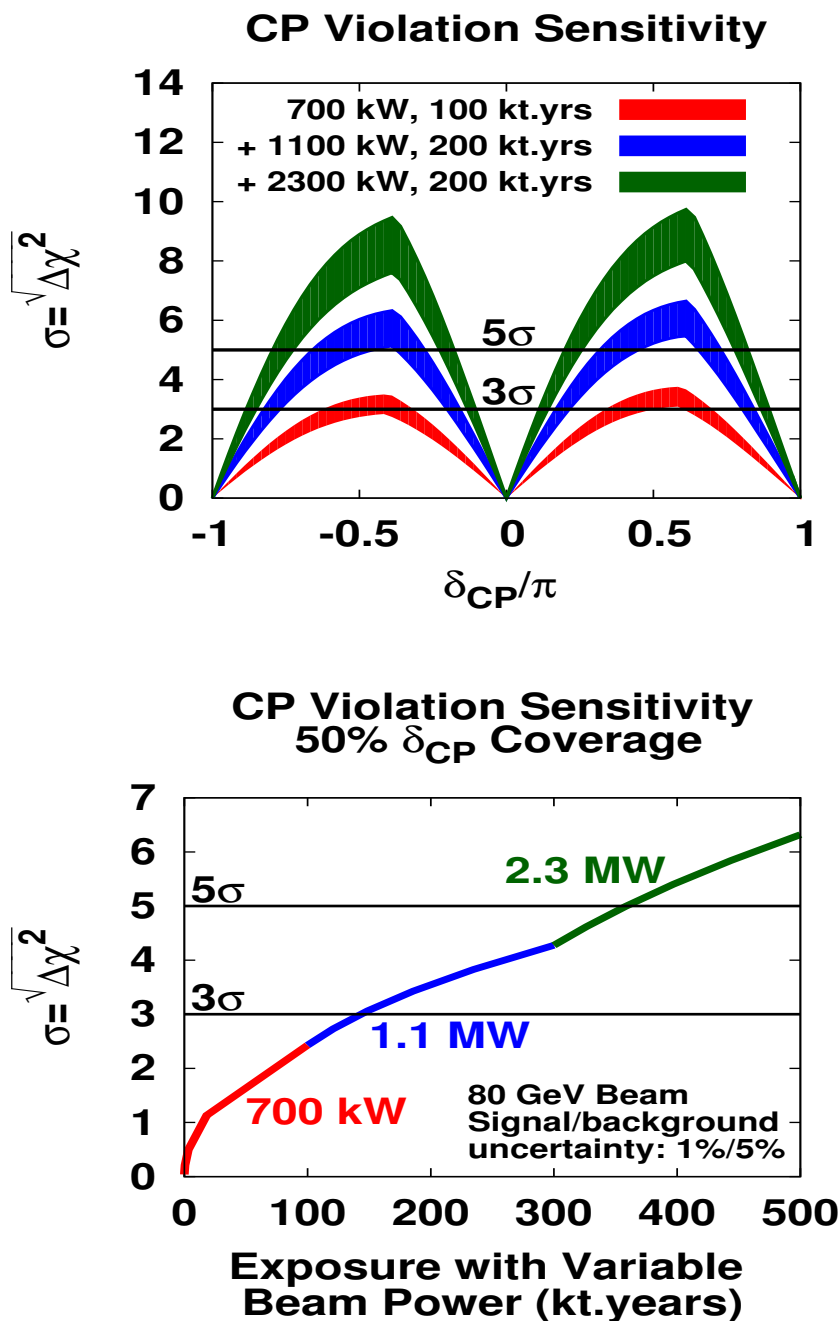
Scenario	MH sensitivity	CP sensitivity
10 kt, CDR beam, no $\nu$ ND	$\geq 4/2\sigma$ 50%/all $\delta_{CP}$	$\geq 2\sigma$ 40% $\delta_{CP}$
10 kt, beam improvements, no $\nu$ ND	$\geq 5/3\sigma$ 50%/all $\delta_{CP}$	$\geq 3/2\sigma$ 23%/55% $\delta_{CP}$
10 kt, beam improvements, with $\nu$ ND	$\geq 5/3\sigma$ 50%/all $\delta_{CP}$	$\geq 3/2\sigma$ 33%/60% $\delta_{CP}$
+ NO $\nu$ A (6 yrs), T2K (6yrs)	$\geq 5/3.8\sigma$ 60%/all $\delta_{CP}$	$\geq 4/3\sigma$ 23%/50% $\delta_{CP}$

Figure 4-15 shows the significance with which the mass hierarchy can be resolved and CP violation determined as a function of increased exposure in LBNE of mass  $\times$  power  $\times$  time<sup>||</sup>. For this study the LBNE beamline improvements discussed in Section 3.4 are used with  $E_p = 80$  GeV, and the signal and background systematics are assumed to be 1% and 5%, respectively. Both  $\nu_e$  and  $\nu_\mu$  appearance signals are used in a combined analysis. Due to the long baseline and the large value of  $\theta_{13}$ , the determination of the mass hierarchy in LBNE to high precision does not require a large exposure. A  $5\sigma$  sensitivity for the worst case (NH,  $\delta_{CP} = \pi/2$ ) or (IH,  $\delta_{CP} = -\pi/2$ ) requires an exposure of  $\sim 200$  kton.MW.years **FIXME:** *is this best way to render these units?*, but  $5\sigma$  sensitivity can be reached for 50% of the allowed values of  $\delta_{CP}$  with an exposure of less than 100 kton.MW.years. On the other hand, reaching discovery-level sensitivities ( $\geq 5\sigma$ ) to leptonic CP violation for at least 50% of the possible values of  $\delta_{CP}$  will require large exposures of  $\approx 450$  kton.MW.years. Figure 4-16 demonstrates the sensitivity to CP violation as a function of  $\delta_{CP}$  and exposure that can be achieved with various stages of Project X (Table 3-2). In this study, Stage 1 and 2 of Project X are assumed to provide to LBNE 1.1 MW at 80 GeV, followed by Stage 3 which will provide 2.3 MW, also at 80 GeV. The study demonstrates that it is possible to reach  $5\sigma$  sensitivity to CP violation over at least 50% of  $\delta_{CP}$  values with a 34-kt LArTPC detector running for a little over 10 years, starting with the current MI power and phasing in Project X upgrades. Other possible staging scenarios of detector mass and beam power are discussed in Chapter 3. **FIXME:** *not sure they're there; check*

<sup>||</sup>Time is denoted in years of running at Fermilab. One year of running at Fermilab corresponds to  $\approx 1.8 \times 10^7$  seconds.



**Figure 4–15:** The minimum significance with which the mass hierarchy (top) and CP violation (bottom) can be resolved as a function of exposure in detector mass (kiloton)  $\times$  beam power (MW)  $\times$  time (years). The red band represents the fraction of  $\delta_{CP}$  values for which the sensitivity can be achieved with at least the minimal significance on the y-axis.



**Figure 4-16:** The significance with which CP violation —  $\delta_{CP} \neq 0$  or  $\pi$  — can be determined as a function of  $\delta_{CP}$  (top) and the minimum significance versus exposure for 50% of  $\delta_{CP}$  values (bottom). The different color curves represent possible exposures from different stages of Project X as follows: 700 kW, 100 kton-years (red), + 1.1MW, 200 kton-years (blue) + 2.3MW, 200 kton-years (green). **FIXME:** I don't understand the + stuff The band on the top figure represents the range of sensitivities obtained from improvements to the beamline design described in the CDR.

With tight control of systematics, LBNE — using conventional beam technologies and a mature detector design — can reach  $5\sigma$  sensitivity to CP violation for a large fraction of  $\delta_{CP}$  values with the minimal combination of power-on-target and far detector mass when compared to current and future proposed neutrino oscillation experiments (see Figure 4-17).

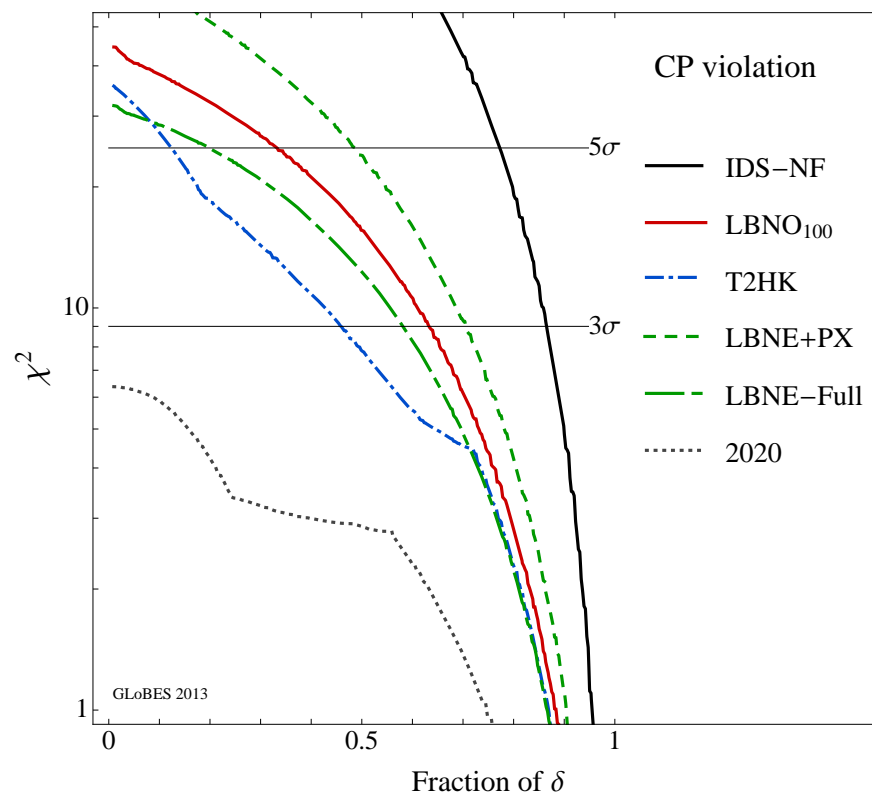


**Figure 4-17:** The minimal CP-violation sensitivity for a given fraction of  $\delta_{CP}$  values for different proposed neutrino oscillation experiments. The dashed black curve labeled “2020” is the expected sensitivity from the current generation of experiments that could be achieved by 2020. LBNE-Full represents a 34-kt LArTPC running in a 700-kW beam for  $5(\nu) + 5(\bar{\nu})$  yrs. LBNE-PX is LBNE staged with Project X beams as shown in Figure 4-16. T2HK is a 560-kt water Cherenkov detector running in a 1.66-MW beam for  $1.5(\nu) + 3.5(\bar{\nu})$  yrs [?]. LBNO<sub>100</sub> is a 100-kton LArTPC at a baseline of 2,300 km running in a 0.8-MW beam from CERN for  $5(\nu) + 5(\bar{\nu})$  yrs [?]. NF-IDS is the Neutrino Factory with a neutrino beam generated from muon decays in a 10-GeV muon storage ring produced from a 4-MW, 8-GeV Project X proton beam coupled with 100-kT magnetized iron detectors at a baseline of 2,000 km ( $\nu + \bar{\nu}$  simultaneously) [?]. Figure courtesy of Pilar Coloma and Patrick Huber. **FIXME:** too long; move some to text

## 4.5 Measurement of $\theta_{23}$ and Determination of the Octant

**FIXME:** *Would be nice to start with a sentence reiterating the significance of theta 2-3, what it means to ‘determine the octant’ and what significance that has.*

**FIXME:** *new* The value of the atmospheric mixing angle  $\sin^2 \theta_{23}$  from global fits given by [?] is  $\sin^2 \theta_{23} = 0.0386^{+0.0024}_{-0.0021}(1\sigma)$  for a normal hierarchy, but as shown in Figure 4-18, the distribution of the  $\chi^2$  from the global fit has another local minimum — particularly if the hierarchy is inverted — at  $\sim \sin^2 \theta_{23} = 0.62$ . A maximal mixing value of  $\sin^2 \theta_{23} = 0.5$  is therefore still allowable and the octant is still largely undetermined.

**FIXME:** *old* The value of the atmospheric mixing angle  $\sin^2 \theta_{23}$  from global fits given by [?] is  $\sin^2 \theta_{23} = 0.0386^{+0.0024}_{-0.0021}(1\sigma)$  for a normal hierarchy, but as shown in Figure 4-18, the distribution of the  $\chi^2$  from the global fit has another local minimum at  $\sim \sin^2 \theta_{23} = 0.62$  — particularly if the hierarchy is inverted. As a result a maximal mixing value of  $\sin^2 \theta_{23} = 0.5$  is still allowable and the octant is still largely undetermined.

**FIXME:** *new* The determination of whether there is maximal mixing in the lepton sector (or a measurement of the deviation from maximal) is of great interest theoretically. Models of quark-lepton universality propose that  $U^{\text{CKM}} = 1 + (\text{Cabbibo})$  and  $U^{\text{PMNS}} = T + (\text{Cabbibo})$  effects **FIXME:** *affects? is this the verb?* where  $T$  is determined by Majorana physics [?]. In such models  $\theta_{23} \sim \pi/4 + \Delta\theta$ , where  $\Delta\theta$  is of order the Cabbibo angle,  $\theta_C$ , and  $\theta_{13} \sim \theta_C/\sqrt{2}$ . **FIXME:** *Says theta 1-3, correct?* It is therefore important experimentally both to determine the value of  $\sin^2 \theta_{23}$  and to determine the octant of  $\theta_{23}$ .

The measurement of  $\nu_\mu \rightarrow \nu_\mu$  oscillations is sensitive to  $\sin^2 2\theta_{23}$ , whereas the measurement of  $\nu_\mu \rightarrow \nu_e$  oscillations is sensitive to  $\sin^2 \theta_{23}$ . A combination of both  $\nu_e$  appearance and  $\nu_\mu$  disappearance measurements can probe both maximal mixing and the  $\theta_{23}$  octant. With the large statistics and rich spectral structure in a wide-band long-baseline experiment like LBNE (see Figure 4-11), precision measurements of  $\sin^2 \theta_{23}$  can be significantly improved compared to existing experiments, particularly for values of  $\theta_{23}$  near  $45^\circ$ . Figure 4-19 demonstrates the measurement precision of  $\theta_{23}$  and  $\Delta m_{31}^2$  that can be achieved by LBNE with a 10-kt detector alone (LBNE10) for different allowed values. For the disappearance mode, systematic uncertainties of 5% on signal and 10% on background are assumed; this is consistent with the assumption of no near neutrino detector. The sub-dominant appearance mode in LBNE10 is dominated by statistical uncertainties.

**FIXME:** *old* The determination of whether there is maximal mixing in the lepton sector or a measurement of the size of the deviation from maximal is of great interest theoretically. Models of quark-lepton universality propose that  $U^{\text{CKM}} = 1 + (\text{Cabbibo})$  and  $U^{\text{PMNS}} = T + (\text{Cabbibo})$  effects where  $T$  is determined by Majorana physics [?]. In such models  $\theta_{23} \sim \pi/4 + \Delta\theta$ , where  $\Delta\theta$  is of order the Cabbibo angle,  $\theta_C$ , and  $\theta_{13} \sim \theta_C/\sqrt{2}$ . It is therefore important experimentally both to determine the value of  $\sin^2 \theta_{23}$  and to determine



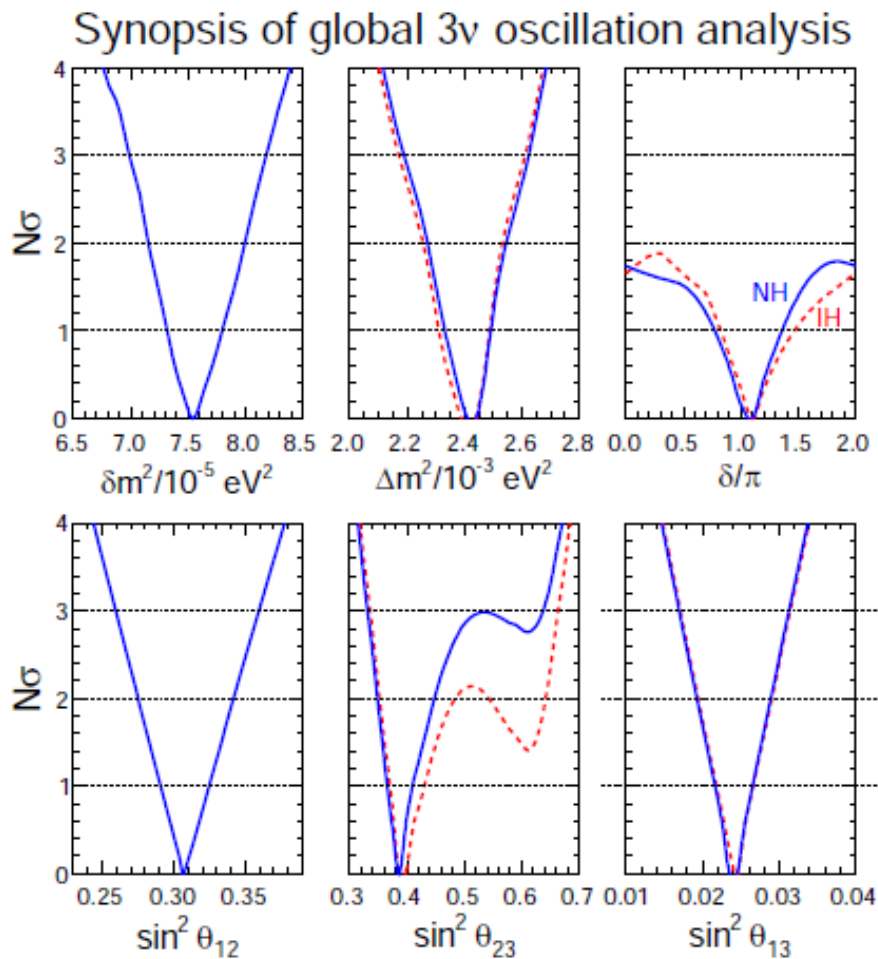


**Figure 4–18:** Results of the global analysis in terms of  $N\sigma$  bounds on the six parameters governing three  $\nu$  flavor oscillations. Blue (solid) and red (dashed) curves refer to NH and IH, respectively. Figure is from ref. [?]

the octant of  $\theta_{23}$ . The measurement of  $\nu_\mu \rightarrow \nu_\mu$  oscillations is sensitive to  $\sin^2 2\theta_{23}$ , whereas the measurement of  $\nu_\mu \rightarrow \nu_e$  oscillations is sensitive to  $\sin^2 \theta_{23}$ . A combination of both  $\nu_e$  appearance and  $\nu_\mu$  disappearance measurements can probe both maximal mixing and the  $\theta_{23}$  octant. With the large statistics and rich spectral structure in a wide-band long-baseline experiment like LBNE (see Figure 4-11), precision measurements of  $\sin^2 \theta_{23}$  can be significantly improved compared to existing experiments, particularly for values of  $\theta_{23}$  near  $45^\circ$ . Figure 4-19 demonstrates the measurement precision of  $\theta_{23}$  and  $\Delta m_{31}^2$  that can be achieved by LBNE with a 10 kton detector alone (LBNE10) for different allowed values. For the disappearance mode systematic uncertainties of 5% on signal and 10% on background are assumed - which is consistent with the assumption of no near neutrino detector. The sub-dominant appearance mode in LBNE10 is dominated by statistical uncertainties.

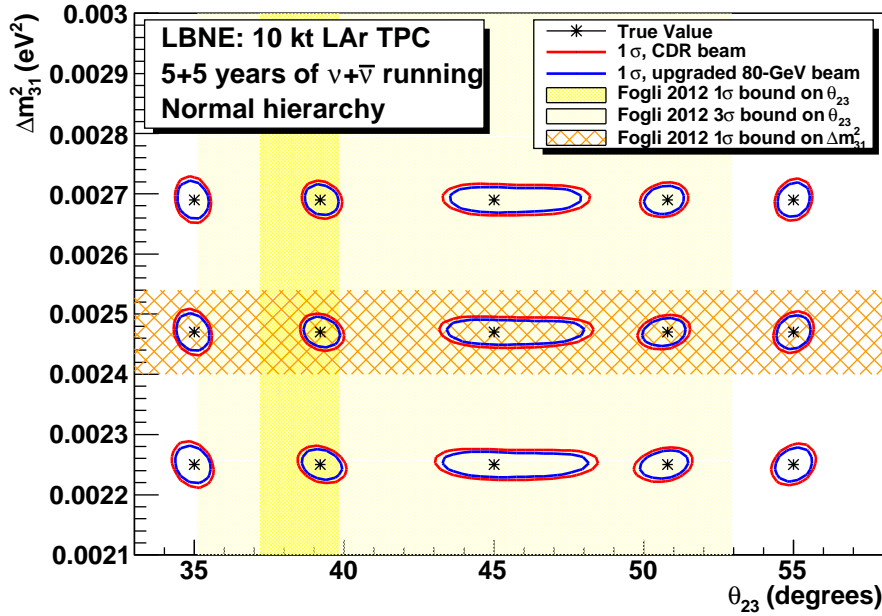


**Figure 4-19:** The precision with which a simultaneous measurement of  $\theta_{23}$  and  $\Delta m_{31}^2$  can be determined in the LBNE10 configuration. The yellow bands represent the  $1\sigma$  and  $3\sigma$  allowed ranges of  $\theta_{23}$  from the 2012 global fit.

The significance with which the  $\theta_{23}$  octant can be determined with LBNE10 is shown in Figure 4-20. If  $\theta_{23}$  is within the current  $1\sigma$  bound of the best fit value from the global fits, LBNE10 alone will determine the octant with  $> 3\sigma$  significance for all values of  $\delta_{CP}$ . Figure 4-21 demonstrates the increasing sensitivity to the  $\theta_{23}$  octant for values closer to maximal mixing that can be achieved with subsequent phases of LBNE coupled with Project X upgrades to the Main Injector power. With sufficient exposure, LBNE can resolve the  $\theta_{23}$  octant with  $> 3\sigma$  significance even if  $\theta_{23}$  is within a few degrees of  $45^\circ$ .

### Octant Sensitivity

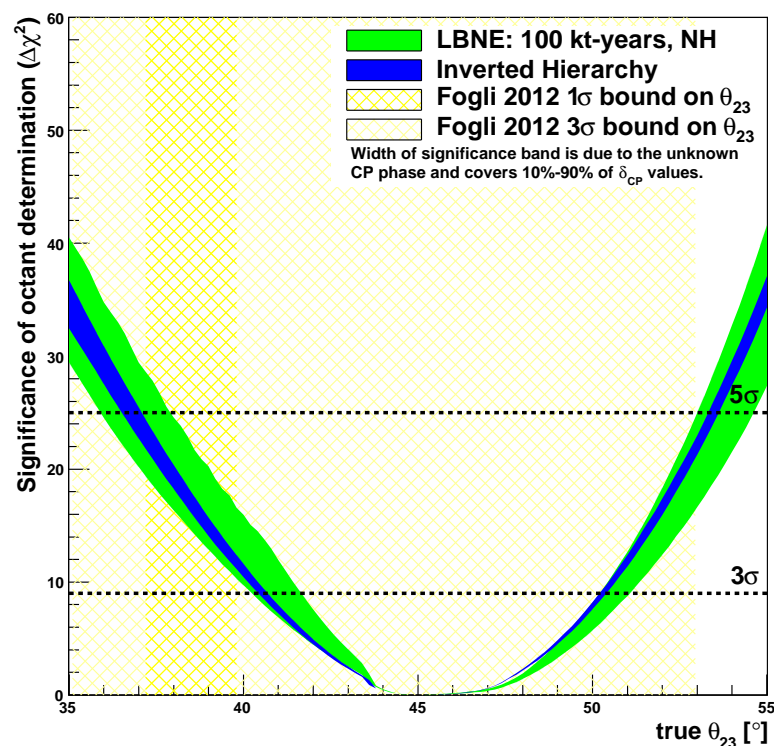


**Figure 4–20:** Significance with which LBNE can resolve the  $\theta_{23}$  octant degeneracy for 5+5 years of  $\nu+\bar{\nu}$  running at 700 kW with a 10-kt detector. The green band is for normal hierarchy and the blue band is for inverted hierarchy. The width of the bands corresponds to the impact of different true values for  $\delta_{CP}$ , ranging from a 10% to 90% fraction of  $\delta_{CP}$ . The yellow bands represent the 1 $\sigma$  and 3 $\sigma$  allowed ranges of  $\theta_{23}$  from the 2012 global fit.

### Octant Sensitivity

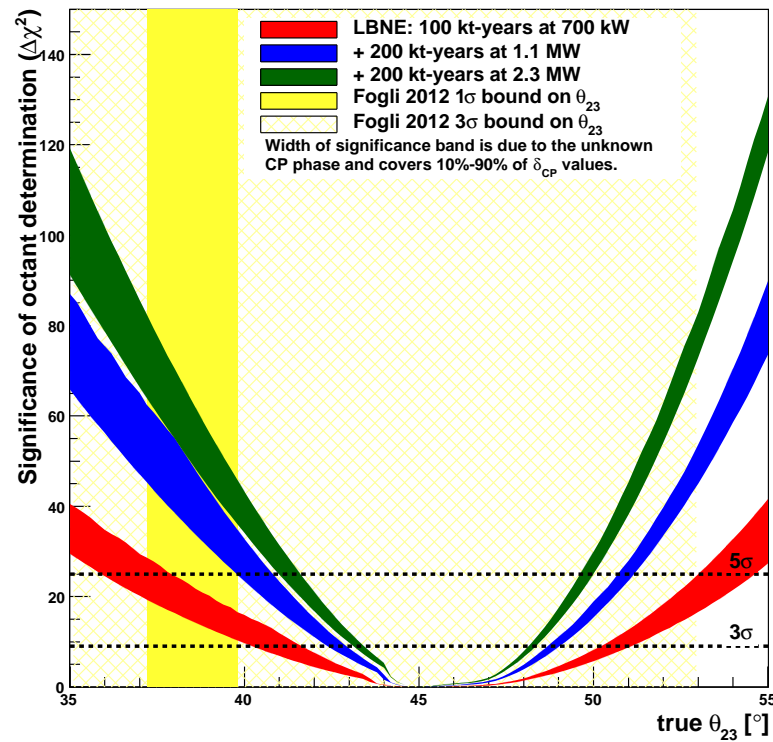


**Figure 4–21:** Significance with which LBNE can resolve the  $\theta_{23}$  octant degeneracy for 5+5 years of  $\nu+\bar{\nu}$  running with increased exposures as follows 700 kW, 100 kt-years (red), + 1.1 MW, 200 kt-years (blue) + 2.3 MW, 200 kt-years (green). Normal mass hierarchy is assumed. The width of the bands corresponds to the impact of different true values for  $\delta_{CP}$ , ranging from a 10% to 90% fraction of  $\delta_{CP}$ .

## 4.6 Precision Measurements of the Oscillation Parameters in the Three-Flavor Model

**FIXME: new** The rich oscillation structure and excellent particle identification of LBNE will enable precision measurement of all the mixing parameters governing the 1-3 and 2-3 mixing in a single experiment. As discussed in Section 4.5, theoretical models probing quark-lepton universality predict specific values of the mixing angles and the relations between them. The reactor mixing angle  $\theta_{13}$  is expected to be measured accurately in reactor experiments by the end of the decade with a precision that will be limited by systematics. The systematic uncertainty on the value of  $\sin^2 2\theta_{13}$  from the Daya Bay reactor neutrino experiment — which has the lowest systematics — is currently 0.005 [?].

**FIXME: old** The rich oscillation structure and excellent particle identification of LBNE will enable precision measurement of all the mixing parameters governing the 1-3 and 2-3 mixing in a single experiment. As discussed in Section 4.5, theoretical models probing quark-lepton universality predict specific values of the mixing angles and the relations between them. The reactor mixing angle  $\theta_{13}$  is expected to be measured accurately in reactor experiments by the end of the decade with a precision that will be limited by systematics. The systematic uncertainty on the value of  $\sin^2 2\theta_{13}$  from the Daya Bay reactor neutrino experiment - which has the lowest systematics - is currently 0.005 [?].

**FIXME: new** While the constraint on  $\theta_{13}$  from the reactor experiments will be important in the early stages of LBNE for determining CP violation, measuring  $\delta_{CP}$  and determining the  $\theta_{23}$  octant, LBNE itself will eventually be able to measure  $\theta_{13}$  independently with a precision on par with the final precision expected from the reactor experiments. Whereas the reactor experiments measure  $\theta_{13}$  using  $\bar{\nu}_e$  disappearance, LBNE will measure it through  $\nu_e$  and  $\bar{\nu}_e$  appearance, thus providing an independent constraint on the three-flavor mixing matrix. Figure 4-22 demonstrates the precision with which LBNE can measure  $\delta_{CP}$  and  $\theta_{13}$  simultaneously with no external constraints on  $\theta_{13}$  as a function of increased exposure starting with LBNE10 and in subsequent phases with different Project X beams. Both appearance and disappearance modes are included in the fit using the upgraded 80-GeV beam, and with 1%/5% systematic uncertainties assumed on signal/background.

**FIXME: old** While the constraint on  $\theta_{13}$  from the reactor experiments will be important in the determination of CP violation, measurement of  $\delta_{CP}$  and the determination of the  $\theta_{23}$  octant in the early stages of LBNE, eventually LBNE will be able to measure  $\theta_{13}$  independently with a precision on par with the final precision expected from the reactor experiments. We note that the reactor experiments measure  $\theta_{13}$  using  $\bar{\nu}_e$  disappearance whereas LBNE will measure it through  $\nu_e$  and  $\bar{\nu}_e$  appearance, thus providing an independent constraint on the 3-flavor mixing matrix. Figure 4-22 demonstrates the precision with which LBNE can measure  $\delta_{CP}$  and  $\theta_{13}$  simultaneously with no external constraints on  $\theta_{13}$  as a function of increased exposure starting with LBNE10 and in subsequent phases with different Project X

beams. Both appearance and disappearance modes are included in the fit using the upgraded 80 GeV beam, and with 1%/5% systematic uncertainties assumed on signal/background.

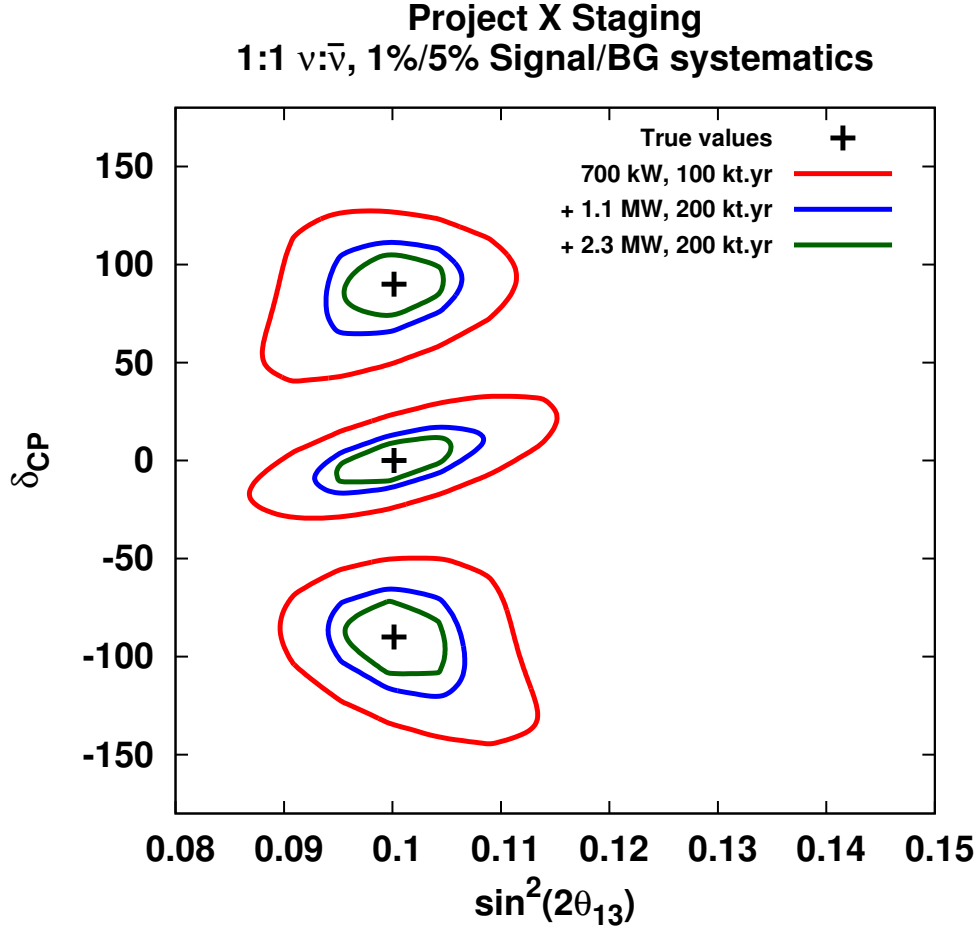


**Figure 4–22:** Measurement of  $\delta_{CP}$  and  $\theta_{13}$  in LBNE with different exposures.

**FIXME:** *new, few little chgs, got rid of old* Figure 4–23 shows the expected  $1\sigma$  resolution on different three-flavor oscillation parameters as a function of exposure in a 700-kW beam with LBNE alone, and LBNE in combination with the expected performance from T2K and NO $\nu$ A. It should be noted that LBNE alone could reach a precision on  $\sin^2 2\theta_{13}$  of 0.005 — on par with the current Daya Bay systematic uncertainty — with an exposure of  $\sim 300$  kt.MW.yrs. LBNE can also significantly improve the resolution on  $\Delta m_{23}^2$  beyond what the combination of NO $\nu$ A and T2K can achieve, reaching a precision of  $< 1 \times 10^{-5} \text{ eV}^2$  with an exposure of  $\sim 300$  kt.MW.yrs.

The precision on  $\Delta m_{23}^2$  will ultimately depend on tight control of energy scale systematics. Initial studies of the systematics reveal that the measurement of  $\nu_\mu$  disappearance in LBNE over a full oscillation interval with two oscillation peaks and two valleys (Figure 4–11),

reduces the dependency of the  $\Delta m_{23}^2$  measurement on the energy scale systematics, which dominated the measurement precision in MINOS [?]. Table 4-7 summarizes the sensitivities

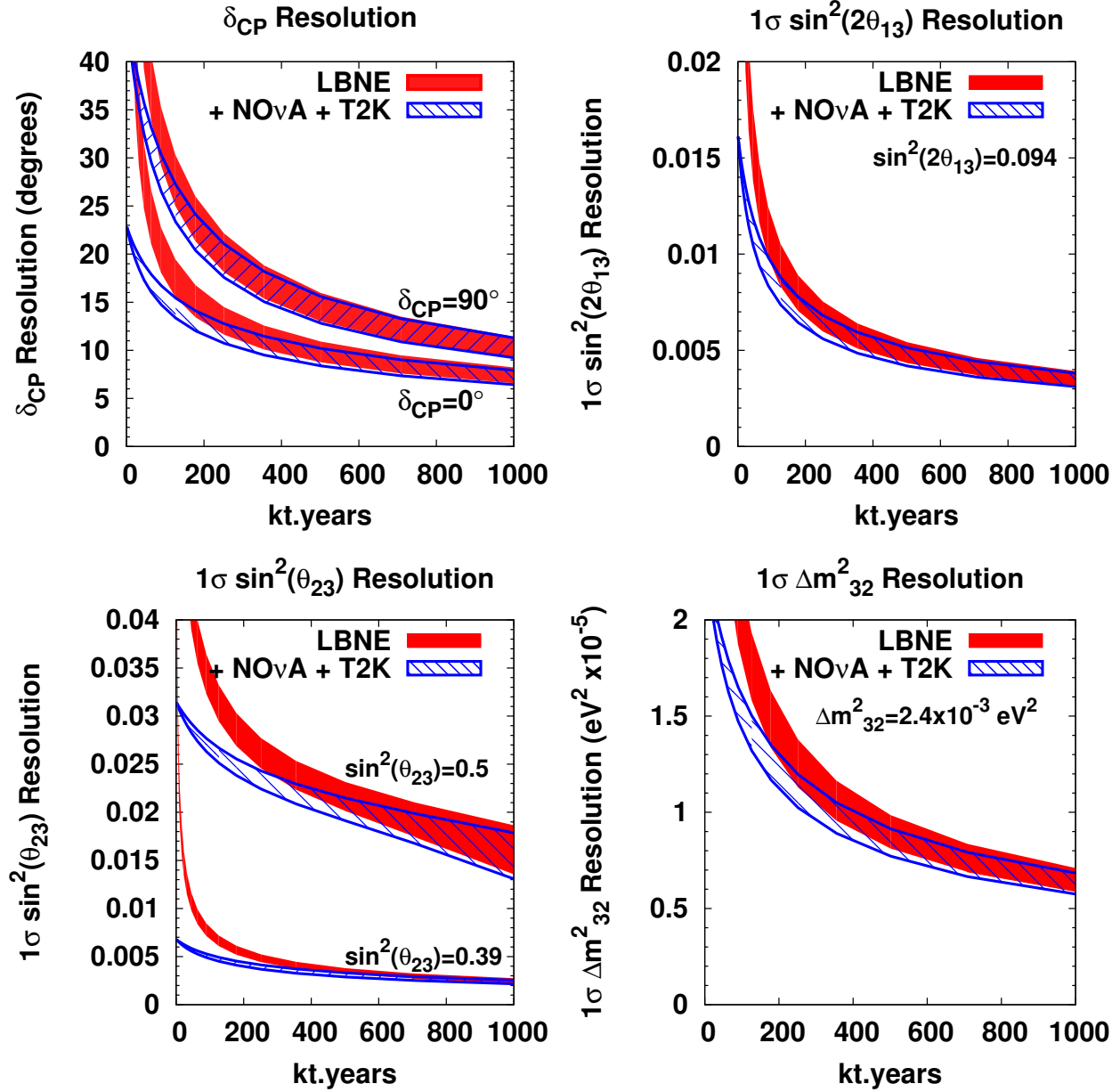


**Figure 4-23:** The expected  $1\sigma$  resolution on different three-flavor oscillation parameters as a function of exposure in a 700-kW beam. The red curve indicates the precision that could be obtained from LBNE alone, and the blue curve represents the combined precision from LBNE and the T2K and NO $\nu$ A experiments. The width of the bands represents the range of performance with the beam improvements under consideration. Clockwise from top left the plots represent:  $\delta_{CP}$ ,  $\sin^2 2\theta_{13}$ ,  $|\Delta m_{31}^2|$ , and  $\sin^2 \theta_{23}$ .

to the mass hierarchy and CP violation and the precision with which the different oscillation

parameters can be measured with different far detector masses in LBNE. A 10-year exposure to the 700-kW beam from the current Main Injector complex is assumed.

Alone, LBNE can potentially reach a precision on  $\delta_{CP}$  between roughly  $6^\circ$  and  $10^\circ$ , i.e., close to the  $4^\circ$  CKM precision on  $\delta_{CP}^{\text{CKM}}$  — but an exposure of  $\sim 700$  kt.MW.years is needed. Nevertheless, as shown in Figure 4-24, wide-band, long-baseline experiments such as LBNE (and LBNO) can achieve nearly CKM precision on  $\delta_{CP}$  with much less exposure when **FIXME:** *does the precision get better than 6 to 10 (stated above) or is it just much better than these other expts can do?* compared to existing experiments such as NO $\nu$ A, T2K and proposed short-baseline, off-axis experiments such as T2HK. It is important to note that the precision on  $\delta_{CP}$  in the off-axis experiments shown in Figure 4-24 assumes the mass hierarchy is resolved. If the mass hierarchy is unknown, the resolution of T2K, NO $\nu$ A and T2HK will be much worse than indicated. LBNE does not require external information on the mass hierarchy to reach the precisions described in this section. Only a neutrino factory can possibly out-perform a wide-band, long-baseline experiment — but not by much — for equivalent power, target mass and years of running. To achieve this precision, however, LBNE will need to tightly control the systematic uncertainties on the  $\nu_e$  appearance signal. A high-resolution near detector will be needed to reach this level of precision, as described in Chapter 3.5.

Future upgrades to the Fermilab accelerator complex — in particular the prospect of high-power, low-energy proton beams such as 3 MW at 8 GeV available in Stage 4 of Project X — could open up further opportunities to probe CP violation using on-axis, low-energy beams specifically directed at the second oscillation maximum where CP effects dominate the asymmetries [?]. Project X could even enable studies in 1-2 mixing in very long-baseline experiments. **FIXME:** *i.e., beyond LBNE?*

## 4.7 Oscillation Studies Using Atmospheric Neutrinos

**FIXME:** *Changed title for consistency*

**FIXME:** *new; basically same as old; ditched old* Atmospheric neutrinos are unique among sources used to study oscillations: the flux contains neutrinos and antineutrinos of all flavors, matter effects play a significant role, both  $\Delta m^2$  values contribute, and the oscillation phenomenology occurs over several decades each in energy (see Figure 2-6) and path length. These characteristics make it ideal for the study of oscillations (in principle sensitive to all of the remaining unmeasured quantities in the PMNS matrix) and provide a laboratory in which to search for exotic phenomena for which the dependence of the flavor-transition and survival probabilities on energy and path length can be defined. The large LArTPC far detector — if placed at sufficient depth to shield from cosmic ray backgrounds — provides a unique opportunity to study atmospheric neutrino interactions with excellent energy and path-length resolutions.



**Table 4-7:** Summary of the oscillation measurements with different configurations given  $\theta_{13} = 8.8^\circ$ ,  $\theta_{23} = 40^\circ$ ,  $\Delta m_{31}^2 = +2.27 \times 10^{-3} \text{eV}^2$ . The fraction of  $\delta_{CP}$  values for which the mass hierarchy (MH) or CP violation (CPV) are determined with  $3\sigma$  sensitivity are given in the first two columns. For the first two columns, all correlations and uncertainties on the known mixing parameters, as well as consideration of the opposite mass hierarchy hypothesis, are included. The measurements assume 5 years of neutrino running and 5 years of antineutrino running at a beam power of 708 kW with  $6 \times 10^{20}$  protons-on-target accumulated per year with an LArTPC. It is assumed that  $\text{NO}\nu\text{A}$  will run for a minimum of 3+3 years with the NuMI ME energy beam ( $\text{NO}\nu\text{A}$  I). It is also assumed that  $5 \times 10^{21}$  protons-on-target will be the total accumulated by T2K ( $\sim 6$  yrs) in neutrino only mode. \* These measurements are for **FIXME**: *represent?* the combination of neutrino and antineutrino running. NOTE: This table is taken from the LBNE Reconfiguration Physics Working Group Study [?] and some performance metrics have changed with beamline design improvements and detector response updates. **FIXME:** *This is awfully long for a caption.*

Configuration	MH* fraction of $\delta$ ( $3\sigma$ )	CPV* fraction of $\delta$ ( $3\sigma$ )	$\sigma(\delta_{cp})^*$ 0, $90^\circ$	$\sigma(\theta_{13})^*$ $\delta = 90^\circ$	$\sigma(\theta_{23})$ $\nu$	$\sigma(\theta_{23})$ $\bar{\nu}$	$\sigma(\Delta m_{31}^2)$ $\nu$ ( $10^{-3} \text{eV}^2$ )	$\sigma(\Delta m_{31}^2)$ $\bar{\nu}$ ( $10^{-3} \text{eV}^2$ )
$\text{NO}\nu\text{A}$ (6yrs) + T2K (6yrs)	0.0	0.0	22,65°	0.62°				
Homestake 5kt	0.66	0.00	25,41°	0.60°	0.92°	1.4°	0.035	0.055
Homestake 10kt	0.75	0.05	17,30°	0.40°	0.69°	0.97°	0.025	0.040
Homestake 15kt	0.90	0.40	15,25°	0.30°	0.52°	0.80°	0.020	0.030
Homestake 20kt	1.0	0.50	13,21°	0.25°	0.46°	0.63°	0.018	0.026
Homestake 5kt + $\text{NO}\nu\text{A}$ + T2K	1.00	0.33	15,31°					
Homestake 10kt + $\text{NO}\nu\text{A}$ + T2K	1.00	0.45	12,25°					
Homestake 15kt + $\text{NO}\nu\text{A}$ + T2K	1.00	0.53	12,24°					

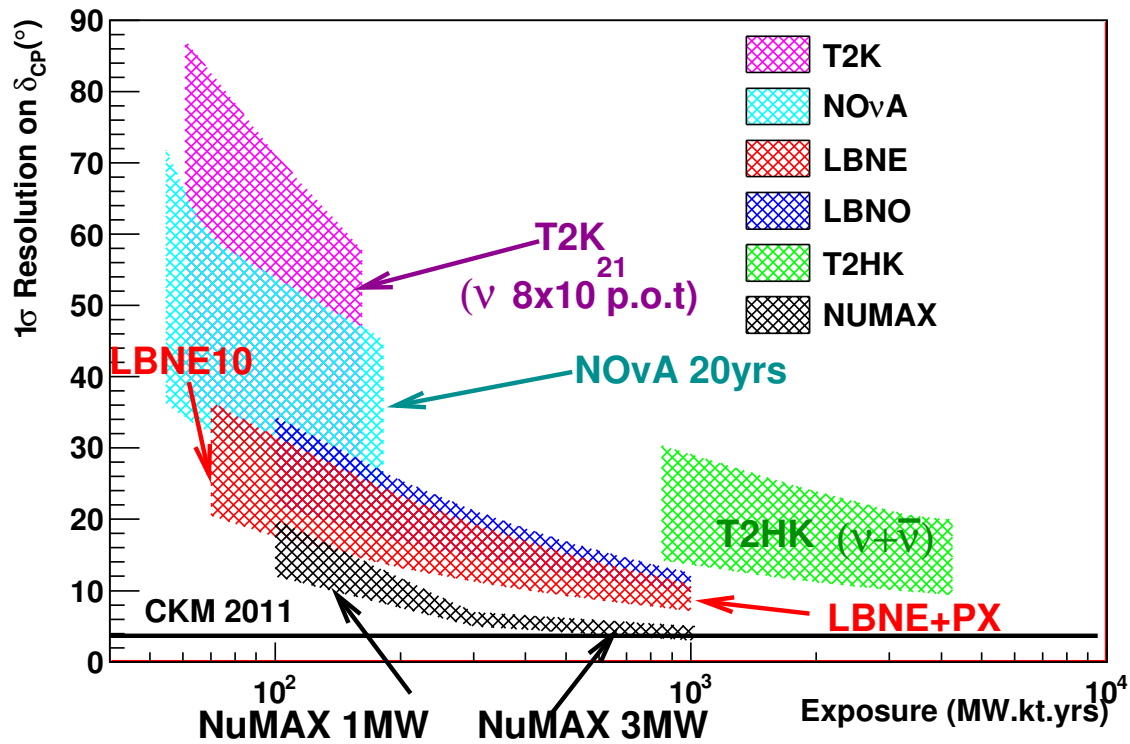


**Figure 4–24:** The  $1\sigma$  resolution on  $\delta_{CP}$  that can be achieved by existing and proposed beamline neutrino oscillation experiments as a function of exposure in terms of mass  $\times$  beam power  $\times$  years of running. The band represents the variation in the resolution as a function of  $\delta_{CP}$  with the lower edge representing the best resolution and the upper edge the worst. The bands start and stop at particular milestones. For example, the LBNE band starts with the resolutions achieved by LBNE10 and ends with the full LBNE running with the first three stages of Project X. The black line denotes the  $4^\circ$  resolution point which is the resolution of  $\delta_{CP}^{\text{CKM}}$  from the 2011 global fits.

LBNE was able to obtain FD physics sensitivities based on information from atmospheric neutrinos by using a Fast MC and a three-flavor analysis framework developed for the MINOS experiment [?].

**FIXME:** *connect this framework with genie and the bartol flux calc, below*

**FIXME:** *new* Four-vector level events are generated using the GENIE neutrino event generator [?]. For atmospheric neutrinos the Bartol [?] flux calculation for the Soudan, MN site was used, and for beam neutrinos the CDR 120 GeV, 700 kW beam [?] as well as the 80 GeV improved beamline designs were used. **FIXME:** *unclear how bartol and genie interact* The expected event rates in 100 kt-yrs are shown in Table 4–8. All interactions occur on argon, and are distributed uniformly throughout a toy detector geometry consisting of two modules, each 14.0 m high, 23.3 m wide, and 45.4 m long. For this study, events with interaction vertices outside the detector volume (e.g., events that produce upward-going stopping or throughgoing muons) have not been considered. Cosmogenic backgrounds have not been studied in detail, but since atmospheric neutrinos are somewhat more tolerant of background than proton decay, a depth that is sufficient for a proton decay search is expected to also be suitable for atmospheric neutrinos. For the SURF 4,850-ft depth, a veto should not be necessary, and one can assume full fiducial mass **FIXME:** *for what?*; at depths around 2,700 feet, a one-meter fiducial cut should be adequate.

**FIXME:** *old* Four-vector level events are generated using the GENIE neutrino event generator [?]. For atmospheric neutrinos the Bartol [?] flux calculation for the Soudan, MN site was used, and for beam neutrinos the CDR 120 GeV, 700 kW beam [?] as well as the 80 GeV improved beamline designs were used. The expected event rates in 100 kt-yrs are shown in Table 4–8. All interactions occur on argon, and are distributed uniformly throughout a toy detector geometry consisting of two modules each 14.0 m high, 23.3 m wide, and 45.4 m long. For this study, events with interaction vertices outside the detector volume, for instance which produce upward-going stopping or throughgoing muons, have not been considered. We have not studied cosmogenic backgrounds in detail, but we expect that since atmospheric neutrinos are somewhat more tolerant of background than proton decay, a depth that is sufficient for a proton decay search should also be suitable for atmospheric neutrinos. For the SURF 4850L depth, a veto should not be necessary, and one can assume full fiducial mass; at depths around 2,700 feet, a one-meter fiducial cut should be adequate.

**FIXME:** *new* A Fast MC runs on the produced four-vectors, placing events into containment and flavor categories. Containment is evaluated by tracking leptons through the LAr detector box geometry and classifying events as either fully or partially contained. A detection threshold of 50 MeV is assumed for all particles. The flavor determination is based on the primary and secondary particles above detection threshold, and events are placed into electron-like or  $\mu$ -like categories based on the identity of these particles **FIXME:** *when were they ID'ed?* Electrons and muons are assumed to be correctly identified with only 90% and 100% probability, whereas other electromagnetic particles (e.g.,  $\pi^0, \gamma$ ) are misidentified as electrons 5% of the time, and charged pions are misidentified as muons 1% of the time.

**Table 4–8:** Expected event rates in 100 kt-yr for the Bartol flux and GENIE Argon cross sections (no oscillations).

Flavor	CC	NC	Total
$\nu_\mu$	10069	4240	14309
$\bar{\nu}_\mu$	2701	1895	4596
$\nu_e$	5754	2098	7852
$\bar{\nu}_e$	1230	782	2012
Total:	19754	9015	28769

**FIXME:** *comparison would be cleaner if it wasn't opposite; misID'ed vs ID'ed* Events in which neither of the two leading particles is identified as a muon or electron are placed into an 'NC-like' category. With these assumptions, the purities of the flavor-tagged samples are 97.8% for the FC electron-like sample, 99.7% for the FC  $\mu$ -like sample, and 99.6% for the PC  $\mu$ -like sample. The NC-like category is not used in this analysis, but would be useful for tau appearance studies.

The energy and direction of the event are then estimated by separately smearing these quantities of the leptonic and hadronic system, **FIXME:** *systems?* where the width of the Gaussian-resolution functions for each flavor/containment category are given in Table 4–9. Detector performance assumptions are taken both from the LBNE CDR and from published results from the ICARUS experiment [?,?].

**FIXME:** *old* A Fast MC then runs on the produced four-vectors, placing events into containment and flavor categories. Containment is evaluated by tracking leptons through the LAr detector box geometry and classifying events as either fully or partially contained. A detection threshold of 50 MeV is assumed for all particles. The flavor determination is based on the primary and secondary particles above detection threshold, and events are placed into e-like or  $\mu$ -like categories based on the identity of these particles. Electrons and muons are assumed to be correctly identified with 90% and 100% probability, while other electromagnetic particles ( $\pi^0, \gamma$ ) are misidentified as electrons 5% of the time, and charged pions are misidentified as muons 1% of the time. Events that do not have an identified muon or electron as one of the two leading particles are placed into an 'NC-like' category. With these assumptions the purities of the flavor-tagged samples are 97.8% for the FC e-like sample, 99.7% for the FC  $\mu$ -like sample, and 99.6% for the PC  $\mu$ -like sample. The NC-like category is not used in this analysis, but would be useful for tau appearance studies.

The energy and direction of the event are then estimated by separately smearing the energy and direction of the leptonic and hadronic system, where the width of the Gaussian resolution functions for each flavor / containment category are given in Table 4–9. Detector performance assumptions are taken from the LBNE CDR and published results from the ICARUS experiment [?,?].

**Table 4–9:** Detector performance assumptions for the atmospheric neutrino and the combined atmospheric+beam neutrino analyses.

Angular Resolutions	Electron	1°
	Muon	1°
	Hadronic System	10°
Energy Resolutions	Stopping Muon	3%
	Exiting Muon	15%
	Electron	$1\%/\sqrt{E(\text{GeV})} \oplus 1\%$
	Hadronic System	$30\%/\sqrt{E(\text{GeV})}$

**FIXME:** *new* Including oscillations, the expected number of events in 100 kt-yrs comes to 4015 events in the FC electron-like sample, 5958 events in the FC  $\mu$ -like sample and 1963 events in the PC  $\mu$ -like sample. Figure 4–25 shows the expected L/E distribution for ‘high-resolution’  $\mu$ -like events from a 350 kt-yr exposure; the latest data from Super-Kamiokande is shown for comparison. LBNE defines ‘high-resolution’ events in a similar way as Super-Kamiokande, either by excluding a region of low-energy events or pointing towards the horizon where the L resolution is poor. The data provides excellent resolution of the first two wavelengths, even taking into account the expected statistical uncertainty. **FIXME:** *does the next sentence belong here?* Unless otherwise specified, in this section, oscillation parameters are taken to be:  $\Delta m^2 = 1/2(\Delta m_{32}^2 + \Delta m_{31}^2) = 2.40 \times 10^{-3} \text{ eV}^2$ ,  $\sin^2 \theta_{23} = 0.40$ ,  $\Delta m_{12}^2 = 7.54 \times 10^{-5} \text{ eV}^2$ ,  $\sin^2 \theta_{12} = 0.307$ ,  $\sin^2 \theta_{13} = 0.0242$ ,  $\delta_{CP} = 0$ , and normal hierarchy.

**FIXME:** *old* Including oscillations, in 100 kt-yrs we expect 4015 events in the FC e-like sample, 5958 events in the FC  $\mu$ -like sample and 1963 events in the PC  $\mu$ -like sample. Figure 4–25 shows the expected L/E distribution for ‘High-Resolution’  $\mu$ -like events from a 350 kt-yr exposure and the latest data from Super-Kamiokande is shown for comparison. ‘High-resolution’ events are defined in a similar way to Super-Kamiokande, by excluding a region of events that are low energy or pointing towards the horizon where the L resolution is poor. The data provides excellent resolution of the first two wavelengths, even taking into account the expected statistical uncertainty. Unless otherwise specified, in this section oscillation parameters are taken to be:  $\Delta m^2 = 1/2(\Delta m_{32}^2 + \Delta m_{31}^2) = 2.40 \times 10^{-3} \text{ eV}^2$ ,  $\sin^2 \theta_{23} = 0.40$ ,  $\Delta m_{12}^2 = 7.54 \times 10^{-5} \text{ eV}^2$ ,  $\sin^2 \theta_{12} = 0.307$ ,  $\sin^2 \theta_{13} = 0.0242$ ,  $\delta_{CP} = 0$ , and normal hierarchy.

In performing oscillation fits the data in each flavor/containment category are binned in energy and zenith angle. Figure 4–26 shows the zenith angle distributions for several ranges of reconstructed energy, where oscillation features are clearly evident.

The power to resolve the mass hierarchy with atmospheric neutrinos comes primarily from the MSW enhancement of few-GeV neutrinos at large zenith angles. This enhancement occurs for neutrinos in the normal hierarchy and antineutrinos in the inverted hierarchy. Figure 4–27 shows zenith angle distributions of events in the relevant energy range for each of the three flavor/containment categories. Small differences are evident in comparing the normal

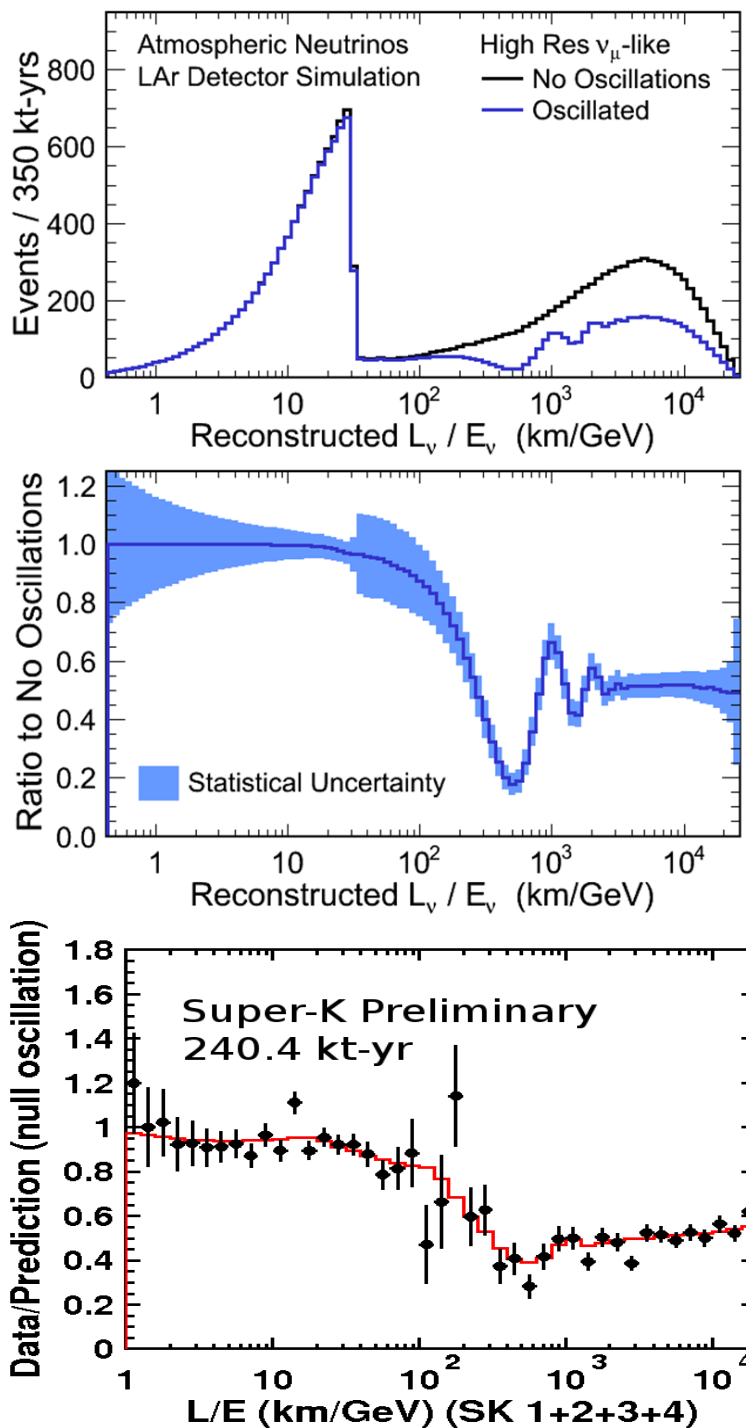


**Figure 4-25:** Reconstructed  $L/E$  Distribution of 'high-resolution'  $\mu$ -like atmospheric neutrino events in LBNE with a 350 kt-yr exposure with and without oscillations (top); the ratio of the two, with the shaded band indicating the size of the statistical uncertainty (center); the ratio of observed data over the null oscillation prediction from the Super-Kamiokande detector with 240.4 kt-yr of exposure (bottom).

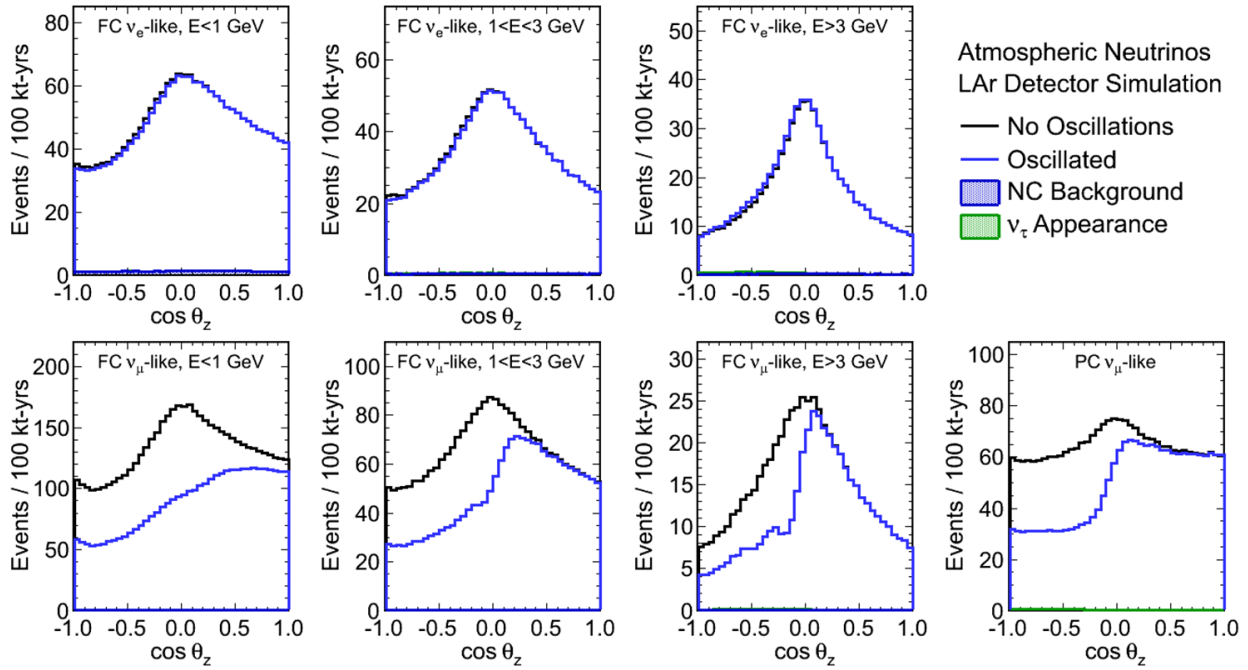


**Figure 4-26:** Reconstructed zenith angle distributions in several ranges of energy for the FC electron-like, FC  $\mu$ -like, and PC  $\mu$ -like samples. The small contributions from NC backgrounds and tau appearance are also shown.

and inverted hierarchy predictions.

**FIXME: new** Since the resonance peak occurs for neutrinos in the normal hierarchy and antineutrinos in the inverted hierarchy, the MH sensitivity can be greatly enhanced if neutrino and antineutrino events can be separated. The LBNE detector will not be magnetized, however the high-resolution imaging does offer some possibilities for tagging features of events that provide statistical discrimination between neutrinos and antineutrinos. For the sensitivity calculations that follow, two such tags are included: a proton tag and a decay-electron tag. Protons are tagged with 100% efficiency if their kinetic energy is greater than 50 MeV (for low-multiplicity events, protons occur preferentially in neutrino interactions). Decay electrons are assumed to be 100% identifiable and are assumed to occur 100% of the time for  $\mu^+$  and 25% of the time for  $\mu^-$ , based on the  $\mu^\pm$  capture probability on Ar40.

In the oscillation analysis 18 *nuisance* parameters are included, with detector performance parameters correlated between beam and atmospheric data. In all cases  $\sin^2 \theta_{12}$ ,  $\Delta m^2 = 1/2(\Delta m_{32}^2 + \Delta m_{31}^2)$ , and  $\Delta m_{12}^2$  are taken to be fixed at the previously given values. The fits then range over  $\theta_{23}$ ,  $\theta_{13}$ ,  $\delta_{CP}$ , and the mass hierarchy. A 2% constraint is assumed on the value of  $\theta_{13}$ . The systematic errors included in this analysis are given in Table 4-10.

**FIXME: old** Since the resonance peak occurs for neutrinos in normal hierarchy and antineutrinos for inverted hierarchy, the MH sensitivity can be greatly enhanced if neutrino and

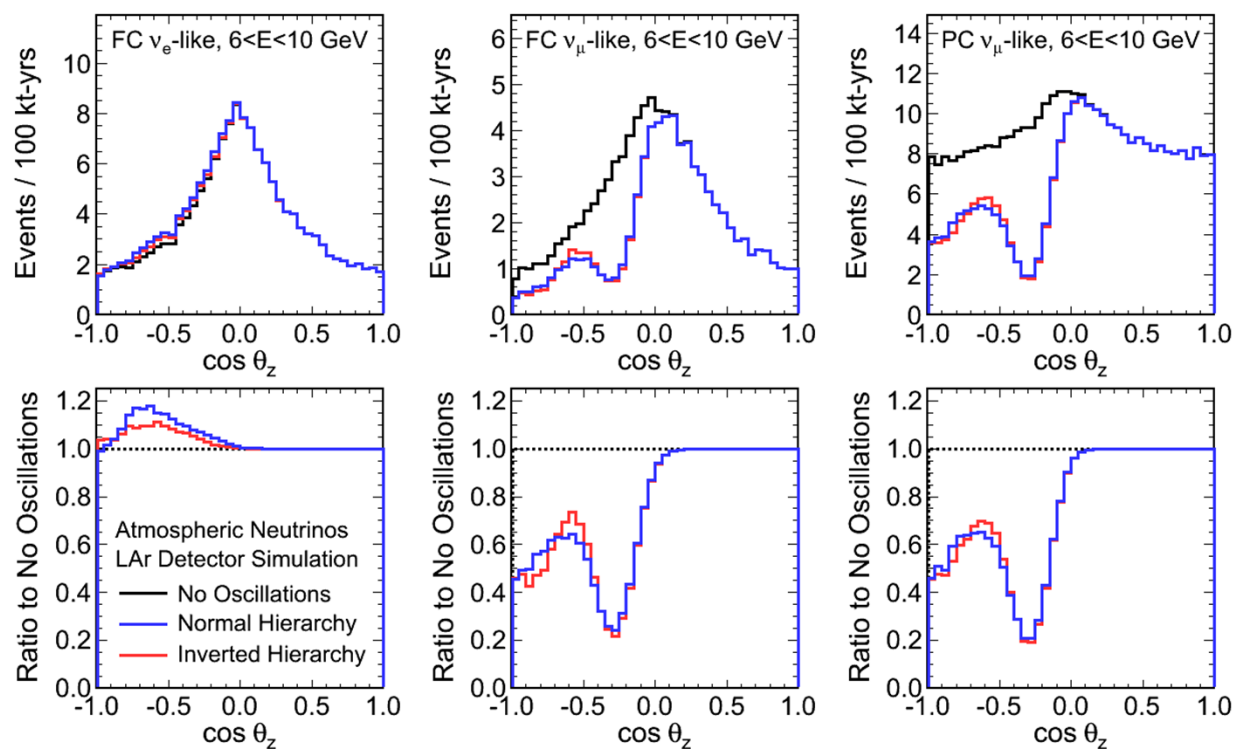


**Figure 4-27:** Reconstructed zenith angle distributions for 6-10 GeV events in the FC electron-like, FC  $\mu$ -like, and PC  $\mu$ -like samples. Top plots show the expected distributions for no oscillations (black), oscillations with normal mass hierarchy (blue), and inverted hierarchy (red). Bottom plots show the ratio of the normal and inverted hierarchy expectations to the no-oscillation distributions for each category.



anti-neutrino events can be separated. The LBNE detector will not be magnetized, however the high-resolution imaging does offer some possibilities for tagging features of events that provide statistical discrimination between neutrinos and anti-neutrinos. For the sensitivity calculations that follow, we have included two such tags: a proton tag and a decay-electron tag. Protons are tagged with 100% efficiency if their kinetic energy is greater than 50 MeV; for low-multiplicity events protons occur preferentially in neutrino interactions. Decay electrons are assumed to be 100% identifiable and are assumed to occur 100% of the time for  $\mu^+$  and 25% of the time for  $\mu^-$  based on the  $\mu^\pm$  capture probability on Ar40.

In the oscillation analysis 18 nuisance parameters are included, with detector performance parameters correlated between beam and atmospheric data. In all cases we take  $\sin^2 \theta_{12}$ ,  $\Delta m^2 = 1/2(\Delta m_{32}^2 + \Delta m_{31}^2)$ , and  $\Delta m_{12}^2$  to be fixed at the previously given values. The fits then range over  $\theta_{23}$ ,  $\theta_{13}$ ,  $\delta_{CP}$ , and the mass hierarchy. A 2% constraint is assumed on the value of  $\theta_{13}$ . The systematic errors included in this analysis are given in Table 4-10.

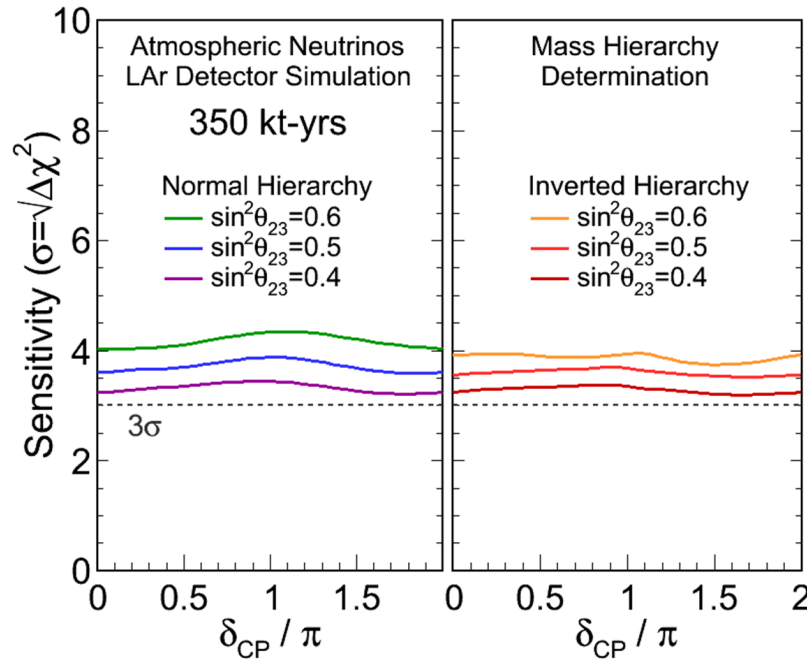
**Table 4-10:** Systematic errors included in the atmospheric and beam+atmospheric neutrino analysis. The beam values assume the existence of a near detector. Atmospheric spectrum ratios include the combined effect of flux and detector uncertainties (e.g., the up/down flux uncertainty as well as the uncertainty on the detector performance for the up/down ratio). The atmospheric spectrum shape uncertainty functions are applied separately for  $\nu_\mu, \nu_e, \bar{\nu}_\mu, \bar{\nu}_e$ .

	Atmospheric	Beam (Assumes ND)
Normalisations	Overall (15%)	$\mu$ -like (1%) e-like (1%)
NC Backgrounds	e-like (10%)	$\mu$ -like (10%) e-like (5%)
Spectrum Ratios	up/down (2%) $\nu_e/\nu_\mu$ (2%) $\bar{\nu}_\mu/\nu_\mu$ (5%) $\bar{\nu}_e/\nu_e$ (5%)	
Spectrum Shape	$f(E < E_0) = 1 + \alpha(E - E_0)/E_0$ $f(E > E_0) = 1 + \alpha \log(E/E_0)$ where $\sigma_\alpha = 5\%$	
Energy Scales (Correlated)	Muons (stopping 1%, exiting 5%) Electrons (1%) Hadronic System (5%)	

**FIXME:** *new* For the hierarchy determination, the  $\Delta\chi^2$  value is calculated between the best fit points in the normal and inverted hierarchies, where at each the nuisance parameters have been marginalized. The sensitivity in the plots that follow is given as  $\sigma = \sqrt{\Delta\chi^2}$ . Figure 4-28 shows the MH sensitivity from a 350 kt-yr exposure of atmospheric neutrino data alone. For all values of the hierarchy and  $\delta_{CP}$ , the hierarchy can be determined at  $> 3\sigma$ . The resolution depends significantly on the true value of  $\theta_{23}$ , and the sensitivity for three values is shown. The sensitivity depends relatively weakly on the true hierarchy and the true value of  $\delta_{CP}$ .

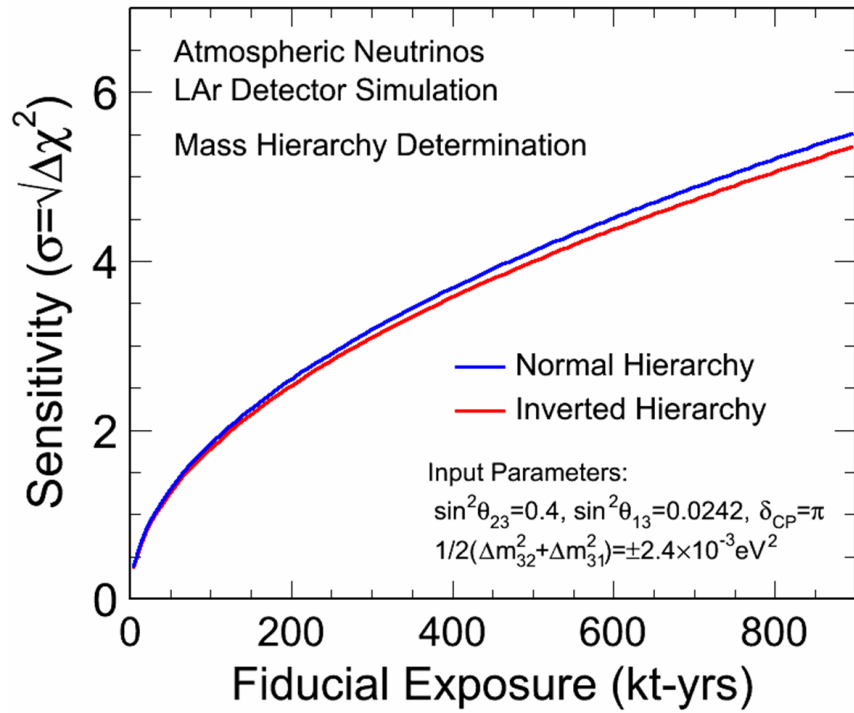
This is in sharp contrast to the MH sensitivity of the beam, which has a strong dependence on the true value of  $\delta_{CP}$ . Figure 4–29 shows the MH sensitivity as a function of the fiducial exposure. Over this range of fiducial exposures the sensitivity goes essentially as the square root of the exposure, indicating that the measurement is not systematics limited.

**FIXME:** *old* For the hierarchy determination, the  $\Delta\chi^2$  value is calculated between the best-fit points in the normal and inverted hierarchies, where at each, the nuisance parameters have been marginalized. The sensitivity in the plots that follow is given as  $\sigma = \sqrt{\Delta\chi^2}$ . Figure 4–28 shows the MH sensitivity from a 350 kt-yr exposure of atmospheric neutrino data alone. For all values of the hierarchy and  $\delta_{CP}$ , the former can be determined at  $> 3\sigma$ . The resolution depends significantly on the true value of  $\theta_{23}$ , and the sensitivity for three values is shown. The sensitivity depends relatively weakly on the true hierarchy and on the true value of  $\delta_{CP}$ . This is in sharp contrast to the MH sensitivity of the beam, which has a strong dependence on the true value of  $\delta_{CP}$ . Figure 4–29 shows the MH sensitivity as a function of the fiducial exposure. Over this range of fiducial exposures the sensitivity goes essentially as the square root of the exposure, indicating that the measurement is not systematics limited.



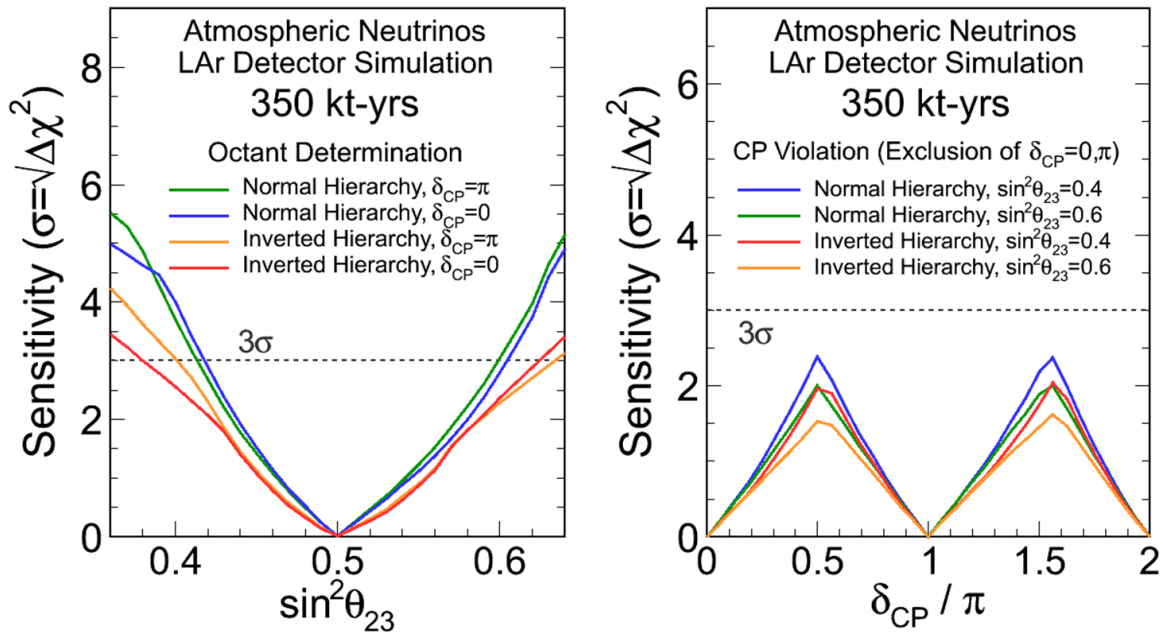
**Figure 4–28:** Sensitivity of 350 kt-yr of atmospheric neutrino data to MH as a function of  $\delta_{CP}$  for true **FIXME:** *normal?* and inverted hierarchy and different assumed values of  $\sin^2 \theta_{23}$ .

Figure 4–30 shows the octant and CPV sensitivity from a 350 kt-yr exposure of atmospheric neutrino data alone. For the determination of the octant of  $\theta_{23}$ , the  $\Delta\chi^2$  value is calculated between the best-fit points in the lower ( $\theta_{23} < 45^\circ$ ) and higher ( $\theta_{23} > 45^\circ$ ) octants, where at each, the nuisance parameters have been marginalized. The discontinuities in the slopes of the octant sensitivity plot are real features, indicating points at which the best fit moves from one hierarchy to the other. For the detection of CP violation, the  $\Delta\chi^2$  exclusion is



**Figure 4-29:** Sensitivity to mass hierarchy using atmospheric neutrinos as a function of fiducial exposure in a LAr detector.

similarly computed for  $\delta_{CP} = (0, \pi)$ .



**Figure 4-30:** Sensitivity to octant (left) and CPV (right) using atmospheric neutrinos.

Figure 4-31 shows the combined sensitivity to beam and atmospheric neutrinos for the mass hierarchy. This assumes a 10-yr run with equal amounts of neutrino and antineutrino running. In the region of  $\delta_{CP}$  where the beam is least sensitive, atmospheric neutrinos offer comparable sensitivity, resulting in a combined sensitivity greater than  $5\sigma$  for all values of  $\delta_{CP}$ . The combined sensitivity is also better than the sum of the separate  $\chi^2$  values, as the atmospheric data helps to remove degeneracies in the beam data. Figure 4-32 shows the combined sensitivity to beam and atmospheric neutrinos for the octant determination and CPV. The role played by atmospheric data in resolving beam degeneracies is also clear from considering the combined and beam-only sensitivities in these plots.

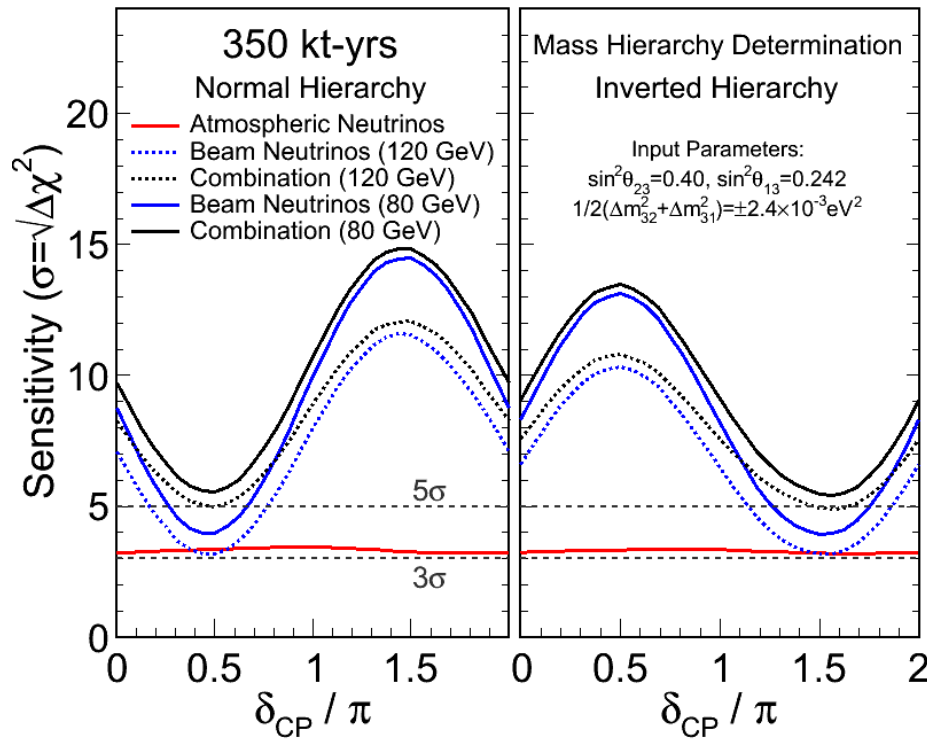


**Figure 4-31:** Sensitivity to mass hierarchy using atmospheric neutrinos combined with beam neutrinos with an exposure of 350 kt-years in a 700-kW beam.

## 4.8 Searches for Physics Beyond $\nu$ SM in Long-Baseline Oscillations

In addition to precision measurements of the standard three-flavor neutrino-oscillation parameters, LBNE provides the best potential for discoveries of physics *beyond* the standard three-flavor model. Full exploitation of the LBNE design's sensitivity to new physics will require higher-precision predictions of the unoscillated neutrino flux at the far detector and larger exposures (detector mass  $\times$  beam power) than currently proposed in the LBNE10

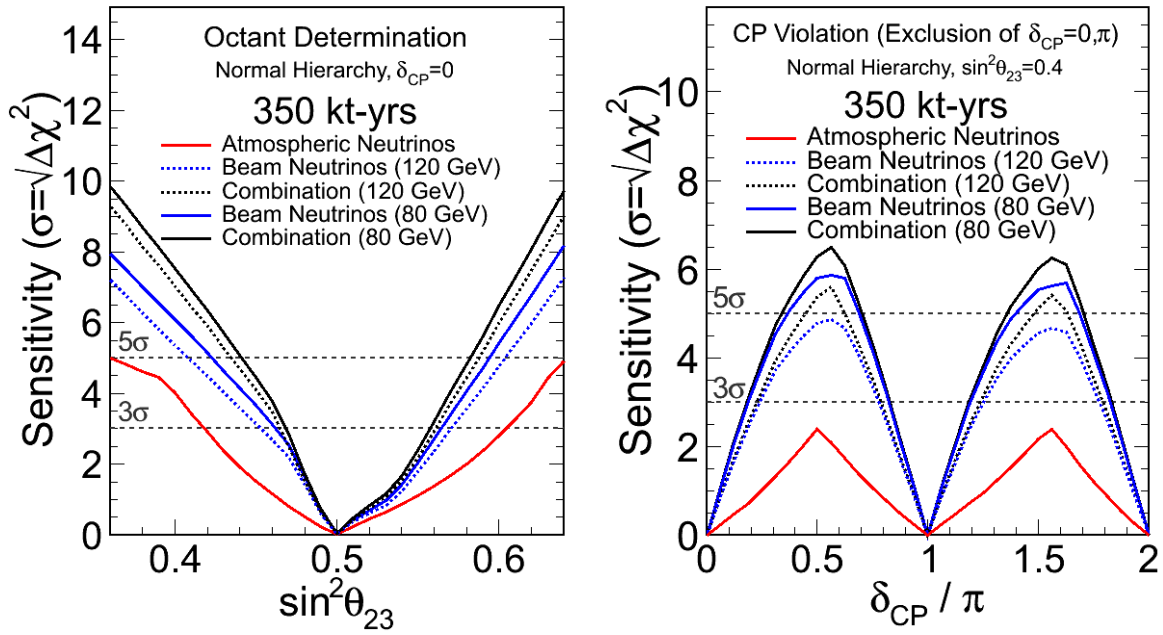


**Figure 4-32:** Sensitivity to octant (left) and CPV (right) using atmospheric neutrinos combined with beam neutrinos with an exposure of 350 kt-years in a 700-kW beam.

configuration. This section presents some examples of new physics that a full-scope LBNE design is well suited to pursue.

#### 4.8.1 Search for Non-Standard Interactions

NC non-standard interactions (NSI) can be understood as non-standard matter effects that are visible only in a far detector at a sufficiently long baseline. LBNE has a unique advantage in this area compared to other long-baseline experiments (except atmospheric-neutrino experiments, which are, however, limited by systematic effects **FIXME: if you're talking baseline, I'd assume you're talking beam. This seems like a separate topic and thus out of place here. ??**). NC NSI can be parameterized as new contributions to the MSW matrix in the neutrino-propagation Hamiltonian:

$$H = U \begin{pmatrix} 0 & & \\ & \Delta m_{21}^2/2E & \\ & & \Delta m_{31}^2/2E \end{pmatrix} U^\dagger + \tilde{V}_{\text{MSW}}, \quad (4.1)$$

with

$$\tilde{V}_{\text{MSW}} = \sqrt{2}G_F N_e \begin{pmatrix} 1 + \epsilon_{ee}^m & \epsilon_{e\mu}^m & \epsilon_{e\tau}^m \\ \epsilon_{e\mu}^{m*} & \epsilon_{\mu\mu}^m & \epsilon_{\mu\tau}^m \\ \epsilon_{e\tau}^{m*} & \epsilon_{\mu\tau}^{m*} & \epsilon_{\tau\tau}^m \end{pmatrix} \quad (4.2)$$

Here,  $U$  is the leptonic mixing matrix, and the  $\epsilon$ -parameters give the magnitude of the NSI relative to standard weak interactions. For new physics scales of a few  $\times 100$  GeV, a value of  $|\epsilon| \lesssim 0.01$  is expected.

### NC NSI discovery reach ( $3\sigma$ C.L.)

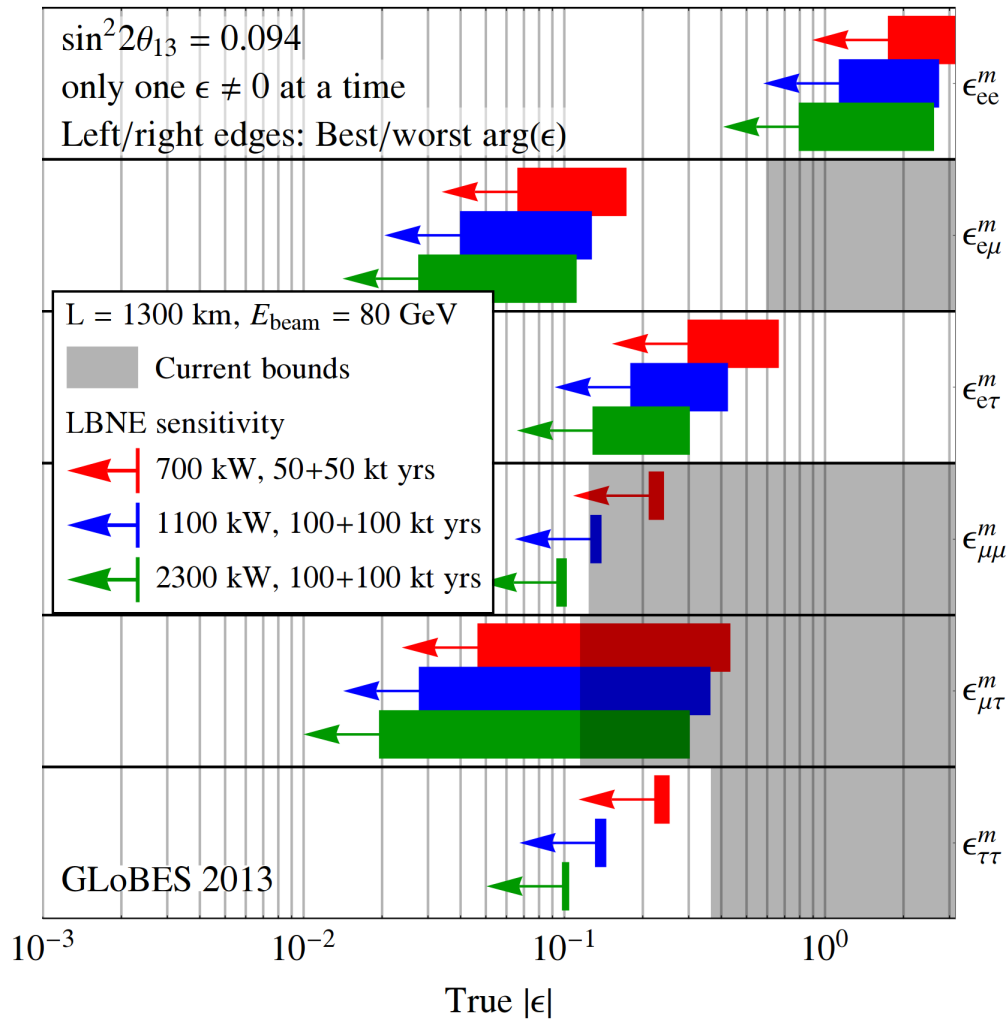


**Figure 4-33:** Non-standard interaction discovery reach in LBNE with increasing exposure: 700 kW 100 kt.years (red) + 1.1MW 200 kt.yrs (blue) + 2.3MW 200 kt.yrs (green). The left and right edges of the error bars correspond to the most favorable and the most unfavorable values for the complex phase of the respective NSI parameters. The gray shaded regions indicate the current model-independent limits on the different parameters at  $3\sigma$  [?] and [?]. For this study the value of  $\sin^2 2\theta_{13}$  was assumed to be 0.09. Figure courtesy of Joachim Kopp.

### 4.8.2 Long-Range Interactions

The small scale of neutrino-mass differences implies that minute differences in the interactions of neutrinos and antineutrinos with background sources can be detected through perturbations to the time evolution of the flavor eigenstates. The longer the experimental baseline, the higher the sensitivity to a new long-distance potential acting on neutrinos. For example, some of the models for such long-range interactions (LRI) as described in [?] (see Figure 4-34) could contain discrete symmetries that stabilize the proton and a dark matter particle and thus provide new connections between neutrino, proton decay and dark matter experiments. The longer baseline of LBNE improves the sensitivity to LRI beyond that possible by the current generation of long-baseline neutrino experiments. The sensitivity will be determined by the amount of  $\nu_\mu/\bar{\nu}_\mu$  CC statistics accumulated and the accuracy with which the unoscillated and oscillated  $\nu_\mu$  spectra can be determined.

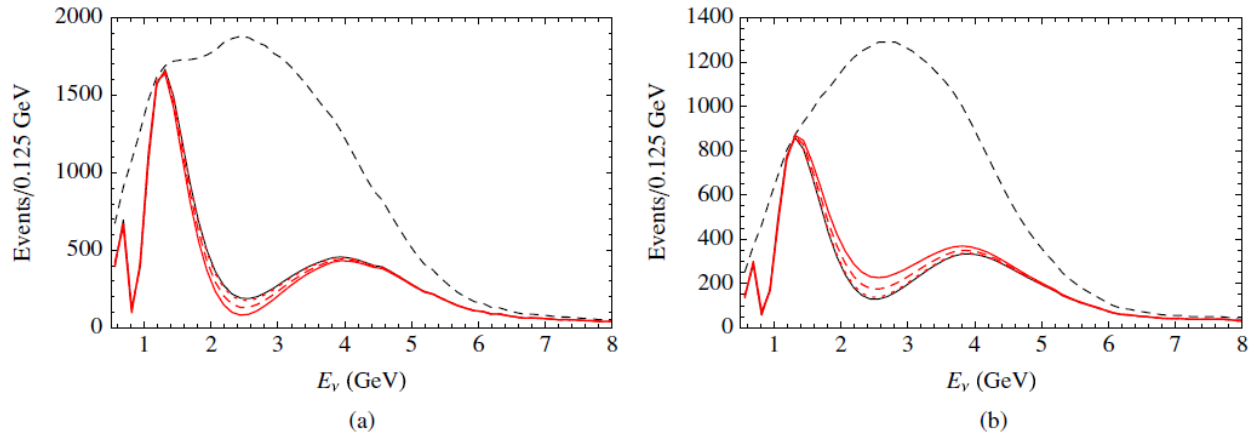


**Figure 4-34:** Long-range Interactions in LBNE. The number of (a) neutrino and (b) antineutrino events versus  $E_\nu$ , in a long-baseline experiment with a 1,300-km baseline. The unoscillated case (top black dashed curves) and the case of no new physics (thin black solid curves) are displayed, as well as the cases with  $\alpha' = 1.0, 0.5, 0.1 \times 10^{-52}$  corresponding to thick solid, dashed, and dotted curves, respectively.  $\alpha'$  is the “fine structure constant” of such interactions, which is constrained to be  $\alpha' \leq 10^{-47}$  [?].

### 4.8.3 Search for Active-Sterile Neutrino Mixing

Searches for evidence of active-sterile neutrino mixing at LBNE can be conducted by examining the NC event rate at the far detector and comparing it to a precision estimate of the expected rate extrapolated from  $\nu_\mu$  flux measurements from the near detector and from beam and detector simulations. Observed deficits in the NC rate could be evidence for active-sterile neutrino mixing. The latest such search in a long-baseline experiment was conducted by the

MINOS experiment [?]. The expected rate of NC interactions in a 10-kt detector with visible energy  $> 0.5$  GeV in LBNE over five years is approximately 2,000 events (see Table 4-1) in the LE beam tune and 3,000 events in the ME beam tune. The NC identification efficiency is high, with a low rate of  $\nu_\mu$  CC background misidentification as shown in Table 4-3.

LBNE will provide a unique opportunity to revisit this search with higher precision over a large range of neutrino energies and a longer baseline. The high-resolution LArTPC far detector will enable a coarse measurement of the incoming neutrino energy in a NC interaction by using the event topology and correcting for the missing energy of the invisible neutrino. This will greatly improve the sensitivity of LBNE to active-sterile mixing as compared to current long-baseline experiments such as MINOS+ since both the energy spectrum as well as the rate of NC interactions can be measured at both near and far detectors. Studies are currently underway to determine the LBNE sensitivity.

#### 4.8.4 Sensitivity to Large Extra Dimensions

Several theoretical models propose that right-handed neutrinos propagate in large compactified extra dimensions, whereas the standard left-handed neutrinos are confined to the 4-dimensional brane [?]. Mixing between the Kaluza-Klein modes and the standard neutrinos would change the mixing patterns beyond that predicted by the three-flavor model. The effects could manifest, for example, as distortions in the disappearance spectrum of  $\nu_\mu$ . The rich oscillation structure visible in LBNE, measured with its high-resolution detector using both beam and atmospheric oscillations, could provide further opportunities to probe for this type of new physics. Studies are underway to understand the limits that **FIXME:** *a full-scope?* LBNE could impose relative to current limits and those expected from other experiments.



## 5 Precision Oscillation Measurements and Short-Baseline Neutrino Physics

**FIXME:** *changed chap title to match exec summ (and maybe shorten it)*

**FIXME:** *new* **FIXME:** *In chap 2, in the PRIMARY objectives (not in italic, and NOT full scope) it says “the mass hierarchy determination and precision determination of theta 2-3 will most likely be complete in the LBNE10 configuration.” Need to reconcile. The reduction of systematic uncertainties for the neutrino oscillation program of the full LBNE scope requires a highly segmented near neutrino detector (ND) to provide excellent resolution in the reconstruction of neutrino events. Combined with the unprecedented large neutrino fluxes available for the LBNE program – which will allow the collection of  $\mathcal{O}(10^8)$  inclusive neutrino charged current (CC) interactions for  $10^{22}$  POT just downstream of the beamline – the inclusion of a near detector offers a unique opportunity to significantly enhance the LBNE long-baseline oscillation program and to produce a range of short-baseline neutrino scattering physics measurements. The combined statistics and precision expected in the ND will allow precise tests of fundamental interactions resulting in a better understanding of the structure of matter.*

Table 5–1 lists the expected number of muon neutrino interactions at the LBNE 459-m near detector site per ton of detector. **FIXME:** *I don’t like this in the intro; but maybe it’s best place; come back to*

**FIXME:** *new* Since the potential of high-intensity neutrino beams as probes of new physics is largely unexplored, and given the broad energy range of the beam, a diverse range of physics measurements – and unexpected discoveries – are possible. These potentially wide-ranging physics measurements would complement physics programs, such as those at Jefferson Laboratory, that are using proton, electron or ion beams from colliders and fixed-target facilities.

**FIXME:** *new* This chapter presents a short description of some of the studies that can be performed at LBNE with a fine-grained near neutrino detector and gives a flavor of the outstanding physics potential. A more detailed and complete discussion of the near detector physics potential can be found in [?].

**Table 5–1:** Estimated  $\nu_\mu$  production rates per ton of detector (water) for  $1 \times 10^{20}$  POT at 459 m assuming neutrino cross sections predictions from NUANCE [?] and a 120 GeV proton beam. Processes are defined at the initial neutrino interaction vertex and thus do not include final state effects. These estimates do not include detector efficiencies or acceptance [?,?]. **FIXME:** *Can you provide a water-to-LAr conversion factor so that this is more relevant to LBNE?*

Production mode	# of $\nu_\mu$ events	# of $\bar{\nu}_\mu$ Events
CC QE ( $\nu_\mu n \rightarrow \mu^- p$ )	50,100	3,310
NC elastic ( $\nu_\mu N \rightarrow \nu_\mu N$ )	18,800	1,100
CC resonant $\pi^+$ ( $\nu_\mu N \rightarrow \mu^- N \pi^+$ )	67,800	0
CC resonant $\pi^-$ ( $\bar{\nu}_\mu N \rightarrow \mu^+ N \pi^-$ )	0	3,300
CC resonant $\pi^0$ ( $\nu_\mu n \rightarrow \mu^- p \pi^0$ )	16,200	1,100
NC resonant $\pi^0$ ( $\nu_\mu N \rightarrow \nu_\mu N \pi^0$ )	16,300	1,030
NC resonant $\pi^+$ ( $\nu_\mu p \rightarrow \nu_\mu n \pi^+$ )	6,930	480
NC resonant $\pi^-$ ( $\nu_\mu n \rightarrow \nu_\mu p \pi^-$ )	5,980	390
CC DIS ( $\nu_\mu N \rightarrow \mu^- X$ or $\bar{\nu}_\mu N \rightarrow \mu^+ X$ , $W > 2$ )	66,800	6,610
NC DIS ( $\nu_\mu N \rightarrow \nu_\mu X$ or $\bar{\nu}_\mu N \rightarrow \bar{\nu}_\mu X$ , $W > 2$ )	24,100	2,950
NC coherent $\pi^0$ ( $\nu_\mu A \rightarrow \nu_\mu A \pi^0$ or $\bar{\nu}_\mu A \rightarrow \bar{\nu}_\mu A \pi^0$ )	2,040	212
CC coherent $\pi^+$ ( $\nu_\mu A \rightarrow \mu^- A \pi^+$ )	3,920	0
CC coherent $\pi^-$ ( $\bar{\nu}_\mu A \rightarrow \mu^+ A \pi^-$ )	0	400
NC resonant radiative decay ( $N^* \rightarrow N \gamma$ )	110	7
Cabbibo-suppressed QE hyperon production ( $\mu^+ \Lambda$ , $\mu^+ \Sigma^0$ , $\mu^+ \Sigma^-$ )	0	240
NC elastic electron ( $\nu_\mu e^- \rightarrow \nu_\mu e^-$ or $\bar{\nu}_\mu e^- \rightarrow \bar{\nu}_\mu e^-$ )	30	3
Inverse Muon Decay ( $\nu_\mu e \rightarrow \mu^- \nu_e$ )	12	0
Other	42,600	2,920
Total CC	236,000	17,000
Total NC+CC	322,000	24,000

**FIXME:** *old*The unprecedented large neutrino fluxes available for the LBNE program will allow the collection of  $\mathcal{O}(10^8)$  inclusive neutrino charged current (CC) interactions for  $10^{22}$  POT at a near detector location. Table 5–1 lists the expected number of muon neutrino interactions at the LBNE 459-m near detector site per ton of detector.

**FIXME:** *old*The reduction of systematic uncertainties for the neutrino oscillation program of the full LBNE scope requires a highly segmented near detector, thus providing excellent resolution in the reconstruction of neutrino events. The combination of this substantial flux with a finely segmented near detector offers a unique opportunity to produce a range of neutrino scattering physics measurements in addition to those needed by the long-baseline oscillation program. The combined statistics and precision expected in the ND will allow precise tests of fundamental interactions resulting in a better understanding of the structure of matter.

**FIXME:** *old* Since the potential of high intensity neutrino beams as probes of new physics is largely unexplored, the substantial step forward offered by the LBNE ND program also provides the opportunity for unexpected discoveries. Given the broad energy range of the beam, a diverse range of physics measurements is possible in the LBNE ND, complementing the physics programs using proton, electron or ion beams from colliders and fixed-target programs such as those at Jefferson Laboratory. This complementarity not only would boost the physics output of LBNE, but it could also attract new collaborators into the LBNE project.

**FIXME:** *old* The following sections list the main physics topics. For a few selected topics, a short description of the studies that can be performed at LBNE gives a flavor of the outstanding physics potential. A more detailed and complete discussion of the near detector physics potential can be found in [?].

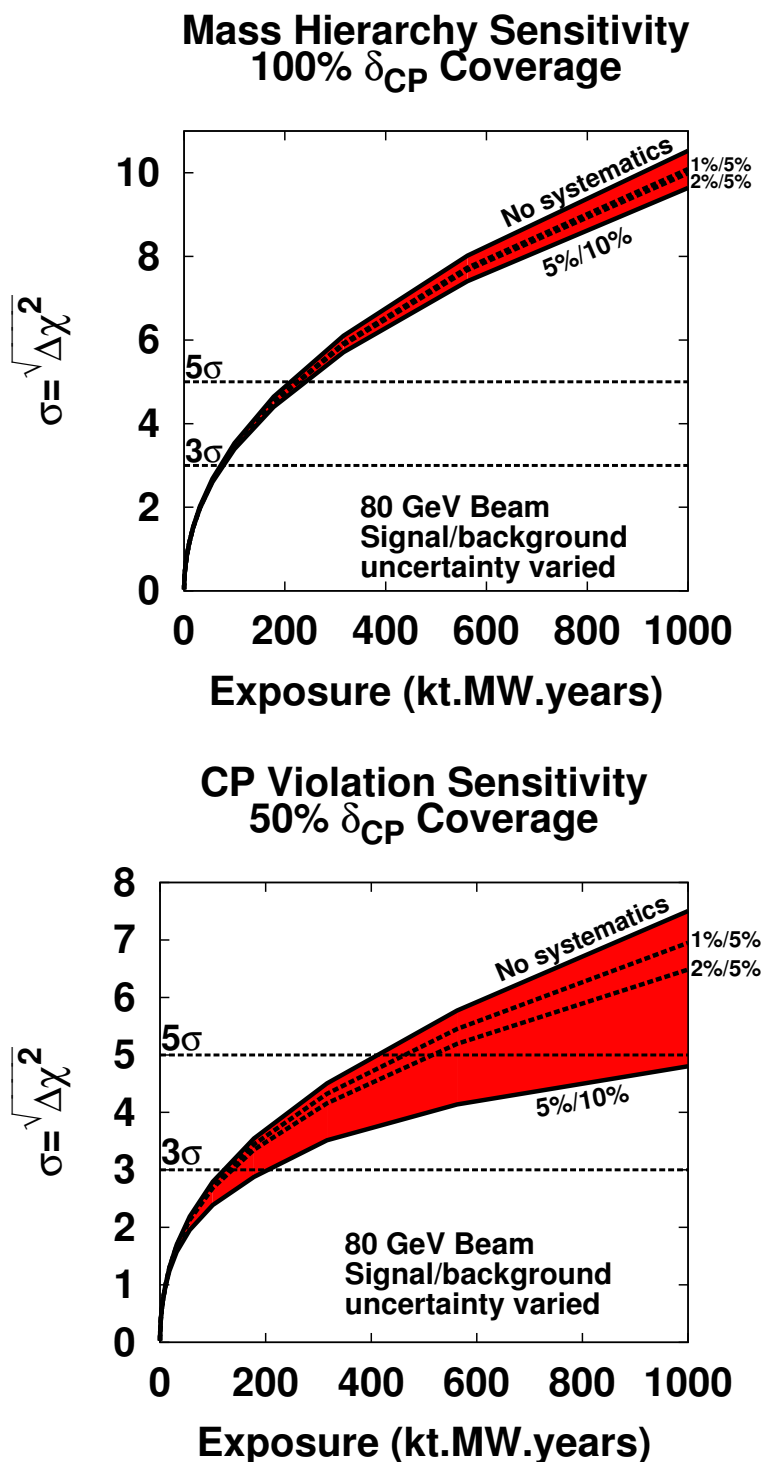
## 5.1 Precision Measurements with Long-Baseline Oscillations

In order to achieve the goals of the full LBNE scientific program – in particular, sensitivity to CP violation and the precision measurement of the three-flavor oscillation parameters – it is necessary to characterize the expected unoscillated neutrino flux and the physics backgrounds to the oscillation signals at the far detector with high precision. In Figure 5-1, the mass hierarchy and CP violation sensitivities as a function of exposure are evaluated using three different sets of assumptions on the the signal/background uncertainties: 1%/5% (the goal of the LBNE scientific program), 2%/5% and 5%/10%. The last is a conservative estimate on the uncertainties that can be achieved in LBNE without unoscillated neutrino-beam measurements at the near site, using the detailed muon flux measurements, target hadron production measurements, and the data-tuned simulation of the NuMI beamline, which uses the same targetry and focusing as LBNE.

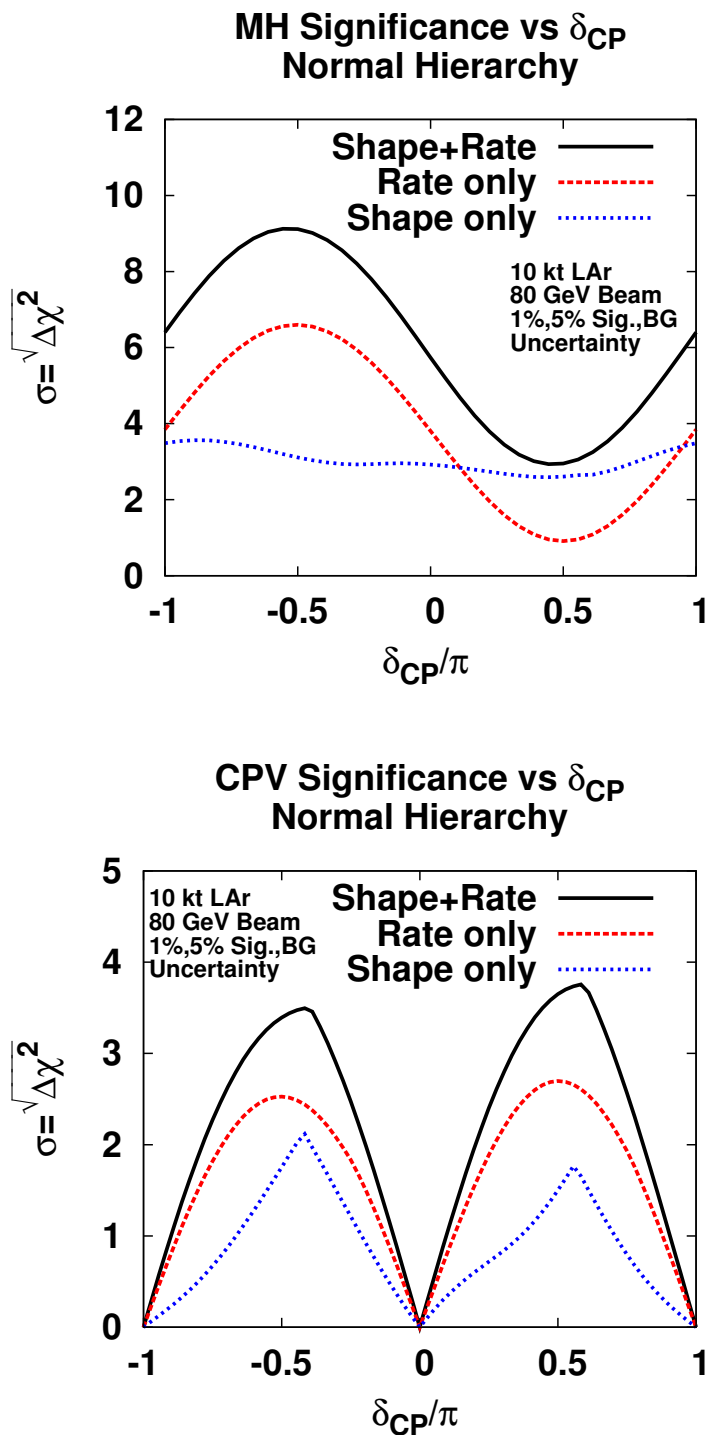
The impact of the systematic uncertainties in the signal and background on the mass hierarchy sensitivity is negligible even at high exposures given the large  $\nu/\bar{\nu}$  asymmetry at 1,300 km. For CP violation, however, the impact is significant at exposures  $\geq 100$  kt-years, as large systematic uncertainties start to dominate the statistical uncertainties.

Table 5-2 summarizes the exposures required to reach  $3, 5\sigma$  sensitivity to CP violation for at least 50% of all possible values of  $\delta_{cp}$ . The resolution on  $\delta_{cp}$  is also shown.

The uncertainties listed in Table 5-2 and shown in the sensitivity figures are on the  $\nu_e$  appearance signal and background normalization. In Figure 5-2 the sensitivities obtained from the rate only, shape only and rate+shape of the appearance spectrum are shown. In a broad-band, long-baseline experiment such as LBNE, the shape information is at least as



**Figure 5–1:** The mass hierarchy (top) and CP violation (bottom) sensitivities as a function of exposure in kt-years. The band represents the range of signal and background normalization errors.



**Figure 5–2:** The mass hierarchy (top) and CP violation (bottom) sensitivities from shape, rate, and shape+rate. The sensitivity is for a 10-kt detector, 700-kW beam, 5+5 ( $\nu + \bar{\nu}$ ) years.

**Table 5–2:** The exposures required to reach 3 and 5 $\sigma$  sensitivity to CP violation for at least 50% of all possible values of  $\delta_{cp}$  as a function of systematic uncertainties. **FIXME:** *for Water?*

Systematic uncertainty	Sensitivity	Required Exposure
0 (statistical only)	3 $\sigma$ , 50% $\delta_{cp}$	100 kt.MW.yr
0 (statistical only)	5 $\sigma$ , 50% $\delta_{cp}$	400 kt.MW.yr
1%/5% (Sig/bkgd)	3 $\sigma$ , 50% $\delta_{cp}$	100 kt.MW.yr
1%/5% (Sig/bkgd)	5 $\sigma$ , 50% $\delta_{cp}$	450 kt.MW.yr
2%/5% (Sig/bkgd)	3 $\sigma$ , 50% $\delta_{cp}$	120 kt.MW.yr
2%/5% (Sig/bkgd)	5 $\sigma$ , 50% $\delta_{cp}$	500 kt.MW.yr
5%/10% (no near $\nu$ det.)	3 $\sigma$ , 50% $\delta_{cp}$	200 kt.MW.yr

important as the rate information. **FIXME:** *because...?*

From the studies of uncertainties and the impact of the spectral shape presented earlier, it is evident that to fully realize the physics potential of possible enhancements to the current LBNE program, a near neutrino detector that can both measure the unoscillated neutrino flux shape and normalization with high precision is highly desirable **FIXME:** *clarify; measure flux and ‘measure normalization’?* . In addition to the precise determination of the neutrino flux, shape and flavor composition, the characterization of different neutrino interactions and interaction cross sections on an LAr target is necessary to estimate the physics backgrounds to the oscillation measurements.

A high-resolution near tracking detector such as that described in Section 3.5 can measure the unoscillated flux normalization, shape and flavor to a few percent using systematically independent techniques that are listed here and discussed in the following sections.

- relative neutrino and antineutrino flux measurement
- measurement of the flavor content of the beam:  $\nu_\mu, \bar{\nu}_\mu, \nu_e, \bar{\nu}_e$
- constraining the unoscillated  $\nu$  spectral shape with the Quasi-Elastic interaction
- low-energy absolute flux measurement: neutrino-electron Neutral Current scattering
- high-energy absolute flux measurement: neutrino-electron Charged Current scattering
- low-energy absolute flux measurement: QE in water and heavy-water targets
- measurement of neutral pions, photons, and  $\pi^\pm$  in Neutral and Charged Current events

### 5.1.1 Relative Neutrino and Antineutrino Flux

The most promising method of determining the shape of the  $\nu_\mu$  and  $\bar{\nu}_\mu$  flux is by measuring the low-hadronic (low- $\nu$ ) charged current events: the Low- $\nu_0$  **FIXME:** *this term is not defined; some value of hadronic energy?* method of relative flux determination [?]. The dynamics of neutrino-nucleon scattering implies that the number of events in a given energy bin with hadronic energy  $E_{\text{had}} < \nu_0$  is proportional to the neutrino (antineutrino) flux in that energy bin up to corrections  $\mathcal{O}(\nu_0/E_\nu)$  and  $\mathcal{O}(\nu_0/E_\nu)^2$ . The method follows from the general expression of the  $\nu$ -nucleon differential cross section:

$$\mathcal{N}(\nu < \nu_0) = C\Phi(E_\nu)\nu_0 \left[ \mathcal{A} + \left(\frac{\nu_0}{E_\nu}\right) \mathcal{B} + \left(\frac{\nu_0}{E_\nu}\right)^2 \mathcal{C} + \mathcal{O}\left(\frac{\nu_0}{E_\nu}\right)^3 \right], \quad (5.1)$$

where the coefficients are  $\mathcal{A} = \mathcal{F}_2$ ,  $\mathcal{B} = (\mathcal{F}_2 \pm \mathcal{F}_3)/2$ ,  $\mathcal{C} = (\mathcal{F}_2 \mp \mathcal{F}_3)/6$ , and  $\mathcal{F}_i = \int_0^1 \int_0^{\nu_0} F_i(x) dx d\nu$  is the integral of structure function  $F_i(x)$ . The number  $\mathcal{N}(\nu < \nu_0)$  is proportional to the flux up to correction factors of the order  $\mathcal{O}(\nu_0/E_\nu)$  or smaller, which are not significant for small values of  $\nu_0$  at energies  $\geq \nu_0$ . It should be pointed out that the coefficients  $\mathcal{A}, \mathcal{B}, \mathcal{C}$  are determined for each energy bin and neutrino flavor within the ND data. LBNE's primary interest is the relative flux determination, i.e., the neutrino flux in one energy bin relative to that in another; variations in the coefficients do not affect the relative flux. The prescription for the relative flux determination is simple: count the number of  $\nu$ -CC events below a certain small value of hadronic energy ( $\nu_0$ ). The observed number of events, up to the correction of the order  $\mathcal{O}(\nu_0/E_\nu)$  due to the finite  $\nu_0$  in each total visible energy bin, is proportional to the relative flux. The smaller the factor  $\nu_0/E_\nu$  is, the smaller is the correction. Furthermore, the energy of events passing the low- $\nu_0$  cut is dominated by the corresponding lepton energy.

It is apparent from the above discussion that this method of relative flux determination is not very sensitive to nucleon structure, QCD corrections or types of  $\nu$ -interactions such as scaling or non-scaling. With the excellent granularity and resolution foreseen in the low-density magnetized tracker it will be possible to use a value of  $\nu_0 \sim 0.5$  GeV or lower, thus allowing flux predictions down to  $E_\nu \sim 0.5$  GeV. A preliminary analysis with the high-resolution tracker achieved a precision  $\leq 2\%$  on the relative  $\nu_\mu$  flux with the low- $\nu_0$  method in the energy region  $1 \leq E_\nu \leq 30$  GeV in the fit with  $\nu_0 < 0.5$  GeV. Similar uncertainties are expected for the  $\bar{\nu}_\mu$  component (the dominant one) in the antineutrino beam mode (negative focusing).

### 5.1.2 Flavor Content of the Beam: $\nu_\mu, \bar{\nu}_\mu, \nu_e, \bar{\nu}_e$

The empirical parametrization (EP) of the pions and kaons, determined from the low- $\nu_0$  flux at the ND, allows prediction of the  $\nu_\mu$  and  $\bar{\nu}_\mu$  flux at the FD location. The EP provides a measure of the  $\pi^+/K^+/\mu^+$  ( $\pi^-/K^-/\mu^-$ ) content of the beam at the ND. Additionally, with an ND capable of identifying  $\bar{\nu}_e$  CC interactions, one can directly extract the elusive  $K_L^0$  content

of the beam. Therefore, an accurate measurement of  $\nu_\mu$ ,  $\bar{\nu}_\mu$  and  $\bar{\nu}_e$  CC interactions provides an absolute prediction of the  $\nu_e$  content of the beam, which is an irreducible background for the  $\nu_e$  appearance search in the FD:

$$\nu_e \equiv \mu^+(\pi^+ \rightarrow \nu_\mu) \oplus K^+(K^+ \rightarrow \nu_\mu) \oplus K_L^0 \quad (5.2)$$

$$\bar{\nu}_e \equiv \mu^-(\pi^- \rightarrow \bar{\nu}_\mu) \oplus K^-(K^- \rightarrow \bar{\nu}_\mu) \oplus K_L^0 \quad (5.3)$$

The  $\mu$  component is well constrained from  $\nu_\mu(\bar{\nu}_\mu)$  CC data at low energy, while the  $K^\pm$  component is only partially constrained by the  $\nu_\mu(\bar{\nu}_\mu)$  CC data at high energy and requires external hadro-production measurements of  $K^\pm/\pi^\pm$  ratios at low energy from MIPP and similar experiments. Finally, the  $K_L^0$  component can be constrained by the  $\bar{\nu}_e$  CC data and by external dedicated measurements at hadron-production experiments. In the energy range  $1(5) \leq E_\nu \leq 5(15)$  GeV the approximate relative contributions to the  $\nu_e$  spectrum are 85% (55%) from  $\mu^+$ , 10% (30%) from  $K^+$  and 3% (15%) from  $K_L^0$ .

Based on the NOMAD experience, we expect to achieve a precision of  $\leq 0.1\%$  on the flux ratio  $\nu_e/\nu_\mu$ . Taking into account the projected precision of the  $\nu_\mu$  flux discussed in the previous section, this translates into an absolute prediction for the  $\nu_e$  flux at the level of 2%.

Finally, the fine-grained ND can directly identify  $\nu_e$  CC interactions from the LBNE beam. The relevance of this measurement is twofold: a) it provides an independent validation for the flux predictions obtained from the low- $\nu_0$  method and b) it can further constrain the uncertainty on the knowledge of the absolute  $\nu_e$  flux.

### 5.1.3 Constraining the Unoscillated $\nu$ Spectral Shape with the Quasi-Elastic Interaction

In any long-baseline neutrino oscillation program, including LBNE, the quasi-elastic (QE) interactions are special. First, the QE cross section is substantial because the energy is low. Secondly, because of the simple topology the interaction provides — a  $\mu^-$  and a proton — to first order, a close approximation to the neutrino energy ( $E_\nu$ ) **FIXME: not complete sentence**. In the context of a fine-grained tracker, precise measurement of QE will impose direct constraints on neutrino interaction associated with Fermi-motion and final state interaction (FSI) dynamics — processes that must be determined empirically since they affect the entire oscillation program. The key to  $\nu_\mu$ -QE is the two-track topology,  $\mu^-$  and  $p$ . A high-resolution ND can efficiently identify the recoil proton and measure its momentum vector as well as  $dE/dx$ . Preliminary studies indicate that in a fine-grained tracking detector the efficiency (purity) is 52% (82%). The high-purity selection will enable the LBNE ND to empirically constrain nuclear motion and the FSI parameters.



### 5.1.4 Low-Energy Absolute Flux: Neutrino-Electron Neutral Current Scattering

Neutrino neutral current interaction with the atomic electron in the target,  $\nu_\mu e^- \rightarrow \nu_\mu e^-$  (NuElas)**FIXME:** *what's NuElas - a name for this interaction? Not clear.* , provides an elegant measure of the absolute flux. The total cross section for NC elastic scattering off electrons is given by [?]:

$$\sigma(\nu_l e \rightarrow \nu_l e) = \frac{G_\mu^2 m_e E_\nu}{2\pi} \left[ 1 - 4 \sin^2 \theta_W + \frac{16}{3} \sin^4 \theta_W \right], \quad (5.4)$$

$$\sigma(\bar{\nu}_l e \rightarrow \bar{\nu}_l e) = \frac{G_\mu^2 m_e E_\nu}{2\pi} \left[ \frac{1}{3} - \frac{4}{3} \sin^2 \theta_W + \frac{16}{3} \sin^4 \theta_W \right], \quad (5.5)$$

where  $\theta_W$  is the weak mixing angle (WMA). For  $\sin^2 \theta_W \simeq 0.23$  **FIXME:** *Value seems pulled out of thin air; what's signif of .23?* the above cross sections are very small:  $\sim 10^{-42} (E_\nu/\text{GeV}) \text{ cm}^2$ . The NC elastic scattering off electrons can be used to determine the absolute flux normalization since the cross section only depends upon the knowledge of  $\sin^2 \theta_W$ . Within the SM the value of  $\sin^2 \theta_W$  at the average momentum transfer expected at LBNE,  $Q \sim 0.07 \text{ GeV}$ , can be extrapolated down from the LEP/SLC measurements with a precision of  $\leq 1\%$ . The  $\nu_\mu e^- \rightarrow \nu_\mu e^-$  will produce a single  $e^-$  collinear with the  $\nu$ -beam ( $\leq 40 \text{ mrad}$ ). The background, dominated by the asymmetric conversion of a photon in an ordinary  $\nu$ -N neutral current event, will produce  $e^-$  and  $e^+$  in equal measure with much broader angular distribution. A preliminary analysis of the expected elastic scattering signal in the high-resolution tracking near detector shows that the scattering signal can be selected with an efficiency of about 60% with a small background contaminant. The measurement will be dominated by the statistical error. We estimate that the absolute flux of the LBNE neutrinos will be determined to a  $\simeq 2.5\%$  precision for  $E_\nu \leq 10 \text{ GeV}$ . The measurement of NC elastic scattering off electrons can only provide the integral of all neutrino flavors.

### 5.1.5 High-Energy Absolute Flux: Neutrino-Electron Charged Current Scattering

The  $\nu_\mu e^-$  CC interaction,  $\nu_\mu + e^- \rightarrow \mu^- + \nu_e$  (inverse muon decay or *IMD*), offers an elegant way to determine the absolute flux. Given the **FIXME:** *energy?* threshold due to **FIXME:** *of?* the massive muon, IMD requires  $E_\nu \geq 10.8 \text{ GeV}$ . A high-resolution near detector such as that described in Section 3.5 **FIXME:** *in the LBNE neutrino beam* will observe  $\geq 2000$  IMD events in three years. The reconstruction efficiency of the single, energetic forward  $\mu^-$  will be  $\geq 98\%$ ; the angular resolution of the  $\text{IMD-}\mu$  is  $\leq 1 \text{ mrad}$ . The background, primarily from the  $\nu_\mu$ -QE, can be precisely constrained using control samples. In particular, the systematic limitations of the CCFR ([?]) and [?] and the CHARM-II [?] IMD measurements can be substantially alleviated with the proposed near detector design. A preliminary analysis indicates that the absolute flux can be determined with an accuracy of  $\approx 3\%$  for  $E_\nu \geq 11 \text{ GeV}$  (average  $E_\nu \approx 25 \text{ GeV}$ ).

### 5.1.6 Low-Energy Absolute Flux: QE in Water and Heavy-Water Targets

Another independent method to extract the absolute flux is through the Quasi-Elastic (QE) CC scattering ( $\nu_\mu n(p) \rightarrow \mu^- p(n)$ ) on deuterium at low  $Q^2$ . Neglecting terms in  $(m_\mu/M_n)^2$  at  $Q^2 = 0$  the QE cross section is independent of neutrino energy for  $(2E_\nu M_n)^{1/2} > m_\mu$ :

$$\frac{d\sigma}{dQ^2} \big|_{Q^2=0} = \frac{G_\mu^2 \cos^2 \theta_c}{2\pi} [F_1^2(0) + G_A^2(0)] = 2.08 \times 10^{-38} \text{ cm}^2 \text{GeV}^{-2}, \quad (5.6)$$

which is determined by neutron  $\beta$  decay and has a theoretical uncertainty  $< 1\%$ . The flux can be extracted experimentally by measuring low  $Q^2$  QE interactions ( $0 - 0.05$  GeV) and extrapolating the result to the limit of  $Q^2 = 0$ . The measurement requires a deuterium or hydrogen (for antineutrino) target to minimize the smearing due to Fermi motion and other nuclear effects. This requirement can only be achieved by using both  $\text{H}_2\text{O}$  and  $\text{D}_2\text{O}$  targets embedded in the fine-grained tracker and extracting the events produced in deuterium by statistical subtraction of the larger oxygen component. The experimental resolution on the muon and proton momentum and angle is crucial. Dominant uncertainties of the method are related to the extrapolation to  $Q^2 = 0$ , to the theoretical cross section on deuterium, to the experimental resolution, and to the statistical subtraction. Sensitivity studies and the experimental requirements are under study.

### 5.1.7 Neutral Pions, Photons, and $\pi^\pm$ in Neutral and Charged Current Events

The principal background to the  $\nu_e$  and  $\bar{\nu}_e$  appearance comes from the NC-events where a photon from the  $\pi^0$  decay produces a signature identical to that produced by  $\nu_e$ -induced electron; the second source of background is due to  $\pi^0$ s from  $\nu_\mu$ -CC where the  $\mu^-$  evades identification — typically at high  $y_{BJ}$ . Since the energy spectra of NC and CC are different, it is critical for the ND to measure  $\pi^0$ 's in NC and CC in the full kinematic phase space.

The proposed ND is designed to measure  $\pi^0$ s with high accuracy in three topologies: (a) both photons convert in the tracker ( $\simeq 25\%$ ), (b) one photon converts in the tracker and the other in the calorimeter ( $\simeq 50\%$ ), and (c) both photons convert in the calorimeter. The first two topologies afford the best resolution because the tracker provides precise  $\gamma$ -direction measurement.

The  $\pi^0$  reconstruction in the proposed fine-grained tracker is expected to be  $\geq 75\%$  if photons that reach the ECAL are included. By contrasting the  $\pi^0$  mass in the tracker versus in the calorimeter, the relative efficiencies of photon reconstruction will be well constrained.

Finally, the  $\pi^\pm$  will be measured by the tracker including the  $dE/dx$  information. **FIXME:** *means both  $\pi^\pm$  and  $dE/dx$  will be measured?* An in situ determination of the charged pions in the  $\nu_\mu/\bar{\nu}_\mu$ -CC events — with  $\mu\text{ID}$  and without  $\mu\text{ID}$  — and in the  $\nu$ -NC events is crucial

to constrain the systematic error associated with the  $\nu_\mu(\bar{\nu}_\mu)$ -disappearance, especially at low  $E_\nu$ .

**Table 5–3:** Precisions achievable from in situ  $\nu_\mu$  and  $\nu_e$  flux measurements in the fine-grained high resolution ND with different techniques. **FIXME:** *Table not yet referenced in text.*

Flavor	Technique	Relative abundance	Absolute normalization	Relative flux $\Phi(E_\nu)$	Detector requirements
$\nu_\mu$	$\nu_\mu e^- \rightarrow \nu_\mu e^-$	1.00	2.5%	$\sim 5\%$	$e^-$ ID $\theta_e$ Resolution $e^-/e^+$ Separation
$\nu_\mu$	$\nu_\mu e^- \rightarrow \mu^- \nu_e$	1.00	3%		$\mu^-$ ID $\theta_\mu$ Resolution 2-Track ( $\mu+X$ ) Resolution $\mu$ energy scale
$\nu_\mu$	$\nu_\mu n \rightarrow \mu^- p$ $Q^2 \rightarrow 0$	1.00	3 – 5%	5 – 10%	$D$ target $p$ Angular & Energy resolution Back-Subtraction
$\bar{\nu}_\mu$	$\bar{\nu}_\mu p \rightarrow \mu^+ n$ $Q^2 \rightarrow 0$	0.70	5%	10%	$H$ target Back-Subtraction
$\nu_\mu$	Low- $\nu_0$	1.00		2.0%	$\mu^-$ vs $\mu^+$ $E_\mu$ -Scale Low- $E_{Had}$ Resolution
$\bar{\nu}_\mu$	Low- $\nu_0$	0.70		2.0%	$\mu^-$ vs $\mu^+$ $E_\mu$ -Scale Low- $E_{Had}$ Resolution
$\nu_e/\bar{\nu}_e$	Low- $\nu_0$	0.01	1-3%	2.0%	$e^-/e^+$ Separation ( $K_L^0$ )

## 5.2 Electroweak Precision Measurement: Weak Mixing Angle

**FIXME:** *This section needs references for all the experiments and other proper names it references*

It is natural to use neutrinos as probes to investigate electroweak physics. Interest in a precise determination of the weak mixing angle ( $\sin^2 \theta_W$ ) at LBNE energies via neutrino scattering is twofold: (a) it provides a direct measurement of neutrino couplings to the  $Z$  boson and (b) it probes a different scale of momentum transfer than LEP by virtue of not being on the  $Z$  pole. The weak mixing angle can be extracted experimentally from three main NC physics processes:

1. deep inelastic scattering off quarks inside nucleons:  $\nu N \rightarrow \nu X$
2. elastic scattering off electrons:  $\nu e^- \rightarrow \nu e^-$

### 3. elastic scattering off protons: $\nu p \rightarrow \nu p$

Figure 5–3 shows the Feynman diagrams corresponding to the three processes.

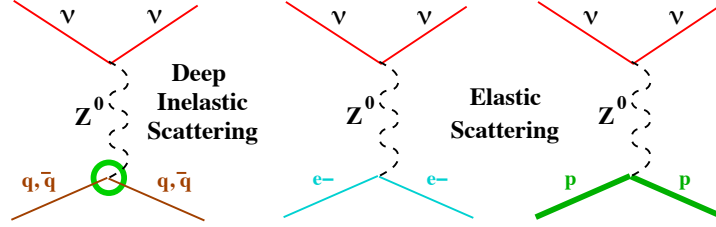


**Figure 5–3:** Feynman diagrams for the three main Neutral Current processes which can be used to extract  $\sin^2 \theta_W$  with the LBNE Near Detector.

#### 5.2.1 Deep Inelastic Scattering

The most precise measurement of  $\sin^2 \theta_W$  in neutrino deep inelastic scattering (DIS) comes from the NuTeV experiment, which reported a value that is  $3\sigma$  from the Standard Model [?]. The LBNE ND can perform a similar analysis in the DIS channel by measuring the ratio of NC and CC interactions induced by neutrinos:

$$\mathcal{R}^\nu \equiv \frac{\sigma_{\text{NC}}^\nu}{\sigma_{\text{CC}}^\nu} \simeq \rho^2 \left( \frac{1}{2} - \sin^2 \theta_W + \frac{5}{9} (1 + r) \sin^4 \theta_W \right). \quad (5.7)$$

Here  $\rho$  is the relative coupling strength of the neutral-to-charged current interactions ( $\rho = 1$  at tree-level in the Standard Model) and  $r$  is the ratio of antineutrino to neutrino cross section ( $r \sim 0.5$ ). The absolute sensitivity of  $\mathcal{R}^\nu$  to  $\sin^2 \theta_W$  is 0.7, which implies that a measurement of  $\mathcal{R}^\nu$  of 1% precision would provide  $\sin^2 \theta_W$  with a precision of 1.4%. Contrary to the NuTeV experiment, the antineutrino interactions cannot be used for this analysis at LBNE due to the large number of  $\nu_\mu$  DIS interactions in the  $\bar{\nu}_\mu$  beam compared to the  $\bar{\nu}_\mu$  DIS interactions.

The measurement of  $\sin^2 \theta_W$  from DIS interactions can only be performed with the low-density magnetized tracker since an accurate reconstruction of the NC event kinematics and of the  $\nu$  CC-interactions are crucial for keeping the systematic uncertainties on the event selection under control. The analysis selects events in the ND after imposing a cut on the visible hadronic energy of  $E_{\text{had}} > 3$  GeV, as in the NOMAD  $\sin^2 \theta_W$  analysis (the CHARM analysis had  $E_{\text{had}} > 4$  GeV). With a 700-kW primary beam about  $3.3 \times 10^6$  CC events and  $1.1 \times 10^6$  NC events are expected, giving a statistical precision of 0.11% on  $\mathcal{R}^\nu$  and 0.15% on  $\sin^2 \theta_W$  (Table 5–4).

The use of a low-density magnetized tracker can substantially reduce systematic uncertainties compared to a massive calorimeter. Table 5–4 shows a comparison of the different

uncertainties on the measured  $\mathcal{R}^\nu$  between NuTeV and LBNE. While NuTeV measured both  $\mathcal{R}^\nu$  and  $\mathcal{R}^{\bar{\nu}}$ , the largest experimental uncertainty in the **FIXME:** *its* single measurement of  $\mathcal{R}^\nu$  is related to the subtraction of the  $\nu_e$ -CC contamination from the NC sample. Since the low-density tracker at LBNE can efficiently reconstruct the electron tracks, the  $\nu_e$ -CC interactions can be identified on an event-by-event basis, reducing the corresponding uncertainty to a negligible level. Similarly, uncertainties related to the location of the interaction vertex, noise, counter efficiency and so on are removed by the higher resolution and by changing the analysis selection. The experimental selection at LBNE will be dominated by two uncertainties: the knowledge of the  $\bar{\nu}_\mu$  flux and the kinematic selection of NC interactions. The former is relevant due to the larger NC/CC ratio for antineutrinos. The total experimental systematic uncertainty on  $\sin^2 \theta_W$  is expected to be about 0.14%.

**Table 5–4:** Comparison of uncertainties on the  $\mathcal{R}^\nu$  measurement between NuTeV and LBNE with the reference beam. The corresponding relative uncertainties on  $\sin^2 \theta_W$  must be multiplied by a factor of 1.4, giving for LBNE a projected overall precision of 0.36%.

Source of uncertainty	$\delta R^\nu / R^\nu$	
	NuTeV	LBNE
Data statistics	0.00176	0.00110
Monte Carlo statistics	0.00015	
Total Statistics	0.00176	0.00110
$\nu_e, \bar{\nu}_e$ flux ( $\sim 1.7\%$ )	0.00064	0.00010
Energy measurement	0.00038	0.00040
Shower length model	0.00054	n.a.
Counter efficiency, noise	0.00036	n.a.
Interaction vertex	0.00056	n.a.
$\bar{\nu}_\mu$ flux	n.a.	0.00070
Kinematic selection	n.a.	0.00060
Experimental systematics	0.00112	0.00102
d,s $\rightarrow$ c, s-sea	0.00227	0.00130
Charm sea	0.00013	n.a.
$r = \sigma^{\bar{\nu}} / \sigma^\nu$	0.00018	n.a.
Radiative corrections	0.00013	0.00013
Non-isoscalar target	0.00010	N.A.
Higher twists	0.00031	0.00070
$R_L (F_2, F_T, xF_3)$	0.00115	0.00140
Nuclear correction		0.00020
Model systematics	0.00258	0.00206
TOTAL	0.00332	0.00255

The measurement of  $\mathcal{R}^\nu$  will be dominated by model **FIXME:** ? systematic uncertainties on the structure functions of the target nucleons. The estimate of these uncertainties for LBNE is based upon the extensive work performed for the NOMAD analysis and includes a NNLO

**FIXME:** ? QCD calculation of structure functions (NLO **FIXME:** *related to NNLO?* for charm production) [?, ?, ?], parton distribution functions (PDFs) extracted from dedicated low- $Q$  global fits, high-twist contributions [?], electroweak corrections [?] and nuclear corrections [?, ?, ?]. The charm quark production in CC, which has been the dominant source of uncertainty in all past determinations of  $\sin^2 \theta_W$  from  $\nu$ N DIS, is reduced to about 2.5% of the total  $\nu_\mu$ -CC DIS with **FIXME:** *for  $E_{\text{had}} > 3$  GeV* with the low-energy beam spectrum at LBNE. This number translates into a systematic uncertainty of 0.13% on  $\mathcal{R}^\nu$  (Table 5-4), assuming a knowledge of the charm production cross section to 5%. It is worth noting that the recent measurement of charm dimuon production by the NOMAD experiment allowed a reduction of the uncertainty on the strange sea distribution to  $\sim 3\%$  and on the charm quark mass  $m_c$  to  $\sim 60$  MeV [?]. The lower neutrino energies available at LBNE reduce the accessible  $Q^2$  values with respect to NuTeV, increasing in turn the effect of non-perturbative contributions (High Twists) and  $R_L$ . The corresponding uncertainties are reduced by the recent studies of low- $Q$  structure functions and by improved modeling with respect to the NuTeV analysis (NNLO vs. LO). The total model systematic uncertainty on  $\sin^2 \theta_W$  is expected to be about 0.29% with the 700-kW reference beam configuration. The corresponding total uncertainty on the value of  $\sin^2 \theta_W$  extracted from  $\nu$ N DIS is 0.36%.

Most of the model uncertainties will be constrained by in situ dedicated measurements using the large CC samples and employing improvements in theory that will have evolved over the course of the experiment. The low-density tracker will collect about 80,000 neutrino-induced inclusive charm events with the 700-kW beam. The precise reconstruction of charged tracks will allow measurement of exclusive decay modes of charmed hadrons (e.g.  $D^{*+}$ ) and measurement of charm fragmentation and production parameters. The average semileptonic branching ratio  $B_\mu$  is of order 5% with the low-energy LBNE beam. The most precise sample of 15,400 dimuon events is collected by the NOMAD experiment [?]. **FIXME:** *Why important to know here?* Finally, precision measurements of CC structure functions in the fine-grained tracker would further reduce the uncertainties on PDFs and on High Twist contributions.

The precision that can be achieved from  $\nu$ N DIS interactions is limited by both the event rates and by the energy spectrum of the reference 700-kW beam configuration. The high-statistics beam exposure **FIXME:** *from something different?* combined with a dedicated run with the high-energy beam option would increase the statistics by more than a factor of 20. This major step forward would not only reduce the statistical uncertainty to a negligible level, but would provide large control samples and precision auxiliary measurements to reduce the systematic uncertainties on structure functions. The two dominant systematic uncertainties, charm production in CC interactions and low  $Q^2$  structure functions, are essentially defined by the available data at present. Overall, the use of a high-energy beam with an upgraded intensity can potentially improve the precision achievable on  $\sin^2 \theta_W$  from  $\nu$ N DIS to about 0.2%. It is worth mentioning that the high-energy beam is also required for the determination of the fluxes in case high  $\Delta m^2$  oscillations are present.

### 5.2.2 Elastic Scattering

A second independent measurement of  $\sin^2 \theta_W$  can be obtained from NC  $\nu_\mu e$  elastic scattering. This channel has lower systematic uncertainties since it does not depend upon the knowledge of the structure of nuclei, but has limited statistics due to its very low cross section. The value of  $\sin^2 \theta_W$  can be extracted from the ratio of neutrino to antineutrino interactions [?]:

$$\mathcal{R}_{\nu e}(Q^2) \equiv \frac{\sigma(\bar{\nu}_\mu e \rightarrow \bar{\nu}_\mu e)}{\sigma(\nu_\mu e \rightarrow \nu_\mu e)}(Q^2) \simeq \frac{1 - 4 \sin^2 \theta_W + 16 \sin^4 \theta_W}{3 - 12 \sin^2 \theta_W + 16 \sin^4 \theta_W}, \quad (5.8)$$

in which systematic uncertainties related to the selection and electron identification cancel out. The absolute sensitivity of this ratio to  $\sin^2 \theta_W$  is 1.79, which implies a measurement of  $\mathcal{R}_{\nu e}$  of 1% precision would provide  $\sin^2 \theta_W$  with a precision of 0.65%.

**FIXME:** *sensitivity of 1.79 implies THAT R of 1% would provide precision of .65%? OR sensitivity of 1.79 implies that R is 1% and this 1% would provide precision of .65%?*

The event selection was described earlier in Section 5.2.1 **FIXME:** *check* since the NC elastic scattering off electrons is also used for the absolute flux normalization. The WMA analysis can be performed only with the low-density magnetized tracker in conjunction with a large LAr detector. In the former case **FIXME:** *sorry, which former case? DIS?* the total statistics available is limited to about a few thousand  $\nu(\bar{\nu})$  events. These numbers do not allow a competitive determination of  $\sin^2 \theta_W$  by using the magnetized tracker alone. However, a 100-ton LAr detector in the ND would be expected to collect about 20,000 (12,000)  $\nu(\bar{\nu})$  events; and an additional factor of four with a high-intensity beam.

A combined analysis of both detectors can achieve the optimal sensitivity: the fine-grained tracker is used to reduce systematic uncertainties (measurement of backgrounds and calibration), while the LAr ND provides the statistics required for a competitive measurement. Overall, the use of the massive LAr detector can provide a statistical accuracy on  $\sin^2 \theta_W$  of about 0.3%. However, the extraction of the WMA is dominated by the systematic uncertainty on the  $\bar{\nu}_\mu/\nu_\mu$  flux ratio in Equation (5.8). This uncertainty has been evaluated with the low- $\nu_0$  method for the flux extraction and a systematic uncertainty of about 1% was obtained on the ratio of the  $\bar{\nu}_\mu/\nu_\mu$  flux integrals. Therefore, the overall precision on  $\sin^2 \theta_W$  achievable from NC elastic scattering off electrons is limited to about 0.9%.

Together, the DIS and the NC elastic scattering channels involve substantially different scales of momentum transfer, providing a tool to test the running of  $\sin^2 \theta_W$  in a single experiment. To this end, the study of NC elastic scattering off protons can provide additional information since it occurs at a momentum scale which is intermediate between the two other processes. Figure 5-4 summarizes the target sensitivity from the LBNE ND, compared with existing measurements as a function of the momentum scale.

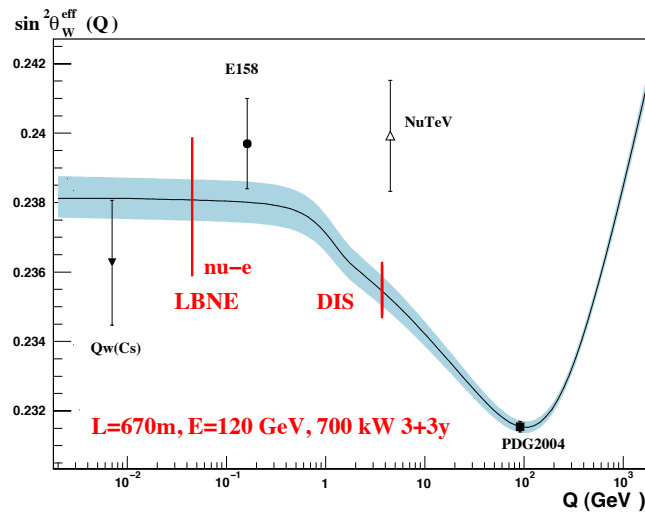


**Figure 5-4:** Expected sensitivity to the measurement of  $\sin^2 \theta_W$  from the LBNE ND with the reference 700 kW beam. The curve shows the Standard Model prediction as a function of the momentum scale [?]. Previous measurements from Atomic Parity Violation [?,?], Moeller scattering (E158 [?]),  $\nu$  DIS (NuTeV [?]) and the combined  $Z$  pole measurements (LEP/SLC) [?] are also shown for comparison. The use of a high-energy beam **FIXME: ambiguous - in GeV or kW?** can reduce the LBNE uncertainties by almost a factor of two.

### 5.3 Observation of the Nucleon's Strangeness Content

The strange-quark content of the proton and its contribution to the proton spin remain enigmatic. The question is whether the strange quarks contribute substantially to the vector and axial-vector currents of the nucleon. A large observed value of the strange-quark contribution to the nucleon spin (axial current),  $\Delta s$ , would change our understanding of the proton structure. The spin structure of the nucleon also affects the couplings of axions and supersymmetric particles to dark matter. The salient topics in this section include:

- Neutral Current Elastic Scattering and Measurement of  $\Delta s$
- Strange Form Factors
- Charm Production and (anti)strange Parton Distribution Function
- Strange Particle Production in NC and CC

The strange *vector* elastic form factors of the nucleon have been measured to high precision in parity-violating electron scattering (PVES) at Jefferson Lab, Mainz and elsewhere. A recent global analysis [?] of PVES data finds a strange magnetic moment  $\mu_s = 0.37 \pm 0.79$  (in



units of the nucleon magneton), so that the strange quark contribution to proton magnetic moment is less than 10%. For the strange electric charge radius parameter,  $\rho_s$ , defined in terms of the Sachs electric form factor at low  $Q^2$  as  $G_E^s = \rho_s Q^2 + \rho'_s Q^4 + \mathcal{O}(Q^6)$ , one finds a very small value,  $\rho_s = -0.03 \pm 0.63 \text{ GeV}^{-2}$ , consistent with zero.

Both results are consistent with theoretical expectations based on lattice QCD and phenomenology [?]. In contrast, the strange *axial vector* form factors are poorly determined. A global study of PVES data [?] finds  $\tilde{G}_A^N(Q^2) = \tilde{g}_A^N (1 + Q^2/M_A^2)^2$ , with the effective proton and neutron axial charges  $\tilde{g}_A^p = -0.80 \pm 1.68$  and  $\tilde{g}_A^n = 1.65 \pm 2.62$ .

The strange axial form factor at  $Q^2 = 0$  is related to the *spin* carried by strange quarks,  $\Delta s$ . Currently the world data on the spin-dependent  $g_1$  structure function constrain  $\Delta s$  to be  $\approx -0.055$  at a scale  $Q^2 = 1 \text{ GeV}^2$ , with a significant fraction coming from the region  $x < 0.001$ . In addition, the HERMES collaboration [?] extracted the strange-quark spin from semi-inclusive DIS data over the range  $0.02 \leq x \leq 0.6$ , yielding a *negative* central value,  $\Delta s = 0.037 \pm 0.019 \pm 0.027$ , although still consistent with the above global average.

**Table 5–5:** Coefficients entering Equation 5.9 for NC elastic scattering and CC QE interactions, with  $\tau = Q^2/4M_p$ .

A	B	C
$\frac{1}{4} [G_1^2 (1 + \tau) - (F_1^2 - \tau F_2^2) (1 - \tau) + 4\tau F_1 F_2]$	$-\frac{1}{4} G_1 (F_1 + F_2)$	$\frac{1}{16} \frac{M_p^2}{Q^2} (G_1^2 + F_1^2 + \tau F_2^2)$

An independent extraction of  $\Delta s$ , which does not rely on the difficult measurements of the  $g_1$  structure function at very small  $x$  values, can be obtained from (anti)neutrino NC elastic scattering off protons, see Figure 5–5. Indeed, this process provides the most direct measurement of  $\Delta s$ . The differential cross section for NC elastic and CC QE scattering of (anti)neutrinos from protons can be written as:

$$\frac{d\sigma}{dQ^2} = \frac{G_\mu^2 Q^2}{2\pi E_\nu^2} (A \pm BW + CW^2); \quad W = 4E_\nu/M_p - Q^2/M_p^2, \quad (5.9)$$

where the positive (negative) sign is for neutrino (antineutrino) **FIXME:** *check* scattering and the coefficients  $A$ ,  $B$ , and  $C$  contain the vector and axial form factors as listed in Table 5–5.

The axial-vector form factor for NC scattering can be written as the sum of the known axial form factor  $G_A$  plus a strange form factor  $G_A^s$ :

$$G_1 = \left[ -\frac{G_A}{2} + \frac{G_A^s}{2} \right], \quad (5.10)$$

while the NC vector form factors can be written as:

$$F_{1,2} = \left[ \left( \frac{1}{2} - \sin^2 \theta_W \right) (F_{1,2}^p - F_{1,2}^n) - \sin^2 \theta_W (F_{1,2}^p + F_{1,2}^n) - \frac{1}{2} F_{1,2}^s \right], \quad (5.11)$$

where  $F_1^{p(n)}$  is the Dirac form factor of the proton (neutron),  $F_2^{p(n)}$  is the corresponding Pauli form factor, and  $F_{1,2}^s$  are the strange-vector form factors. These latter are expected to be small from the PVES measurements summarized above. In the limit  $Q^2 \rightarrow 0$ , the differential cross section is proportional to the square of the axial-vector form factor  $d\sigma/dQ^2 \propto G_1^2$  and  $G_A^s \rightarrow \Delta s$ . The value of  $\Delta s$  can therefore be extracted experimentally by extrapolating the NC differential cross section to  $Q^2 = 0$ .

Previous neutrino scattering experiments have been limited by the statistics and by the systematic uncertainties on background subtraction. One of the earliest measurements available comes from the analysis of 951 NC  $\nu p$  and 776 NC  $\bar{\nu} p$  collected by the experiment BNL E734 [?, ?, ?]. There are also more recent results with high statistics from MiniBooNE where a measurement of  $\Delta s$  was carried out using neutrino NC elastic scattering with 94,531  $\nu N$  events [?]. The MiniBooNE measurement was limited by the ability to distinguish the proton and neutron from  $\nu N$  scattering. The LBNE neutrino beam will be sufficiently intense that a measurement of NC elastic scattering on proton in the fine-grained ND can provide a definitive statement on the contribution of the strange sea to either the axial or vector form factor.

Systematic uncertainties can be reduced by measuring the NC/CC ratios for both neutrinos and antineutrinos as a function of  $Q^2$ :

$$\mathcal{R}_{\nu p}(Q^2) \equiv \frac{\sigma(\nu_\mu p \rightarrow \nu_\mu p)}{\sigma(\nu_\mu n \rightarrow \mu^- p)}(Q^2); \quad \mathcal{R}_{\bar{\nu} p}(Q^2) \equiv \frac{\sigma(\bar{\nu}_\mu p \rightarrow \bar{\nu}_\mu p)}{\sigma(\bar{\nu}_\mu p \rightarrow \mu^+ n)}(Q^2), \quad (5.12)$$

Figure 5-5 shows the absolute sensitivity of both ratios to  $\Delta s$  for different values of  $Q^2$ . The sensitivity for  $Q^2 \sim 0.25 \text{ GeV}^2$  is about 1.2 for neutrinos and 1.9 for antineutrinos, which implies that a measurement of  $\mathcal{R}_{\nu p}$  and  $\mathcal{R}_{\bar{\nu} p}$  of 1% precision would enable the extraction of  $\Delta s$  with an uncertainty of 0.8% and 0.5%, respectively.

The design of the high-resolution tracker ND for LBNE includes several different nuclear targets. Therefore, most of the neutrino scattering is from nucleons embedded in a nucleus, requiring nuclear effects to be taken into account. Fortunately, in the ratio of NC/CC the nuclear corrections are expected to largely cancel out. The  $\Delta s$  analysis requires a good proton reconstruction efficiency as well as high resolution on both the proton angle and energy. To this end, the low-density magnetized tracker at LBNE can increase the range of the protons inside the ND, allowing the reconstruction of proton tracks down to  $Q^2 \sim 0.07 \text{ GeV}^2$ . This capability will reduce the uncertainties in the extrapolation of the form factors to the limit  $Q^2 \rightarrow 0$ .

Table 5-6 summarizes the expected proton range for the low-density ( $\rho \sim 0.1 \text{ g/cm}^3$ ) straw tube tracker (STT) in the ND tracking detector design described in Section 3.5. About  $1 \times 10^5$   $\nu p(\bar{\nu} p)$  events are expected after the selection cuts in the low-density tracker, yielding a statistical precision on the order of 0.3%.

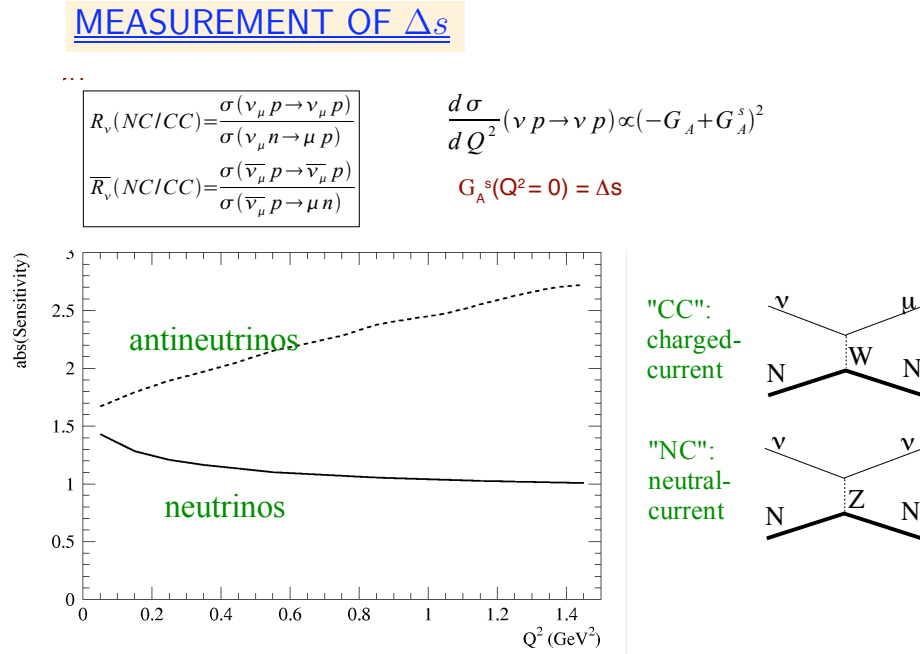


**Figure 5–5:** Absolute sensitivity of the ratios  $\mathcal{R}_{\nu p}$  (solid) and  $\mathcal{R}_{\bar{\nu} p}$  (dashed) to the strange contribution to the spin of the nucleon,  $\Delta s$ , as a function of  $Q^2$  **FIXME:** *This doesn't read well; can we say 'to the strange quark's contribution to spin of nucleon'?* (both main caption and short caption.

The determination of  $\Delta s$  in the LBNE ND design follows the analysis performed by the FINESS collaboration [?] and in the SciBooNE experiment. **FIXME:** *follows the ANALYSES of these two expts? Sounds like the finesse collab analyzed their own AND the sciboone data. Plz clarify.* In particular, based upon the latter, with the scintillator tracker LBNE expects a purity of about 50%, with background contributions of 20% from neutrons produced outside of the detector, 10%  $\nu n$  events and 10% NC pion backgrounds. The dominant systematic uncertainty will be related to the background subtraction. The low-energy beam spectrum at LBNE provides the best sensitivity for this measurement since the external background from neutron-induced proton recoils will be reduced by the strongly suppressed high-energy tail. The low-density magnetized tracker is expected to increase the purity by reducing the neutron background and the NC pion background. The outside neutron background, it should be noted, can be determined using the  $n \rightarrow p + \pi^-$  process in the STT. The sensitivity analysis is still in progress, however LBNE is confident of achieving a precision on  $\Delta s$  of about 0.02 – 0.03.

## 5.4 Tests of Isospin Physics and Sum-Rules

One of the most compelling physics topics accessible to a high-resolution near detector in LBNE is the isospin physics using neutrino and antineutrino interactions. This physics

**Table 5–6:** Expected proton range for the low-density ( $\rho \sim 0.1 \text{ g/cm}^3$ ) tracker. The first column gives the proton kinetic energy and the last column the proton momentum. The  $Q^2$  value producing  $T_p$  is calculated assuming the struck nucleon is initially at rest.

$T_p$ MeV	$Q^2$ $\text{GeV}^2/c^2$	Range STT $cm$	$P_p$ $\text{GeV}/c$
20	0.038	4.2	0.195
40	0.075	14.5	0.277
60	0.113	30.3	0.341
80	0.150	50.8	0.395
100	0.188	75.7	0.445

involves the Adler sum rule and tests of isospin (charge) symmetry in nucleons and nuclei.

The Adler sum rule relates the integrated difference of the antineutrino and neutrino  $F_2$  to the isospin of the target:

$$\mathcal{S}_A(Q^2) = \int_0^1 dx \left[ F_2^{\bar{\nu}}(x, Q^2) - F_2^{\nu}(x, Q^2) \right] / (2x) = 2 I_z, \quad (5.13)$$

where the integration is performed over the entire kinematic range of the Bjorken variable  $x$  and  $I_z$  is the projection of the target isospin vector on the quantization axis ( $z$  axis). For the proton  $\mathcal{S}_A^p = 1$  and for the neutron  $\mathcal{S}_A^n = -1$ .

In the quark parton model the Adler sum is the difference between the number of valence  $u$  and  $d$  quarks of the target. The Adler sum rule survives the strong interaction effects because of the conserved vector current (CVC) and provides an exact relation to test the local current commutator algebra of the weak hadronic current. We note that in the derivation of the Adler sum rule the effects of both non-conservation of the axial current and heavy-quark production are neglected.

Experimental tests of the Adler sum rule require the use of a hydrogen target to avoid nuclear corrections to the bound nucleons inside the nuclei. The structure functions  $F_2^{\bar{\nu}}$  and  $F_2^{\nu}$  have to be determined from the corresponding differential cross sections and must be extrapolated to small  $x$  values in order to evaluate the integral. The test performed in bubble chambers by the BEBC collaboration — the only test available — is limited by the modest statistics; it used about 9,000  $\bar{\nu}$  and 5,000  $\nu$  events collected on hydrogen [?].

The LBNE program can provide the first high-precision test of the Adler sum rule. To this end, the use of the high-energy beam configuration **FIXME:** *again, GeV or kW? (intensity or p energy?)*, although not essential, would increase the sensitivity, allowing attainment of higher  $Q^2$  values. Since the use of a liquid  $\text{H}_2$  bubble chamber is excluded in the ND hall due to safety concerns, the (anti)neutrino interactions off a hydrogen target can only be extracted with a subtraction method from the composite materials of the ND targets. Using this technique to determine the position resolution in the location of the primary vertex is

crucial to reducing systematic uncertainties. **FIXME:** *“For this reason a precision test of the Adler sum rule can be only performed with the low-density magnetized ND.” Is this an argument for why we need the low-dens mag’d ND? It sounds like “sigh, we’ll have to use this crappy thing instead of a bubble chamber.” Need to reword. Here’s a proposal:* LBNE would perform a precision test of the Adler sum rule using the low-density magnetized ND.

A combination of two different targets — the polypropylene ( $C_3H_6$ )<sub>n</sub> foils placed in front of the STT modules and pure carbon foils — are used **FIXME:** *in the low-dens mag’d ND* to provide a fiducial hydrogen mass of about 1 tonne. The statistical subtraction **FIXME:** *used for testing the Adler sum rule* increases the statistical uncertainty **FIXME:** *of what?* by a factor of four. With the LBNE fluxes from the standard exposure, about  $1 \times 10^6$  inclusive  $\nu(\bar{\nu})$  CC events would be collected on the hydrogen target. This level of precision will open up the possibility of making new discoveries in the quark and hadron structure of the proton. **FIXME:** *This level of precision, although reduced, is sufficient to open up this possibility? The flow here isn’t quite right.*

## 5.5 Nucleon Structure, Parton Distribution Functions, and QCD Studies

Precision measurements of (anti)neutrino structure functions and differential cross sections would directly affect **FIXME:** *improve?* LBNE’s oscillation measurements by providing accurate simulation of neutrino interaction **FIXME:** *why would measurements provide simulation?* and offer an estimate of all background processes that are dependent upon the angular distribution of the outgoing particles in the FD. Furthermore, certain QCD analyses — i.e., global fits used for extraction of parton distribution functions (PDF) via the differential cross sections measured in ND data — would constrain systematic error in precision electroweak measurements. This would apply not only in neutrino physics but also in hadron-collider measurements.

Under the rubric of nucleon-structure, this chapter discusses:

- Measurement of Form Factors and Structure Functions
- QCD Analysis of Parton Distribution Functions
- $d/u$  Parton Distribution Functions at Large  $x$
- GLS Sum Rule and  $\alpha_s$
- Non-perturbative Contributions and High Twists
- Quark-hadron Duality

- Generalized Parton Distributions

For quantitative studies of inclusive deep-inelastic lepton-nucleon scattering, it is vital to have precise  $F_3$  structure functions, which can only be measured with neutrino and antineutrino beams, as input into global PDF fits. Because it depends on weak axial quark charges, the  $F_3$  structure function is unique in its ability to differentiate between the quark and antiquark content of the nucleon. On a proton target, for instance, the neutrino and antineutrino  $F_3$  structure functions (at leading order in  $\alpha_s$ ) are given by

$$xF_3^{\nu p}(x) = 2x(d(x) - \bar{u}(x) + \bar{s}(x) + \dots), \quad (5.14)$$

$$xF_3^{\bar{\nu} p}(x) = 2x(u(x) - \bar{d}(x) - \bar{s}(x) + \dots). \quad (5.15)$$

In contrast, electromagnetic probes are sensitive only to a sum of quark and antiquark PDFs. Unfortunately, the neutrino scattering cross sections have considerably larger uncertainties than the electromagnetic inclusive cross sections at present. The proposed high-resolution tracker for LBNE promises to reduce the gap between the uncertainties on the weak and electromagnetic structure functions, and would have a major impact on global PDF analyses.

Recent experiments at JLab have collected high-precision data on the individual  $F_1$  and  $F_2$  (or  $F_T$  and  $F_L$ ) structure functions at large  $x$  from Rosenbluth-separated cross sections. This avoids the need for model-dependent assumptions about the ratio  $R = \sigma_L/\sigma_T$  of the longitudinal to transverse cross sections in the extraction of the structure functions from the measured cross sections. **FIXME:** *The fact that JLab collected this data allows LNBE to avoid making these assumptions? Reword according to meaning.* LBNE's ND would provide similar-quality data on the individual  $F_T$  and  $F_L$  structure functions from neutrino scattering, which would maximally complement and facilitate the flavor decomposition of these functions.

In addition to data in the DIS region, there is considerable interest in obtaining data at low  $Q^2$  (down to  $Q^2 \sim 1 \text{ GeV}^2$ ) and low  $W$  ( $W < 2 \text{ GeV}$ ) to complement data from JLab. Unpolarized structure functions can be expressed in terms of powers of  $1/Q^2$  (power corrections):

$$F_{2,T,3}(x, Q^2) = F_{2,T,3}^{\tau=2}(x, Q^2) + \frac{H_{2,T,3}^{\tau=4}(x)}{Q^2} + \frac{H_{2,T,3}^{\tau=6}(x)}{Q^4} + \dots \quad (5.16)$$

where the first term ( $\tau = 2$ ), expressed in terms of PDFs, represents the Leading Twist (LT), which describes the scattering off a free quark, and is responsible for the scaling of SF via perturbative QCD  $\alpha_s(Q^2)$  corrections. The Higher Twist (HT) terms ( $\tau = 4, 6$ ) reflect instead the strength of multi-parton correlations ( $qq$  and  $qg$ ). The ND data at LBNE would allow a good separation of target mass and Higher Twist **FIXME:** *should be upper case H and T?* corrections, both of which are  $1/Q^2$ -suppressed at high  $Q^2$ , due to leading twist contributions [?], [?]. **FIXME:** *check*

Global PDF fits show that at large values of  $x$  ( $x > 0.5 - 0.6$ ) the  $d$  quark distribution (or the  $d/u$  ratio) is very poorly determined. The main reason for this is the absence of free

neutron targets. Because of the larger electric charge on the  $u$  quark than on the  $d$ , the electromagnetic proton  $F_2$  structure function data provide strong constraints on the  $u$  quark distribution, but are relatively insensitive to the  $d$  quark distribution.

To constrain the  $d$  quark distribution a precise knowledge of the corresponding neutron  $F_2^n$  structure functions is required, which in practice is extracted from inclusive deuterium  $F_2$  data. At large values of  $x$  the nuclear corrections in deuterium become large and, more importantly, strongly model-dependent, leading to large uncertainties on the resulting  $d$  quark distribution.

With the energy-upgraded 12-GeV beam at JLab, several planned experiments will measure the  $d/u$  ratio up to  $x \sim 0.85$ , using several different methods in order to minimize the nuclear corrections. For example, the “BoNuS” experiment [?] will use semi-inclusive DIS from deuterium. A low-momentum ( $|\vec{p}| < 100$  MeV) spectator proton detected in the backward center-of-mass hemisphere will ensure scattering on an almost free neutron (th). Preliminary results have confirmed the feasibility of this method at the current 6-GeV energies, and a proposal for the extension at 12 GeV has been approved.

Perhaps the cleanest and most direct method to determine the  $d/u$  ratio at large  $x$  is from neutrino and antineutrino DIS on hydrogen. Existing neutrino data on hydrogen have relatively large errors and do not extend beyond  $x \sim 0.5$ . A new measurement of neutrino and antineutrino DIS from *hydrogen* **FIXME:** *why italics? what's different, it's still hydrogen?* at LBNE with significantly improved uncertainties would therefore make an important discovery about the  $d/u$  behavior as  $x \rightarrow 1$ . This measurement might be possible with a statistical subtraction of pure-carbon from the hydro-carbon target with negligible systematic errors due to acceptance. To well complement the proposed JLab 12-GeV experiments, the kinematical reach would need to be up to  $x \sim 0.85$  and with as large a  $Q^2$  range as possible to control for higher twist and other sub-leading effects in  $1/Q^2$ . **FIXME:** “*And the ND can do this...*” or *some such...*

## 5.6 Studies of Neutrino-Nuclear Interactions and Nuclear Effects

An integral part of the physics program envisioned for the LBNE ND involves detailed measurements of (anti)neutrino interactions in a variety of nuclear targets. The most important nuclear target is of course the argon target that comprises the LBNE FD. Regarding the ND, the standard target is hydro-carbon, largely provided by the mass of the the STT radiators. An additional proposed ND target is argon gas in pressurized aluminium tubes with sufficient mass to provide  $\simeq 5$  times the  $\nu_\mu$ -CC and NC statistics as expected in the LBNE FD. Equally important nuclear targets are iron, which is used in the ICAL of INO, and carbon. The modularity of the STT provides for successive measurements using thin nuclear targets

such as lead, calcium and other materials. An arrangement of nuclear targets positioned upstream of the detector provides the desired sample in (anti)neutrino interactions. **FIXME:** *this is pretty vague; ANY arrangement?* For example, a single 1-mm-thick lead sheet at the upstream end of the detector will provide about  $2 \times 10^5$   $\nu_\mu$ -CC interactions in one year.

Potential ND studies in nuclear effects include the following:

- nuclear modifications of form factors
- nuclear modifications of structure functions
- mechanisms for nuclear effects in coherent and incoherent regimes
- a dependence of exclusive and semi-exclusive processes
- effect of final-state interactions
- effect of short-range correlations
- two-body currents

The study of nuclear effects in (anti)neutrino interactions off nuclei is directly relevant for the long-baseline oscillation studies. The use of argon or iron in the LBNE FD requires a measurement of nuclear cross sections on the same targets in the ND. **FIXME:** *No, but something like high-precision measurements made using argon or iron in the FD ... may require similar targets in ND* In addition to the different  $p/n$  ratio in argon or iron or water, nuclear modifications of cross sections can differ from 5% to 15% between oxygen and argon, while the difference in the final state interactions could be larger. Additionally, nuclear modifications can introduce a substantial smearing of the kinematic variables reconstructed from the observed final-state particles. Detailed measurements of the  $A$  **FIXME:** *as in atomic number? I had to guess, but that's what comes to mind anyway* dependence of different processes are then required in order to understand the absolute energy scale of neutrino events and to reduce the corresponding systematic uncertainties on the oscillation parameters.

Furthermore, an important question in nuclear physics is how the structure of a free nucleon is modified when said nucleon is inside a nuclear medium. **FIXME:** *Makes it sound like the ND plans to perform some nuclear physics measurements...? Why is this important for ND?* **FIXME:** *Other question: I can't find a definition of 'nuclear medium'; I'm going to assume it's a nucleus. What does it mean to have a free nucleon inside a nucleus? (This is not for the paper, I'm just curious.)* Studies of the ratio of structure functions of nuclei to those of free nucleons (or in practice, the deuteron) reveal nontrivial deviations from unity as a function of  $x$  and  $Q^2$ . These have been well explored in charged-lepton scattering experiments, but little empirical information exists from neutrino scattering. **FIXME:** *How does this relate to LBNE goals? Or is it just an independent physics study thing?*



Another reason to investigate the medium modifications of neutrino structure functions is that most neutrino scattering experiments are performed on nuclear targets, from which information on the free nucleon is inferred by performing a correction for the nuclear effects. **FIXME:** *aha, here's the relevance, but wait... this also refers to indep ND neutrino 'scattering' expts, right?* In practice this often means applying the same nuclear correction as for the electromagnetic structure functions, which introduces an inherent model dependence in the result. In particular, significant differences between photon-induced and weak-boson-induced nuclear structure functions are predicted, especially at low  $Q^2$  and low  $x$ , which have not been tested. A striking example is offered by the ratio  $R$  of the longitudinal-to-transverse structure functions [?]. While the electromagnetic ratio tends to zero in the photoproduction limit,  $Q^2 \rightarrow 0$ , by current conservation, the ratio for neutrino structure functions is predicted to be *finite* in this limit. Thus, significant discovery potential exists in the study of neutrino scattering from nuclei.

Finally, the extraction of (anti)neutrino interactions on deuterium from the statistical subtraction of  $\text{H}_2\text{O}$  from  $\text{D}_2\text{O}$ , which is required to measure the fluxes (Section 5.1), would allow the first direct measurement of nuclear effects in deuterium. This measurement can be achieved since the structure function of a free isoscalar nucleon is given by the average of neutrino and antineutrino structure functions on hydrogen ( $F_2^{\nu n} = F_2^{\bar{\nu} p}$ ). A precise determination of nuclear modifications of structure functions in deuterium would play a crucial role in reducing systematic uncertainties from the global PDF fits.

## 5.7 Search for Heavy Neutrinos

The most economic way to handle the problems of neutrino masses, dark matter and baryon asymmetry of the universe in a unified way may be to add to the SM three Majorana singlet fermions with masses roughly on the order of the masses of known quarks and leptons. The appealing feature of this theory (called the  $\nu\text{MSM}$  for “Neutrino Minimal SM”) is that every left-handed fermion has a right-handed counterpart, leading to an equal way of treating quarks and leptons. The lightest of the three new leptons is expected to have a mass from 1 keV to 50 keV and to play the role of the dark matter particle. Two other neutral fermions are responsible for giving masses to ordinary neutrinos via the see-saw mechanism at the *electroweak scale* and for creation of the baryon asymmetry of the Universe (for a review see [?]). The masses of these particles and their coupling to ordinary leptons are constrained by particle physics experiments and cosmology. They should be almost degenerate, thus nearly forming Dirac fermions (this is coming from **FIXME:** *i.e., 'dictated by'?* the requirement of successful baryogenesis). Different considerations indicate that their mass should be in the region of  $\mathcal{O}(1)$  GeV [?].

**FIXME:** *new* The  $\nu\text{MSM}$  is described by the most general renormalizable Lagrangian containing all the particles of the SM and three singlet fermions. For the purpose of the present discussion the lightest singlet fermion  $N_1$  (the “dark matter sterile neutrino”), which is cou-

pled extremely weakly to the ordinary leptons, is ignored. In addition,  $N_2$  and  $N_3$  are assumed degenerate in mass,  $M_2 = M_3 = M$ . Then the convenient parametrization of the interaction of the  $N$ 's with the leptons of SM is:

**FIXME:** *old* The  $\nu$ MSM is described by the most general renormalizable Lagrangian containing all the particles of the SM and three singlet fermions. For the purpose of the present discussion we take away from it the lightest singlet fermion  $N_1$  (the “dark matter sterile neutrino”), which is coupled extremely weakly to the ordinary leptons. In addition, we take  $N_2$  and  $N_3$  degenerate in mass,  $M_2 = M_3 = M$ . Then the convenient parametrization of the interaction of  $N$ 's with the leptons of SM is:

$$L_{\text{singlet}} = \left( \frac{\kappa M m_{\text{atm}}}{v^2} \right)^{\frac{1}{2}} \left[ \frac{1}{\sqrt{\epsilon e^{i\eta}}} \bar{L}_2 N_2 + \sqrt{\epsilon e^{i\eta}} \bar{L}_3 N_3 \right] \tilde{H} - M \bar{N}_2^c N_3 + \text{h.c.}, \quad (5.17)$$

where  $L_2$  and  $L_3$  are the combinations of  $L_e$ ,  $L_\mu$  and  $L_\tau$

$$L_2 = \sum_{\alpha} x_{\alpha} L_{\alpha}, \quad L_3 = \sum_{\alpha} y_{\alpha} L_{\alpha}. \quad (5.18)$$

with  $\sum_{\alpha} |x_{\alpha}|^2 = \sum_{\alpha} |y_{\alpha}|^2 = 1$ .

In Equation (5.17)  $v = 246$  GeV is the vacuum expectation value of the Higgs field  $H$ ,  $\tilde{H}_i = \epsilon_{if} H_j^*$ ,  $m_{\text{atm}} \simeq 0.05$  eV is the atmospheric neutrino mass difference, and  $\kappa = 1$  (2) for normal (inverted) hierarchy of neutrino masses. The  $x_{\alpha}$  and  $y_{\alpha}$  can be expressed through the parameters of the active neutrino-mixing matrix (explicit relations can be found in [?]). The parameter  $\epsilon$  (by definition,  $\epsilon < 1$ ) and the CP-breaking phase  $\eta$  cannot be fixed by using neutrino masses and mixings.

If the mass of  $N$  is fixed, smaller  $\epsilon$  yields stronger interactions of singlet fermions to the SM leptons. This would have led to equilibration of these particles in the early universe above the electroweak temperatures, and, therefore, to erasing of the baryon asymmetry. In other words, the mixing angle  $U^2$  between neutral leptons and active neutrinos must be small, explaining why these new particles have not been seen previously. For small  $\epsilon$ ,

$$U^2 = \frac{\kappa m_{\text{atm}}}{4M\epsilon}. \quad (5.19)$$

The most efficient mechanism of sterile neutrino production is through weak decays of heavy mesons and baryons, as can be seen from the left panel of Figure 5–6, showing some examples of relevant two- and three-body decays. Heavy mesons can be produced by energetic protons scattering off the target material.

Several experiments have conducted searches for heavy neutrinos, for example BEBC [?], CHARM [?], NuTeV [?] and the CERN PS191 experiment [?,?] (see also discussion of different experiments in [?]). In the search for heavy neutrinos, the strength of the proposed

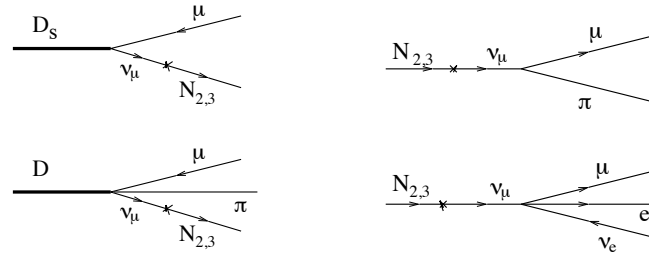


**Figure 5-6:** Left panel: Feynman diagrams of meson decays producing heavy sterile neutrinos. Right panel: Feynman diagrams of sterile neutrino decays.

high-resolution ND, compared to earlier experiments, lies in reconstructing the exclusive decay modes, including electronic, hadronic and muonic. Furthermore, the detector offers a means to constrain and measure the backgrounds using control samples. Preliminary investigations suggest that the LBNE high-resolution near detector will have an order of magnitude higher sensitivity in exclusive channels than previous experiments. The sensitivity evaluation is being actively advanced.

## 5.8 Search for High $\Delta m^2$ Neutrino Oscillations

## 5.9 Search for Non-Standard Interactions: High $\Delta m^2$ Neutrino Oscillations

The evidence for neutrino oscillations obtained from atmospheric, long-baseline accelerator, solar and long-baseline reactor data from different experiments consistently indicates two different scales, with  $\Delta m_{32}^2 \sim 2.4 \times 10^{-3} \text{ eV}^2$  defining the atmospheric oscillations and  $\Delta m_{21}^2 \sim 7.9 \times 10^{-5} \text{ eV}^2$  defining the solar oscillations. **FIXME:** *nothing about accel or reactor oscill scales?* The only way to accommodate oscillations with relatively high  $\Delta m^2$  at the  $\text{eV}^2$  scale **FIXME:** *Why do we care about the 1-eV<sup>2</sup> scale?* is therefore to add one or more sterile neutrinos to the conventional three light neutrinos.

Recently, the MiniBooNE experiment reported that their antineutrino data might be consistent with the LSND  $\bar{\nu}_\mu \rightarrow \bar{\nu}_e$  oscillation with  $\Delta m^2 \sim \text{eV}^2$  [?]. Contrary to the antineutrino data, the MiniBooNE neutrino data seem to exclude high  $\Delta m^2$  oscillations, possibly indicating a different behavior between neutrinos and antineutrinos.

Models with five (3+2) or six (3+3) neutrinos can potentially explain the MiniBooNE results. In addition to the cluster of the three neutrino mass states accounting for “solar” and “atmospheric” mass splitting two (or three) states at the  $\text{eV}$  scale are added, with a small admixture of  $\nu_e$  and  $\nu_\mu$  to account for the LSND signal. One distinct prediction from such models is a significant probability for  $\bar{\nu}_\mu$  disappearance into sterile neutrinos, on the order

of 10%, in addition to the small probability for  $\bar{\nu}_e$  appearance.

Since the ND at LBNE is located at a baseline of 460 m and uses the LE beam, it can reach the same value  $L/E_\nu \sim 1$  of MiniBooNE and LSND. The large fluxes and the availability of fine-grained detectors make the LBNE program well suited to search for oscillations at the  $\text{eV}^2$  scale. Due to the potential differences between neutrinos and antineutrinos, four possibilities have to be considered in the analysis:  $\nu_\mu$  disappearance,  $\bar{\nu}_\mu$  disappearance,  $\nu_e$  appearance and  $\bar{\nu}_e$  appearance. As discussed in Section 5.1, the search for high  $\Delta m^2$  oscillations has to be performed simultaneously with the in situ determination of the fluxes.

To this end, an independent prediction of the  $\nu_e$  and  $\bar{\nu}_e$  fluxes starting from the measured  $\nu_\mu$  and  $\bar{\nu}_\mu$  CC distributions are required since the  $\nu_e$  and  $\bar{\nu}_e$  CC distributions could be distorted by the appearance signal. The low- $\nu_0$  method can provide such predictions if external measurements for the  $K_L^0$  component are available from hadro-production experiments (Section 5.1).

The study will implement an iterative procedure:

1. extraction of the fluxes from  $\nu_\mu$  and  $\bar{\nu}_\mu$  CC distributions assuming no oscillations are present
2. comparison with data and determination of oscillation parameters (if any)
3. new flux extraction after subtraction of the oscillation effect
4. iteration until convergence

The analysis has to be performed separately for neutrinos and antineutrinos due to potential CP or CPT violation according to MiniBooNE/LSND data.

The ratio of electron-to-muon CC events will be measured:

$$\mathcal{R}_{e\mu}(L/E) \equiv \frac{\# \text{ of } \nu_e N \rightarrow e^- X}{\# \text{ of } \nu_\mu N \rightarrow \mu^- X}(L/E); \quad \bar{\mathcal{R}}_{e\mu}(L/E) \equiv \frac{\# \text{ of } \bar{\nu}_e N \rightarrow e^+ X}{\# \text{ of } \bar{\nu}_\mu N \rightarrow \mu^+ X}(L/E) \quad (5.20)$$

This is then compared with the predictions obtained from the low- $\nu_0$  method. Deviations of  $\mathcal{R}_{e\mu}$  or  $\bar{\mathcal{R}}_{e\mu}$  from the expectations as a function of  $L/E$  would provide evidence for oscillations. It must be noted that this procedure only provides a relative measurement of  $\nu_e(\bar{\nu}_e)$  vs  $\nu_\mu(\bar{\nu}_\mu)$ ; since the fluxes are extracted from the observed  $\nu_\mu$  and  $\bar{\nu}_\mu$  CC distributions, an analysis of the  $\mathcal{R}_{e\mu}(\bar{\mathcal{R}}_{e\mu})$  ratio cannot distinguish between  $\nu_\mu(\bar{\nu}_\mu)$  disappearance and  $\nu_e(\bar{\nu}_e)$  appearance.

The process of NC elastic scattering off protons (Section ??) can provide the complementary measurement needed to disentangle the two hypotheses of  $\nu_\mu(\bar{\nu}_\mu)$  disappearance into sterile

neutrinos and  $\nu_e(\bar{\nu}_e)$  appearance. In order to cancel systematic uncertainties, the NC/CC ratio with respect to quasi-elastic scattering will be measured:

$$\mathcal{R}_{NC}(L/E) \equiv \frac{\# \text{ of } \nu p \rightarrow \nu p}{\# \text{ of } \nu_\mu n \rightarrow \mu^- p}(L/E); \quad \bar{\mathcal{R}}_{NC}(L/E) \equiv \frac{\# \text{ of } \bar{\nu} p \rightarrow \bar{\nu} p}{\# \text{ of } \bar{\nu}_\mu p \rightarrow \mu^+ n}(L/E) \quad (5.21)$$

**FIXME: new** It is possible to reconstruct the neutrino energy from the proton angle and momentum under the assumption of neglecting the nuclear smearing (the same for the neutrino CC sample). **FIXME: assume that you neglect something? Do you assume that you CAN neglect this? Why not ‘assuming no nucl smearing’ or ‘neglecting nule smearing’?** In the oscillation analysis, only the *relative* distortions of the ratio  $\mathcal{R}_{NC}(\bar{\mathcal{R}}_{NC})$  as a function of  $L/E$  are of interest, not their absolute values. For  $Q^2 > 0.2 \text{ GeV}^2$  the relative shape of the total cross sections is not very sensitive to the details of the form factors. To improve the energy resolution, it is possible to use events originating from the deuterium inside the D<sub>2</sub>O target embedded into the fine-grained tracker. **FIXME: Sentence unclear. Deuterium is inside target which is embedded in tracker; events (not particles that cause events?) originate from this deuterium; how to use them to improve energy resolution? Are they a known energy or something?**

**FIXME: old** We can reconstruct the neutrino energy from the proton angle and momentum under the assumption of neglecting the nuclear smearing (the same for the neutrino CC sample). In the oscillation analysis we are only interested in relative distortions of the ratio  $\mathcal{R}_{NC}(\bar{\mathcal{R}}_{NC})$  as a function of  $L/E$  and not in the absolute values of the ratios. For  $Q^2 > 0.2 \text{ GeV}^2$  the relative shape of the total cross sections is not very sensitive to the details of the form factors. To improve the energy resolution we can use events originating from the deuterium inside the D<sub>2</sub>O target embedded into the fine-grained tracker.

An improved oscillation analysis is based on a simultaneous fit to both  $\mathcal{R}_{e\mu}(\bar{\mathcal{R}}_{e\mu})$  and  $\mathcal{R}_{NC}(\bar{\mathcal{R}}_{NC})$ . The first ratio provides a measurement of the oscillation parameters while the latter constrains the  $\nu_e(\bar{\nu}_e)$  appearance vs the  $\nu_\mu(\bar{\nu}_\mu)$  disappearance. This analysis imposes two main requirements on the ND:

- $e^+/e^-$  separation to provide an unambiguous check of the different behavior between neutrinos and antineutrinos suggested by MiniBooNE
- accurate reconstruction of proton momentum and angle

**FIXME: new** Validation of the unfolding of the high  $\Delta m^2$  oscillations from the in situ extraction of the (anti)neutrino flux would also require changes to the beam conditions, since the ND cannot be easily moved. This would require a short run with a high-energy beam and the capability to change/switch off the beam focusing system.

**FIXME: old** In order to validate the unfolding of the high  $\Delta m^2$  oscillations from the in situ extraction of the (anti)neutrino flux, we would also need to change the beam conditions,

since the ND cannot be easily moved. To this end, it will be important to have the possibility of a short run with a high energy beam and to change/switch off the beam focusing system.

## 5.10 Light (sub-GeV) Dark Matter Searches

According to the latest cosmological and astrophysical measurements, nearly eighty percent of the matter in the universe is in the form of cold, non-baryonic dark matter (DM). The search to find evidence of the particle (or particles) that make up DM, however, has so far turned up empty. Direct detection experiments and measurements at the LHC alike, however, are starting to severely constrain the parameter space of Weakly-Interacting Massive Particles (WIMPs), one of the leading candidates for DM. The lack of evidence for WIMPs at these experiments has forced many in the theory community to reconsider.

**FIXME:** *new* Some theories consider an alternative possibility to the WIMP paradigm in which the DM mass is much lighter than the electroweak scale (e.g., below the GeV level). In order to satisfy constraints on the relic density of DM, these theories require that DM particles be accompanied by light “mediator” particles that would have allowed for efficient DM annihilation in the early universe. In the simplest form of these theories an extra U(1) gauge field mixes with the Standard Model (SM) U(1) gauge field, but with an additional kinetic term. This mixing term provides a “portal” from the dark sector to the charged particles of the SM. In this model, the mediators are called “dark photons” and are denoted by  $\mathbf{V}$ .

Recently, a great deal of interest has been paid to the possibility of studying these models at low-energy, fixed-target experiments (see Refs. [?,?,?]). High-flux neutrino beam experiments have been shown to provide coverage of DM+mediator parameter space which cannot be covered by either direct detection or collider experiments. Upon striking the target, the proton beam can produce the dark photons either directly through  $pp(pn) \rightarrow \mathbf{V}$  as in Figure 5-7 (left) or indirectly through the production of a  $\pi^0$  or a  $\eta$  meson which then promptly decays into a SM photon and a dark photon as in Figure 5-7 (center). For the case where  $m_V > 2m_{DM}$ , the dark photons will quickly decay into a pair of DM particles. The LBNE ND will provide an excellent setup for making this measurement. **FIXME:** *sentence added by anne*

**FIXME:** *old* One alternative possibility to the WIMP paradigm is that DM has a mass which is much lighter than the electroweak scale (e.g., below the GeV level). In these theories, in order to satisfy constraints on the relic density of DM, the DM particles must be accompanied by light “mediator” particles that allow for efficient DM annihilation in the early universe. The simplest form of these theories is that of an extra U(1) gauge field mixes with the Standard Model (SM) U(1) gauge field with an additional kinetic term. This mixing term provides a “portal” from the dark sector to the charged particles of the SM. In this model, the mediators are called “dark photons” and are denoted by  $\mathbf{V}$ . Recently, a great deal of

interest has been paid to the possibility of studying these models at low-energy, fixed-target experiments (see Refs. [?, ?, ?, ?]). High flux neutrino beam experiments, such as LBNE, have been shown to provide coverage of DM+mediator parameter space which cannot be covered by either direct detection or collider experiments. Upon striking the target, the proton beam can produce the dark photons either directly through  $pp(pn) \rightarrow V$  as in Figure 5-7 (left) or indirectly through the production of a  $\pi^0$  or a  $\eta$  meson which then promptly decays into a SM photon and a dark photon as in Figure 5-7 (center). For the case where  $m_V > 2m_{DM}$ , the dark photons will quickly decay into a pair of DM particles.

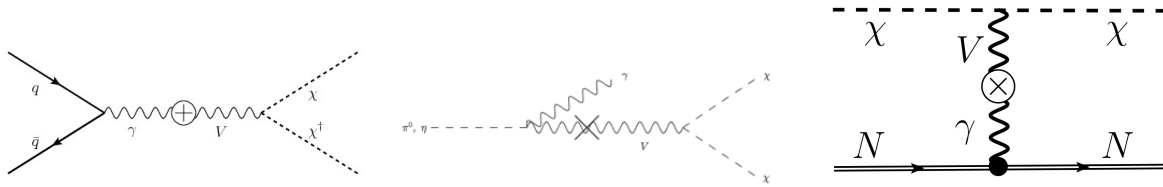


**Figure 5-7:** On the left is shown the direct production of a dark photon, while, in the center, the dark photon is produced via the decay of a neutral pion or eta meson. In both cases, the dark photon promptly decays into a pair of DM particles. Right: Tree-level scattering of a DM particle off of nuclei. Analogous interactions with electrons in the detector are also possible.

These relativistic DM particles from the beam will travel along with the neutrinos to the LBNE near detector. The DM particles can then be detected through neutral-current-like interactions either with electrons or nucleons in the detector, as shown in Figure 5-7 (right). Since the signature of DM events looks just like those of the neutrinos, the neutrino beam provides the major source of background for the DM signal.

Several ways have been proposed to suppress neutrino backgrounds using the unique characteristics of the DM beam. Since DM will travel much more slowly than the higher-mass neutrinos, the timing of the DM events in the near detector. **FIXME:** *incomplete sentence* In addition, since the electrons struck by DM will be in a much more forward direction **FIXME:** *than what? I thought the signal was indistinguishable*, the angle of these electrons may be used to reduce backgrounds, taking advantage of fine angular resolution LBNE can provide. Finally, a special run can be devised to turn off the focusing horn to significantly reduce the charged particle flux that will produce neutrinos. Figure 5-8 shows an example of the number of DM neutral-current-like events which would have been produced in the MINOS near detector (980t) depending on the mass of the DM particle and the size of the mixing between the SM and dark photons ( $\kappa$ ). If the LBNE near detector were of the type LArTPC and with the entire detector volume active, the effective number of DM events detected would be much higher with the detector of the same mass **FIXME:** *not same type?*. Much more thorough studies must be conducted to obtain reliable sensitivity. This requires an integration of theoretical predictions into a simulation package for the detector.

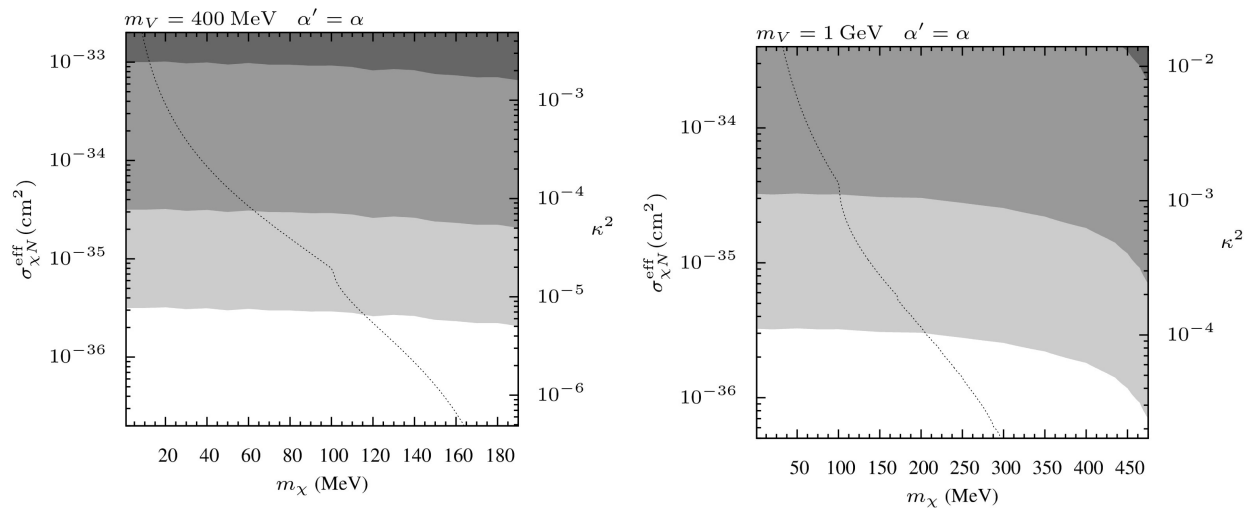


**Figure 5-8:** Expected number of neutral-current-like events from DM scattering. On the left is shown the case where  $V$  is directly produced, while the right plot shows the case where  $V$  is produced from  $\eta$  decay. The contours show greater than 10 (light), 1000 (medium) and 106 (dark) events. These plots were taken from [?].



## 6 Baryon Physics Motivated by Grand Unified Theories

**FIXME:** *new* Baryon number is an unexplained symmetry **FIXME:** *relate how it's a conserved quantity to how it's a 'symmetry' with deep connections in* **FIXME:** *to both? cosmology and particle physics* **FIXME:** *or connects cosmology and particle physics? or has deep 'implications' for both?* As one of the conditions underlying the observed matter-antimatter asymmetry of the universe, baryon number should be violated **FIXME:** *or 'should not be conserved'.* This violation is a hallmark of **FIXME:** *all? many? some?* grand unified theories (GUTs), theories that connect quarks and leptons in ways not envisioned by the Standard Model. Observation of proton or bound neutron decay would provide a key experimental signature of baryon number violation. Predicted rates for nucleon decay based on GUTs are uncertain but cover **FIXME:** *overlap?* a range directly accessible with the **FIXME:** *today's? proposed for tomorrow?* large underground detectors. LBNE, configured with its massive far detector deep underground **FIXME:** *and made more massive than 10 kt, right?* may allow us to observe a process such as proton decay or neutron-antineutron oscillation for the first time. At the very least it would provide an excellent opportunity to extend the search for baryon number violation by nearly an order of magnitude past the limits set by the current generation, which has so far produced negative results.

**FIXME:** *old* Baryon number is an unexplained symmetry with deep connections in cosmology and particle physics. Baryon number is expected to be violated as one of the conditions for the observed matter-antimatter asymmetry of the universe, and baryon number violation is a hallmark of grand unified theories (GUTs), theories which connect quarks and leptons in a manner beyond the standard model. A key experimental observable of baryon number violation is the decay of the proton or bound neutron. Predicted rates for nucleon decay based on GUTs are uncertain but cover a range directly accessible with the large underground detectors. An underground installation of a massive LBNE far detector provides an excellent opportunity extend the search for baryon number non-conservation by nearly an order of magnitude past the limits set by the current generation of negative results, or more hopefully, to observe a process such as proton decay or neutron-antineutron oscillation for the first time.

## 6.1 LBNE and the Current Experimental Context

**FIXME:** *new, 4 pgraphs* Current limits on nucleon decay via numerous channels are dominated by Super-Kamiokande (SK) [?], for which the most recently reported preliminary results are based on an overall exposure of 260 kt-yr. **FIXME:** *Does it matter that this exposure is for water?* **FIXME:** *as a wcd, it only sees one channel (or one category of channel), right? but its results in this channel dominate all other results?* The SK search has so far failed to observe nucleon decay, however it has established strict limits (90% CL) on the partial lifetimes for modes of particular interest **FIXME:** *per GUTs?* such as  $\tau/B(p \rightarrow e^+\pi^0) < 1.3 \times 10^{34}$  yr and  $\tau/B(p \rightarrow K^+\bar{\nu}) < 0.59 \times 10^{34}$  yr [?]. These are significant limits **FIXME:** *significant in size or significant to the community?* that constrain model builders and set a high threshold for the next generation detectors such as LBNE and Hyper-Kamiokande. With more than 10 years of exposure, the SK limits will improve only slowly. A much more massive detector such as Hyper-Kamiokande is required to make a significant (order-of-magnitude) improvement using the water Cherenkov technique. **FIXME:** *with HK, how fast or slowly is it expected to improve?*

**FIXME:** *Add a word about the signature in an LArTPC, in contrast to that in a WCD* The uniqueness of proton decay signatures in an LArTPC and the potential for reconstructing them with redundant information has long been recognized as a key strength of this technology. An LArTPC can reconstruct all final-state charged particles and make an accurate assessment of particle type, distinguishing between muons, pions, kaons and protons. Electromagnetic showers are readily measured, and those that originate from photons generated by  $\pi^0$  decay can be distinguished to a significant degree from those that originate from charged-current electron neutrino interactions. Kiloton-per-kiloton, LArTPC technology will **FIXME:** *is known to or is expected to?* outperform water Cherenkov in both detection efficiency and atmospheric neutrino background rejection for most nucleon decay modes, although intranuclear effects are smaller for oxygen and non-existent for hydrogen. **FIXME:** *what effect does this last caveat have?*

When mass and cost are taken into account, water Cherenkov technology is optimum for the  $p \rightarrow e^+\pi^0$  final-state topology, where the signal efficiency is roughly 40% and the background rate is 2 events per megaton-year. The efficiency estimate [?] for an LArTPC is 45% with 1 event per megaton year — not a significant enough improvement in efficiency to overcome the penalty of lower mass. **FIXME:** *Here you've just assumed lower mass, but it's not explicitly stated*

For the  $p \rightarrow K^+\bar{\nu}$  channel, on the other hand, the LArTPC technology is superior based on the same criteria. In the LArTPC, the  $K^+$  track is reconstructed and identified as a charged kaon. The efficiency for the  $\nu K^+$  mode **FIXME:** *why is it designated differently here?* in LAr is estimated to be as high as 97.5% with a background rate of 1 event per megaton year. In water Cherenkov detectors the efficiency for this mode is roughly 19% for a low-background search, with a background rate of 4 events per megaton year. Based on these numbers and

a ten-year exposure, LBNE's full-scope 34-kt LArTPC and the 560-kt Hyper-Kamiokande WCD have comparable sensitivity (at 90% CL), but the estimated LArTPC background of 0.3 events is dramatically better than the 22 estimated for Hyper-K (assuming no further improvement in analysis technique past that executed for SK-4). **FIXME:** *The next sentence doesn't seem necessary.* Experimental searches for rare events in the presence of significant backgrounds are notoriously more problematic than background-free searches.

**FIXME:** *old* Current limits on nucleon decay via numerous channels are dominated by Super-Kamiokande (SK) [?], for which the most recently reported preliminary results are based on an overall exposure of 260 kt-yr. The SK search has so far been negative, resulting in strict limits (90% CL) on the partial lifetimes for modes of particular interest such as  $\tau/B(p \rightarrow e^+\pi^0) < 1.3 \times 10^{34}$  yr and  $\tau/B(p \rightarrow K^+\bar{\nu}) < 0.59 \times 10^{34}$  yr [?]. These are significant limits that constrain model builders and set a high threshold for the next generation detectors such as LBNE and Hyper-Kamiokande. With more than 10 years of exposure, the SK limits will improve only slowly. A much more massive detector such as Hyper-Kamiokande is required to make a significant (order-of-magnitude) improvement using the water Cherenkov technique.

The uniqueness of proton decay signatures in the LArTPC and the potential for reconstructing them with redundant information has been long recognized as a key strength for this technology. The LAr TPC can reconstruct all final state charged particles including an accurate assessment of particle type, distinguishing muons from pions from kaons from protons. Electromagnetic showers are readily measured with a significant ability to distinguish those that originate from photons from  $\pi^0$  decay from those that originate from charged-current electron neutrino interactions. Kiloton-per-kiloton, LAr TPC technology will outperform water cherenkov in both detection efficiency and atmospheric neutrino background rejection for most nucleon decay modes, although intranuclear effects are smaller for oxygen and non-existent for hydrogen.

Taking mass and cost into account, water Cherenkov technology is optimum for the  $p \rightarrow e^+\pi^0$  final state topology, where the signal efficiency is roughly 40% and the background rate is 2 events per megaton-year. The estimate [?] for a LAr TPC is 45% efficiency and 1 event per megaton year, not enough of an improvement to overcome the penalty of lower mass.

On the other hand, for the  $p \rightarrow K^+\bar{\nu}$  channel, the efficiency for water Cherenkov detectors is roughly 19% for a low background search with a background rate of 4 events per megaton year. This is the best mode for a LArTPC, where the  $K^+$  track is reconstructed and identified as a charged kaon. The efficiency for the  $\nu K^+$  mode is estimated to be as high as 97.5% with a background rate of 1 event per megaton year. Based on these numbers and a ten year exposure, the 34 kton LBNE detector and 560 kton Hyper-Kamiokande have comparable sensitivity (at 90% CL), but the LArTPC would have an estimated background of 0.3 events whereas Hyper-K would have 22 events (assuming no further improvement in analysis technique past that executed for SK-4). Experimental searches for rare events in the presence of significant backgrounds are notoriously more problematic than background-free

searches.

## 6.2 Signatures for Baryon Number Violation in LAr

**FIXME:** *new, 2 pg* The LBNE LArTPC has a chance to make up for lower detector mass when compared to Hyper-Kamiokande for modes where the water Cherenkov detector has relatively low efficiency or is susceptible to higher background rates. **FIXME:** *prev sentence needs more positive wording; point was made clear in prev section. Something like: “The LBNE LArTPC’s superior detection efficiencies for decay modes that produce kaons will outweigh its relatively low mass compared with Hyper-Kamiokande.”* Because the LArTPC can reconstruct protons that would otherwise be below Cherenkov threshold, it can reject many CC and NC background topologies by vetoing on the presence of a recoil proton. Due to its high spatial resolution it does well for event topologies with displaced vertices (such as  $p \rightarrow \mu^+ K^0$ , a mode preferred in some SUSY GUTs over  $\nu K^+$ ). For modes with no electron in the final state, the same displaced vertex performance that underpins long-baseline neutrino oscillation measurements allows the rejection of charged current  $\nu_e$  interactions. And, as will be stressed for the key mode of  $p \rightarrow \nu K^+$  described in detail below, the capability to reconstruct the charged kaon with the proper range and  $dE/dx$  allows for a high-efficiency, background-free analysis. In general, the above criteria favor all modes with a kaon, charged or neutral, in the final state. Conversely, the efficiency for decay modes to a lepton plus light meson will be limited by intranuclear reactions that plague LAr to a greater extent than they do  $^{16}\text{O}$  in a water Cherenkov detector.

An extensive survey of nucleon decay efficiency and background rates has been published [?]. Table 6-1 lists selected modes where LArTPC technology exhibits a significant performance advantage (per kiloton) over the water Cherenkov technology.

**FIXME:** *old* The LBNE LAr TPC has a chance to make up for lower detector mass when compared to Hyper-Kamiokande for modes where the water Cherenkov detector has relatively low efficiency or is susceptible to higher background rates. Because the LAr TPC can reconstruct protons that would otherwise be below Cherenkov threshold, it can reject many CC and NC background topologies by vetoing on the presence of a recoil proton. Because the LAr TPC has high spatial resolution, it does well for event topologies with displaced vertices (such as  $p \rightarrow \mu^+ K^0$ , a mode preferred in some SUSY GUTs over  $\nu K^+$ ). For modes with no electron in the final state, the same displaced vertex performance we rely on for long-baseline neutrino oscillation allows the rejection of charged current  $\nu_e$  interactions. And as will be stressed for the key mode of  $p \rightarrow \nu K^+$  described in detail below, the ability to reconstruct the charged kaon with the proper range and  $dE/dx$  allows for a high efficiency, background-free analysis. In general, the above criteria favor all modes with a kaon, charged or neutral, in the final state. Conversely, the efficiency for decay modes to a lepton plus light meson will be limited by intranuclear reactions that are, if anything, worse than the case of  $^{16}\text{O}$  in a water Cherenkov detector.

An extensive survey of nucleon decay efficiency and background rates has been published [?]. Table 6-1 lists selected modes where a LArTPC has a significant performance advantage (per kiloton) over the water Cherenkov technique.

**Table 6-1:** Efficiencies and background rates (events per Mt-yr) for nucleon decay channels of interest for a large underground LArTPC [?], and comparison with water Cherenkov detector capabilities. The entries for the water Cherenkov capabilities are based on experience with the Super-Kamiokande detector [?].

Decay Mode	Water Cherenkov		Liquid Argon TPC	
	Efficiency	Background	Efficiency	Background
$p \rightarrow \nu K^+$	19%	4	97%	1
$p \rightarrow \mu^+ K^0$	10%	8	47%	< 2
$p \rightarrow \mu^- \pi^+ K^+$			97%	1
$n \rightarrow e^- K^+$	10%	3	96%	< 2
$n \rightarrow e^+ \pi^-$	19%	2	44%	0.8

**FIXME:** *new, 3 pgph* The key signature for  $p \rightarrow K^+ \bar{\nu}$  is the presence of an isolated, monochromatic, charged kaon ( $p = 340 \text{ MeV}/c$  for the case of free protons). Unlike the case of  $p \rightarrow e^+ \pi^0$ , where the maximum detection efficiency is limited to 40–45% because of inelastic intranuclear scattering of the  $\pi^0$ , the kaon in  $p \rightarrow K^+ \bar{\nu}$  emerges intact (due to strangeness conservation) from the nuclear environment of the decaying proton  $\sim 97\%$  of the time. Nuclear effects come into play in other ways, however: the kaon momentum is smeared by the proton's Fermi motion and shifted downward by rescattering [?]. **FIXME:** *With what consequences?*

The kaon emerging from this process is below Cherenkov threshold, therefore a water detector must detect it after it stops, via its decay products. Not all  $K$  decay modes are reconstructable, however, and even for those that are, insufficient information exists to determine the initial  $K$  momentum. Still, water detectors can reconstruct significant hadronic channels such as  $K^+ \rightarrow \pi^+ \pi^0$  decay, and the 6-MeV gamma from de-excitation of  $O^{16}$  provides an added signature to help with the  $K^+ \rightarrow \mu^+ \nu$  channel. The overall detection efficiency in SK [?] is thus approaching 20%.

In LArTPC detectors, the  $K^+$  can be tracked, its momentum measured by range, and its identity positively resolved via detailed analysis of its energy-loss profile. Additionally, all decay modes can be cleanly reconstructed and identified, including those with neutrinos, since the decay is at rest. **FIXME:** *Is this 'at rest' made clear above? Does it matter if we first hear it here?* With this level of detail, it is possible for a single event to provide overwhelming evidence for the appearance of an isolated kaon of the right momentum originating from a point within the fiducial volume. The strength of this signature is clear from single-event displays of kaons observed by the ICARUS Collaboration in the cosmic ray test run of

the T600 module, performed at a surface installation in Pavia. Figure 6-1 shows a sample event in which the kaon is observed as a heavily ionizing track that stops and decays to  $\mu\nu$ , producing a muon track that also stops and decays such that the Michel electron track is also visible.

**FIXME:** *old* The key signature for  $p \rightarrow K^+\bar{\nu}$  is the presence of an isolated monochromatic ( $p = 340 \text{ MeV}/c$  for the case of free protons) charged kaon. Unlike the case of  $p \rightarrow e^+\pi^0$ , where the maximum detection efficiency is limited to 40–45% because of inelastic intranuclear scattering of the  $\pi^0$ , the kaon in  $p \rightarrow K^+\bar{\nu}$  emerges intact (due to strangeness conservation) from the nuclear environment of the decaying proton  $\sim 97\%$  of the time. On the other hand, nuclear effects are important: the kaon momentum is smeared by the proton's Fermi motion and shifted downward by rescattering. [?] % Stefan and Ankowski, ArXiv:0811.1892 [nucl-th], 2009.

In water detectors, the kaon is below Cherenkov threshold, and must be detected after stopping, via its decay products. Not all  $K$  decay modes are reconstructable, and even for those that are there is insufficient information to determine the initial  $K$  momentum. Still, water detectors enable reconstruction of significant hadronic channels like  $K^+ \rightarrow \pi^+\pi^0$  decay, and the 6 MeV gamma from de-excitation of  $O^{16}$  provides an added signature to help with the  $K^+ \rightarrow \mu^+\nu$  channel, such that the overall detection efficiency is approaching 20% in SK [?].

In the case of LAr detectors, the  $K^+$  can be tracked, its momentum measured by range, and its identity positively resolved via detailed analysis of its energy loss profile. Additionally, all decay modes can be cleanly reconstructed and identified, including those with neutrinos since the decay is at rest. With this level of detail, a single event can provide overwhelming evidence for the appearance of an isolated kaon of the right momentum originating from a point within the fiducial volume. The strength of this signature is clear from single event displays of kaons observed by the ICARUS Collaboration in the cosmic ray test run of the T600 module on the surface at Pavia in

1. One example is shown below in Figure 6-1.

**FIXME:** *new* If it can be demonstrated that background processes mimicking this signature can be rejected at the appropriate level, it is possible that a single  $p \rightarrow K^+\bar{\nu}$  candidate could provide evidence for proton decay. The background rejection capability of the LBNE far detector is the topic of Section ??.

**FIXME:** *old* Provided that it can be demonstrated that background processes that mimic this signature can be rejected at the appropriate level, a single  $p \rightarrow K^+\bar{\nu}$  candidate can be viewed as evidence for proton decay. We discuss the background rejection capability of the LBNE far detector in the section below.

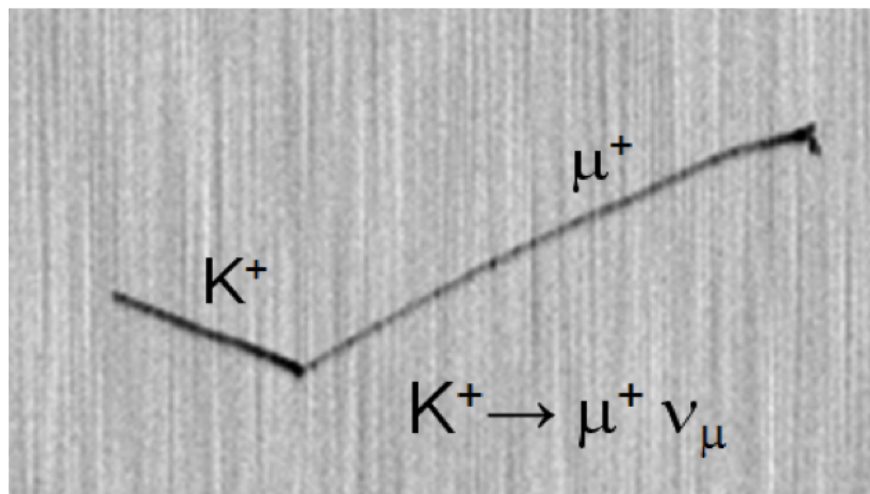


**Figure 6-1:** Single event display for an isolated charged kaon in the ICARUS T600 detector.

### 6.3 Background Levels and Rejection Capabilities

**FIXME:** *new, 3 pgph* Cosmic-ray muons certainly contribute to background when they penetrate the detector, but the most pernicious background in LAr for proton decay with kaon final states comes from cosmic-ray muons that produce entering kaons via photonuclear interactions in the rock near the detector. Backgrounds **FIXME:** *of both types?* as a function of depth have been studied for LAr [?, ?, ?].

At the 4850-ft level, the vertical rock overburden will be approximately 4-km water equivalent, at which depth the muon rate through a 34-kt LArTPC will be approximately  $0.1 \text{ s}^{-1}$ . As this is quite small, a veto on the detection of a muon in the LAr volume can be applied with negligible loss of live-time. Specifically, assuming a maximum drift time of 2 ms, the probability of a muon passing through the detector in time with any candidate event (i.e., a candidate for proton decay or other signal of interest) will be  $2 \times 10^{-4}$ . Thus, any candidate event that coincides in time with a large energy deposition from a muon or muon-induced cascade can be rejected with an **FIXME:** *acceptable?* efficiency loss of 0.02%. Only background from events associated with cosmic-ray muons in which the muon itself does not cross the detector remain to be considered.

The main background for the decay mode  $p^+ \rightarrow K^+ \bar{\nu}$  occurs when a neutral particle (e.g., a  $K_L^0$ ) originating in a muon-induced cascade outside the detector propagates into the detector volume and undergoes a charge-exchange reaction in the fiducial volume. LBNE has simulated cosmic-ray muons and their secondaries at depth, and has found the rate of positive kaons produced inside the 34-kt detector by a neutral particle entering from outside (and with no muon inside) to be 0.9 events per year before any other cuts are applied. Further studies included the following **FIXME:** *successively applied?* cuts:

**FIXME:** *old* In LAr, the most pernicious background for proton decay with kaon final states comes from cosmic rays that produce entering kaons via photonuclear interactions in the rock near the detector. Backgrounds as a function of depth have been studied for LAr in references [?, ?, ?]. At the 4850-foot level, the vertical rock overburden will be approximately 4 km water equivalent. and the muon rate through a 34 kt LArTPC will be approximately  $0.1 \text{ s}^{-1}$ .

With such a small cosmic-ray muon rate, a veto on the detection of a muon in the detector can be applied with negligible loss of live-time. Specifically, taking a maximum 2 ms drift time, the probability of a muon passing through the detector in time with any candidate event will be  $2 \times 10^{-4}$ . (Here the candidate event is defined as an event to be considered as a candidate for the proton decay or other signal of interest.) Thus, any candidate event that coincides in time with a large energy deposition from a muon or muon-induced cascade can be rejected with an efficiency loss of 0.02%. This leaves us to consider only a background from events associated with cosmic-ray muons in which the muon itself does not cross the detector.

We have considered this irreducible cosmic-ray background for the case of  $p^+ \rightarrow K^+ \bar{\nu}$ . The main background for this decay mode occurs when a neutral particle (*i.e.*, a  $K_L^0$ ) originating in a muon-induced cascade outside the detector propagates into the detector volume and undergoes a charge-exchange reaction in the fiducial volume. After simulating cosmic-ray muons and their secondaries at depth, we have found the rate of positive kaons produced inside the 34-kt LBNE detector by a neutral particle coming from outside (and with no muon inside) to be 0.9 events per year before any other cuts are applied. In further studies we considered the following cuts:

**FIXME:** *end old, restart*

1. No muon is in the detector. **FIXME:** *fiducial or total volume?*
2. The  $K^+$  candidate is produced inside the LAr volume at a distance from the wall greater than 10 cm. **FIXME:** *how does this relate to fiducial volume?*
3. The energy deposition from  $K^+$  and its descendants (excluding decay products) is less than 150 MeV.
4. The total energy deposition from the  $K^+$ , its descendants and decay products is less than 1 GeV.
5. Energy deposition from other particles in the muon-induced cascade (*i.e.*, excluding the energy deposition from the positive kaon, its descendants and decay products) is less than 100 MeV.

**FIXME:** *new* No event survived the cuts, resulting in an upper bound on the rate of this type of background event of 0.07 events per year in a 34-kt LArTPC. **FIXME:** *the next sentence*



*is confusing. I don't see that we've established that 'a lot of Ks deposit energy...' or what the other particles are.* The key point here is that although a large number of  $K^+$ 's deposit an energy similar to that which is expected from a proton decay, the energy depositions from  $K^+$ 's are not the only ones recorded for these events: there are other particles entering the detector and depositing more energy making the rejection of background events simpler than expectations based on just the appearance of a kaon in the detector. These studies demonstrate that proton decay searches can be successfully conducted in the LBNE LArTPC at the 4850-ft level, and would not require an external veto system.

**FIXME:** *old* No event survived the cuts, giving an upper bound on the rate of background events that can mimic the  $p \rightarrow K^+\bar{\nu}$  proton decay mode of 0.07 events per year in a 34 kt LArTPC. The key point here is that although a large number of  $K^+$ 's deposit an energy similar to what is expected from a proton decay, the energy depositions from  $K^+$ 's are not the only ones recorded for these events: there are other particles entering the detector and depositing more energy making the rejection of background events simpler than expectations based on just the appearance of a kaon in the detector. These studies show that proton decay searches can be successful at the 4850L at SURF, and would not require an external veto system.

## 6.4 Expected Sensitivity to $p \rightarrow K^+\bar{\nu}$

**FIXME:** *new* A deep underground LArTPC detector of at least 10 kt is needed to improve the current limits on the  $p \rightarrow K^+\bar{\nu}$ , set by Super-Kamiokande, significantly beyond that experiment's continued running. A 34-kt detector will improve the current limits by an order of magnitude after running **FIXME:** *how long - a dozen years?* Clearly a larger detector volume would improve the limits even more in that span of time. Figure 6-2 shows the expected limit on the proton lifetime as a function of running time in LBNE for  $p \rightarrow K^+\bar{\nu}$ . **FIXME:** *Seems like there should be more to say - Where did this info come from? link to the studies referred to in prev section? Unstated conclusion to draw is 'maximize exposure', I guess.*

**FIXME:** *old* Figure 6-2 shows the expected limit on the proton lifetime as a function of time in LBNE for  $p \rightarrow K^+\bar{\nu}$ . According to this plot, at least 10 kton of LAr is required to improve the limits significantly beyond continued Super-Kamiokande running. A 34 kton detector can eventually improve the limits on the  $p \rightarrow K^+\bar{\nu}$  by an order of magnitude compared to Super-Kamiokande. Corresponding sensitivities can be computed for the other decay channels listed in Table 6-1.

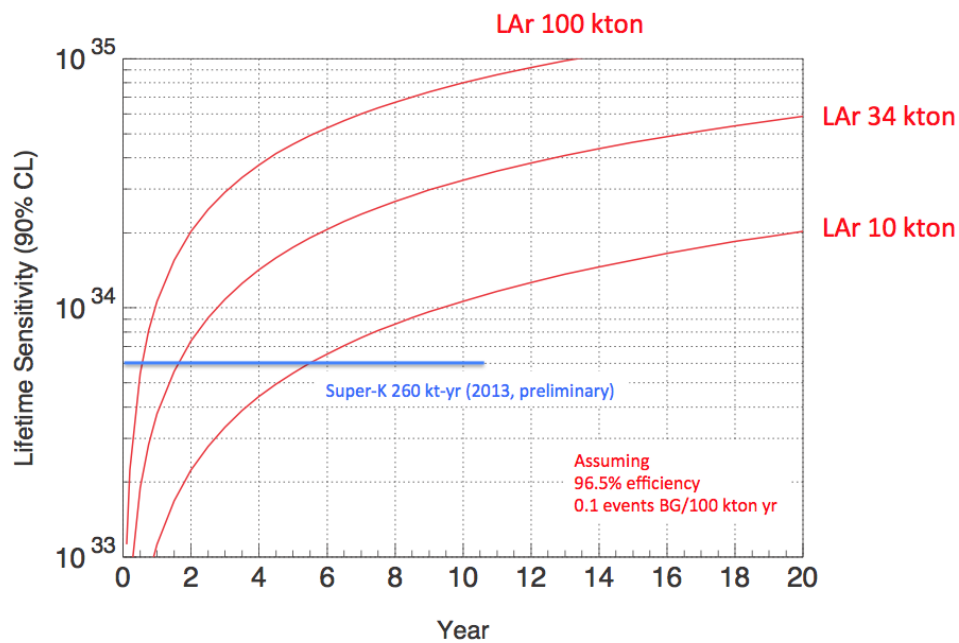


**Figure 6–2:** Proton decay lifetime limit for  $p \rightarrow K^+ \bar{\nu}$  as a function of time for underground LArTPC's of fiducial masses 10, 34 and 50 kt. For comparison, the current limit from Super-Kamiokande is also shown. The limits are at 90% C.L., calculated for a Poisson process including background assuming that the detected events equal the expected background.

## 7 Core-Collapse Supernova Neutrinos

### 7.1 Physics and Astrophysics From Core-Collapse Neutrinos

The information in a supernova neutrino burst is contained in the energy and flavor evolution of the burst as a function of time. This information will shed light both on astrophysics of the collapse, and on neutrino properties. We emphasize here again that liquid argon has unique sensitivity to the  $\nu_e$  component of the burst. It must also be emphasized that the combination of information from different detectors with different flavor sensitivities will bring highly-enhanced information.

Some fairly generic core-collapse signal features are illustrated in Fig. 7-1 reproduced from reference [?]. The event starts with a short, sharp “neutronization” or “break-out” burst primarily composed  $\nu_e$ , and is followed by an “accretion” phase lasting some hundreds of milliseconds. The final “cooling” phase over  $\sim 10$  seconds represents the main part of the signal, over which the proto-neutron star sheds its gravitational binding energy. Flavor content and spectrum changes throughout these phases, and the core collapse’s temperature evolution can be followed with the neutrino signal (see Fig. 7-6).

The core-collapse neutrino spectrum at a given moment in time is expected to be well described by a “pinched-thermal” form, with one popular parameterization [?,?] given by:

$$\phi(E_\nu) = \mathcal{N} \left( \frac{E_\nu}{\langle E_\nu \rangle} \right)^\alpha \exp \left[ -(\alpha + 1) \frac{E_\nu}{\langle E_\nu \rangle} \right], \quad (7.1)$$

where  $E_\nu$  is the neutrino energy,  $\langle E_\nu \rangle$  is the mean neutrino energy,  $\alpha$  is the “pinching parameter”, and  $\mathcal{N}$  is a normalization constant. Large  $\alpha$  corresponds to a more “pinched” spectrum (suppressed high-energy tail). The different  $\nu_e$ ,  $\bar{\nu}_e$  and  $\nu_x$  flavors are expected to have different average energy and  $\alpha$  parameters and to evolve differently in time.

Many phenomena have impact on the flavor-energy time evolution, including neutrino oscillation effects that are determined by the mass hierarchy, and “collective” effects due to

neutrino-neutrino interactions. See *e.g.* references [?, ?, ?, ?, ?, ?, ?, ?] as examples; a voluminous literature exists exploring these phenomena.

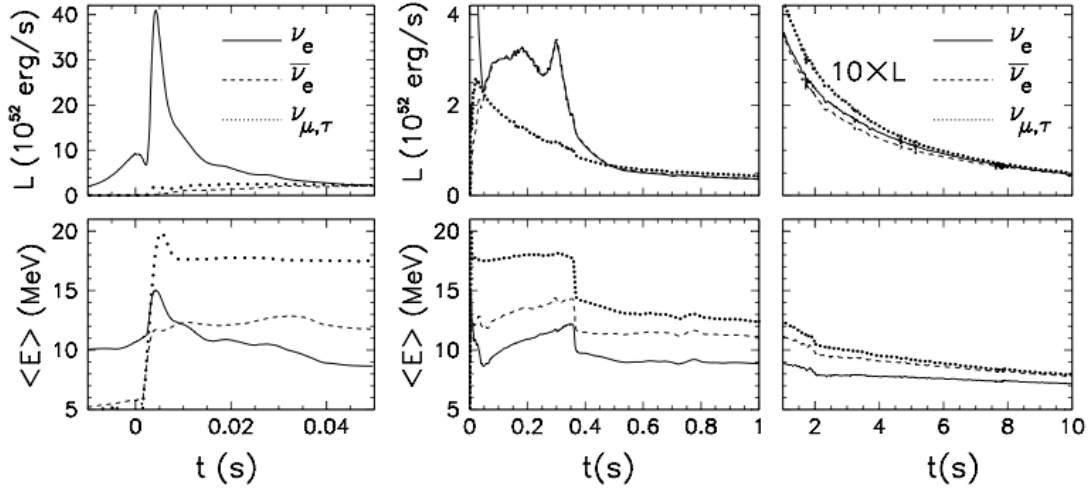


**Figure 7-1:** Expected core-collapse neutrino signal from the “Basel” model [?] (figure from [?]), for a  $10.8 M_{\odot}$  progenitor. The left panel shows the very early signal, including “neutronization burst”; the middle panel shows the “accretion phase”, and the right panel shows the cooling phases. The top plots show luminosities as a function of time and the bottom plots show average energy as a function of time for  $\nu_e$ ,  $\bar{\nu}_e$  and  $\nu_{\mu,\tau}$  flavor components of the flux (note that fluxes for  $\nu_{\mu}$ ,  $\bar{\nu}_{\mu}$ ,  $\nu_{\tau}$ , and  $\bar{\nu}_{\tau}$  should be identical).

The following lists some examples of astrophysical phenomena that should have observable impact on the signal:

- The neutronization burst, which will be mainly composed of  $\nu_e$ .
- Formation of a black hole, which would cause a sharp signal cutoff (*e.g.* [?])
- Shock wave effects [?]
- Standing Accretion Shock Instability (SASI) oscillations [?, ?]
- Turbulence effects [?, ?]

This list is far from comprehensive. In addition there are possible effects that would give indications of beyond-the-standard-model physics [?], *e.g.* axions, extra dimensions, anomalous neutrino magnetic moment (and the non-observation of which would enable constraints on these phenomena).

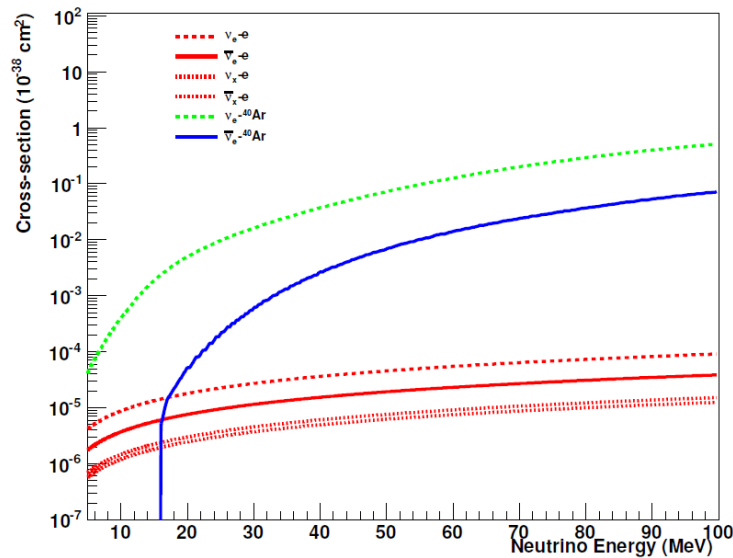
Signatures of collective effects and signatures depending on the mass hierarchy impact many of the above signals (see next section for examples).

The supernova neutrino burst is prompt with respect to the electromagnetic signal and therefore provides an early warning to astronomers [?,?]. Some pointing should also be possible with a liquid argon signal [?] (primarily from elastic scattering on electrons).

One can note also that non-observation of a burst, or non-observation of a  $\nu_e$  component of a burst, in the presence of supernovae (or other astrophysical events) observed in electromagnetic or gravitational wave channels would provide valuable information about the nature of the sources. A long-timescale sensitive search yielding no bursts will also provide limits on the rate of core collapse.

## 7.2 Expected Signal and Detection in Liquid Argon

The predicted event rate from a supernova burst may be calculated by folding expected neutrino differential energy spectra with cross sections for the relevant channels, and with detector response. We use of SNOwGLOBES software [?]. SNOwGLOBES takes as input fluxes, cross sections (see Fig. 7-2), “smearing matrices” and post-smearing efficiencies. The smearing matrices incorporate both interaction product spectra and detector response.



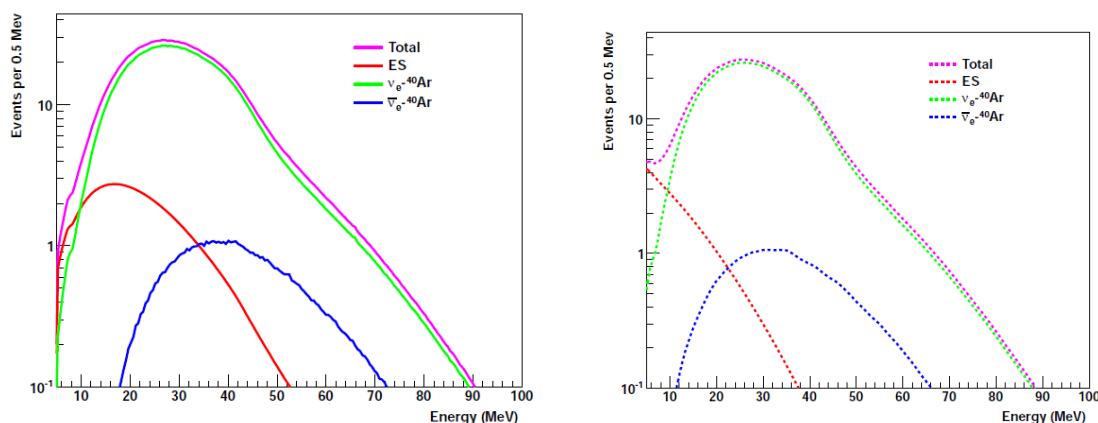
**Figure 7-2:** Cross-sections for SN-relevant interactions in argon.

Table 7-1 shows calculated rates for the dominant interactions in argon for the “Livermore” model [?], and the “GKVM” model [?]. Figure 7-3 shows the expected observed differential event spectra. Clearly  $\nu_e$  flavor dominates.

Another example is for “Duan” fluxes [?] for which different oscillation hypotheses have

**Table 7-1:** Event rates for different models in 17 kt of LAr for a core-collapse at 10 kpc. Event rates will simply scale by active detector mass.

Channel	Events, “Livermore” model	Events, “GKVM” model
$\nu_e + {}^{40}\text{Ar} \rightarrow e^- + {}^{40}\text{K}^*$	1154	1424
$\bar{\nu}_e + {}^{40}\text{Ar} \rightarrow e^+ + {}^{40}\text{Cl}^*$	97	67
$\nu_x + e^- \rightarrow \nu_x + e^-$	148	89
Total	1397	1580



**Figure 7-3:** Supernova neutrino event rates in 17 kton of argon for a core collapse at 10 kpc, for the GKVM model [?] (events per 0.5 MeV), showing three relevant interaction channels. Left: interaction rates as function of true neutrino energy. Right: “smeared” rates as a function of detected energy, assuming resolution from reference [?].

been applied, to illustrate (anecdotally) potential mass hierarchy signatures: see Fig. 7-4. \* Another example is shown in in Figure 7-5, for which a clear feature is visible for the normal mass hierarchy case.

Figure 7-6 shows another example of a preliminary study showing how one might track supernova temperature as a function of time with the  $\nu_e$  signal in liquid argon. Here, a fit is made to the pinched-thermal form of 7.1. Not only can one effectively measure the internal temperature of the supernova, but the time evolution is observably different for different hierarchies.

Most LBNE supernova physics sensitivity studies so far have been done using parameterized detector responses from [?] in SNOwGLoBES. Work is currently underway using LArSoft to characterize low-energy response for LBNE detector configurations. Figure 7-7 shows an example 20-MeV event. Preliminary results show that energy resolutions for baseline detector parameters will not differ too significantly from those in [?]. Also under study is the potential

\*Note that the “Duan” flux represents only a single late time slice of the supernova burst and not the full flux; hierarchy information will be encoded in the time evolution of the signal as well.

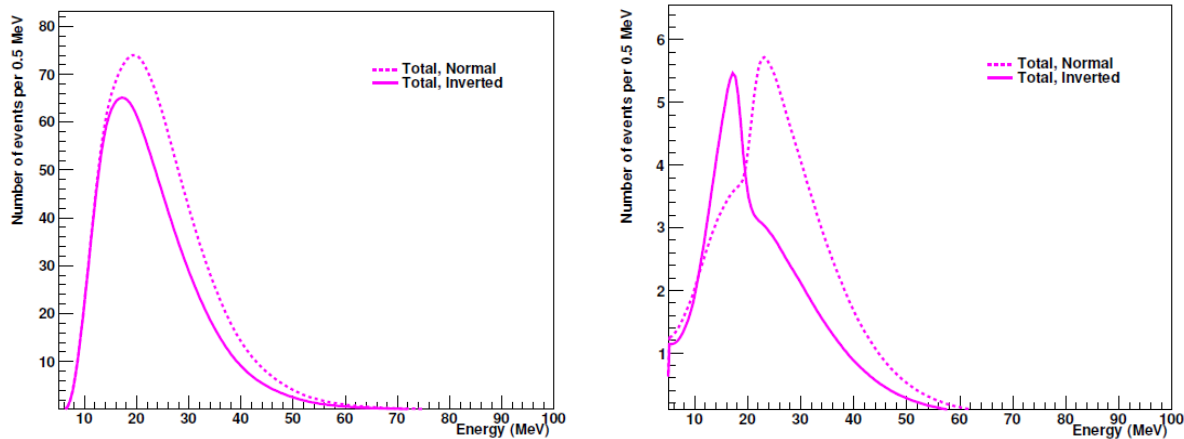


**Figure 7-4:** Comparison of total event rates for normal and inverted hierarchy, for a specific flux example, for a water Cherenkov detector (left) and for a 17 kt LAr (right) configuration, in events per 0.5 MeV. There are distinctive features in LAr for different neutrino mass hierarchies for this supernova model.

for tagging CC  $\nu_e$  absorption events using the cascade of deexcitation  $\gamma$ -rays, which should serve the dual purposes of rejecting background and isolating the CC component of the signal.

### 7.3 Low-Energy Backgrounds

Due to their low energy, supernova events are subject to background, although the short-timescale-burst nature of the signal means that the background can be well known and subtracted. Muons and their associated Michel electrons can in principle be removed. Preliminary studies from reference [?], extended for cosmic-ray rates on the surface, suggest that the 4850L depth available at the Homestake mine is acceptable.

We are in the process of creating a physics driven radioactive background budget and associated event generator for low-energy background events in the LBNE far detector. Radioactive decays will have the capacity to directly overlap with the energy spectrum created by supernova neutrino events in LBNE (these will mostly be from  $\nu_e + {}^{40}\text{Ar} \rightarrow e^- + {}^{40}\text{K}^*$ ). It is also possible that an ensemble of radioactive decay events in and around higher energy particle interactions (e.g. from beam neutrinos) could server to obscure the edges of electromagnetic showers from highly scattering particles like electrons and pions. This would serve as the radiological equivalent of dark noise in a digital image, and would have the potential to introduce a systematic uncertainty in the energy calculated for events even at much higher energy than the decays themselves. It is therefore very important to calculate the radioactive decay backgrounds in the LBNE far detector with sufficient accuracy to properly account for their presence, whether that is as a direct background with the capacity to obscure the

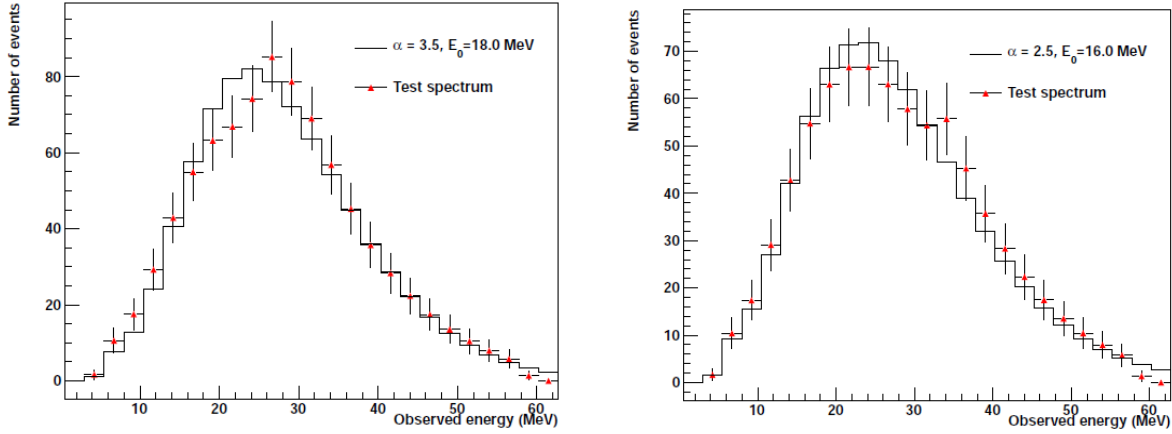


**Figure 7-5:** Observed  $\nu_e$  spectra in 34 kton of LAr for a 10 kpc core collapse, representing about one second of integration time each at one second intervals during the supernova cooling phase. The solid line represents the best fit to a parameterized pinched-thermal spectrum. Clear “non-thermal” features in the spectrum that change with time are visible, on the left at around 20 MeV and on the right at around 35 MeV. Error bars are statistical. These features are present *only* for normal mass hierarchy.

supernova neutrino signal or as a systematic effect in energy calculations.

The radioactive background budget will have many components, each of which will fall into one of two categories: intrinsic radioactive contamination in the argon or support materials, and cosmogenic radioactivity produced *in situ* from cosmic ray showers interacting with the argon or the support materials. The former is dependent on the materials comprising the detector itself, and is therefore independent of far detector site depth. The latter is strongly coupled to the cosmic ray flux and spectrum, so any depth dependence to the background model will play a role here. Both of these background categories are of course in addition to the direct energy depositions from cosmic rays themselves and associated showers. Those have been discussed and well-studied elsewhere, so we will simply refer to their existence here.

### 7.3.1 Intrinsic Backgrounds

Intrinsic backgrounds in the far detector come from the radioactive material that is ubiquitous in the materials comprising the detector (both active and instrumentation/support materials), the cryostat, cavern walls, and dust. The isotopes of interest will largely be “the usual suspects” in experiments where radioactive backgrounds must be controlled:  $^{232}\text{Th}$  and  $^{238}\text{U}$  (and their associated decay chains),  $^{40}\text{K}$ , and  $^{60}\text{Co}$ . In addition to these, there will also be a large component from  $^{39}\text{Ar}$ , which is present in natural argon harvested from the atmosphere at the level of approximately 1 Bq/kg. This means that a 10 kT far detector filled with



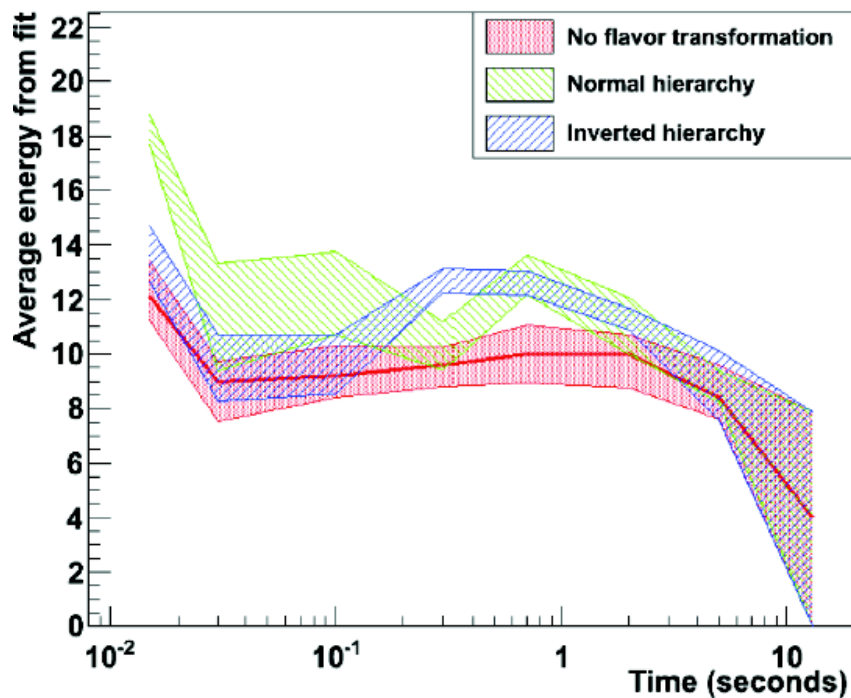


**Figure 7-6:** Average  $\nu_e$  energy from fit to SNOwGLoBES-smeared pinched-thermal spectrum as a function of time, for a flux model based on [?] and including collective oscillations, for two different hierarchy assumptions (34 kton at 10 kpc). The bands represent  $1\sigma$  error bars from the fit. The solid red line is the truth  $\langle E_\nu \rangle$  for the unoscillated spectrum. This plot shows that there is meaningful information to be obtained by tracking  $\nu_e$  spectra as a function of time.

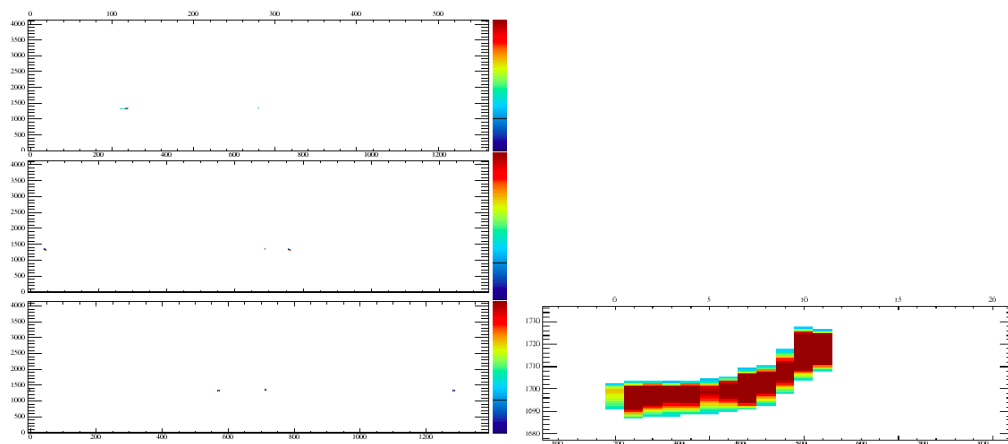


**Figure 7-7:** Left: raw event display of a typical 20-MeV event in the LBNE 10-kton geometry; the top panel shows the collection plane, and the lower two panels show the induction planes (with multiple images due to wire wrapping). Right: zoom of collection plane image.

$^{\text{nat.}}\text{Ar}$  will have a rate from  $^{39}\text{Ar}$  of approximately 10 MHz across the whole detector. The beta decay spectrum from  $^{39}\text{Ar}$  is thankfully quite low in energy ( $Q_\beta = 0.565$  MeV), so it will not interfere directly with the supernova signal, but can contribute to the “dark noise” effect discussed earlier. Furthermore, the product of the average beta energy with this rate sets the scale of the power being introduced into the detector at which we should be concerned about controlling backgrounds. This radioactive power from  $^{39}\text{Ar}$  is approximately:

$$P_{\text{Rad}} \sim 0.25 \text{ MeV} \times 10 \text{ MHz} = 2.5 \times 10^6 \text{ MeV/s.} \quad (7.2)$$

Because the backgrounds in this category can be not just in the bulk argon, but on the surface of or embedded in any of the supporting materials (*e.g.* wire frames, signal wires, photon collectors, readout electronics, cryostat lining/insulation, cavern walls, concrete cavern lining, *etc.*), we must also be mindful of which type of radioactive decay is produced by each intrinsic isotope and not just the total energy released. For instance, an alpha decay from an isotope in the U or Th decay chain will deposit its full energy into the detector if it occurs in the active region of the detector, but will deposit no energy if it occurs inside of some macroscopically thick piece of support material because of the very short range ( $\lesssim 1 \mu\text{m}$ ) in most solids. We must therefore account for energy depositions from intrinsic contamination in different locations (or groups of locations differently. This is clearly a tractable problem, but one which must be handled with some level of care and forethought.

There is clearly a large body of work on the control of radiological backgrounds in experiments like LBNE, so much of the work in this area will be cited from experiments like DARKSIDE, ICARUS, BOREXINO, KamLAND, and Super Kamiokande. Some work will remain however on understanding backgrounds particular to the SURF campus—either on the surface or at the 4850 level (radon levels and dust activity, for instance), and there remains a significant required effort to integrate existing and new work into the LBNE simulation, reconstruction, and analysis framework.

### 7.3.1.1 Cleanliness Database

Radioactive decays, including cosmogenic spallation products, tend to make  $<10$  MeV signals, but may have impact on the detector performance due to the large number of charged particles and scintillation photons they produce in liquid argon. While backgrounds from radioactive decay lie below the main supernova signal range, they inhabit a potential region of interest for physics signatures. The decay events are mainly from radioactive isotope  $^{39}\text{Ar}$  in natural argon, the  $^{238}\text{U}$  and  $^{232}\text{Th}$  decay chains through the airborne (dust) contamination in the detector, and radioactive elements in detector construction materials (which will also have a significant U/Th component). Measurements were made of the decay of  $^{39}\text{Ar}$  in natural argon [?], purity in liquid argon due to outgassing from various materials [?]. The LBNE Collaboration also endeavors to build up a cleanliness database that includes material outgassing characteristics and radioactivity of detector construction materials. Systematic studies of the airborne contamination are also carried out at Homestake and South

Dakota School of Mines and Technology (SDSMT) [?], which include, (1) the survey of the radioactivity data of rock samples and other substances in the Sanford Underground Research Facility (SURF), (2) simulation study of decay events in liquid argon, and (3) the characterization of dust particles on the surface at SURF and in the Davis Cavern at 4850 feet level. More efforts are planned by the LBNE Radiological and Cleanliness Control Group to make progress in the following aspects,

1. Developing more effective dust deposition monitoring method that can also be sensitive to smaller dust particles.
2. Determining the radioactivity of dust particles collected from underground site.
3. Implementing radioactive noise simulation in LBNE simulation tools and study the cleanliness requirements for various physics goals.
4. Tracing impact from decay events that may affect the performance of particular detector units, such as the HV units, TPC wires, etc.
5. Developing material purity model using material test data from the MTS.

The goal is to develop a reliable cleanliness control and monitoring procedure that can guarantee the contamination in the multi kiloton LBNE far detector at a level low enough so that we can extend the experiment threshold down to 5 MeV to 10 MeV in a detector that is also highly stable over 10 - 20 years of data taking.

### 7.3.2 Cosmogenic Backgrounds

As mentioned earlier in this Section, the cosmogenic backgrounds are where the depth of the far site will contribute to the signals seen in LBNE. We have compiled a list of potential cosmogenic nuclides (all either  $\beta^-$  or  $\beta^+$  emitters) produced in argon, along with the nuclear data required to calculate their decay spectra and the software infrastructure necessary to store and recall them as needed. We are now in the process of compiling the activation cross sections, which along with the decay lifetimes will determine the proportions with which we will sample these spectra to simulate background events in LBNE. We will, of course, have different proportions and overall numbers of these cosmogenic nuclides that will be added to LBNE simulations for operation on the surface, and 4850 ft. (we will probably also look at 800 ft.) at SURF. These decays will be added to those from intrinsic radioactivity discussed in Section 7.3.1, to build up the complete radioactive background model for LBNE.

## 8 Other Physics Opportunities with the LBNE Far Detector

In this chapter we summarize several physics topics that in principal could be addressed by the LBNE LAr-FD in a deep underground location. Detection of low energy neutrinos such as geo-neutrinos and relic supernova neutrinos are challenging because of the intrinsic high detection thresholds ( $> 1\text{MeV}$ ) of a LAr detector. Solar neutrino searches require large detectors of order 100kton or more to be competitive, although the high energy and pointing resolutions of a LAr-TPC could be advantageous and offset some of the loss in performance due to the smaller masses of such detectors. Nevertheless, these topics are scientific opportunities that could be pursued by LBNE, in particular with the deployment of larger mass detectors at the far site. An aggressive R&D effort on radiopurity and cleanliness could potentially reduce the detection thresholds of a LAr detector and enhance the low energy scientific reach.

### 8.1 Solar Neutrinos

Even after the long standing mystery of missing solar neutrinos [?] was explained by data from the Super-Kamiokande and SNO [?,?] experiments as flavor transformation of solar neutrinos, there are still interesting open questions in solar neutrino physics. Some of these are astrophysical (like a measurement of the fraction of energy production via CNO cycle in the sun, or flux variations due to helio-seismological modes which reach the solar core, or long-term stability of the solar core temperature). But even particle physics questions remain. Can the MSW model explain the amount of flavor transformation as a function of energy, or are non-standard neutrino interactions required? Do solar neutrinos and reactor anti-neutrinos oscillate with the same parameters? Some of these questions will be answered by experimental data in the immediate future (like SNO+, KamLAND solar phase, further Borexino data, etc.), but high statistics measurements will be necessary to further constrain alternatives to the standard oscillation scenario.

The solar neutrino physics potential of a large liquid Argon TPC largely depends on the energy threshold and depth. The decay of the naturally occurring  $^{39}\text{Ar}$  produces  $\beta$ 's with

a 567 keV endpoint and with an expected background of 10 MHz in a 10 kton LAr-TPC limits the fundamental reach of LAr detectors to  $\nu$  with  $\geq 1$  MeV. The number of solar neutrinos expected in a 10 kton LAr-TPC is 9 events per day from Fermi transition and 26 events per day from Gamow-Teller transitions assuming a 4.5 MeV threshold and 31%  $\nu_e$ . The ICARUS collaboration has reported a 10 MeV neutrino energy threshold [?]. With such a high threshold the LBNE LArFD could measure the CC/NC ratio of  $^8\text{B}$  solar neutrinos with high statistical accuracy and thereby test the MSW flavor transformation curve (see Figure 8-1) with high precision if the detector itself has low radioactivity levels. To significantly improve on existing measurements of the MSW transition and limits on the day/night effect, a LAr detector of 34 kton or more is required. [!htbp] In addition, since the spallation of

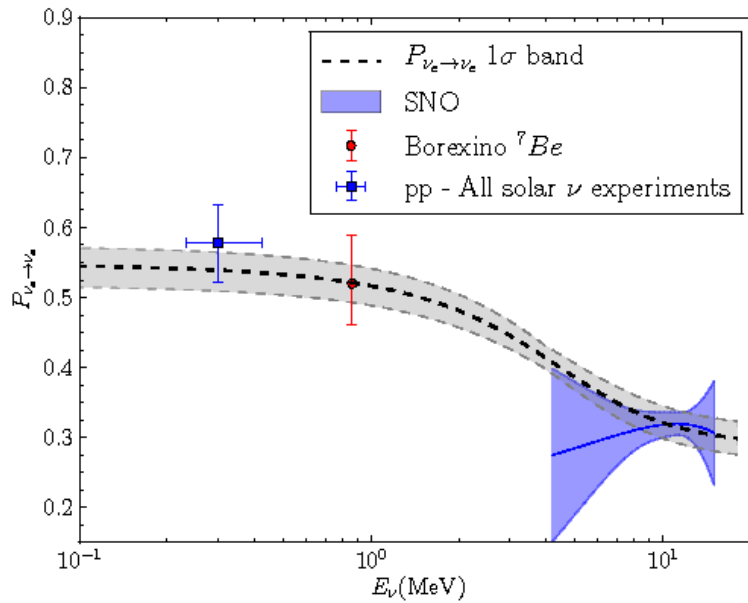


**Figure 8-1:** Measurements of the solar MSW transition [?].

the  $^{40}\text{Ar}$  (a rather complex nucleus compared to  $^{16}\text{O}$ ) is likely to produce many long-lived spallation products which could limit the detection threshold for low energy neutrinos. Only a TPC at the deepest location has a reasonable chance of detecting solar neutrinos. Studies of the spallation background in the LAr-FD are underway. As an example, Figure 8-2 shows the  $^{40}\text{Cl}$  production rate in a 10kton LAr-TPC as a function of depth.  $^{40}\text{Cl}$  is a beta emitter with an endpoint of 7.48 MeV.

## 8.2 Geoneutrinos

Within the earth it is believed that radioactive decays of uranium and thorium are the most significant source of heat that causes mantle convection, the fundamental geological process

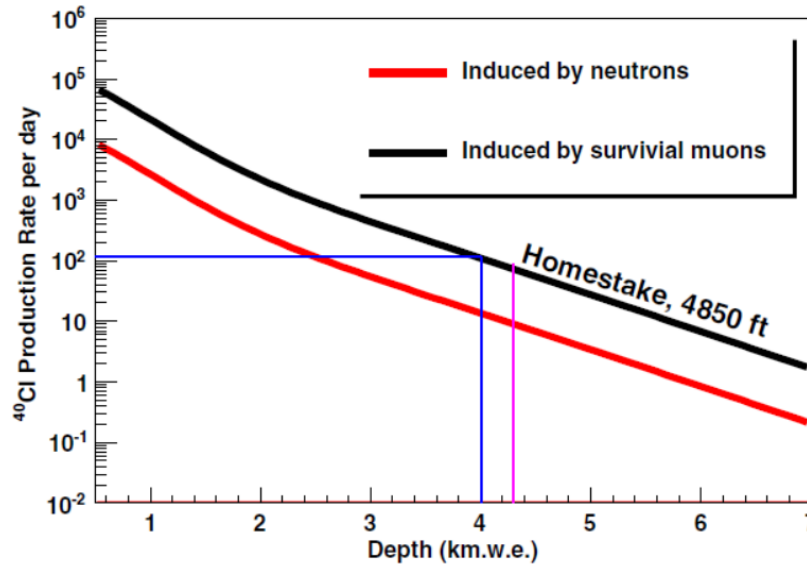


**Figure 8-2:**  $^{40}\text{Cl}$  production rates in a 10 kton detector produced by (n,p) reaction as a function of depth.

that regulates the thermal evolution of the earth and shapes its surface. Until recently, estimates of the total uranium and thorium content of the earth were inferred from earth formation models. However, it has been known for a long time that the uranium and thorium decays produce electron anti-neutrinos, so-called geo-neutrinos, and the detection of these geo-neutrinos near the surface of the earth can directly inform us of the deep earth uranium and thorium content. The low flux of electron anti-neutrinos from reactors, so called reactor neutrinos, at SURF makes it a suitable site to probe geo-neutrinos.

In a liquid Ar detector electron anti-neutrinos can be detected by Ar inverse-beta-decay



The threshold for this reaction is approximately 8.5 MeV, which means that it cannot be used to detect either geo-neutrinos or reactor neutrinos. There are also elastic scattering reactions; however, these are sensitive to neutrinos as well as antineutrinos, so in order to eliminate backgrounds from solar neutrinos we need to be able to reject these by pointing at a level better than one in a thousand. Detecting geo-neutrinos with a massive LAr detector deep underground at SURF hence will be very difficult.

### 8.3 Indirect Searches for WIMP Dark Matter

If the true nature of Dark Matter (DM) does indeed involve a weakly-interacting particle with a mass in the range of 1 GeV, one of the main search strategies involves looking for

anomalous signals in astrophysical data from its annihilation (or decay) into SM particles, like neutrinos [?]. Signals of DM decay via neutrinos can come from such distant objects as the galactic center, the center of the Sun or even the Earth. As our solar system moves through the DM halo, WIMP's interact with the nuclei of celestial bodies and become trapped in the body's gravitational well. Over time, the WIMPs accumulate near the core of the body, enhancing the possibility of annihilation. The high-energy neutrinos ( $E \sim m_{\text{WIMP}}$ ) from these annihilations can free-stream through the astrophysical body and emerge roughly unaffected (although oscillation and matter effects can slightly alter the energy spectrum). For the Sun, the background of neutrinos are produced at much lower energies via the nuclear fusion process. Thus, the detection of high-energy neutrinos pointing to the Sun and detected in the LBNE far detector would be clear evidence of DM annihilation (see Reference [?]). Since the LBNE far detector has relatively large mass of the order 10s of kt, it can act as a "neutrino telescope" and be used to search for signals of DM annihilations coming from the Sun and/or the core of the Earth. IMB [?], IceCube [?] and Super-Kamiokande have searched for DM through this method but have not observed a signal of DM annihilation into neutrinos. Compared to these experiments which are based on Cherenkov light detection using large PMT's, LBNE's LArTPC can provide much better angular resolution that can achieve a far more accurate pointing resolution. More thorough studies [?] are needed to design an optimized analysis to accomplish a competitive detection of dark matter.

## 8.4 GUT Monopoles

GUT monopoles left over from the big bang have the ability to catalyze nucleon decay that could be detectable in large underground detectors [?]. The signature would be multiple proton decays occurring during the monopole's transit of the detector. The imaging ability and low thresholds of the LArTPC provide an opportunity to view this phenomenon through the window of proton decays for which water is an ineffective detection medium. Catalyzed proton decay may still be observable even if the spontaneous proton decay lifetime is too long to be observed with acceptable exposures.

## 8.5 Neutron Anti-neutron Oscillations ( $\Delta B = 2$ )

Some Grand Unified Theories suggest that there may be double baryon number violating transitions that change nucleons into anti-nucleons [?]. The subsequent nucleon anti-nucleon annihilation would be an unmistakable signal in the LBNE detector. The imaging properties of LBNE give it the ability to observe a much broader range of nucleon annihilation final states - an advantage over water detectors - where the signal would be broadened by the mix of charged and neutral hadrons in the final state. It is suspected that the neutron to anti-neutron transition rate is suppressed for bound neutrons via interactions with the other nucleons.

## 9 Conclusion

In this document we have presented the wealth of physics opportunities and capabilities of the Long-Baseline Neutrino Experiment program. We conclude this document with a discussion of possible timeframes for the different stages for LBNE. With DOE CD-1 approval in hand the LBNE Project is working toward the technical design specifications, including detailed costs and schedule, in preparation for CD-2. At CD-2 the LBNE Phase-I project will be baselined. Currently, the timescale for CD-2 is projected to be 2016, although the DOE has indicated flexibility in this specifically to allow for incorporation of scope changes enabled by additional partners. It is also expected that CD-3a approval will be on the same timescale or before CD2, and will allow expenditures for long-leadtime components and construction activities. The CD-4 milestone (completion of the construction project and transition to experiment operations) is currently projected for 2024. We expect that commissioning and operations for LBNE to have started well before CD4, which is considered the formal termination of the construction project.

**Timeline Scenario:** The exact timeframe for accessing LBNE science goals will depend on how a complex sequence of developments take place. However, here we provide an example of one plausible long-term scenario that integrates evolution of LBNE detector mass with development of the Project X beam.

1. Begin operation in 2023 with 700-kW beam and a 10-kt detector.
2. Three years later, in 2026, Project X phase 1 is completed, increasing the beam power to 1.2 MW [?], and the LBNE far detector fiducial mass is increased to 20 kt.
3. Two years later, in 2028, the LBNE far detector mass is increased to 34 kt.
4. Four years later (6 years after the completion of Project X phase 1), Project X phase 3 is completed, increasing the beam power to 2.4 MW.
5. Operate for six years with “full” detector mass and “full” beam power.

The evolution of the LBNE sensitivity to CP-violation under this scenario is illustrated in Fig. 9-1. In this graph, the accumulated exposure is plotted as a function of calendar year,



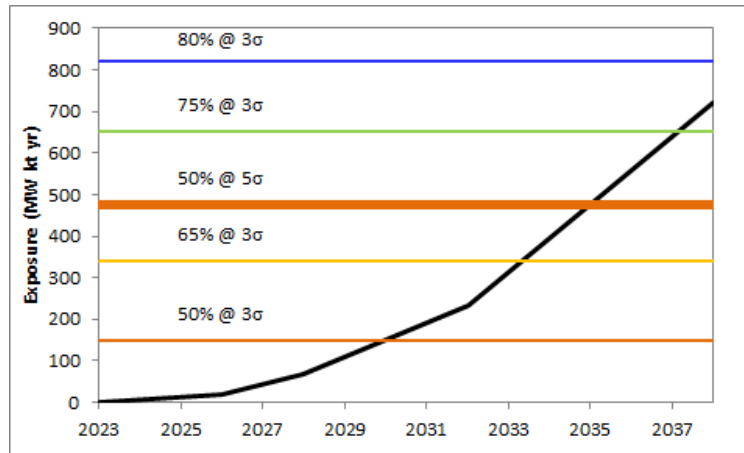


**Figure 9–1:** Evolution of exposure and sensitivity to non-zero or  $\pi$  value for  $\delta_{CP}$  as a function of calendar year, under the scenario for rapid development of the later stages of LBNE and integration with Project X as described in the text.

beginning in 2023. Horizontal lines indicate exposure values that yield particular benchmarks in the sensitivity to leptonic CP violation. These benchmarks are specified in terms of the fraction of the range of  $\delta_{CP}$  for which a non-zero (or  $\pi$ ) value would be established at the stated level of statistical significance ( $3\sigma$  or  $5\sigma$ ) or better. In this scenario, LBNE would achieve 50% coverage of  $\delta_{CP}$  at better than  $5\sigma$  (and 70% coverage at better than  $3\sigma$ ) by 2035 (Note: no experiment will approach 100% in this metric). During the same time frame, LBNE will measure the value of the CP phase,  $\delta_{CP}$ , as well as other mixing parameters including  $\theta_{23}$  with increasing precision with no ambiguities. If the CP phase is near 0 or  $\pi$ , then CP violation cannot be determined by any experiment, but LBNE will have a precise measurement of the parameter. Also in this scenario the mass hierarchy will have been determined unambiguously within about 5 years.

The scenario described above is just one of a number of possibilities. An advantage of a staged approach to LBNE is the flexibility to coordinate with other major activities so that high points in the time profiles of costs do not overlap.

**Alternatives** Considering the time it has taken to reach the current state of development of LBNE, it is unlikely that another program of similarly ambitious scope would be able to begin operation before 2025, particularly in light of the current constrained budget conditions in HEP. We note that similar-cost alternatives for the first phase of LBNE utilizing the existing NuMI beam were considered during the reconfiguration exercise in 2012. The conclusion of the panel was that none of these alternatives presented a path toward an experiment capable of a  $5\text{--}\sigma$  CP violation signal. We also note that careful consideration of a large water Cherenkov option for LBNE was given prior to selection of the LArTPC technology for the far detector. While both options could satisfy the scientific requirements, the LArTPC was expected to have a better scientific performance and presented an attractive advanced technological approach.

**Intensity Frontier Leadership** Massive neutrinos constitute the only palpable evidence we have that the standard model of electroweak and strong interactions (SM) does not describe all observed phenomena. Other puzzling features are the extremely small masses and very large mixings of neutrinos compared to other quarks and leptons. These discoveries have moved the study of neutrino properties to the forefront of experimental and theoretical particle physics as a crucial tool for understanding the fundamental nature of the physical world.

LBNE represents a world-class US based effort to address the science of neutrinos with technologically advanced experimental techniques. By anchoring the U.S. Intensity Frontier program, LBNE provides a platform around which to grow and sustain core infrastructure for the community. This is especially the case for the development of Project X, which will accelerate progress towards the science goals of LBNE while also greatly expanding the capability of Fermilab to host compelling experimental programs that will explore other sectors of the Intensity Frontier.

Understanding the fundamental nature of fermion flavor, the existence of CP violation in the lepton sector and how this relates to the baryon asymmetry of the universe; knowing whether proton decay occurs and how; and elucidating the dynamics of supernova explosions all count among the grand questions of our field. The bold approach adopted for LBNE provides the most rapid and cost-effective means of addressing these questions. With the support of the HEP community, the vision articulated in this document can be realized in a way that maintains the level of excitement for Particle Physics and the inspirational impact it has in the U.S and worldwide.

# **A Summary of the LBNE Reconfiguration Steering Committee Report**

In March of 2012, the Office of Science Director W. F. Brinkman charged Fermilab with finding a path forward to reach the scientific goals of the Long-Baseline Neutrino Experiment in a phased approach as detailed in the following letter:



**Department of Energy**  
Office of Science  
Washington, DC 20585

**Office of the Director**

March 19, 2012

Dr. Pier Oddone  
Director  
Fermilab  
Wilson and Kirks Road  
Batavia, IL 60510-5011

Dear Pier,

Thank you for your recent presentation on the status and plans for the Long Baseline Neutrino Experiment (LBNE). The project team and the scientific collaboration have done an excellent job responding to our requests to assess the technology choices and refine the cost estimates for LBNE. We believe that the conceptual design is well advanced and the remaining technical issues are understood.

The scientific community and the National Academy of Sciences repeatedly have examined and endorsed the case for underground science. We concur with this conclusion, and this has been the motivator for us to determine a path forward as quickly as possible following the decision of the National Science Board to terminate development of the Homestake Mine as a site for underground science.

We have considered both the science opportunities and the cost and schedule estimates for LBNE that you have presented to us. We have done so in the context of planning for the overall Office of Science program as well as current budget projections.

Based on our considerations, we cannot support the LBNE project as it is currently configured. This decision is not a negative judgment about the importance of the science, but rather it is a recognition that the peak cost of the project cannot be accommodated in the current budget climate or that projected for the next decade.

In order to advance this activity on a sustainable path, I would like Fermilab to lead the development of an affordable and phased approach that will enable important science results at each phase. Alternative configurations to LBNE should also be considered. Options that allow us to independently develop the Homestake Mine as a future facility for dark matter experiments should be included in your considerations.



Printed with soy ink on recycled paper

A report outlining options and alternatives is needed as soon as practical to provide input to our strategic plan for the Intensity Frontier program. OHEP will provide additional details on realistic cost and schedule profiles and on the due date for the report.

Thank you,

A handwritten signature in black ink, appearing to read 'W. F. Brinkman', with a stylized flourish extending to the right.

W. F. Brinkman  
Director, Office of Science

A Steering Committee was formed by Fermilab to study phased approaches and alternative experimental configurations. The membership of the Steering Committee was as follows:

**Membership** Young-Kee Kim, FNAL, Chair

Jon Bagger, JHU  
Charlie Baltay, Yale  
Gary Feldman, Harvard  
Kevin Lesko, LBNL  
Ann Nelson, Washington, Seattle  
Mark Reichenadter, SLAC (chair of cost group)  
Mel Shochet, U.Chicago (chair of physics group)  
Bob Svoboda, UC Davis  
James Symons, LBNL  
Steve Vigdor, BNL

**Ex-officio members** HEPAP chair, NRC study chair: Andy Lankford, UC Irvine

PASAG chair: Steve Ritz, UC Santa Cruz  
DOE's DUSEL review committee co-chairs: Jay Marx, Caltech and Mark Reichenadter, SLAC  
DPF chair: Pierre Ramond, U. Florida  
DOE Intensity Frontier Workshop co-chairs: Harry Weerts, ANL and JoAnne Hewett, SLAC  
LBNE Project Manager: Jim Strait  
Fermilab Director: Pier Oddone  
LBNE Lab Oversight Group member: Susan Seestrom, LANL

**Scientific Secretary** Jeffrey Appel, FNAL served as the scientific secretary for the Steering Committee and the two working groups.

The Executive Summary of the LBNE Reconfiguration Steering Group Report is reproduced below:

# Executive Summary

## Introduction

The Department of Energy (DOE) Office of Science (SC) is planning investments in the next generation neutrino experiment, the Long-Baseline Neutrino Experiment (LBNE).

In light of the current budget climate, on March 19<sup>th</sup>, Dr. W.F. Brinkman, Director of the DOE Office of Science, asked Fermilab to find a path forward to reach the goals of the LBNE in a phased approach or with alternative options. His letter notes that this decision is not a negative judgment about the importance of the science, but rather it is a recognition that the peak cost of the project cannot be accommodated in the current budget climate, or that projected for the next decade. Pier Oddone, Director of Fermilab, formed a Steering Committee and two working groups, a Physics Working Group and an Engineering/Cost Working Group, to address this request. The Steering Committee is charged to provide guidance to the working groups, to identify viable options and to write the report to the DOE. The Physics Working Group is charged to analyze the physics reach of various phases and alternatives on a common basis, and the Engineering/Cost Working Group is charged to provide cost estimates and to analyze the feasibility of the proposed approaches with the same methodology. Dr. Brinkman's letter to Pier Oddone is given in *Appendix A*, and the membership of the Steering Committee, the committee's ex-officio members and the membership of the working groups are listed in *Appendix B*.

The Steering Committee produced an interim report and presented it to Pier Oddone on June 4. Pier Oddone briefed the interim conclusions to Dr. Brinkman on June 6. On June 29, Dr. Brinkman wrote a letter to Pier Oddone, asking the laboratory to proceed with planning a Critical Decision 1 review later this year based on the reconfigured LBNE options that we presented. Dr. Brinkman's letter is given to *Appendix C*.

The Steering Committee had twelve conference call meetings and had two face-to-face meetings on April 26, 2012 and May 22-23, 2012 at Fermilab. The Steering Committee organized and held a workshop on April 25-26, 2012 at Fermilab to inform the high-energy physics community, to discuss the status of the work in progress and to seek input from the community. *Appendix D* gives the agenda for the workshop. The Physics Working Group and the Engineering/Cost Working Group enlisted the necessary experts from Fermilab, other national laboratories, universities and the LBNE and other neutrino experiment collaborations to carry out the studies. Each working group provided a report of their analysis and their reports can be found at [http://www.fnal.gov/directorate/lbne\\_reconfiguration/](http://www.fnal.gov/directorate/lbne_reconfiguration/). Meeting agendas and minutes of the Steering Group and the working groups, and the workshop presentations are posted on the LBNE reconfiguration webpage ([http://www.fnal.gov/directorate/lbne\\_reconfiguration/](http://www.fnal.gov/directorate/lbne_reconfiguration/)).

The Steering Committee wishes to thank the Physics Working Group, the Engineering/Cost Working Group and many experts who participated in the studies, whose work is the foundation of this report. The committee would also like to thank those who provided their input to this process via presenting at the workshop or writing letters to the committee.

## Neutrinos and LBNE

The discovery that neutrinos spontaneously change type – a phenomenon called neutrino oscillation – was one of the most revolutionary particle-physics discoveries of the last several decades. This discovery was unexpected by the very successful Standard Model of particle physics. It points to new physics phenomena at energies much higher than those that can directly be discovered at particle colliders, and it raises other challenging questions about the fundamental workings of the universe.

Neutrinos are the most elusive of the known fundamental particles. To the best of our knowledge, they interact with other particles only through the weak interactions. For this reason, neutrinos can only be observed and studied via intense neutrino sources and large detectors. Particle accelerators, nuclear reactors, cosmic ray air showers, and neutrinos originating in the sun and in supernovae provide important neutrino sources, and have all played critical roles in discovering neutrinos and their mysterious properties. These discoveries led to the 1988 Nobel Prize in Physics (Leon Lederman, Melvin Schwartz and Jack Steinberger), the 1995 Nobel Prize in Physics (Frederick Reines), and the 2002 Nobel Prize in Physics (Raymond Davis and Masatoshi Koshiba).

The experimental achievements of the past 15 years have been astonishing. A decade ago, the space of allowed oscillation parameters spanned many orders of magnitude. Within the three-neutrino picture, allowed regions have now shrunk to better than the 10% precision level for most of the parameters. By the end of this decade, invaluable new information is expected from the current generation of neutrino-oscillation experiments, namely the long-baseline beam experiments NOvA, T2K, MINOS, ICARUS and OPERA and the reactor experiments Double Chooz, Daya Bay and RENO. These experiments will measure the known oscillation parameters much more precisely, and may provide nontrivial hints regarding the neutrino mass hierarchy. However, it is unlikely that these experiments will be able to determine the ordering of the neutrino masses unambiguously, nor provide any significant information regarding possible violation of CP-invariance in the lepton sector. Nor is it expected that they will be able to test definitively the standard three-neutrino paradigm. That will be the task of next-generation experiments.

Future opportunities for testing the paradigm and probing new physics using next-generation neutrino-oscillation experiments are broad and exciting. The focus for the U.S. has been the Long Baseline Neutrino Experiment (LBNE), which would employ a 700 kW beam from Fermilab and a large liquid argon time-projection chamber at the Homestake mine in South Dakota, 1,300 km away. With the 1,300 km baseline, a broad-band neutrino beam designed specifically for this purpose, and the highly capable detector, LBNE would measure many of the oscillation parameters to high precision and, in a single experiment, test the internal consistency of the three-neutrino oscillation model. Placed deep underground, the detector would also allow for a rich physics program beyond neutrino-oscillation studies. It would include a high-sensitivity search for proton decay, and high-sensitivity studies of neutrinos coming from supernovae within our galaxy.

The LBNE would answer a number of important scientific questions:

1. Is there CP violation in the neutrino sector? The existence of matter this late in the universe's development requires CP violation at an early stage, but the amount seen in the quark sector is much too small to account for the matter that we observe in the universe. CP violation in the lepton sector may provide the explanation.
2. Is the ordering of the neutrino mass states the same as that of the quarks, or is the order inverted? In addition to being an important question on its own, the answer has a major



impact on our ability to determine whether the neutrino is its own antiparticle. If true, it could reflect physics at energy scales much greater than those probed at the LHC.

3. Is the proton stable? Proton decay would require violation of baryon number conservation, and such violation is needed to account for the matter-antimatter asymmetry in the universe. The answer will provide clues to the unification of the forces of nature.
4. What physics and astrophysics can we learn from the neutrinos emitted in supernova explosions?

The importance of these questions and the unique ability of LBNE to address them led to strong support by the scientific community for LBNE. LBNE was a feature of the plan proposed by the Particle Physics Project Prioritization Panel (P5) of the High Energy Physics Advisory Panel (HEPAP) in 2008 and was a key element of the strong endorsement for underground physics by the National Research Council, in July, 2011. The importance of LBNE to U.S leadership in neutrino physics was also recognized in the report of the DOE-sponsored workshop on Fundamental Physics at the Intensity Frontier, held in December 2011.

A very strong collaboration formed around LBNE with the participation of 65 institutions, including 6 U.S. national laboratories, from 5 countries.

## Conclusions

To achieve all of the fundamental science goals listed above, a reconfigured LBNE would need a very long baseline (>1,000 km from accelerator to detector) and a large detector deep underground. However, it is not possible to meet both of these requirements in a first phase of the experiment within the budget guideline of approximately \$700M – \$800M, including contingency and escalation. The committee assessed various options that meet some of the requirements including underground detector only options (no accelerator-base neutrino beam) and a range of baselines from the existing 700-800 km available with Fermilab's NuMI beam to as far as 2,600 km, and identified three viable options for the first phase of a long-baseline experiment that have the potential to accomplish important science at realizable cost. These options are (not priority ordered):

- Using the existing NuMI beamline in the low energy configuration with a **30 kton** liquid argon time projection chamber (LAr-TPC) **surface detector** 14 mrad off-axis at Ash River in Minnesota, **810 km** from Fermilab.
- Using the existing NuMI beamline in the low energy configuration with a **15 kton** LAr-TPC **underground (at the 2,340 ft level) detector** on-axis at the Soudan Lab in Minnesota, **735 km** from Fermilab.
- Constructing a new low energy LBNE beamline with a **10 kton** LAr-TPC **surface detector** on-axis at Homestake in South Dakota, **1,300 km** from Fermilab.

The committee looked at possibilities of projects with significantly lower costs and concluded that the science reach for such projects becomes marginal.

We list pros and cons of each of the viable options below (not priority ordered).

- 30 kton surface detector at Ash River in Minnesota (NuMI low energy beam, 810 km baseline)

Pros	<ul style="list-style-type: none"> <li>• Best Phase 1 CP-violation sensitivity in combination with NOvA and T2K results for the current value of <math>\theta_{13}</math>. The sensitivity would be enhanced if the mass ordering were known from other experiments.</li> <li>• Excellent (<math>3\sigma</math>) mass ordering reach in nearly half of the <math>\delta_{CP}</math> range.</li> </ul>
Cons	<ul style="list-style-type: none"> <li>• Narrow-band beam does not allow measurement of oscillatory signature.</li> <li>• Shorter baseline risks fundamental ambiguities in interpreting results.</li> <li>• Sensitivity decreases if <math>\theta_{13}</math> is smaller than the current experimental value.</li> <li>• Cosmic ray backgrounds: impact and mitigation need to be determined.</li> <li>• Only accelerator-based physics.</li> <li>• Limited Phase 2 path: <ul style="list-style-type: none"> <li>◦ Beam limited to 1.1 MW (Project X Stage 1).</li> <li>◦ Phase 2 could be a 15-20 kton underground (2,340 ft) detector at Soudan.</li> </ul> </li> </ul>

- 15 kton underground (2,340 ft) detector at the Soudan Lab in Minnesota (NuMI low energy beam, 735 km baseline)

Pros	<ul style="list-style-type: none"> <li>• Broadest Phase 1 physics program: <ul style="list-style-type: none"> <li>◦ Accelerator-based physics including good (<math>2\sigma</math>) mass ordering and good CP-violation reach in half of the <math>\delta_{CP}</math> range. CP-violation reach would be enhanced if the mass ordering were known from other experiments.</li> <li>◦ Non-accelerator physics including proton decay, atmospheric neutrinos, and supernovae neutrinos.</li> </ul> </li> <li>• Cosmic ray background risks mitigated by underground location.</li> </ul>
Cons	<ul style="list-style-type: none"> <li>• Mismatch between beam spectrum and shorter baseline does not allow full measurement of oscillatory signature.</li> <li>• Shorter baseline risks fundamental ambiguities in interpreting results. This risk is greater than for the Ash River option.</li> <li>• Sensitivity decreases if <math>\theta_{13}</math> is smaller than the current experimental value.</li> <li>• Limited Phase 2 path: <ul style="list-style-type: none"> <li>◦ Beam limited to 1.1 MW (Project X Stage 1).</li> <li>◦ Phase 2 could be a 30 kton surface detector at Ash River or an additional 25-30 kton underground (2,340 ft) detector at Soudan.</li> </ul> </li> </ul>

- 10 kton surface detector at Homestake (new beamline, 1,300 km baseline)

Pros	<ul style="list-style-type: none"> <li>• Excellent (<math>3\sigma</math>) mass ordering reach in the full <math>\delta_{CP}</math> range.</li> <li>• Good CP violation reach: not dependent on <i>a priori</i> knowledge of the mass ordering.</li> <li>• Longer baseline and broad-band beam allow explicit reconstruction of oscillations in the energy spectrum: self-consistent standard neutrino measurements; best sensitivity to Standard Model tests and non-standard neutrino physics.</li> <li>• Clear Phase 2 path: a 20 – 25 kton underground (4850 ft) detector at the Homestake mine. This covers the full capability of the original LBNE physics program.</li> <li>• Takes full advantage of Project X beam power increases.</li> </ul>
Cons	<ul style="list-style-type: none"> <li>• Cosmic ray backgrounds: impact and mitigation need to be determined.</li> <li>• Only accelerator-based physics. Proton decay, supernova neutrino and atmospheric neutrino research are delayed to Phase 2.</li> <li>• ~10% more expensive than the other two options: cost evaluations and value engineering exercises in progress.</li> </ul>

The LBNE collaboration has conducted initial studies to verify whether the cosmic ray backgrounds are manageable for the operation of LAr-TPCs on the surface. The studies were concentrated on photon induced cascades as the major source of background events, as this is potentially the most serious problem. Two independent techniques have been investigated to reduce these backgrounds using the ability of the LAr detector to reconstruct muon tracks and electron showers and separate electron- from gamma-induced showers. Both techniques have been shown to be viable, even without the assumption of a photon trigger system or fast timing veto. It was found that a combination of simple cuts together with the low (2%) expected probability of  $e\text{-}\gamma$  misidentification can reject this background to a level well below the expected  $\nu_e$  appearance signal. Studies will continue in the next few months. In addition, the shorter drift distance for surface options is chosen to mitigate the effects of space charge build-up due to cosmic rays. Detailed information is documented and available at [http://www.fnal.gov/directorate/lbne\\_reconfiguration/](http://www.fnal.gov/directorate/lbne_reconfiguration/).

The Phase 1 experiment will use the existing detectors (MINOS near detector, MINERvA, and NOvA near detector) as near detectors for the two NuMI options, and use muon detectors to monitor the beam for the Homestake option. For the Homestake case, the LBNE collaboration has examined strategies to maintain the initial scientific performance without a full near detector complex. Although detailed evaluation must await full simulations, the conclusion is that there are viable strategies that will be adequate for the initial period of LBNE running. However, a complete LBNE near detector system will be required in a later stage to achieve the full precision of the experiment. Studies will continue as the design of LBNE is developed. Details information is documented and available at [http://www.fnal.gov/directorate/lbne\\_reconfiguration/](http://www.fnal.gov/directorate/lbne_reconfiguration/).

Studies have been done to understand the possibilities for optimizing the NuMI beamline for a lower-neutrino-energy spectrum and a higher flux to enhance the physics sensitivity for the two NuMI options. The conclusion is that modest increases in the flux below 2 GeV are possible, but that no options for large gains are known. Detailed information is documented and available at [http://www.fnal.gov/directorate/lbne\\_reconfiguration/](http://www.fnal.gov/directorate/lbne_reconfiguration/).

While each of these first-phase options is more sensitive than the others in some particular physics domain, the Steering Committee in its discussions strongly favored the option to build a new beamline to Homestake with an initial 10 kton LAr-TPC detector on the surface. The physics reach of this first phase is very strong; it would determine the mass hierarchy and explore the CP-violating phase  $\delta_{CP}$ , and measure other oscillation parameters:  $\theta_{13}$ ,  $\theta_{23}$ , and  $|\Delta m^2_{32}|$ . Moreover this option is seen by the Steering Committee as a start of a long-term world-leading program that would achieve the full goals of LBNE in time and allow probing the Standard Model most incisively beyond its current state. Subsequent phases will include:

- A highly capable near neutrino detector, which will reduce systematic errors on the oscillation measurements and enable a broad program of short-baseline neutrino physics.
- An increase in far detector mass to 35 kton fiducial mass placed at the 4850 ft level, which will further improve the precision of the primary long-baseline oscillation measurements, enable measurement of more difficult channels to make a fully comprehensive test of the three-neutrino mixing model, and open or enhance the program in non-accelerator-based physics, including searches for baryon-number-violating processes and measurements of supernova neutrinos.
- A staged increase in beam power from 700 kW to 2.3 MW with the development of Project X, which will enhance the sensitivity and statistical precision of all of the long- and short-baseline neutrino measurements.

The actual order and scope of the subsequent stages would depend on where the physics leads and the available resources.

At the present level of cost estimation, it appears that this preferred option may be ~15% more expensive than the other two options, but cost evaluations and value engineering exercises are continuing.

Although the preferred option has the required very long baseline, the major limitation of the preferred option is that the underground physics program including proton decay and supernova collapse cannot start until later phases of the project. Placing a 10 kton detector underground instead of the surface in the first phase would allow such a start, and increase the cost by about \$135M.

Establishing a clear long-term program will make it possible to bring in the support of other agencies both domestic and foreign. The opportunities offered by the beam from Fermilab, the long baseline and ultimately underground operation are unique in the world. Additional national or international collaborators have the opportunity to increase the scope of the first phase of LBNE or accelerate the implementation of subsequent phases. In particular, partnerships with institutions and agencies could add sufficient additional resources to place the initial 10 kton LAr TPC detector 4850 feet underground and provide a full near detector in the first phase. Studies of proton decay and neutrinos from supernova collapse are complementary to those being performed with existing water Cerenkov detectors. For the study of supernova collapse, LAr TPCs are sensitive to neutrinos whereas water Cerenkov detectors are sensitive to antineutrinos; for the study of proton decay, the LAr TPC is much more sensitive to the decay of protons into kaons as preferred by supersymmetric theories. There are also a large number of other nucleon decay modes for which liquid argon has high detection efficiency. Detection of even a single event in any of these modes would be revolutionary for particle physics.

Finally, Dr. Brinkman's response to the Reconfiguration Steering Group Report follows:



**Department of Energy**  
Office of Science  
Washington, DC 20585

**Office of the Director**

June 29, 2012

Dear Pier,

I would like to thank you and your management team for your recent presentation on the revised plans for the Long Baseline Neutrino Experiment (LBNE). The steering group and project team have done an excellent job responding to our request to reconfigure the project in ways that lead to an affordable and phased approach that will enable important science results at each phase. The report of the LBNE steering group outlining the options and alternatives considered provides clear and thoughtful input to our strategic plan for the Intensity Frontier program.

We would like you to proceed with planning a Critical Decision 1 review later this year based on the reconfigured LBNE options you presented. Please work with Jim Siegrist and Dan Lehman on the timing of this review.

I am hopeful that we can put the LBNE project on a sustainable path and thereby secure a leadership position for Fermilab in the Intensity Frontier. We look forward to working with you to achieve this goal.

Sincerely yours,

A handwritten signature in dark ink, appearing to read "W.F. Brinkman", is written over the "Sincerely yours," line.

W.F. Brinkman

